UNIVERSITÀ DEGLI STUDI DI CAGLIARI

Scuola di Dottorato di Ingegneria Civile e Architettura

Direttore: Prof. Ing. Gaetano Ranieri

Dottorato in Ingegneria Strutturale

Coordinatore: Prof. Ing. Barbara De Nicolo

XXIV CICLO

Fire resistance of Laminated Veneer Lumber (LVL) and Cross-Laminated Timber (XLAM) elements

Dottoranda: Agnese Menis

Tutor: Prof. Ing. Massimo Fragiacomo

SSD: ICAR 09: Tecnica delle Costruzioni

Marzo 2012

SUMMARY

Engineering design of timber structures in fire conditions is crucial to ensure high safety levels. Wood is subjected to degradation under fire exposure therefore its thermal and mechanical behaviours change. Timber design must take the decrease of timber performance into account to calculate structural elements that can carry external loads also if exposed to high temperatures. Analytical and numerical approaches can be adopted in fire design practice.

This research investigates the fire behaviour of laminated veneer lumber elements and cross-laminated timber panels. The study focused on some research questions regarding the fire resistance of unprotected and protected timber structural elements, the possibility to predict accurately the fire behaviour of timber elements through numerical modelling, and the accuracy of analytical estimations of fire resistance using simplified design methods.

Experimental tests of small and large specimens exposed to fire on one or more sides and subjected to different types and levels of load were performed. The results highlight the good performance of timber structural elements in fire conditions. The collected data were used to validate two- and three-dimensional models implemented in the general purpose finite element code Abaqus. Thermal and mechanical analyses were carried out to estimate the temperature distribution within unprotected and protected cross-sections of different sizes, the fire resistance and the displacement of timber elements loaded in-plane and out-of-plane. Further, parametric studies assuming different timber properties-temperature relationships were also performed. The proposed numerical modelling can be used to investigate the fire behaviour of timber members made of other wood-based products and subjected to different loads and fire conditions.

Experimental and numerical results were compared with analytical predictions obtained by using simplified design methods proposed by current codes of practice and recent research proposals. Numerical and analytical methods provide overall acceptable

estimations of fire behaviour of timber members, especially considering the high variability that characterizes the wood material and the experimental tests, in particular the fire tests.

SOMMARIO

La progettazione di strutture in legno esposte al fuoco è di fondamentale rilevanza al fine di garantire elevati livelli di sicurezza. Il comportamento termico e meccanico del legno cambia a seguito dell'esposizione al fuoco che causa il degrado del materiale. La riduzione delle prestazioni strutturali di elementi lignei in condizione d'incendio deve essere considerata nella progettazione delle strutture affinché siano in grado di resistere alle sollecitazioni esterne anche se esposte al fuoco. Metodi analitici e numerici possono essere utilizzati nella progettazione al fuoco.

Questa ricerca analizza il comportamento al fuoco di elementi in legno microlamellare e di pannelli in legno lamellare incrociato. Lo studio si è indirizzato su alcuni aspetti fondamenti riguardanti la resistenza al fuoco di elementi lignei protetti e non protetti, la possibilità di descrivere il reale comportamento al fuoco di elementi lignei mediante la modellazione numerica e l'accuratezza delle previsioni ottenute analiticamente con metodi di calcolo semplificati.

Prove sperimentali sono state eseguite su provini di piccole e grandi dimensioni esposti al fuoco su uno o più lati e caricati con diversi tipi e livelli di forze. I risultati hanno dimostrato le buone prestazioni in condizione d'incendio degli elementi lignei aventi sezioni adatte all'impiego strutturale. I dati acquisiti sono stati utilizzati per validare i modelli numerici implementati nel codice di calcolo agli elementi finiti Abaqus. Con analisi termiche e meccaniche sono stati stimati la distribuzione di temperatura in sezioni, protette e non, aventi diverse dimensioni, la resistenza al fuoco e lo spostamento di elementi lignei caricati nel piano e fuori piano. Indagini parametriche sono state inoltre condotte adottando diverse leggi di variazione delle proprietà del legno con la temperatura. La modellazione numerica proposta può essere estesa a studi sul comportamento al fuoco di elementi lignei strutturali realizzati con altri prodotti derivati del legno e soggetti a diverse condizioni di carico e d'incendio.

I risultati sperimentali e numerici sono stati confrontati con le previsioni analitiche ottenute con metodi semplificati proposti dalle normative di progettazione e da recenti ricerche. Complessivamente i metodi numerici e analitici permettono accettabili previsioni del comportamento al fuoco di elementi strutturali in legno, considerando soprattutto l'alta variabilità che caratterizza il materiale e le prove sperimentali, in particolari quelle al fuoco.

TABLE OF CONTENTS

LIST OF FIGURES

PART I

PART II

LIST OF TABLES

PART I

PART II

LIST OF PUBLICATIONS

Fragiacomo M., **Menis A.**, Moss P.J., Buchanan A.H. and Clemente I. (2009). *Comparison between the conductive model of Eurocode 5 and the temperature distribution within a timber cross-section exposed to fire*. Proceedings of the 42nd Meeting – CIB-W18, Duebendorf, Switzerland.

Fragiacomo M., **Menis A.**, Moss P.J., Buchanan A.H. and Clemente I. (2010) *Numerical and experimental evaluation of the temperature distribution within laminated veneer lumber (LVL) exposed to fire*. Journal of Structural Fire Engineering; 1(3):145-159, DOI: 10.1260/2040-2317.1.3.145.

Fragiacomo M., **Menis A.**, Moss P.J., Clemente I. and Buchanan A.H. (2010). *Numerical and experimental thermal-structural behaviour of laminated veneer lumber (LVL) exposed to fire*. Proceedings of the 11th World Conference on Timber Engineering, Riva del Garda, Italy.

Fragiacomo M., **Menis A.**, Clemente I. and Bochicchio G. (2011) *Resistenza all'incendio di solai a pannelli in legno lamellare incrociato.* Proceedings of the 23rd CTA Conference - Special Session, Ischia, Italy (in Italian).

Fragiacomo M., **Menis A**., Moss P.J., Clemente I., Buchanan A.H. and De Nicolo B. (2012). *Predicting the fire resistance of timber members loaded in tension.* Fire and Materials, Wiley, published online. DOI: 10.1002/fam.2117

Fragiacomo M., **Menis A.**, Bochicchio G., Clemente I. and Ceccotti A. (2012). *Fire resistance of cross-laminated timber floors. Part 1: Experimental study.* ASCE Journal of Structural Engineering, in review.

Fragiacomo M., **Menis A.** and Clemente I. (2012). *Fire resistance of cross-laminated timber floors. Part 2: Numerical modeling.* ASCE Journal of Structural Engineering, in review.

Menis A., Fragiacomo M. and Clemente I. (2012). *Numerical investigation of the fire resistance of protected cross-laminated timber floor panels*. IABSE Structural Engineering International, in review.

Fragiacomo M., **Menis A.**, Bochicchio G. and Clemente I. (2012). *Fire behaviour of cross-laminated timber walls.* Proceedings of the 7th International Conference on Structures in Fire, Zurich, Switzerland.

Fragiacomo M., **Menis A.** and Clemente I. (2012). F*ire resistence of cross-laminated timber floors*. Proceedings of the 7th International Conference Wood and Fire Safety, Strbské Pleso, Slovakia.

Fragiacomo M., **Menis A.**, Clemente I., Bochicchio G. and Tessadri B. (2012). *Experimental and numerical behaviour of cross-laminated timber floors in fire conditions*. Proceedings of the 12th World Conference on Timber Engineering, Auckland, New Zealand.

INTRODUCTION

Fire performance of structural elements is an important issue of building design in order to ensure the attainment of the required safety level. This aspect is essential for timber buildings that are becoming more widespread in Europe for public, domestic and commercial purposes. The fire behaviour of different timber construction systems must be considered with special care since wood is a combustible material. Wood is characterized by complex physical and chemical phenomena that occur when it is exposed to high temperatures. The material degradation with temperature leads to a consequent decrease of mechanical performance of timber structural elements.

Simplified and advanced calculation methods are recommended for fire design of timber elements in common practice and research investigations, respectively. Both the approaches need extensive experimental tests for validation purposes. The numerical modelling is nowadays an effective and inexpensive alternative method to investigate the behaviour of timber structures in fire conditions without performing expensive fire tests. It is of interest to develop robust numerical models calibrated on available experimental data to understand more in detail the behaviour of elements made of different wood-based products, and to carry out parametric studies when geometrical, mechanical and thermal properties, applied loads, protective claddings and boundary conditions are varied with respect to test conditions.

The objective of this research is the investigation of the behaviour of laminated veneer lumber elements and cross-laminated timber panels exposed to fire. The present study was undertaken in an attempt to address some important research questions:

- What is the actual resistance of large-scale timber structural elements exposed to fire on one or more sides and subjected to different types of load?
- What is the effect of protective cladding on the actual fire resistance of large-scale timber structural elements?

- Is it possible to model accurately the thermal state within protected and unprotected timber members, and the thermo-mechanical behaviour under load in fire conditions using general purpose software packages?
- What is the influence of the temperature-dependent properties of wood on the thermal and mechanical behaviour of timber members in fire conditions?
- What is the accuracy of simplified design methods provided by current code of practice and new research proposals to estimate the fire resistance of timber elements under different load levels?

Experimental and numerical approaches were mainly employed in this research to investigate these important aspects of structural fire design.

Experimental tests on small- and large-scale specimens subjected to in-plane and out-of-plane external loads and exposed to fire on one or more sides were carried out to analyse the thermal and mechanical performances of laminated veneer lumber and cross-laminated timber. Two- and three-dimensional numerical models were implemented in the general purpose finite element code Abaqus to simulate the fire tests and to predict the resistance of laminated veneer lumber elements and cross-laminated timber panels in fire conditions. Heat transfer analyses were performed to obtain reliable information on temperature distribution within cross-sections subjected to one- and two-dimensional fire exposures. The thermal results were compared with experimental data collected by thermocouples inserted in small and large specimens tested in furnaces with different sizes. An accurate numerical description of the thermal state is crucial to evaluate the residual cross-section with load-bearing capacity and therefore to estimate the fire resistance of structural elements. The mechanical behaviour of timber elements under fire conditions was investigated by carrying out sequential coupled thermo-structural analyses. The numerical estimations of fire resistance and displacement were compared with experimental measurements and analytical predictions obtained by using simplified design methods proposed by code of practice and recent research. The thermal and structural models were used to perform parametric studies adopting different thermal and mechanical properties for wood, load levels, and fire exposures.

This thesis is subdivided into two main parts dealing with laminated veneer lumber elements and cross-laminated timber panels. Each part describes the experimental tests and the numerical studies on thermal and mechanical behaviour of the analysed wood-based product. An abstract summarizes the content of the part. The primary experimental and numerical observations are highlighted in the conclusions of each part.
An introductory chapter before the two main parts discusses the state-of-the-art on numerical models recently implemented in different software packages to investigate the behaviour of structural timber elements exposed to fire.

Part I concerns the fire behaviour of laminated veneer lumber. After introducing the wood-based product (*Chapter 1*), the thermal investigation on unloaded specimens is presented in *Chapter 2*. The fire tests of small and large elements carried out in different furnaces are described. The two-dimensional thermal models implemented in Abaqus finite element code to simulate the fire tests are presented and numerical results in terms of temperature distribution and residual cross-section are discussed. *Chapter 3* describes the fire tests performed on small elements loaded in tension and the three-dimensional model developed to simulate the thermal and mechanical behaviour of those elements. The numerical outcomes of the thermo-structural analyses in terms of temperature and stress distribution, displacement and fire resistance are discussed and compared with experimental data and analytical predictions.

Part II deals with the thermal and mechanical behaviour of cross-laminated timber floor panels exposed to fire. After introducing the wood-based product (*Chapter 4*), the experimental tests of specimens loaded out-of-plane at ambient temperature and in fire conditions are described in *Chapter 5*. Data collected during the tests in terms of deflection, temperature distribution, residual cross-section and fire resistance are discussed and compared with analytical predictions. The thermal states within cross-sections protected with different materials are compared. *Chapter 6* and *Chapter 7* present the numerical investigations on fire behaviour of unprotected and protected cross-laminated timber floor panels, respectively. Both the chapters describe the implementation of finite element models in Abaqus and discuss the numerical results of thermal and thermo-structural analyses in terms of temperature and stress distributions, deflection, charred depth and fire resistance. Furthermore, a parametric study and a numerical-analytical comparison are discussed.

The main chapters of this thesis have been either published or submitted to peer-reviewed international journals. Each chapter was completed with additional information, details and results that were not included in the papers.

The state-of-the-art is based on the paper "*Numerical investigation of the fire resistance of protected cross-laminated timber floor panels*" submitted to IABSE Structural Engineering International.

Chapter 2 is based on the paper "Numerical and experimental evaluation of the temperature distribution within laminated veneer lumber (LVL) exposed to fire" published in the Journal of Structural Fire Engineering.

Chapter 3 is based on the paper "*Predicting the fire resistance of timber members loaded in tension*" published in Fire and Materials.

Chapter 5 is based on the paper "*Fire resistance of cross-laminated timber floors. Part 1: Experimental study*" submitted to ASCE Journal of Structural Engineering.

Chapter 6 is based on the paper "*Fire resistance of cross-laminated timber floors. Part 2: Numerical modeling*" submitted to ASCE Journal of Structural Engineering.

Chapter 7 is based on the paper "*Numerical investigation of the fire resistance of protected cross-laminated timber floor panels*" submitted to IABSE Structural Engineering International.

NUMERICAL INVESTIGATIONS: STATE-OF-THE-ART

Structural fire performance is an important part of building design. Timber structures must be considered with special care since wood is combustible. Experimental testing is needed to assess the fire performance of a timber structure in a realistic and accurate way, and several results are available in literature [e.g. Bénichou et al. 2002; Frangi 2009a; Moss et al. 2009c; Schmid and König 2010; Teibinger and Matzinger 2010; Yang at al. 2009a]. Experimental fire tests, however, are very expensive and can be performed only in few laboratories. The possibility to use advanced numerical models to extend the few experimental results available to specimens with different configurations, load levels, and boundary conditions is therefore very appealing. The models can also be used to validate simplified design methods such as the 'reduced cross-section method' (RCSM) proposed by the Eurocode 5, Part 1-2 [CEN 2004] used in common practice.

Different finite element codes can be used to perform thermal and mechanical analyses to investigate, respectively, the temperature and the stress distributions within members or structures made of different materials such as steel, concrete and wood exposed to fire [Buchanan 2002]. Some of these are general purpose software packages such as Abaqus and Ansys, and their use is recommended especially for research investigations. Other programs such as Safir [Franssen 2005] are specific for fire design. An extensive bibliography on finite element investigations of wood thermal and mechanical behaviour, timber connections, wood-based products and timber structural elements is reported in literature by Mackerle [2005].

The fire performance of structural elements has to be evaluated considering their thermal and mechanical behaviours when exposed to high temperatures. The material properties, the geometrical characteristics, the boundary conditions and the surrounding environment have a strong influence on the structural fire behaviour. Wood is a

combustible material subjected to physical degradation. Different phenomena such as evaporation of moisture, pyrolysis, charring and cracking of charred material take place in wood when exposed to fire. Many studies were performed on physical, thermal and mechanical properties of wood at ambient temperature and in fire conditions. Some finite element models focused on microscopic and macroscopic wood behaviour were developed to consider those complex phenomena, but they are not suitable for structural purposes due to heavy computational demand. The thermal behaviour of wood exposed to fire can be described by assuming in numerical modelling 'effective', rather than real, values for the thermo-physical properties that govern the internal heat transmission [König 2006]. Different proposals of effective density, specific heat and thermal conductivity can be found in literature to consider implicitly the wood degradation [e.g. CEN 2004; Frangi 2001; Hopkin et al. 2011; König 2006]. These parameters were implemented in numerical investigations of structural elements made of various wood products subjected to different fire conditions such as standard [ISO 834-1 1999] and parametric fires [CEN 2002b]. Furthermore, the thermal state depends upon the interactions in terms of radiation and convection with the surrounding environment. Values for the radiation and convection coefficients are recommended in the Eurocode 5, Part 1-2 [CEN 2004] and Eurocode 1 [CEN 2002b].

Heat transfer numerical models describe the temperature distribution within members exposed to fire, and can be used to determine the un-charred cross-section. The charring of protected and unprotected timber members subjected to one-dimensional (1D) standard and parametric fire exposures was investigated experimentally and numerically by König and Walleij [1999]. A heat transfer model was implemented in the computer program Tempcalc to calibrate the variation of the thermal properties of charcoal and wood with temperature. The coupled heat and moisture transfer in timber beams subjected to 1D or two-dimensional (2D) standard fire exposure was analysed by Schnabl and Turk [2006]. The differential equations describing the heat conduction and the moisture diffusion in a timber volume were solved using a computer program written in Matlab. Results in terms of charring were comparable with analytical predictions and experimental data. The validated model was then used to evaluate also the fire behaviour of loaded timber composite beams [Schnabl et al. 2008].

The thermal behaviour of different wood-based products exposed to high temperatures was investigated by using different finite element codes. 2D numerical

models were implemented in Abaqus [Fragiacomo et al. 2010a; Menis 2008] and Safir [Tsai 2010] to predict the temperature distribution within small and large cross-sections made from radiata pine laminated veneer lumber (LVL) exposed to fire on three or four sides. Parametric studies using coarse and fine meshes and adopting different input values for thermal properties, moisture content, convection coefficient and emissivity were performed. Experimental and numerical comparisons between the fire behaviour of cross-laminated timber (XLAM) and homogenous timber panels with the same depths were also conducted [Frangi et al. 2009a,b]. The numerical simulations of timber panels subjected to 1D standard fire exposure were performed using the finite element code Ansys. The falling of the charred layers due to the use of a polyurethane adhesive was assumed in the modelling of the 3- and 5-layer XLAM panels. The numerical results proved the influence of the number and thickness of layers on the fire behaviour of XLAM panels. Further, their charring rate was found to be strongly dependent upon the time when the charred layers fall off causing the direct exposure of the heated wood to high temperatures.

An accurate prediction of the inner thermal state is fundamental for a correct evaluation of the fire resistance of structural elements in fire conditions. Sequential thermal and structural analyses where the output in terms of temperature becomes an input for the mechanical model were carried out by using different software packages to simulate the fire behaviour of loaded timber members. Like the thermal parameters, also the mechanical properties of wood are dependent upon the temperature and different proposals can be found in literature [e.g. Buchanan 2002; CEN 2004; Jong and Clancy 2004]. The load-bearing capacity of heated wood reduces progressively as the temperature rises within the cross-section. Charred material loses completely its strength and stiffness leading to the reduction of the resistant cross-section. The variation of mechanical properties with temperature should be implemented in numerical models for an accurate description of the timber behaviour.

Several numerical models were implemented in different codes to carry out investigations on the behaviour of structural elements loaded out-of-plane or in-plane and exposed to fire on one or more sides. Thermal and mechanical analyses carried out in Abaqus [Fragiacomo et al. 2012b] and Ansys [Bobacz 2006] codes were performed to examine the fire performance of axially loaded timber members. Different computer programs were used to investigate the fire behaviour of protected and unprotected

XLAM panels with different depths and structural layout [König and Schmid 2007; Schmid and König 2010]. The thermal state within the cross-sections was described by numerical models implemented in both software packages and Safir. The computer program CSTFire, written as a Visual Basic macro embedded in Excel, was used for the structural analysis. The numerical outcomes in terms of bending resistance and depth of the so-called 'zero-strength' layer were discussed and compared with the corresponding numerical results obtained for the homogenous timber deck plates [König and Schmid 2007]. Moreover, comparisons between the numerical results and the analytical predictions using the simplified RCSM suggested by the Eurocode 5 [CEN 2004] and a recent modified version for XLAM were carried out [Schmid and König 2010]. The same programs were employed to analyse the fire performance of wooden I-joists used in floor assemblies [König and Källsner 2006]. The falling off of the protective claddings at specific times was considered in the thermal model, and found to markedly affect the results. Numerical results in terms of resistance, temperature and charring depth were presented and critically discussed.

Almost all numerical models proposed in literature do not consider do not consider the adhesives used to manufacture the wood products. However their influence on the fire behaviour of structural members might not be negligible. This was observed, for example, during a research on timber-concrete composite slabs exposed to fire where a shear failure occurred in a glued laminated timber (GLT) beam [Frangi et al. 2004]. The fire resistance of that GLT beam was numerically estimated considering the reduction of both timber and adhesive shear strengths with temperature. A recent experimental and numerical investigation has been carried out with the aim to evaluate the influence of the adhesive on the fire resistance of GLT elements [Klippel et al. 2011]. The thermal state within members exposed to standard fire on three sides was obtained through a 2D modelling implemented in Abaqus. The accuracy of the thermal model was verified comparing the temperature distributions with the experimental data recorded at different depths in cross-sections subjected to 1D fire exposure. The sequential mechanical analyses were carried out using the computer program CSTFire. The thermal and mechanical properties of wood proposed by the Eurocode 5 were adopted. The numerical modelling was used to analyse the influence of the adhesives used in the finger joints and between laminations in GLT. The numerical investigation highlighted that the reduction of the adhesive strength with temperature was negligible since the beam failed

in bending. Conversely, the finger joint failures may be affected by the adhesive behaviour at high temperatures.

Several numerical simulations of thermal and mechanical behaviour of timber connections exposed to fire can be found in literature. A thermal modelling was implemented in Ansys to investigate the thermal interaction between steel and timber in multiple shear steel-to-timber connections exposed to fire [Erchinger et al. 2006; Erchinger et al. 2010]. A 2D finite element model of timber members was initially implemented and validated, then a three-dimensional (3D) model of steel-to-timber connections was developed. The model was validated on experimental data recorded during fire tests carried out by other authors. Another thermal investigation on wood-steel-wood and steel-wood-steel connections with bolts and dowels was performed by implementing a 3D model in Abaqus code [Peng et al. 2008; Peng 2010]. These connection types were tested in standard fire conditions under two different load levels. Parametric studies using different meshes and adopting different input for the thermal properties were also carried out. The thermal influence of the gaps between bolts and holes, and between steel plates and wood members was also investigated, as the gaps tend to enlarge during fire exposure due to the wood shrinkage, and worsens significantly the connection performance in fire conditions. In the modelling a small gap between bolts and wood was defined, while a perfect steel-wood contact was assumed. The thermal and mechanical behaviour of timber-to-timber and steel-to-timber connections loaded in tension parallel to grains in normal and fire conditions was examined using 3D models implemented in the finite element software Marc by Racher et al. [2010] and Audebert et al. [2011]. The thermal properties proposed by different authors were previously verified through a 2D model by comparing numerical and experimental results [Laplanche et al. 2004]. The non-linear geometrical and mechanical behaviour, and the contact between connection components were considered in the model. The evolution of the contacts between steel, timber and connectors (bolts and dowels) during the fire was also modelled [Audebert et al. 2011]. The Hill criterion was used to define the plasticity of an anisotropic material such as wood, even if this criterion assumed a symmetric behaviour in tension and compression. The asymmetry in the wood mechanical behaviour has been taken into account in some 3D numerical investigations of timber connections at ambient temperature [Xu et al. 2009a,b]. These finite element models implemented in Marc software consider also a failure criterion.

Racher et al. [2010] carried out a parametric study to estimate the influence of the timber member thickness on the connection load-carrying capacity.
A different numerical approach based on a component model was adopted by Cachim and Franssen [2009b] to simulate the fire behaviour of steel dowelled timber connections. The mechanical behaviour of timber and dowel components was defined separately. Beam elements and springs were used to schematize the dowel and the timber, respectively. The component model implemented in Safir code was initially validated for connections in ambient conditions. In fire conditions, two numerical steps were required to perform the investigation. A thermal analysis was carried out on a 3D schematization of the connection to determine the temperature distribution within the timber and the steel dowel assuming a perfect contact throughout the fire exposure. The thermal outcomes were converted in input for the following mechanical analysis using the component model. The accuracy of the modelling was verified for different connection types by comparing the numerical results with experimental data.

Another important research topic is the fire behaviour of floor and wall assemblies. Numerical tools were used to estimate the fire resistance of wood structural elements and to perform parametric studies considering different assembly compositions in terms of material, position and thicknesses of the protective layers. A 2D computer model called Wall2D was developed in Canada to predict the heat transmission through non-insulated wood-stud walls exposed to fire [Takeda and Mehaffey 1998]. Since the thermal results were in good agreement with all experimental data, the authors concluded that the model can be used in fire safety design. The same computer model was used to evaluate the fire resistance of load-bearing wood frame wall assemblies [Bénichou et al. 2002]. The Wall2D model was then extended to Wall2DN to simulate also the fire behaviour of insulated wood-stud walls and the opening of the joints between gypsum boards due to their shrinkage at high temperature [Takeda 2003]. The influence of the insulation in the cavity on the fire resistance of the wall assembly was evaluated. An advanced thermal model was implemented by Winter and Meyn [2009] in the finite element code Ansys to simulate more realistically the fire behaviour of timber wall assemblies. The formation of cracks in the panel materials and the opening of joints caused by the material shrinkage were considered in the thermal modelling.

The fire behaviour of timber frame floor assemblies with void cavities was investigated experimentally and numerically to propose a simplified design model based

on the charring rate concept [Frangi and Erchinger 2007; Frangi et al. 2008b]. The temperature distribution in the timber members of the floor assembly exposed to standard fire was computed implementing a finite element model in Ansys code. A parametric study on charring depth of initially protected timber beams was carried out assuming different cross-sections, types of fire protection, and start of charring caused by the cladding falling off. The thermal modelling was validated on experimental results collected during fire tests on specimens subjected to 1D fire exposure, and then used to check the accuracy of analytical predictions made with the RCSM and the new charring model developed by the authors. A computer model was also developed to analyse the effect of an insulation layer in a wood frame floor/ceiling assembly [Takeda 2010]. A heat transfer model describes the thermal state in the assembly and the charring of wood joists. The fire resistance of joists was also determined by a structural model. A numerical investigation of solid wood joist floor assemblies exposed to fire was carried out also by Lu et al. [2010]. The temperature distribution within the assembly was obtained by performing thermal analyses with a 3D model implemented in Abaqus code. The falling off of the protective cladding made of gypsum board was assumed in the modelling. The outcomes of the 3D heat transfer model were compared with other numerical results obtained with a 2D model and with experimental data of a full-scale test. Thermal and structural analyses were performed by using a 3D model implemented in Ansys code to simulate large-scale fire tests on two different loaded wood floor assemblies [Tabaddor 2008].

PART I

FIRE BEHAVIOUR OF LAMINATED VENEER LUMBER (LVL) ELEMENTS

Abstract

The thermal and structural performance of laminated veneer lumber (LVL) elements was investigated experimentally and numerically. Tests of small and medium LVL beam members subjected to two-dimensional fire exposure were performed in different fire laboratories of New Zealand. Two- and three-dimensional finite element models were implemented in the Abaqus software to simulate the fire tests and to carry out parametric studies. Experimental data, numerical results and analytical predictions based on simplified design methods were compared.

Chapter 1 reports a brief introduction on LVL product that is widely utilized for structural purposes in Australasia and Northern Europe due to the good mechanical properties.

Chapter 2 describes experimental tests of unloaded LVL elements exposed to fire on three and four sides, and discusses experimental-numerical comparisons in terms of temperature distribution within the members. Different LVL cross-sections were instrumented with several thermocouples to measure the inner temperature during the fire tests. A two-dimensional numerical model implemented in Abaqus finite element code was used to performed thermal analyses assuming different conductive models

suggested by Eurocode 5, Part 1-2 and by recent research proposals. The numerical results were characterized by acceptable approximation close to the surface exposed to fire. Since the accuracy reduced for deeper fibres, a new proposal based on a different variation of the thermal conductivity with the temperature was made. The proposal led to acceptable approximation throughout the tested cross-sections.

Chapter 3 describes experimental tests of LVL elements subjected to tension loads and exposed to fire on three and four sides. Furthermore, a three-dimensional model for predicting the fire resistance of LVL members is presented. Fire resistance is evaluated numerically in a two-step process implemented in the Abaqus finite element code: first, a time-dependent thermal analysis of the member exposed to fire is performed, followed by a structural analysis under constant load in fire conditions. The mechanical analysis considers the reduction in mechanical properties (stiffness and strength) of timber with temperature. The analysis terminates when the LVL element can no longer redistribute stresses from the hottest to the coldest parts, leading to structural failure. Experimental data in terms of temperature, charring depth, displacement and failure time were compared with numerical results obtained by assuming the thermal properties and degradation of mechanical properties with temperature suggested by Eurocode 5, Part 1-2, showing an overall acceptable approximation. The fire resistance of the LVL elements was then predicted depending upon the applied tensile loads using the numerical model and simplified design formulas, showing that the latter ones lead to acceptable approximation.

CHAPTER 1.

LAMINATED VENEER LUMBER (LVL)

Laminated veneer lumber (LVL) is an engineering wood product composed by veneers of 2.5-4.4 mm glued with durable adhesive and laid up with grain parallel to the main axis of the structural element (Fig. 1.1). This wood-based product appeared commercially initially in 1970s and it was introduced for structural applications in New Zealand in 1990s. Radiate pine is the most used wood species for LVL production in New Zealand.

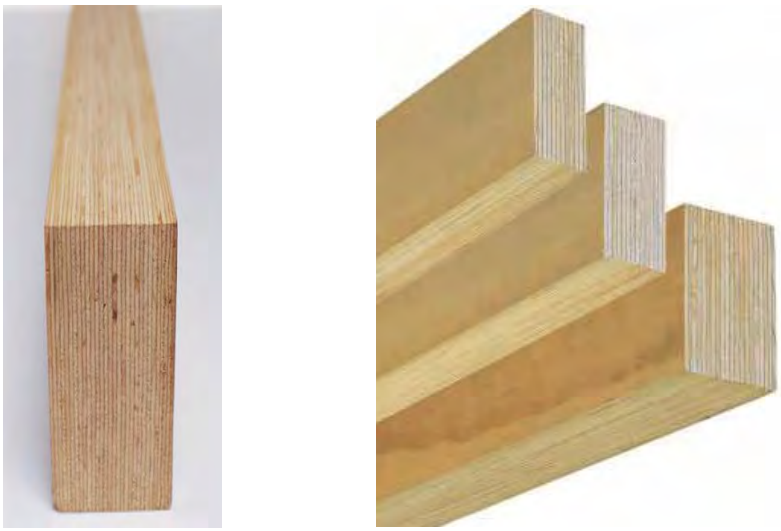

Fig. 1.1 - *Laminated veneer lumber product (left) and different LVL cross-sections (right) [Nelson Pine Industries Ltd. 2008].*

The great variability that characterizes sawn timber is considerably reduced in wood products made from laminations glued together such as LVL and glued laminated timber. The wood defects are almost negligible in LVL because of the large number of thin layers that randomise wood weak points such as knots. Therefore LVL structural product has high strength and stiffness properties and its mechanical performance is reliable and predictable. Since it is a wood-based product, LVL is anisotropic with different properties parallel and perpendicular to the grain. The design properties of LVL

are specific to the layups used by each individual manufacturer. LVL with defined properties for specific purposes can be product by combined graded veneers. Higher grade veneers on the outer faces will increase the fastener strength for nail plates in elements loaded on the edge and provide better stiffness for elements loaded on the flat (Fig. 1.2).

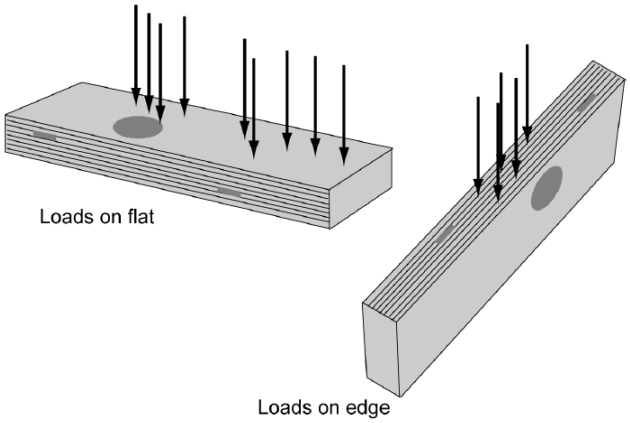

Fig. 1.2 - *Laminated veneer lumber loaded on flat or on edge [Buchanan 2007].*

LVL is manufactured according to the Australian and New Zealand standard AS/NZS 4357 [2005] and the European standard EN 14374 [CEN 2004]. The phases of LVL manufacturing process (Fig. 1.3) are herein listed:

- log selection and debarking;
- logs are conditioned in hot water (85°C for 24 hours);
- steamed logs are peeling in a rotary lathe;
- ribbon of veneer is clipped to a fixed wet width;
- veneers are dried with hot air perpendicular to surface. The drying process takes about 10 min to obtain a moisture content of between 8 and 10%;
- ultrasound measurement of veneer stiffness;
- veneer grading for moisture content and visual appearance;
- veneer edge is scarfed for an uniform thickness at the joints between veneers;
- application of adhesive for structural purposes, usually phenol formaldehyde resin;
- overlapping of veneers to form 1.2 m wide bi-dimensional elements with thickness and length that vary from 12 to 120 mm and from 8 to 18 m, respectively;
- heating process and pressing;
- cutting to required widths and marking of each LVL element.

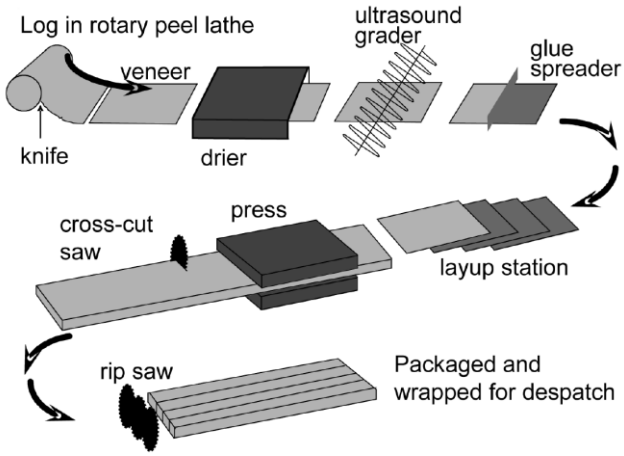

Fig. 1.3 - *Schematic view of LVL manufacturing process [Buchanan 2007].*

LVL may be used for beams or portal frame structures as an alternative to steel or reinforced concrete (Fig. 1.4). It is suitable for a wide range of applications where high performance and defined reliable properties are required. Long LVL structural elements (up to 18 m) can be manufactured, therefore reduced section depths can be used over continuous span. Moreover, larger spans and structures, and high continuous studs or columns are possible with fewer end joints.

Fig. 1.4 - *A LVL portal frame in New Zealand [CHH Woodproducts New Zealand].*

CHAPTER 2.

THERMAL INVESTIGATION

2.1. INTRODUCTION

Timber is a natural and sustainable resource which is being used more and more as structural material in buildings. Since timber is combustible, the fire design needs special attention. When a timber structural member is exposed to fire, physical, thermal and mechanical degradation phenomena occur in the material [Buchanan 2002] leading to a very complex behaviour. Simplified design methods suggested by current codes of practice such as Eurocode 5, Part 1-2 [CEN 2004] and New Zealand Standard [SNZ 1993] assume strength capacity under fire to be dependent upon the residual cross-section, which is evaluated by computing the thickness of the charring layer lost from the original unburned section during the time of exposure to fire. In such simplified design approaches, the charring rate is defined as the rate of movement of the 300ºC isotherm in the wood. Information on the temperature distribution within a timber cross-section during a fire is therefore crucial to compute the charring rate for different wood species and wood-based materials such as laminated veneer lumber [Tsai 2010] or glued laminated timber [e.g. Yang et al. 2009a,b]. The temperature distribution is also required for advanced numerical models where the structural fire resistance is calculated by taking into account the degradation of the mechanical properties (strength and modulus of elasticity) of timber with the temperature.

Analytical models based on experimental results for the temperature profiles of sections, beams and slabs exposed to standard ISO fire [ISO 834-1 1999] or different fire conditions were proposed by Frangi and Fontana [2003], Janssens [2004] and Shrestha et al. [1994]. Experimental tests of timber connections in tension were performed with the aim to evaluate the fire resistance and the temperature distribution within the timber and mechanical fasteners in fire conditions [e.g. Moss et al. 2009c]. The temperature profiles

can also be calculated using numerical models calibrated on experimental test results [e.g. König and Walleij 1999; Moss et al. 2009b; Peng et al. 2008; Takeda 2003]. A rigorous modelling of the heat conduction process within timber members exposed to fire should consider all complex phenomena taking place in the material, including the mass transport of water vapour after evaporation, the charring of wood, the crack formation and the physical properties of the char layer [e.g. Winter and Meyn 2009]. Due to the complexity of such rigorous models, reference to simplified conventional heat transfer models is usually made, where the phenomena listed above are implicitly accounted for in the thermal and physical properties of the material [König 2006]. Until now, most of the numerical analyses were performed using thermal parameters derived by calibration of the models on experimental results. Different proposals can be found in literature for the variation of thermal and mechanical parameters with temperature, showing little agreement among them [e.g. Cachim and Franssen 2009a; CEN 2004; Frangi 2001; Hopkin et al. 2011; König and Walleij 1999; Moss et al. 2009a]. Such relationships are affected by several variables such as the shape of the fire curve, the wood species, the moisture content, the type of wood–based material, the conditions of the surrounding environment, etc. It is therefore important to perform further research into the thermal and physical parameters of timber when exposed to fire in order to improve the accuracy of the temperature prediction and, consequently, the accuracy of the fire resistance of timber members.

The chapter investigates the temperature distribution within cross-sections made from spruce timber and radiata pine laminated veneer lumber (LVL) exposed to fire. Small (146×60 mm) and medium (300×105 mm and 360×133 mm) LVL members were tested in New Zealand under two-dimensional fire exposure in a custom-made furnace at the University of Canterbury [Menis 2008] and in the pilot furnace of the Building Research Association of New Zealand (BRANZ) [Lane 2005], respectively. Experimental results of one- and two-dimensional fire exposures were then compared with numerical values obtained by implementing a model of the thermal conduction process in the Abaqus finite element code [ABAQUS v.6.6]. Different proposals among those found in literature for the variation of thermal and physical properties with temperature were compared. A new proposal is made which leads to a more accurate prediction of temperature distribution, particularly for larger sections subjected to two-dimensional fire exposure.

2.2. EXPERIMENTAL TESTS

2.2.1. *LVL elements tested in custom-made furnace*

Three similar fire tests on unloaded radiata pine LVL members were carried out in the Fire Engineering Laboratory of the University of Canterbury, Christchurch, New Zealand [Menis 2008]. The purpose was to investigate the temperature distribution within the cross-sections exposed to fire on four sides.

The tests were performed in a small custom-made furnace made up of a 500 mm long cylinder and a steel frame as support (Fig. 2.1a). The cylinder has a diameter of 500 mm and a square opening of 180×180 mm at each end. It is composed by two stainless steel skins of 0.9 and 2 mm separated by 100 mm of Kaowool mineral insulation. The electrical furnace is heated up by three spiral heating coils fixed to the inner cylinder skin (Fig. 2.1b). The average temperature inside the furnace is measured by three K-type thermocouples.

(a)

(b)

Fig. 2.1 *- Photos of the custom-made furnace.*

The specimens had a cross-section of 146×60×1000 mm due to the small sizes of the furnace. They were cut into four parts and instrumented with 15 thermocouples placed parallel to the grain at the interface between the adjacent parts (Fig. 2.2a). The specimens were then rebuilt by gluing the four parts together (Fig. 2.2b) using phenol resorcinol formaldehyde resin, which was also used to produce LVL [Nelson Pine Industries Ltd. 2008]. Such glue does not interfere with the thermal properties of LVL and, apparently, with the temperature gradient in the timber [König et al. 2008], even though more specific studies would be necessary on this topic to fully evaluate the effect of the glue on the temperature distribution.

This experimental set-up allows the thermocouples to be inserted parallel to the grain into the specimens, and parallel to the temperature contours, leading to the best accuracy when measuring the temperature. The utilized thermocouples were type K (Chromel-Alumel), in particular 'K24-GG', suitable for high temperatures up to 1370°C (Fig. 2.3). Figure 2.4 displays the layout of the thermocouples (left) and the cross-section of an instrumented specimen before the test (right). Six thermocouples were inserted every 5 mm in half breadth of specimens (horizontal direction). The other nine thermocouples recorded the temperature every 5 and 10 mm along half specimen depth (vertical direction).

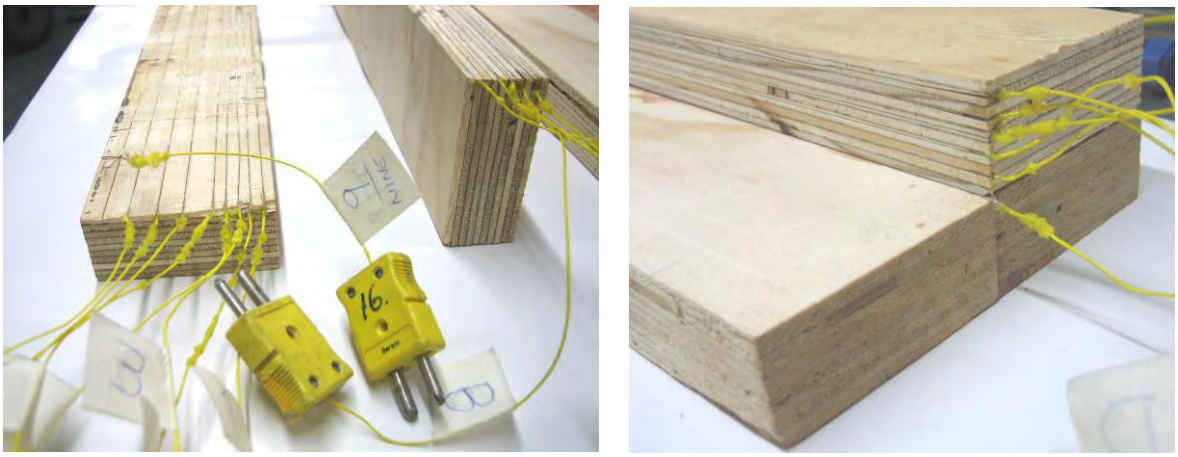

(a) (b)

Fig. 2.2 - *Preparation of the specimens: (a) insertion of the thermocouples in two pieces of LVL, (b) construction of specimens by gluing the four pieces of LVL.*

Fig. 2.3 - *K-type thermocouples inserted in the specimens.*

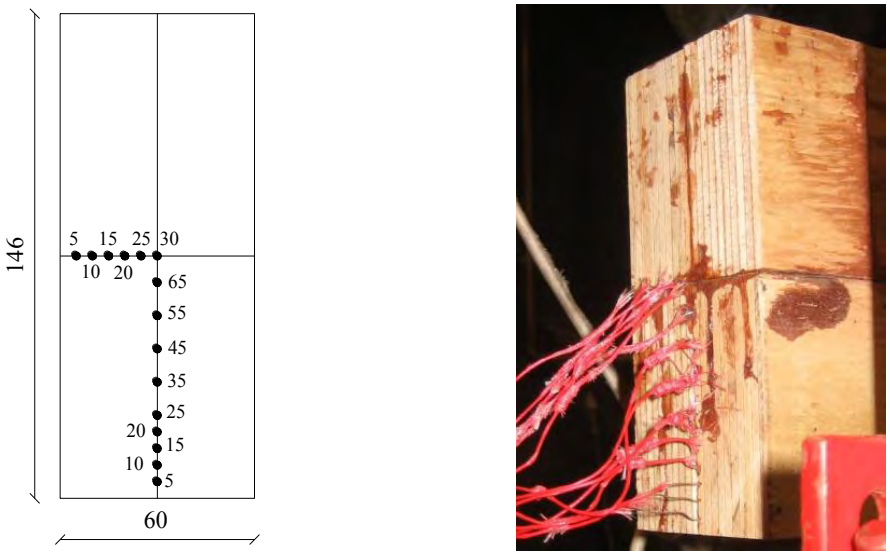

Fig. 2.4 - *Thermocouple layout with dimensions in mm (left) and instrumented specimen cross-section (right).*

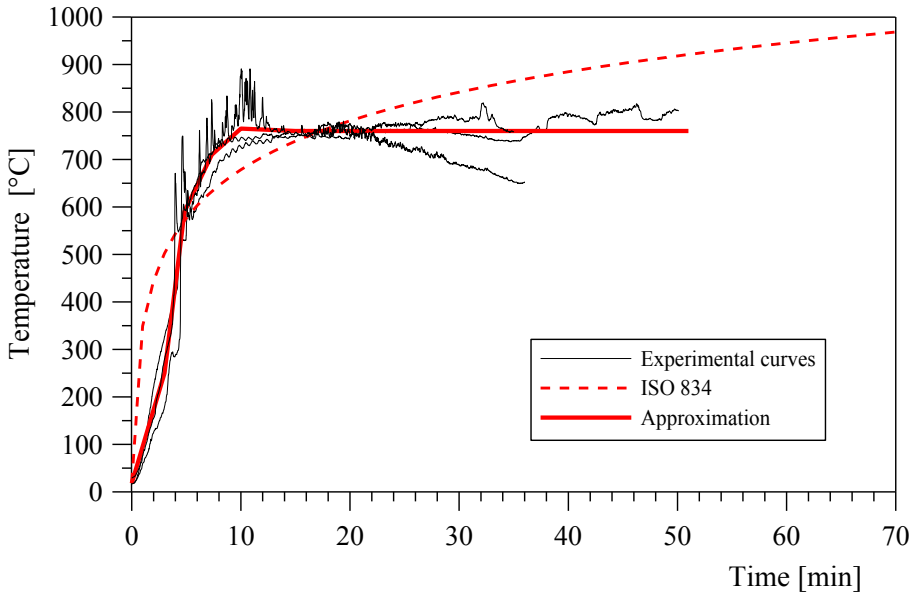

Fig. 2.5 - *Temperature in the custom-made furnace during the fire tests.*

A further K-type thermocouple was placed in the furnace to monitor the inner temperature during the fire test. Figure 2.5 plots the temperature recorded in the furnace during the three tests. The experimental curves did not reach the higher values of the standard ISO 834 fire curve [1999] in order not to damage the furnace. The furnace was turned off 30 min after ignition, when specimens 2 and 3 were immediately removed and cooled down with water. Specimen 1, however, was left in the furnace until complete disintegration occurred. The temperature within specimen 1, 2 and 3 before the fire exposure was 18, 20 and 16.5°C, respectively.

Table 2.1 reports the times recorded during the three tests relating to the charring, the ignition, the furnace switching off and the test duration. The charring and ignition times were noted when the emission of smoke from the furnace and the flames inside the furnace were observed, respectively (Fig. 2.6).

Each plot of Figure 2.7 displays the temperatures in the furnace and at different depths along the longer dimension (left-hand graphs) and shorter dimension (right-hand graphs) for tested specimens. All curves of temperature within the cross-section exhibit a plateau, more marked in the interior fibres, around the value of 100°C, when the evaporation of the bound water occurs.

(a) (b)

Fig. 2.6 *- Start of charring (a) and ignition (b) of a specimen tested in the custom-made furnace.*

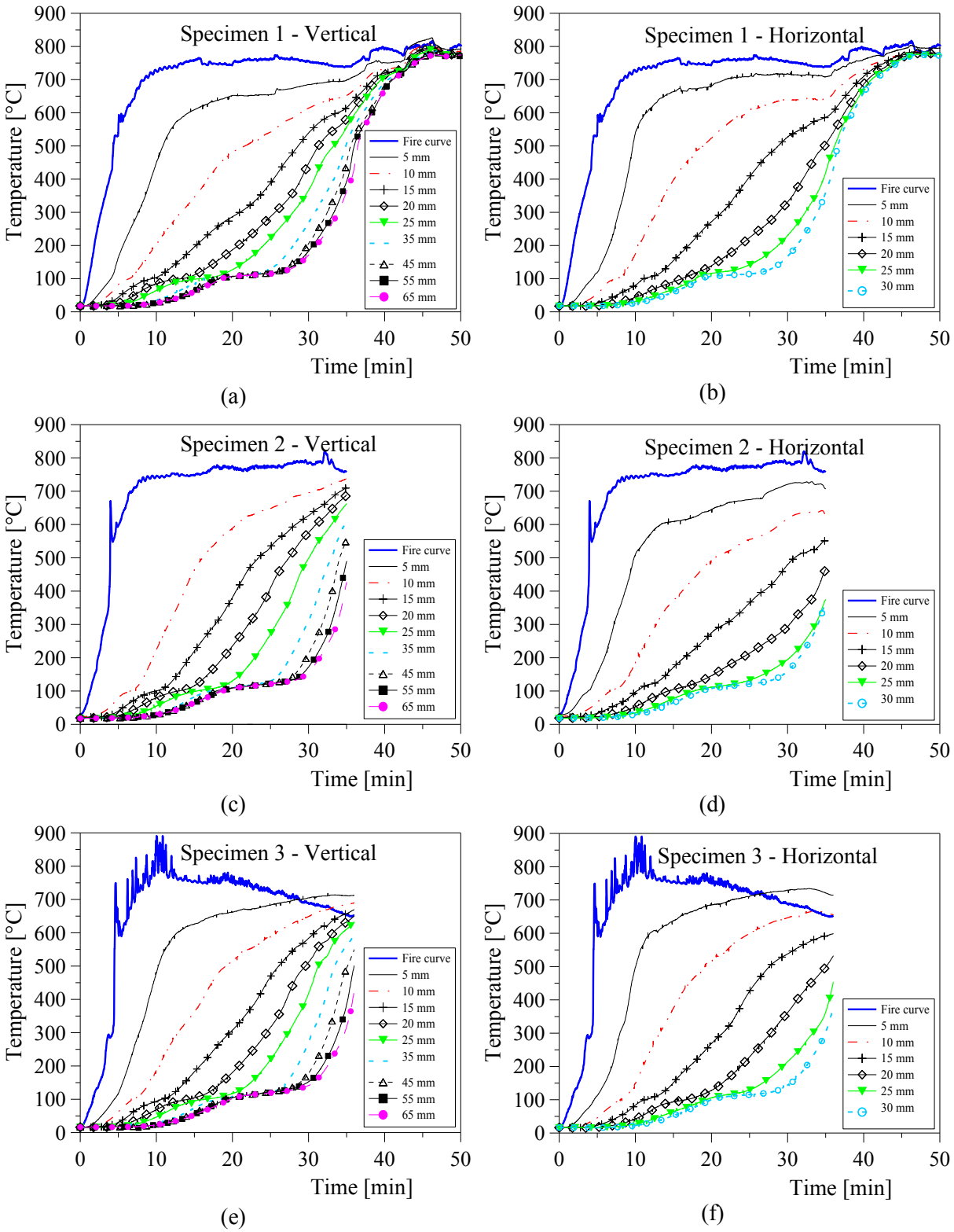

Fig. 2.7 - *Temperature distribution within the samples. Specimen 1: (a) vertical and (b) horizontal direction. Specimen 2: (c) vertical and (d) horizontal direction. Specimen 3: (e) vertical and (f) horizontal direction.*

Test	Charring time	Ignition time	Switching off furnace	Test duration
1	3’ 19”	4’ 40”	35’ 00”	50’
2	2’ 54”	3’ 45”	31’ 32”	35’
3	3’ 02”	4’ 18”	33’ 00”	36’

Table 2.1 - *Main times recorded during the tests.*

2.2.2. *LVL beams tested in pilot furnace*

Further fire tests were performed in the pilot furnace at Building Research Association of New Zealand (BRANZ) Fire Research facility in Wellington. Three radiata pine LVL beams spanning 2.20 m were exposed to the standard ISO 834 fire [1999] (Fig. 2.8). The unloaded beams were protected on the upper side by two gypsum plasterboard panels rated 60 min fire resistance [Winstone Wallboards]. Figure 2.9 shows a LVL beam positioned in the specimen holder of the pilot furnace. Specimens 1 and 2 had a 300×105 mm cross-section, whilst specimen 3 had a slightly larger cross-section of 360×133 mm. Every specimen had two cross-sections instrumented with 12 K-type thermocouples at depth of 18 mm and 36 mm from the exposed surfaces (Fig. 2.10). The thermocouples were exposed to fire on one side except those at the corners that had a double fire exposure. The beams were cut in order to install the thermocouples and then assembled using heat resistant resorcinol glue. The average measured moisture content and density were 12% and 605 kg/m^3, respectively, which were used in the numerical modelling. Pilot tests went on at least until all thermocouples reached the temperature of 300°C. A photo of residual cross-section of specimen 3 at the end of the 60-minute fire test is shown in Figure 2.11. More details about the preparation of the specimens, the experimental set-up and the outcomes of the fire tests are discussed in Lane’s report [Lane 2005]. This report presents also results of cone calorimeter tests performed for the purpose of determining ignition properties and charring rates, and load-bearing fire resistance tests. Finally some design recommendations for a simple method to predict the fire performance of radiata pine LVL exposed to fire are provided.

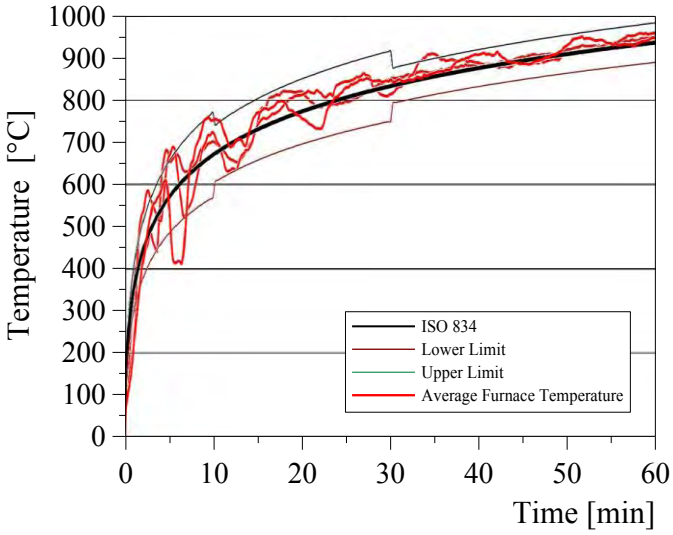

Fig. 2.8 - *Temperature in the pilot furnace during the fire tests [Lane 2005].*

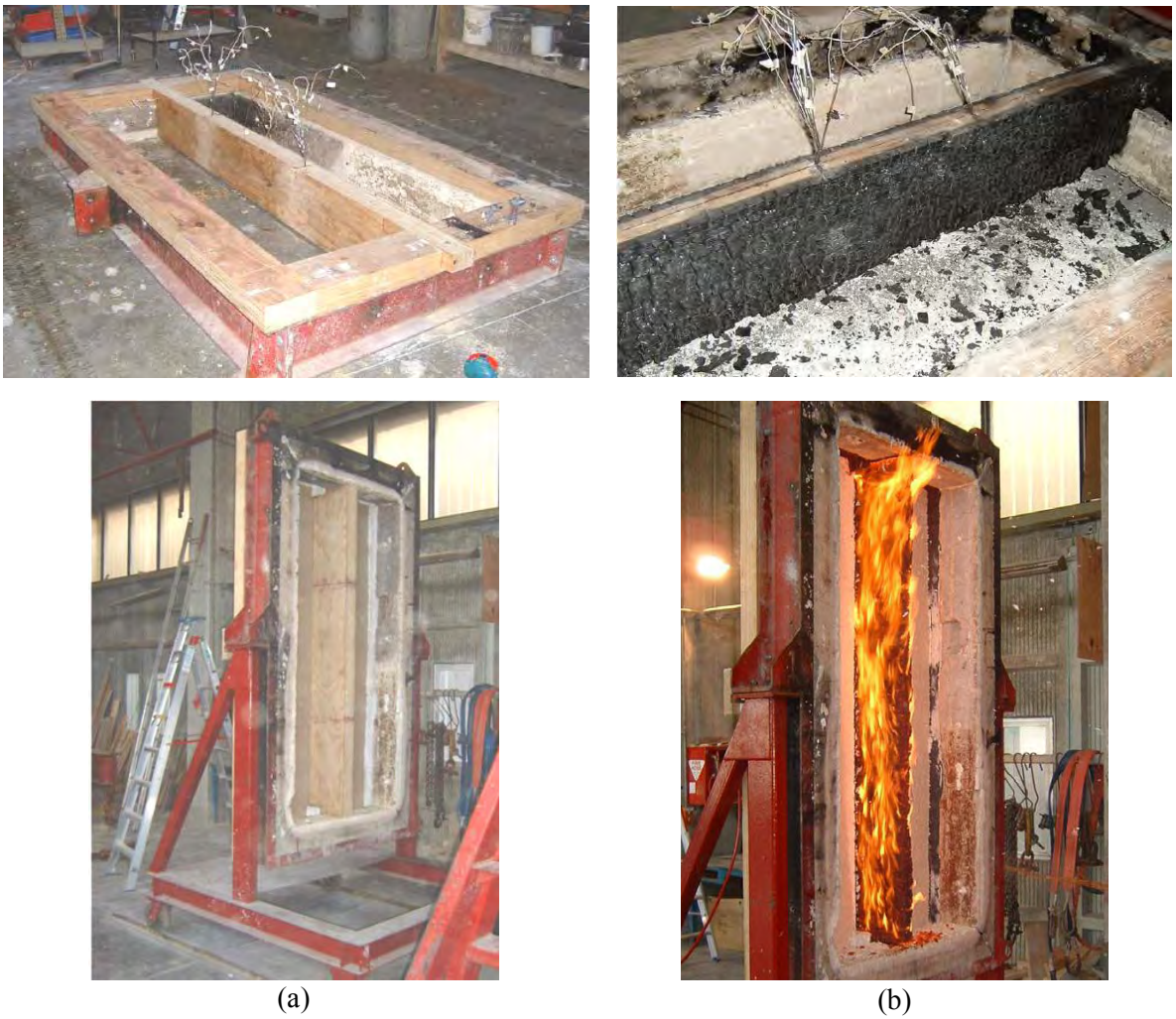

(a) (b)

Fig. 2.9 - *Pilot furnace specimen holder with a LVL beam installed in position before the test (a) and after the fire exposure (b) [Lane 2005].*

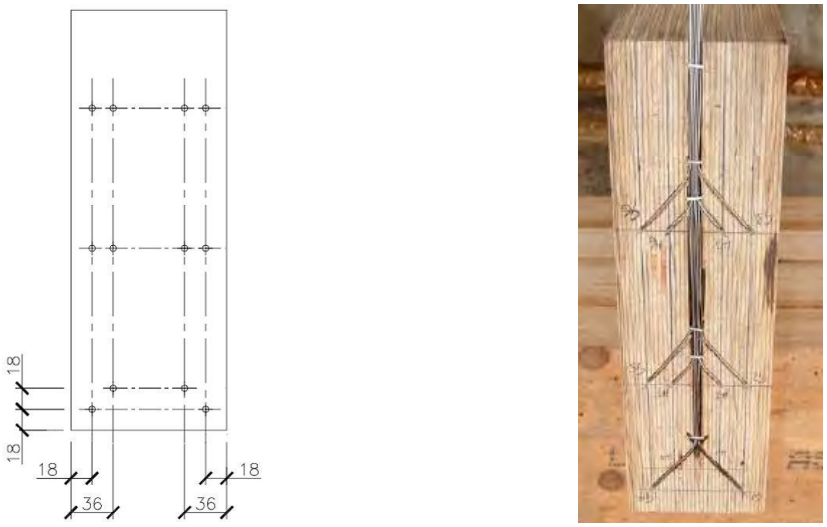

Fig. 2.10 - *Thermocouple layout with dimensions in mm (left) and instrumented beam cross-section (right) [Lane 2005].*

Fig. 2.11 - *Two slices of the residual section of the specimen 3 tested in the pilot furnace [Lane 2005].*

2.3. NUMERICAL ANALYSES

Numerical analyses were carried out using a two-dimensional (2D) model implemented in the general purpose finite element code Abaqus [ABAQUS v.6.6], rather than in a specific software for fire resistance of structural members such as Safir [Franssen 2005]. The temperature distribution in the LVL cross-section during a fire was computed by performing uncoupled heat transfer analyses using four-node quadrilateral, linear elements type 'DC2D4', which are available in the library of Abaqus for thermal analyses. Due to symmetry, only one-fourth and one half of the cross-section was modelled for the specimens tested in the custom-made and in the pilot furnace, respectively (Fig. 2.12). The gypsum plasterboard on the upper side of LVL beams was modelled in Abaqus.

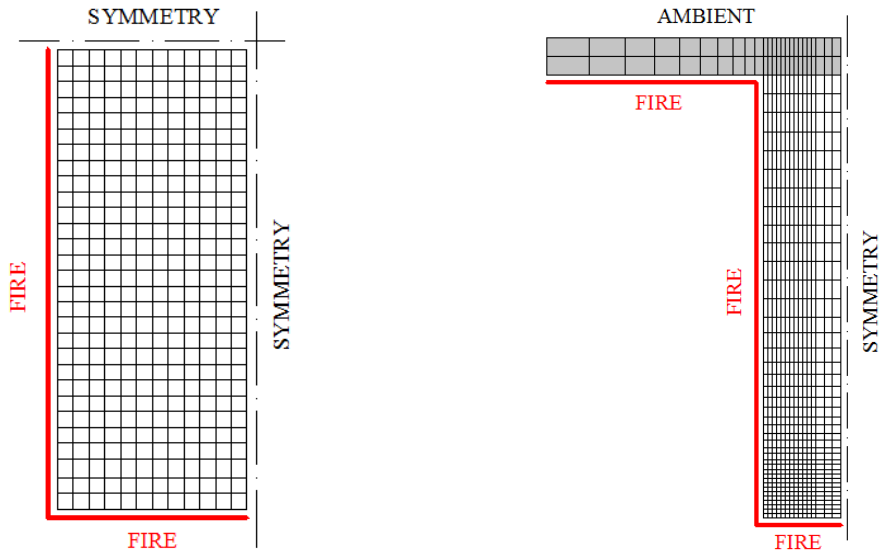

Fig. 2.12 - *Two-dimensional numerical modelling of cross-sections. (a) LVL specimens tested in the custom-made furnace, (b) LVL beams tested in the pilot furnace.*

Exposure to fire was modelled by using the temperature recorded in the furnace as an input, and by imposing the boundary conditions of radiation and convection along the perimeter of the cross-section exposed to the fire through the Abaqus function 'Interactions'. The emissivity ε and convection coefficient h were assumed equal to 0.8 and 25 W/m^{2}K, respectively, as suggested by Eurocode 5 [CEN 2004] and Eurocode 1

[CEN 2002b]. In the uncoupled heat transfer analyses, the material is described through the thermo-physical properties of density, specific heat and thermal conductivity which govern the heat conduction process. Abaqus allows the user to implement a variation of such quantities with the temperature as a piecewise linear without any limitation on the number of points used to describe those relationships. This opportunity offered by Abaqus is very important as the thermo-physical properties of wood are characterized by a high variation with temperature. The assumption of isotropic behaviour of LVL was made in the numerical modelling of the conduction process, where no difference was considered between the radial and tangential directions. The meshes used are displayed in Figure 2.12, chosen so as to ensure accuracy of the results, and coincidence of the nodes with the location of the thermocouples. The 2D models of the cross-sections tested in the custom-made and pilot furnace were subdivided in 348 and 650 elements, respectively. An uniform mesh with elements of 2.5×2.5 mm size were utilized for the analyses on one-fourth of the cross-sections exposed to fire in the custom-made furnace. The modelled beam section was divided into elements of different sizes using a dense mesh in the parts more exposed to fire, in particular close to the edges where the heat fluxes coming from two sides are superimposed. This choice was made to avoid problems of numerical convergence caused by a coarse mesh.

2.3.1. *Thermal properties*

The uncertainty in the dependency of the thermo-physical properties of wood with temperature suggested the opportunity to carry out more numerical analyses, assuming the relationships proposed by different authors (Fig. 2.13). Numerical results obtained according to the Moss et al. proposal [Moss et al. 2009a] highlighted a significant difference in the evaluation of the evaporation process in terms of specific heat with respect to Eurocode 5 [CEN 2004]. The Moss et al. conductive model, in fact, was based on the results of tests where wood specimens were heated at temperatures of up to 250°C and neither ignition nor charring occurred, whilst the Eurocode 5 model was based on results of fire tests. Acceptable predictions of the temperature distributions within specimens exposed to fire were obtained using the relationships proposed by the Eurocode 5 [CEN 2004] and by Frangi [2001]. Cachim and Franssen [2009a; 2010] proposed a modified conductive model to account for the influence of different values of

moisture content on the behaviour of wood exposed to fire using a specific heat capacity curve directly dependent upon moisture. Experimental outcomes, in fact, pointed out the significant influence of moisture content and timber density on charring rate and, therefore, on the temperature distribution within wood sections. Since the moisture content was about 12% in all specimens tested, analyses carried out using the proposed modified conductive model led to insignificant differences compared to analyses carried out using the Eurocode 5 relationships. The value of density at ambient temperature equal to 570 kg/m^3, as suggested by the producer [Nelson Pine Industries Ltd. 2008], was adopted in the thermal analyses.

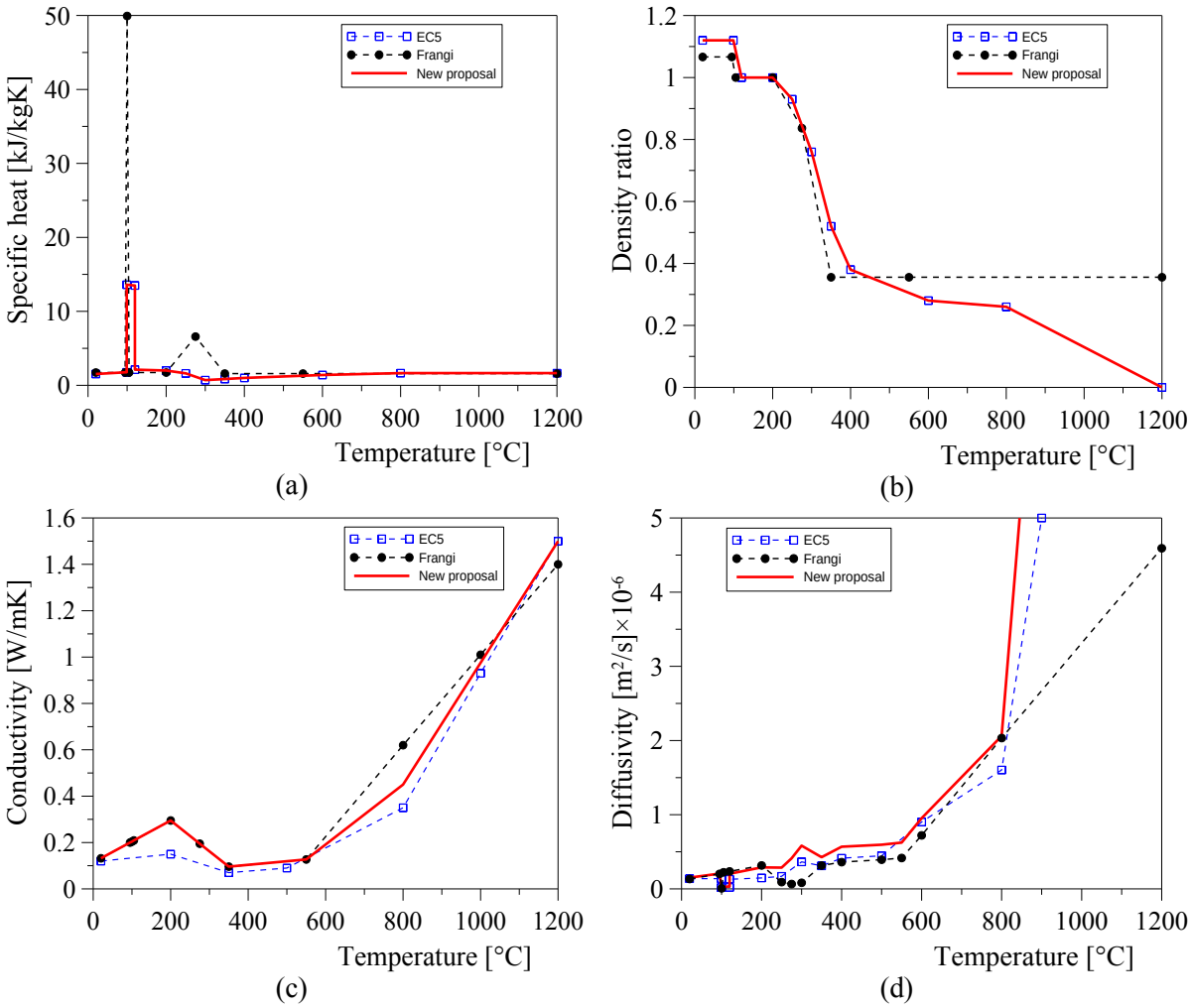

Fig. 2.13 - *Different relationships adopted for the thermo-physical properties of softwood: (a) specific heat, (b) density ratio, assuming an initial moisture content of 12% for Eurocode 5 (EC5) and New Proposal, and 14% for Frangi's proposal, (c) conductivity, (d) diffusivity.*

Also Frangi and Fontana [2003] did not notice any significant effect of moisture content on temperature within wood sections if the moisture content of the material is within the range 8% to 15%.

By comparing the Eurocode 5 and Frangi's proposals, it can be noted that they are conceptually similar for the specific heat, except for single values (Fig. 2.13a). Both proposals assume a peak of the specific heat at the evaporation temperature of water, although the quantity of heat released is different. A further heat release is considered around the charring temperature (300°C) by Frangi's proposal. The reduction in density with temperature is almost the same until 300°C (Fig. 2.13b), although Eurocode 5 considers a more marked drop due to the evaporation process of moisture inside the wood. Conversely, the properties of the charring layer (for temperatures higher than 300°C) are modelled quite differently, with the Frangi's proposal based on a density ratio constant with temperature rather than dropping to zero for high temperature as suggested by the Eurocode 5 (Fig. 2.13b), and the conductivity higher than in the Eurocode 5 (Fig. 2.13c). The diffusivity, which is the conductivity divided by the product of the density and the specific heat [Buchanan 2002], is plotted in Figure 2.13d for all proposals. Since the curves are fairly close to each other, it is not surprising that both proposals led to overall similar numerical results, as will be shown in the following paragraphs.

Since both proposals predicted a slower rise in temperature in the interior fibres than measured in the pilot furnace (as shown by numerical results presented later), a new proposal was made to improve the accuracy of the numerical modelling. This new proposal is based on the density ratio and specific heat variations suggested by Eurocode 5. The conductivity values proposed by Frangi were assumed up to 550°C, and the Eurocode 5 values were considered for higher temperatures. Since there was still a delay in the numerical prediction of temperatures with respect to the experimental values, the conductivity was slightly increased (Fig. 2.13c) in the range 550°C to 1200°C, so as to account for an increased thermal exchange in the charring layer due to convection and radiation through the cracks. The new proposal is summarized in Table 2.2.

TEMPERATURE	SPECIFIC HEAT	DENSITY RATIO	CONDUCTIVITY		
	EC5 and New Proposal	EC5 and New Proposal	New Proposal	Frangi	EC5
°C	kJ $kg^{-1}K^{-1}$	-	W $m^{-1}K^{-1}$		
20	1.53	1+ω	0.132	0.132	0.120
99	1.77	1+ω	0.203	0.203	0.133
99	13.60	1+ω	0.203	0.203	0.133
120	13.50	1.00	0.223	0.223	0.137
120	2.12	1.00	0.223	0.223	0.137
200	2.00	1.00	0.295	0.295	0.150
250	1.62	0.93	0.228	0.228	0.123
300	0.71	0.76	0.162	0.162	0.097
350	0.85	0.52	0.096	0.096	0.070
400	1.00	0.38	0.104	0.104	0.077
500	1.20	0.33	0.119	0.119	0.090
550	1.30	0.31	0.127	0127	0.133
600	1.40	0.28	0.180	0.225	0.177
800	1.65	0.26	0.450	0.617	0.350
1200	1.65	0.00	1.500	1.400	1.500

Table 2.2 - *Different variations of thermal properties with temperature (ω is the moisture content).*

2.4. EXPERIMENTAL-NUMERICAL COMPARISONS

2.4.1. *LVL elements tested in custom-made furnace*

The average temperature measured during the three fire tests was used as an input in the numerical modelling because there was a noticeable difference between the ISO 834 fire curve [1999] and the actual trends of temperature in the furnace versus time during the fire tests (Fig. 2.5). Figures 2.14 and 2.15 display both experimental and numerical results as temperature versus time plots along the horizontal and vertical directions up to 20 mm depth. Such a value can be regarded as the depth of technical interest in structural fire design for the small cross-section tested in the custom-made furnace as it corresponds to one-third of the total breadth. By the time this depth has charred, the member has lost most of its strength capacity. It is therefore pointless to investigate the temperature distribution for larger depths.

Numerical analyses were carried out by adopting different variations of density, specific heat and conductivity with temperature. Two proposals were initially considered: Eurocode 5 [CEN 2004] and Frangi [2001]. As anticipated in the previous paragraph, both proposals lead to very similar curves. This result can be justified by both proposals having similar trends of the diffusivity with temperature, as clearly appears from Figure 2.13d. Both proposals slightly anticipate the heating up of the specimen along the vertical direction (long dimension) (Fig. 2.14), and show a delay in the heating up process along the horizontal direction (short dimension), particularly for the deeper fibres (Fig. 2.15). The overall approximation, however, is acceptable in both directions given the significant scatter of the experimental curves.

The new proposal leads to slightly better results in the horizontal direction and somewhat worse results in the vertical direction, with a worse approximation for deeper fibres. The reason for the worse approximation is not fully clear at this point. A possible reason, however, could be the hypothesis of thermal isotropy perpendicular to the grain, where the same properties are assumed in radial and tangential directions. This hypothesis is commonly made for solid and glued laminated timber, where the radial and tangential directions change over the cross-section due to the cylindrical symmetry of wood. For LVL, however, the manufacturing production process leads to a cross-section

where the radial and tangential directions are parallel in each point to the horizontal and vertical direction, respectively (Fig. 2.4, right). It may therefore be inferred that in an LVL cross-section the difference between the radial and tangential direction may cause a larger discrepancy with respect to the hypothesis of isotropy than in a solid or glued laminated timber section where the radial and tangential directions rotate in the different points. In other words, LVL may be regarded as an overall more anisotropic material than solid or glued laminated timber. This would be partially confirmed by Rogowski [1967], who found different charring rates considering the direction parallel or perpendicular to laminations for softwood glue-laminated columns exposed to fire.

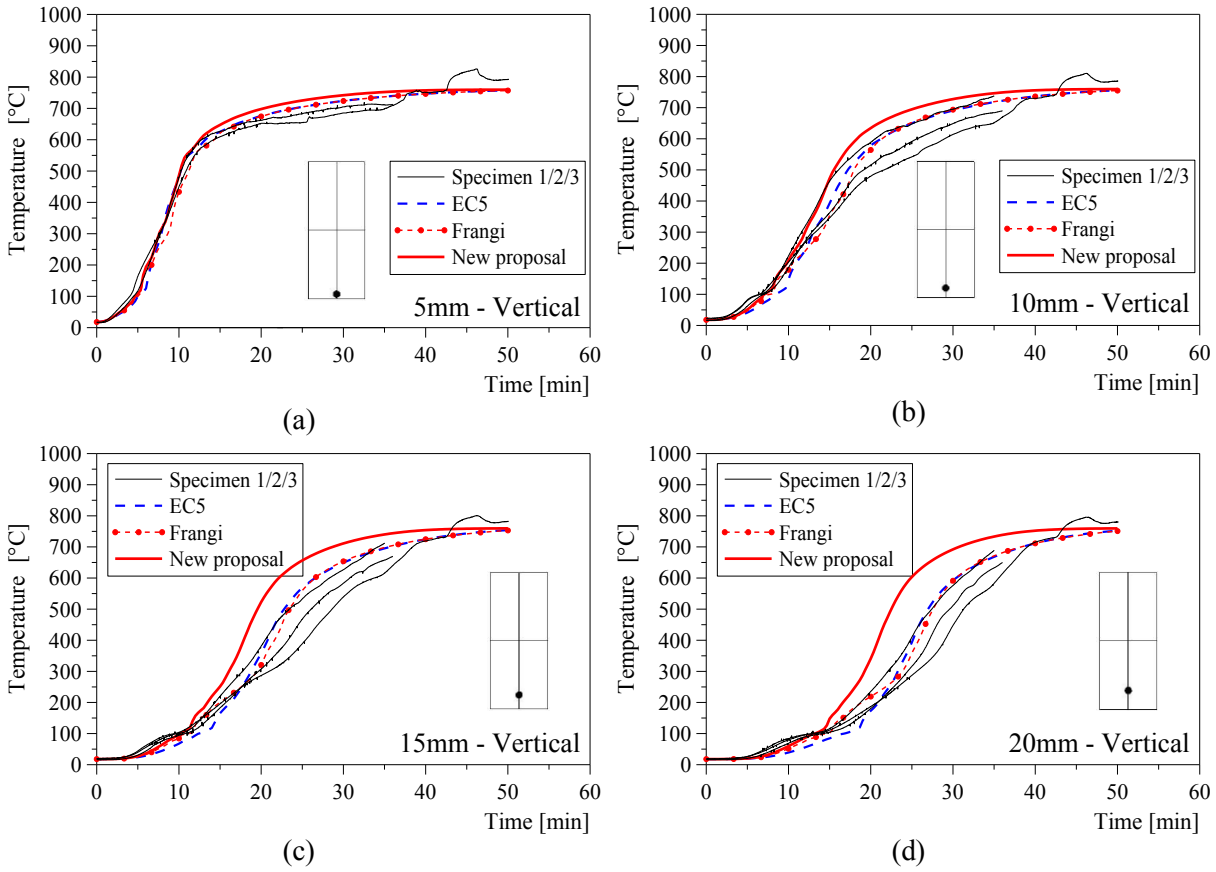

Fig. 2.14 - *Comparison between experimental and numerical results in vertical direction at different depths: (a) 5 mm, (b) 10 mm, (c) 15 mm, (d) 20 mm.*

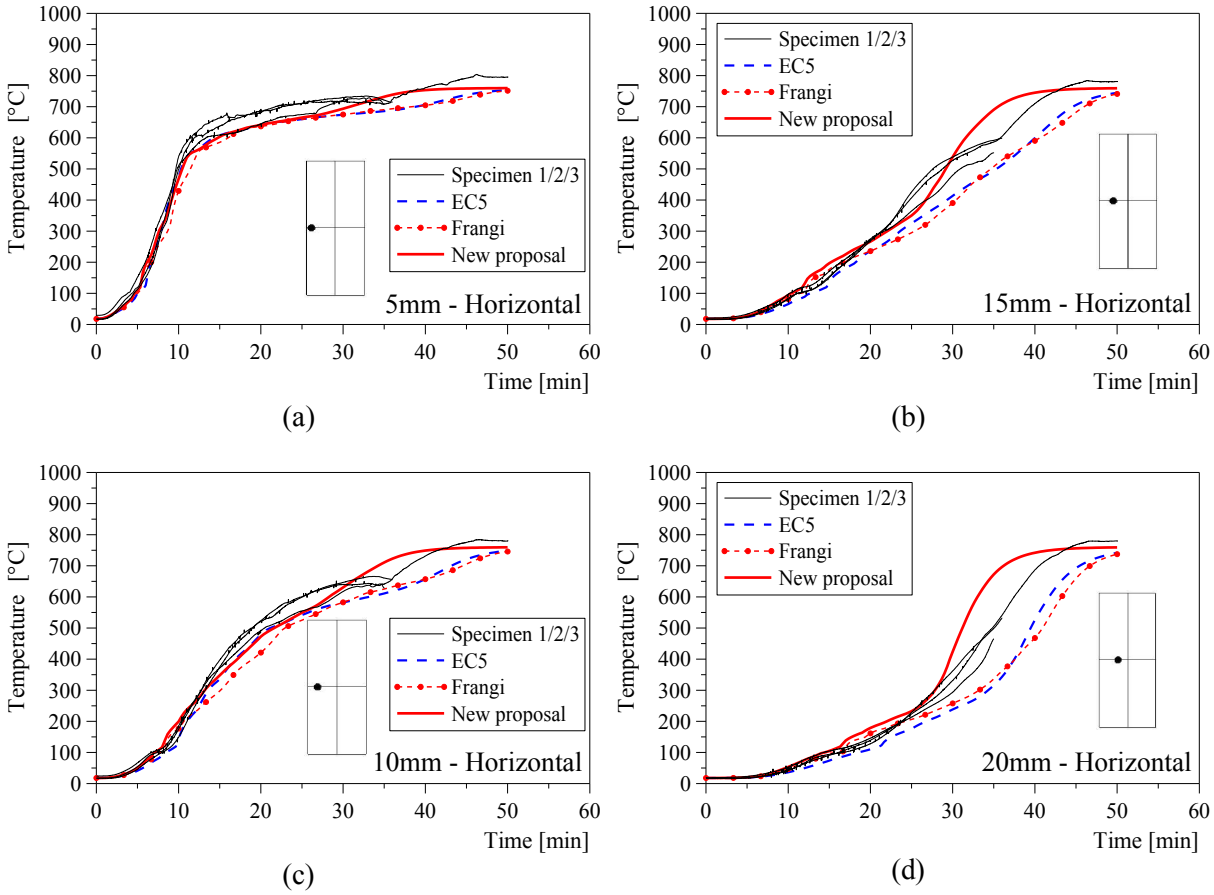

Fig. 2.15 - *Comparison between experimental and numerical results in horizontal direction at different depths: (a) 5 mm, (b) 10 mm, (c) 15 mm, (d) 20 mm.*

The movement of the 300°C isotherm, assumed as the boundary between charred and heated wood, allows the evaluation of the residual cross-section. Figure 2.16 displays a graphic visualization of the charring progress in the modelled section at different times of fire exposure. The grey and red colours represent the charred material and the 300°C isotherm, respectively. The blue contour corresponds to temperature close to the ambient temperature.

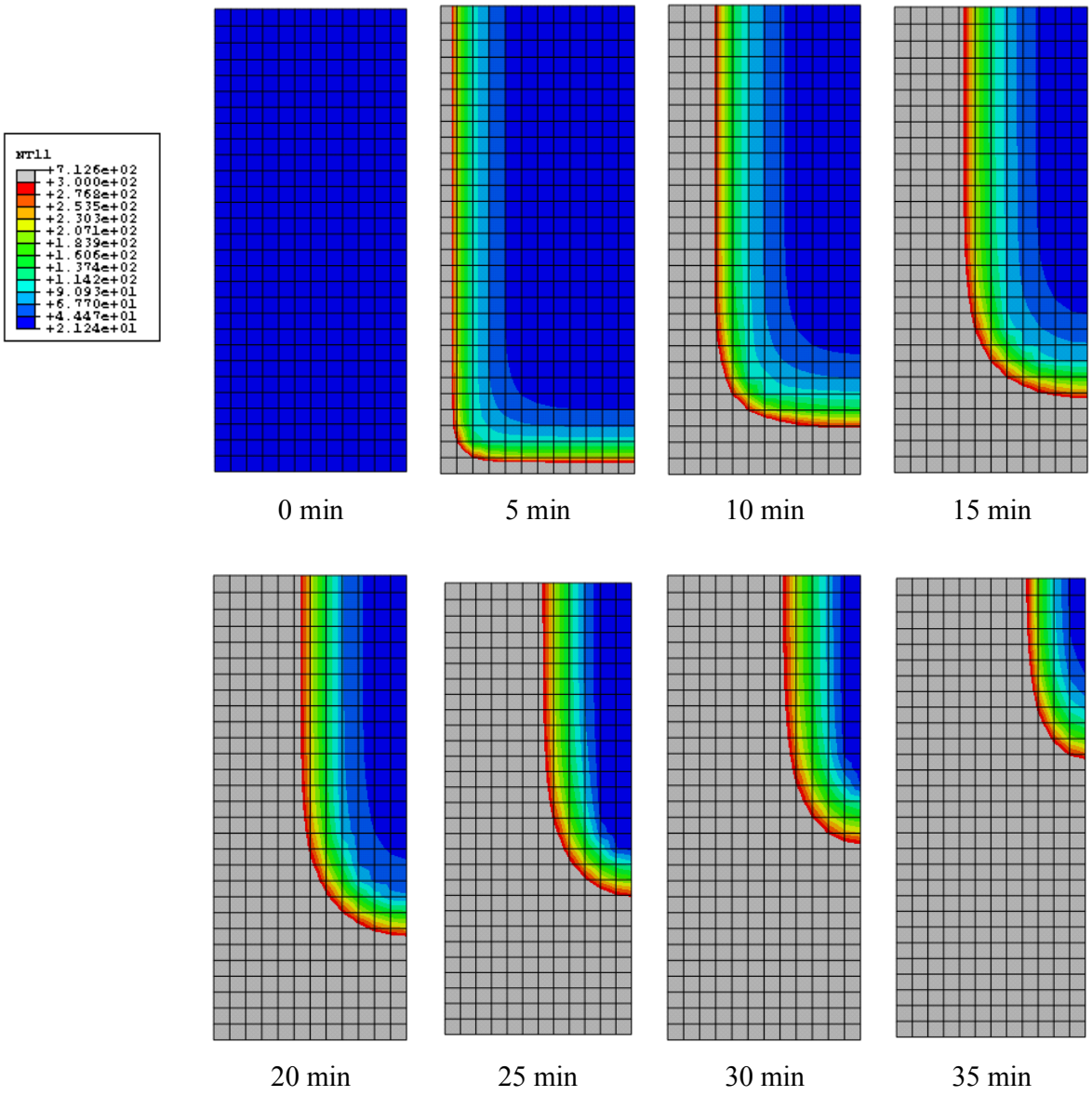

Fig. 2.16 - *Graphic visualization of the residual cross-section at different fire exposure times.*

2.4.2. *LVL beams tested in pilot furnace*

Thermal analyses were carried out to simulate the fire tests on LVL beam specimens performed in the pilot furnace at BRANZ [Lane 2005]. The two different cross-sections, section 'A' (300×105 mm) and 'B' (360×133 mm), were investigated using the 2D Abaqus finite element model. The gypsum plasterboard panel on top of the beam was modelled using the thermo-physical properties suggested by Jones [2001]. The standard fire curve [ISO 834-1 1999] was used as input (Fig. 2.8). Figures 2.17 and 2.18 display the experimental-numerical comparisons for both cross-sections ('A' and 'B'), different depths instrumented with thermocouples (18 and 36 mm) as in Figure 2.10, different exposure conditions, and different proposals for the thermo-physical parameters of LVL. The cross-sections are subjected to two exposure conditions in particular a double face exposure close to the corner of the cross-section (Fig. 2.17) and a single face exposure (Fig. 2.18).

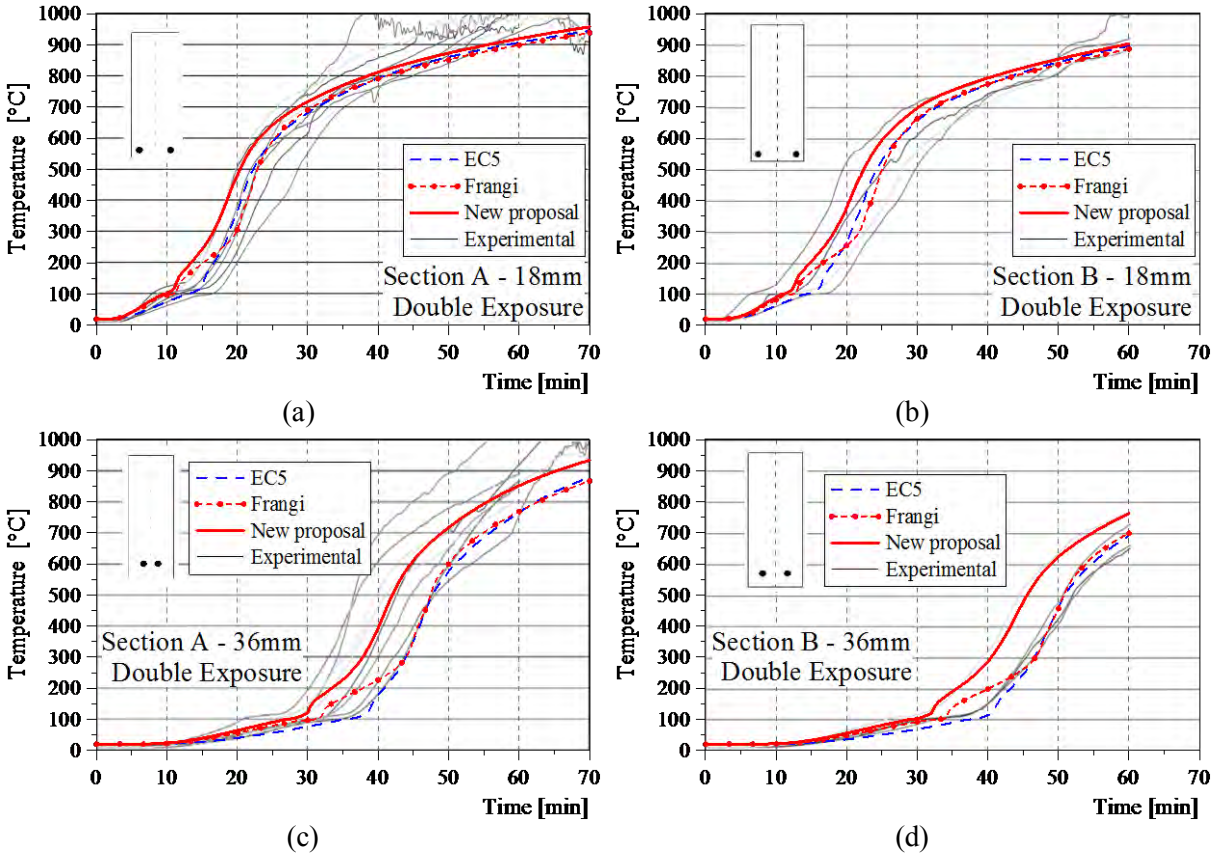

Fig. 2.17 - *Comparison between experimental and numerical results at different depths for sections 'A' (left) and 'B' (right) subjected to a double face exposure.*

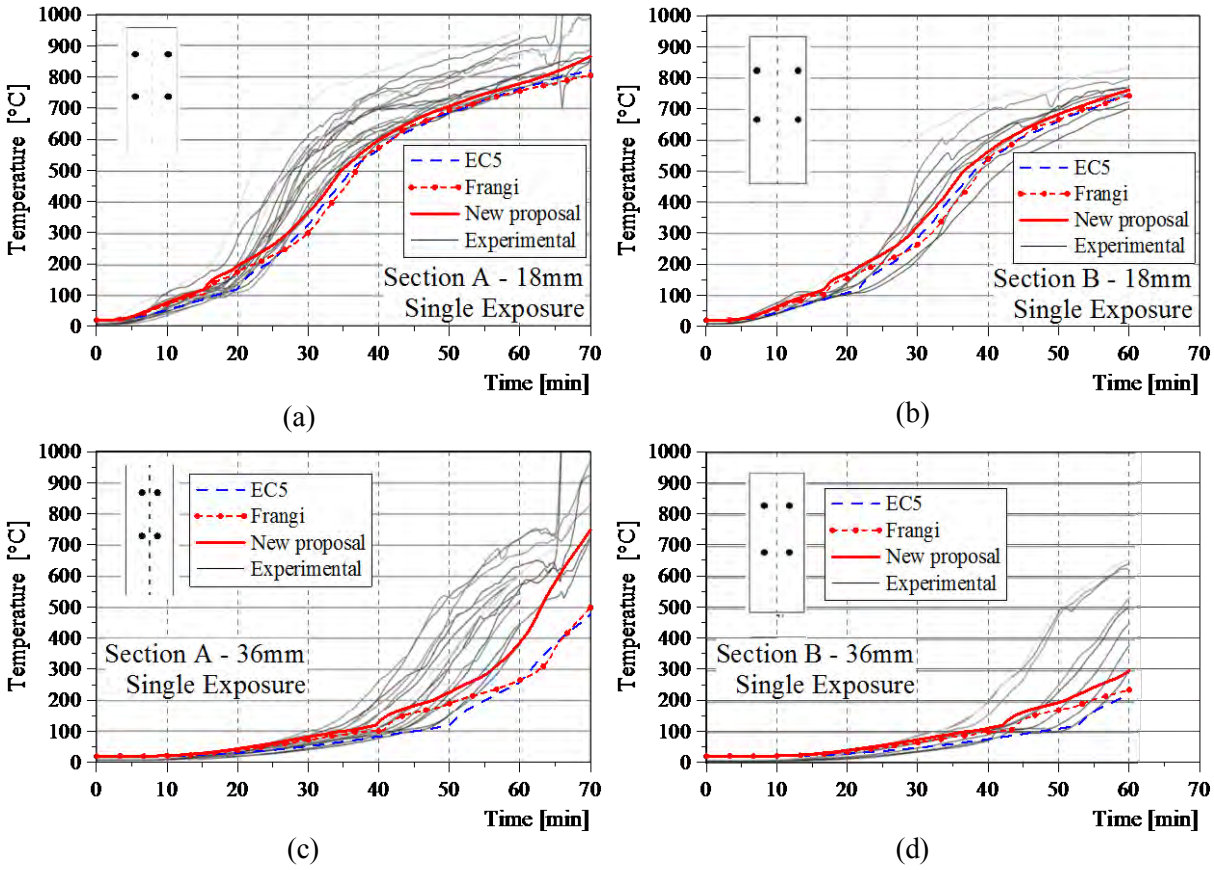

Fig. 2.18 - *Comparison between experimental and numerical results at different depths for sections 'A' (left) and 'B' (right) subjected to a single face exposure.*

Similar to the LVL sections tested in the custom-made furnace, both Frangi's [2001] and Eurocode 5 [CEN 2004] proposals lead to numerical curves close to each other. Both proposals, for both cross-sections, lead to fairly close agreement with the experimental results at the 18 mm depth under double face exposure (Fig. 2.17a,b). The Eurocode 5 curve is, however, preferable as it is characterized by more uniform inclination closer to the experimental curves. At 36 mm depth, the heating process of LVL is predicted with a delay with respect to the experimental tests for both double and single face exposures and cross-sections (Fig. 2.17c,d and Fig. 2.18c,d) particularly for the smallest one. A delay in the heating process can also be recognized for the numerical curves at 18 mm depth in the case of single face exposure (Fig. 2.18a,b), where the numerical curves appear to be less inclined than the experimental ones. It should be highlighted, however, the notable scatter of the experimental values measured by the thermocouples. In some cases (e.g. Fig. 2.17c and 2.18c), the charring temperature equal

to 300°C, as suggested by Eurocode 5, was reached with a 10 min delay between the first and the last thermocouple.

As mentioned in the introduction, an accurate prediction of the temperature distribution is meaningful in order to evaluate the fire resistance of a timber cross-section. In this respect, it is crucial to know the temperature versus time curve at 36 mm depth until charring has occurred and, hence, the temperature of 300°C has been reached. When charring takes place at that depth, the total breadth has reduced down to less than half of the original size, leading to a small residual cross-section with little strength which is very likely to have reached failure conditions. For fibres closer to the surface, however, an accurate prediction of the temperature is critical at any temperature as it markedly affects the conduction process inside the cross-section. With the aim of improving the numerical prediction of the temperatures, some attempts were made to change the thermo-physical parameters of the LVL in order to obtain closer agreement between experimental and numerical results for both cross-sections, types of exposure, and depths from the surface. Since the Eurocode 5 curves had a shape closer to the experimental ones, the variation of density and specific heat with temperature were assumed in accordance with such proposals. The conductivity, however, was varied as described in paragraph 2.3.1 and displayed in Figure 2.13c. The new proposal led to closer agreement with all the experimental curves for sections 'A' and 'B' (Fig. 2.17 and Fig. 2.18).

Figure 2.19 presents a comparison between the experimental and numerical residual cross-section of specimen 3 after a fire exposure of 60 min. The black dashed line indicates the size of the cross-section before the fire test, whilst the red solid line represents the 300°C isotherm and, therefore, the residual cross-section at the end of the fire test using the finite element model with the new proposal. Lane [2005] found a charring rate of 0.72 mm/min for radiata pine LVL. The residual cross-section in the numerical model has the same depth as in the pilot furnace at the end of the test, however it is wider (61 mm instead of 46.6 mm). Hence, the charring rate on lateral faces is smaller than the charring rate on the bottom face. This is a consequence of the delayed increase in temperature predicted numerically even by the new proposal in the inner fibres exposed to fire along the lateral faces. The approximation of the finite element model is instead good for the predictions of the residual cross-section and charring rate in the vertical direction.

The residual cross-section evolution obtained numerically at different fire exposure times is reported in Figure 2.20. The grey and red colours represent the charred material and the 300°C isotherm, respectively. The blue contour corresponds to temperature close to the ambient temperature.

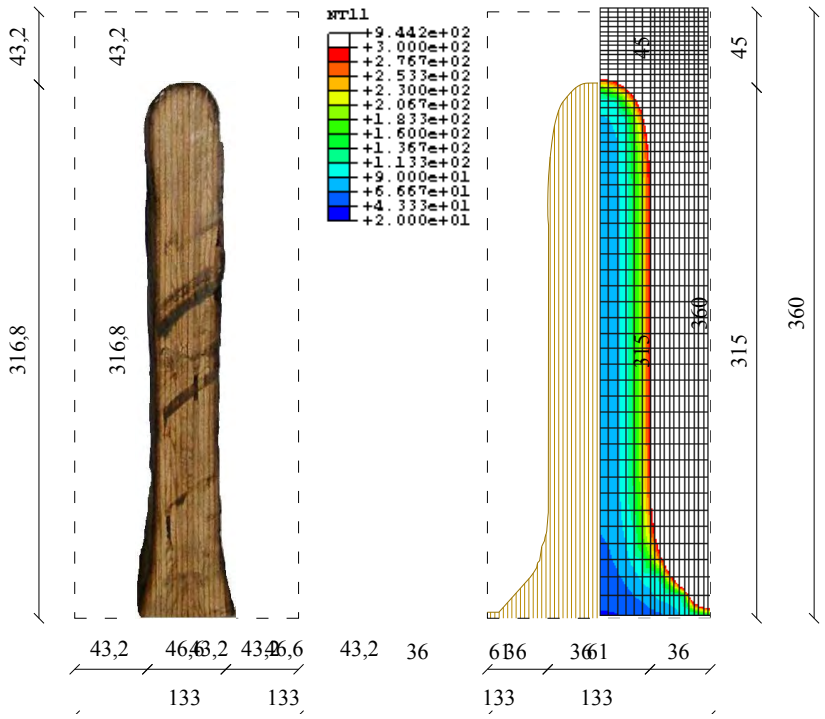

Fig. 2.19 - *Comparison between experimental and numerical residual cross-section of specimen 3 after 60-minute fire exposure (dimensions in mm).*

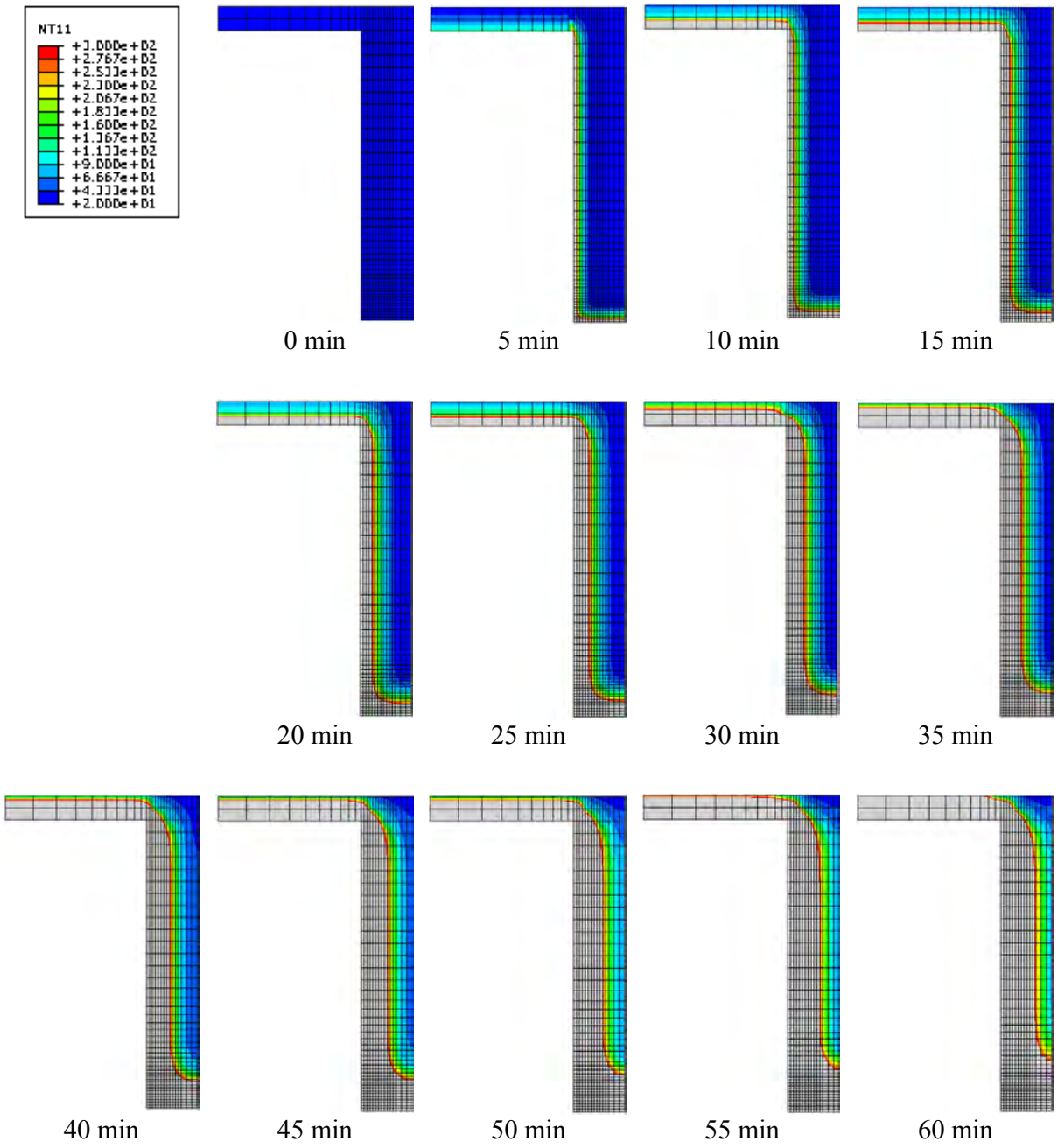

Fig. 2.20 - *Graphic visualization of the residual cross-section at different fire exposure times.*

2.4.3. *Timber elements tested in small furnace*

Four unprotected timber members made from spruce were tested under standard fire [ISO 834-1 1999] in a small furnace at SP Technical Research Institute of Sweden (Trätek). The specimens had 225×95 mm cross-section made from five 45×95 mm laminations and were subjected to one-dimensional (1D) exposure along the larger dimension so as to simulate the case of a 95 mm thick timber slab subjected to fire on the underside. The unloaded specimens were protected on three sides by fire resistant gypsum plasterboards to ensure the 1D heat transfer in the element. Six thermocouples were located at different depths within the cross-section (Fig. 2.21c).

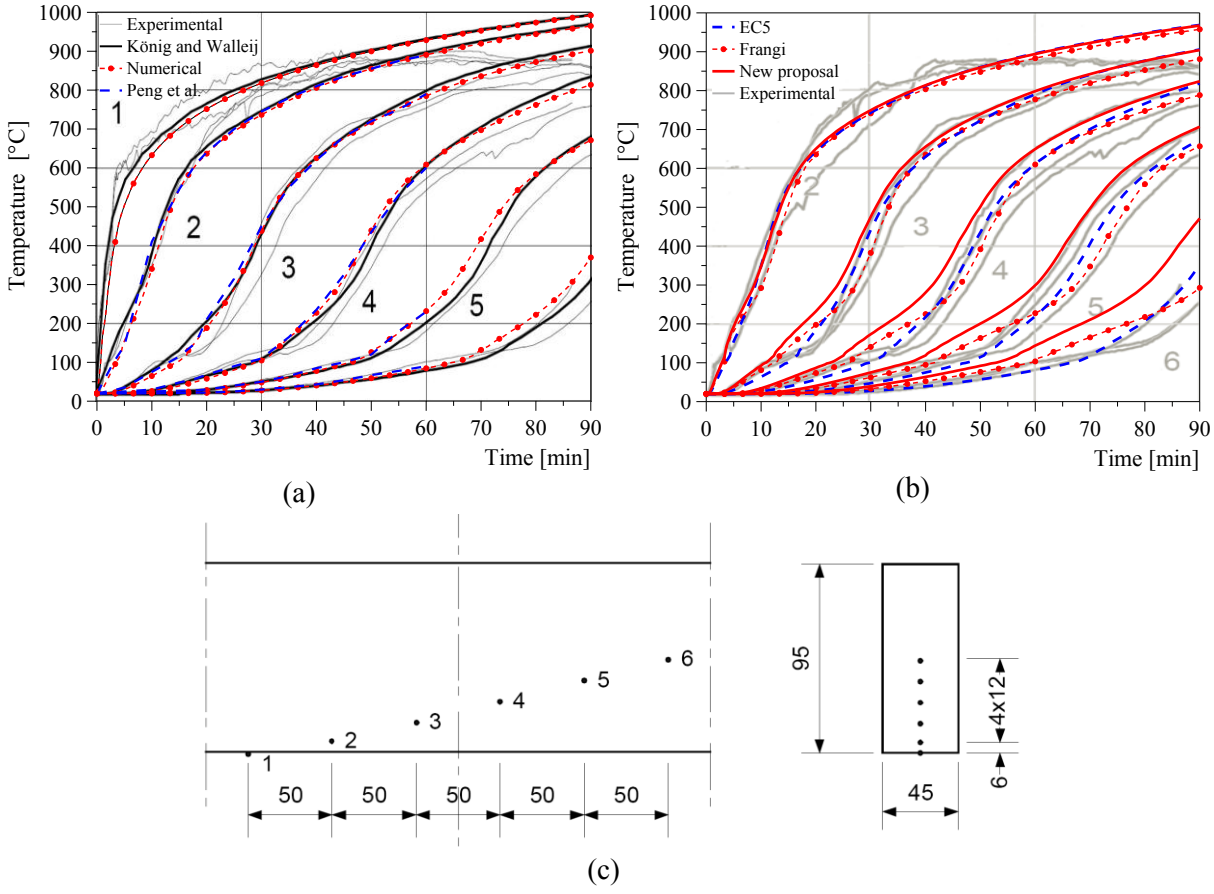

Fig. 2.21 - *Comparison between experimental and numerical temperatures at different depths: (a) numerical results from different authors [König and Walleij 1999; Peng et al. 2008], (b) numerical results obtained with different thermo-physical properties, (c) thermocouple layout on elevation (left) and cross-section (right) of a specimen lamination (dimensions in mm) [König and Walleij, 1999].*

More information on test set-up, specimens, thermocouple location and experimental results can be found in the report by König and Walleij [1999]. The outcomes of the experimental tests and numerical analyses presented in the aforementioned report were used as further validation of the 2D finite element model implemented in Abaqus to simulate the fire tests of LVL elements.

The 1D heat conduction process along the 95 mm depth of the specimens was modelled using a 1.5×1.5 mm mesh, which was found to provide a stable and accurate numerical solution. The comparison with the experimental results, the numerical curves obtained by König and Walleij [1999] using the computer program TempCalc [Fire Safety Design 1990], and the numerical curves obtained by Peng at al. [2008] using Abaqus is displayed in Figure 2.21a for the temperature at different depths. The thermal properties suggested by König and Walleij were used in these analyses. A good correspondence between all the numerical and experimental curves can be noted at all thermocouple locations. Figure 2.21b compares the experimental curves with the numerical outcomes obtained using the presented finite element model with three different proposals for the thermo-physical properties, as discussed in the previous paragraph: the Eurocode 5 [CEN 2004], Frangi's proposal [2001], and the new proposal. The Eurocode 5 leads to an excellent approximation, with the numerical curves in close proximity to the experimental ones. The new proposal anticipates the heating process, particularly for the deeper fibres, however the approximation is still acceptable. The Frangi's proposal is slightly worse than the Eurocode 5 but better than the new proposal.

CHAPTER 3.

THERMAL AND MECHANICAL STUDY

3.1. INTRODUCTION

Timber is a structural material with good mechanical properties parallel to the grain. However, it is combustible, and the fire exposure involves very complex behaviour because physical, thermal and mechanical degradation phenomena occur together. Different proposals can be found in literature for the variation of thermal and mechanical properties of wood with temperature [e.g. Buchanan 2002; Cachim and Franssen 2009a; CEN 2004; Frangi 2001; Hopkin et al. 2011; Jong and Clancy 2004; König 2006; König and Walleij 1999]. Several variables affect the change of material properties such as wood species, moisture content, fire conditions, stress direction with respect to the grain and level of applied load.

Simplified design methods suggested by current codes of practice such as Eurocode 5, Part 1-2 [CEN 2004] and New Zealand Standard [SNZ 1993] assume the strength capacity under fire to be dependent upon the residual cross-section, which is evaluated by computing the thickness of the charred layer during time of exposure to fire. When wood is converted to char, it loses its strength and stiffness, whereas the cooler part of the initial cross-section maintains its load-bearing capacity. In order to compute the structural fire resistance of timber members, the degradation of mechanical properties with temperature has to be considered. To this purpose, the temperature distribution within the wood member is required so that the residual cross-section can be estimated on the basis of the time of exposure to the fire. The temperature profiles can be determined using analytical and numerical models calibrated on experimental results [e.g. Erchinger et al. 2006; Frangi and Fontana 2003; Janssens 2004; Laplanche et al. 2006; Peng et al. 2008; Winter and Meyn 2009]. An accurate temperature prediction

improves the fire resistance estimation of wood structural elements and their connections [e.g. Frangi et al. 2010a; Moss et al. 2009c; Schmid et al. 2010a].

The chapter investigates the thermal–structural behaviour of loaded timber members exposed to fire. The timber members are made from laminated veneer lumber (LVL) manufactured from radiata pine grown in New Zealand. Small LVL members (150×63 mm) were tested at the University of Canterbury (New Zealand) under two-dimensional fire exposure and three different tensile load levels [Menis 2008].

The experimental results were compared with numerical predictions obtained by implementing a three-dimensional model in the Abaqus finite element code [ABAQUS v.6.6]. Thermal and mechanical properties suggested by Eurocode 5 including variations with temperature were assumed in the numerical modelling. The fire resistance of small LVL elements was predicted for different levels of the applied tensile forces, using the numerical model and the simplified analytical approaches.

3.2. EXPERIMENTAL TESTS

Five fire tests on radiata pine LVL specimens were carried out in the Fire Engineering Laboratory of the University of Canterbury, Christchurch, New Zealand [Menis 2008]. The purpose was to investigate the behaviour of timber elements loaded in tension and exposed to fire on four sides.

The tests were performed in the same custom-made electrical furnace described in Chapter 2. Because the small sizes of the furnace, the specimens had a cross-section of 150×63 mm and a length of 900 mm. Only the portion of the sample inside the furnace was exposed to heat flux (hatched part in Fig. 3.1a), while the member ends were outside the furnace. The testing frame of the furnace allows an axial load to be applied on the specimens using a manual pump. Figure 3.1b shows a specimen inside the custom made furnace before testing. The hydraulic jack is on the right of the testing frame, and the load cell is on the left. Steel supports fastened to both sample ends using four 16-mm diameters bolts (8.8 steel grade) allowed load to be transferred from the testing frame to the specimen (Fig. 3.2 and Fig. 3.3). Each specimen was monotonically loaded until the required tension load was reached. Three different levels of load were chosen: 75 kN on two specimens, 54 kN on one specimen and 40 kN on two specimens, corresponding to 22%, 16% and 12% of the estimated mean failure load at ambient temperature. The tensile axial force was kept constant by pumping more oil into the loading jack throughout the test, as shown by the experimental data plotted in Figure 3.4a.

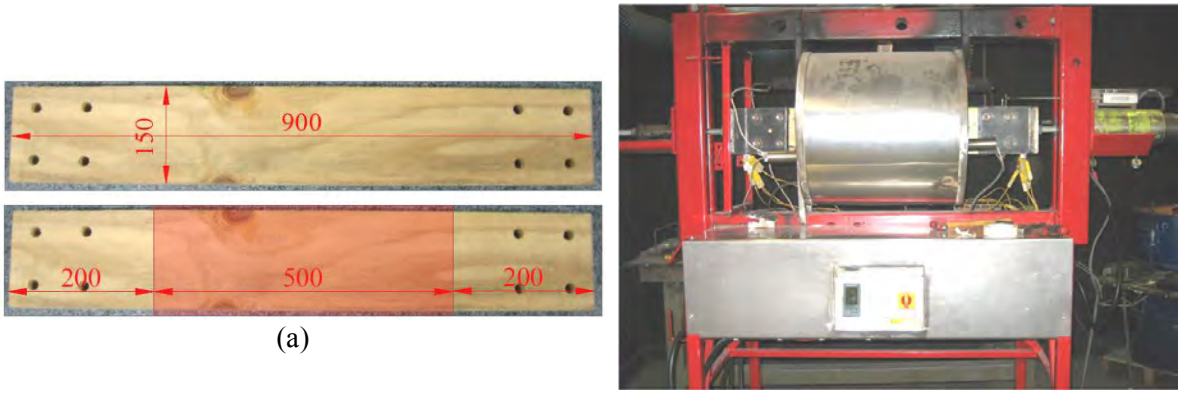

(a) (b)

Fig. 3.1 *- (a) Photos of the specimens with dimensions in mm. (b) Specimen in the custom-made furnace before testing.*

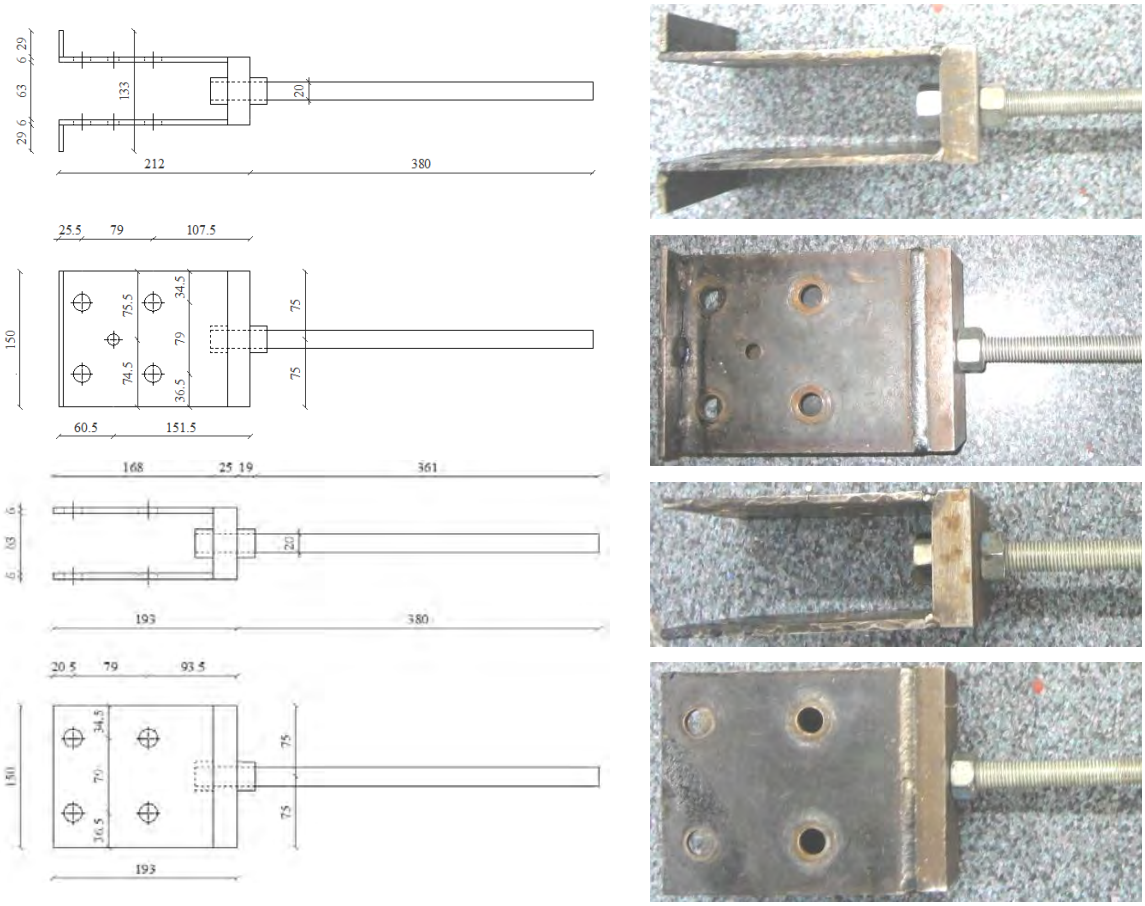

Fig. 3.2 - *Drawings and photos of the two steel supports.*

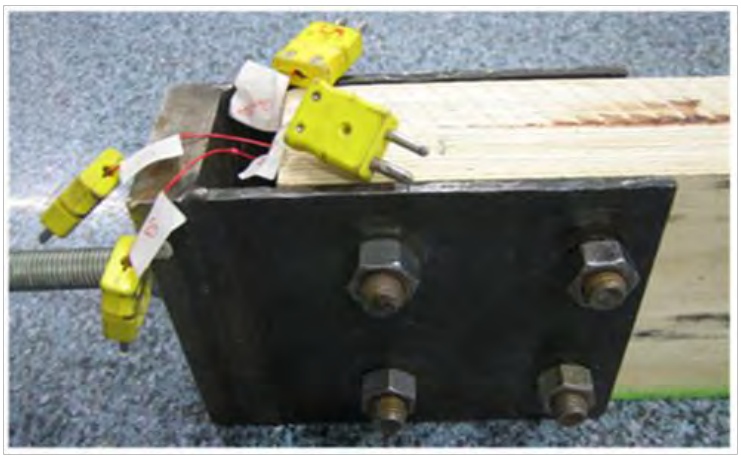

Fig. 3.3 - *Specimen end fastened with bolts.*

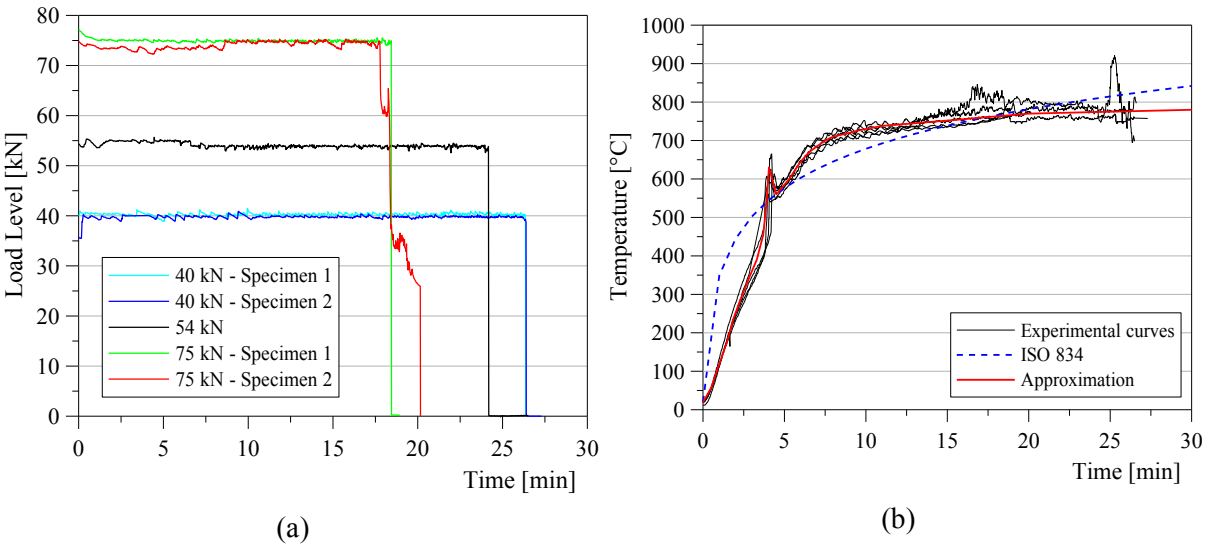

Fig. 3.4 - *(a) Applied loads on LVL specimens vs. time. (b) Temperature in the custom-made furnace during fire tests and approximation adopted in numerical modelling.*

Figure 3.4b displays the temperature in the furnace recorded by a thermocouple during the fire tests. The furnace was switched on after the specimens were loaded with the required tension load. The experimental fire curves did not follow the standard ISO 834 fire [ISO 834-1 1999] because the electrical furnace was not able to reach high temperatures rapidly. A piecewise linear approximation of the recorded fire curves (red curve) was adopted in the numerical modelling described in the following paragraph.

One specimen loaded with 75 kN was instrumented with four K-type thermocouples at a depth of 10, 20, 65 and 75 mm from the surface along the long dimension of the cross-section (Fig. 3.5a). The recorded temperature distribution in the cross-section was compared with experimental data of the fire tests previously performed in the same furnace on unloaded LVL specimens, already presented in Chapter 2. In those fire tests, the small specimens were instrumented with fifteen thermocouples since the aim was investigated accurately the temperature distribution in the cross-section.

As the fire was ignited, the perimeter of the specimen began charring, leading to a reduction in residual cross-section, a reduction in axial stiffness and an increase in elongation. The elongation of the specimens was measured with a potentiometer on one side of the testing frame. The displacements show an approximately linear increase until failure occurred as reported in Figure 3.5b for specimens subjected to a constant tension load of 40 and 75 kN.

After the specimen had failed, the furnace was switched off and the burnt element was quickly removed and cooled down with water. The failure time was the time at which the applied load was not able to be sustained by the specimen exposed to fire on four sides. Brittle failure of specimens occurred due to the high stresses in the small residual cross-section (Fig. 3.6). One LVL member loaded with 75 kN failed unexpectedly close to the connection with the steel support (Fig. 3.7).

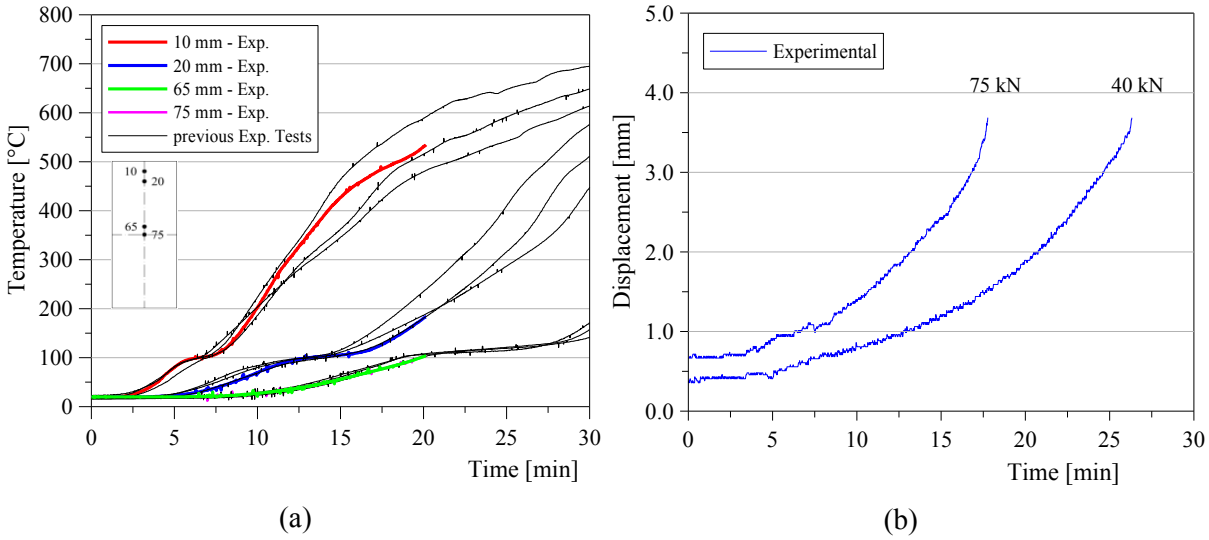

Fig. 3.5 - *(a) Temperature distribution within instrumented specimen. (b) Elongation of specimens loaded with 40 and 75 kN.*

Fig. 3.6 - *Typical brittle failure of specimens loaded in tension.*

Fig. 3.7 - *Failure close to the connection with the steel support.*

3.3. NUMERICAL ANALYSES

Numerical analyses were carried out using Abaqus [ABAQUS v.6.6], a general purpose finite element code. The aim was to simulate the fire behaviour of LVL elements in tension under fire conditions and validate the numerical modelling with the experimental results obtained from tests described previously.

A three-dimensional (3D) finite element model was implemented in Abaqus to take into account the effects of temperature and load at the same time. Sequential coupled thermal-stress analyses were performed, where a thermal analysis simulating fire conditions was conducted, followed by a mechanical analysis that assumed as an input the variation of thermal state in the model obtained as output from the previous numerical simulation. This procedure was chosen because thermal gradients are not affected by the distribution of the mechanically induced stresses in the cross-section.
The 3D model represents one-fourth of cross-section and half of the total length of the tested specimens (Fig. 3.8). Three planes of symmetry were defined in the model due to the double symmetry of the cross-section and the symmetric load application.

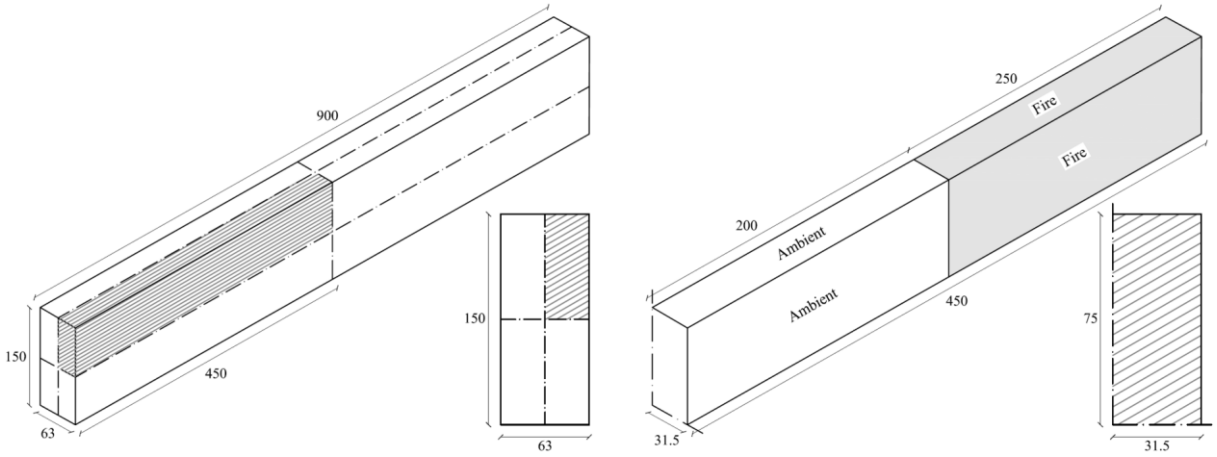

Fig. 3.8 - *Geometry of specimens (a) and three-dimensional finite element model (b) with dimensions in mm.*

3.3.1. *Mesh sensitivity study*

Some preliminary numerical analyses were performed using different meshes (Fig. 3.9) to investigate the dependency of the results upon the chosen mesh. Three meshes were tested, and the results were compared as shown in the following paragraph. Using mesh 'A', the cross-section is divided into 90 square elements of about 5 mm length, whereas the cross-section with the other two meshes is divided into elements of different sizes. Mesh 'B' is denser in the inner part of the section that corresponds to the residual cross-section at the end of the thermo-mechanical analysis. This choice was made to avoid the situation where the combined analyses terminate because of problems of numerical convergence due to the presence of a coarse mesh. The cross-section with mesh 'B' is divided into 150 elements of 2×5 mm and 4.3×5 mm. The third mesh instead is denser in the parts of the section more exposed to fire, in particular close to the top surface and along the small dimension of the cross-section. Mesh 'C' subdivides the cross-section in 228 elements of about 2.5×2.5 mm and 2.5×5 mm.

After comparing the thermal and mechanical results, most of the numerical analyses were carried out using the 3D finite model with mesh 'B'. The selected mesh was the best compromise between accuracy of solution and computational time needed for the analyses. The whole 3D model is subdivided into 7500 elements with 8976 nodes (Fig. 3.10a).

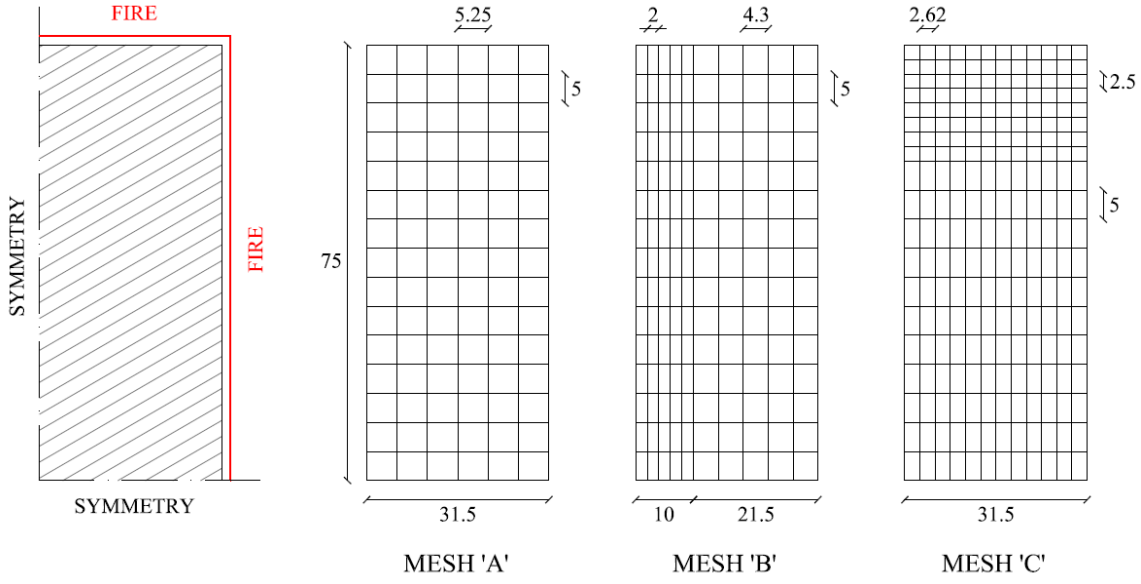

Fig. 3.9 - *Modelled cross-section and different meshes (dimensions in mm).*

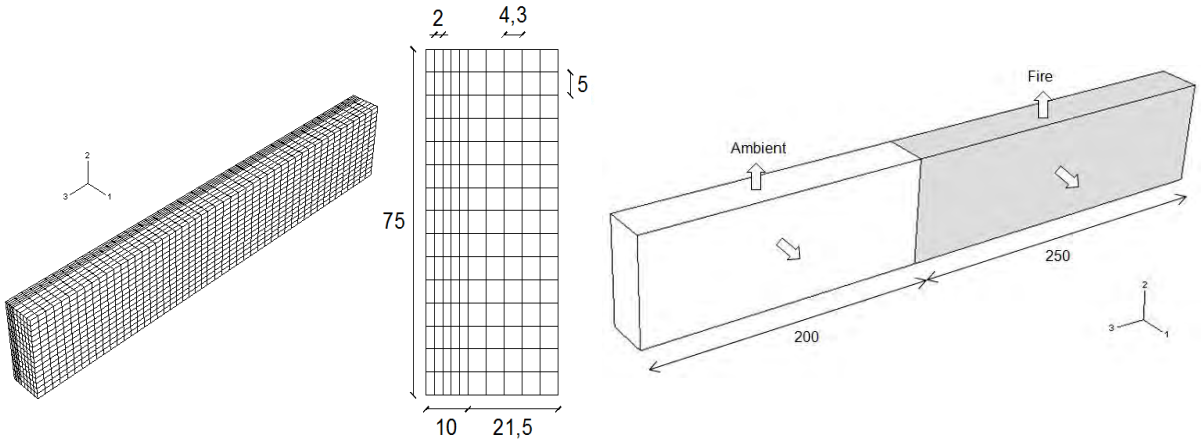

Fig. 3.10 - *(a) Mesh adopted in the numerical modelling and (b) thermal interactions (dimensions in mm).*

3.3.2. *Thermal analysis*

The temperature distribution in the LVL cross-section exposed to fire on four surfaces was computed by performing uncoupled heat transfer analysis using eight-node linear solid elements type 'DC3D8', which are available in the library of Abaqus for thermal analyses.

Exposure to fire was modelled by using an approximation of the furnace temperature as an input (Fig. 3.4b) and by imposing the boundary conditions of radiation and convection on all surfaces exposed to the fire, no heat flux across the symmetry planes, and the environment at ambient temperature. As shown in Figure 3.1a, about half of the specimen length was under fire conditions, while the remaining part was outside the furnace, remaining at room temperature (Fig. 3.10b). The emissivity ε and convection coefficient h were assumed equal to 0.8 and 25 W/m^2 K, respectively, as suggested by Eurocode 5 [CEN 2004] and Eurocode 1 [CEN 2002b].

The influence of temperature on thermal properties is implemented in Abaqus by defining the material through its thermo-physical parameters that govern the heat conduction process. The finite element code in fact allows the user to implement a variation of such quantities with the temperature as a piecewise linear curve. Different proposals can be found in the literature for the variation of thermal properties with

temperature [e.g. Buchanan 2002; Cachim and Franssen 2009a; CEN 2004; Frangi 2001; Hopkin et al. 2011; König 2006]. Such variation depends on the fire curve, and many proposals such as the Eurocode 5 one refer to standard fire exposure [ISO 834-1 1999]. In the presented modelling, the Eurocode 5 relationships were adopted for conductivity, specific heat and density. Such relationships account implicitly for the complex phenomena taking place in wood exposed to fire so simplified conventional heat transfer analyses can be carried out. Moisture content and density at ambient temperature were assumed as 12% and 570 kg/m^3, respectively.

A similar two-dimensional (2D) thermal model was already implemented in Abaqus and validated on numerical results from different authors and on experimental results of fire tests carried out on unloaded specimens under one- dimensional and 2D fire exposure (Chapter 2).

3.3.3. *Mechanical analysis*

The numerical model is the same model described for the thermal analysis. The elements used for the mechanical analyses were eight-node linear, reduced-integration elements type 'C3D8R', which are available in the library of Abaqus for static stress analyses. Some analyses with the coarse mesh 'A' (Fig. 3.9) were conducted also using twenty-node quadratic elements (elements 'C3D20R' in Abaqus), but the computational time was at least 10 times longer than using linear elements. Furthermore, the burden of that analysis was not justified by a significant improvement of the results, because the fire resistance of members modelled using quadratic instead of linear elements increased less than 1%. Therefore, linear elements were chosen for all analyses.

Like the thermal parameters, the mechanical properties of wood also depend upon the temperature. Several proposals related to different fire curves can be found in the literature [e.g. Buchanan 2002; CEN 2004; Jong and Clancy 2004]. The relationships proposed by the Eurocode 5 [CEN 2004] for a standard fire exposure whereby the strength and modulus of elasticity reduce to zero at 300°C were assumed in this modelling (Fig. 3.11).

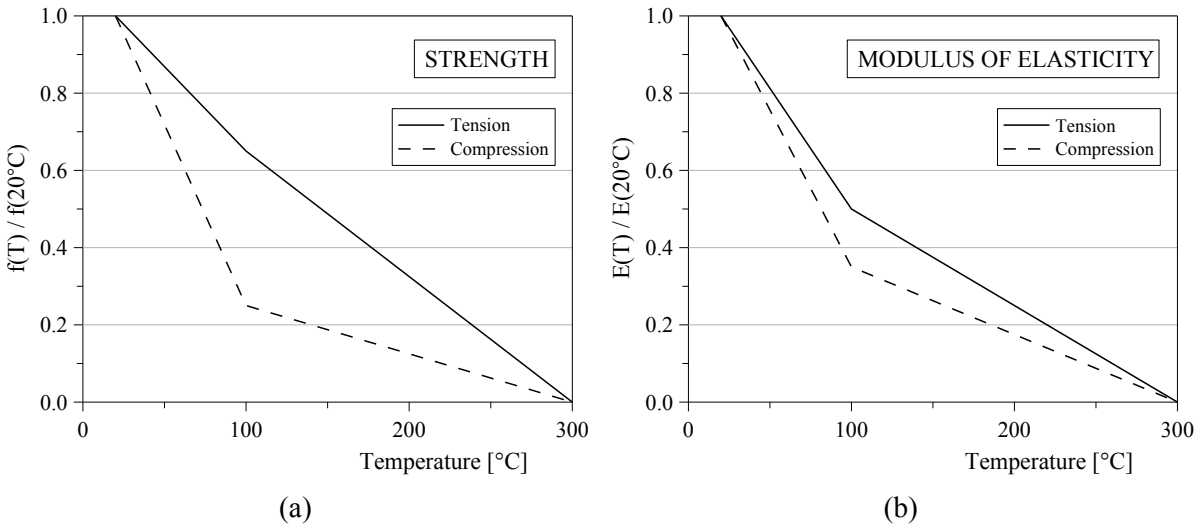

Fig. 3.11 - *Reductions of strength (a) and modulus of elasticity (b) in tension and compression with temperature according to Eurocode 5 [CEN 2004].*

In the Abaqus code it is not possible to define these as equal to zero; therefore, values two orders of magnitude smaller than the values at ambient temperature were adopted. Timber behaviour in compression can be schematized with an elasto-plastic strength–strain relationship, whereas a brittle behaviour characterizes the material in tension (Fig. 3.12). According to the Eurocode 5, the reduction of strength with temperature is greater in compression than in tension and different from the reduction of the modulus of elasticity with temperature. These differences markedly influence the structural performance of timber under fire conditions. Therefore, it is necessary to consider different strength–strain relationships and variation of mechanical properties with temperature to obtain a more realistic description of the wood behaviour under fire conditions.

The timber mechanical properties were implemented using a plasticity model readily available in Abaqus for concrete, because there is not a specific model for wood. The 'concrete damaged plasticity' (CDP) model allows the definition of different strength–strain relationships in compression and tension; moreover, those laws can be related to temperature, creating a direct correlation between mechanical and thermal material behaviour. In particular, different strength reduction factors with temperature can be implemented in compression and tension, whereas only one modulus of elasticity–temperature relationship can be adopted for both types of stresses.

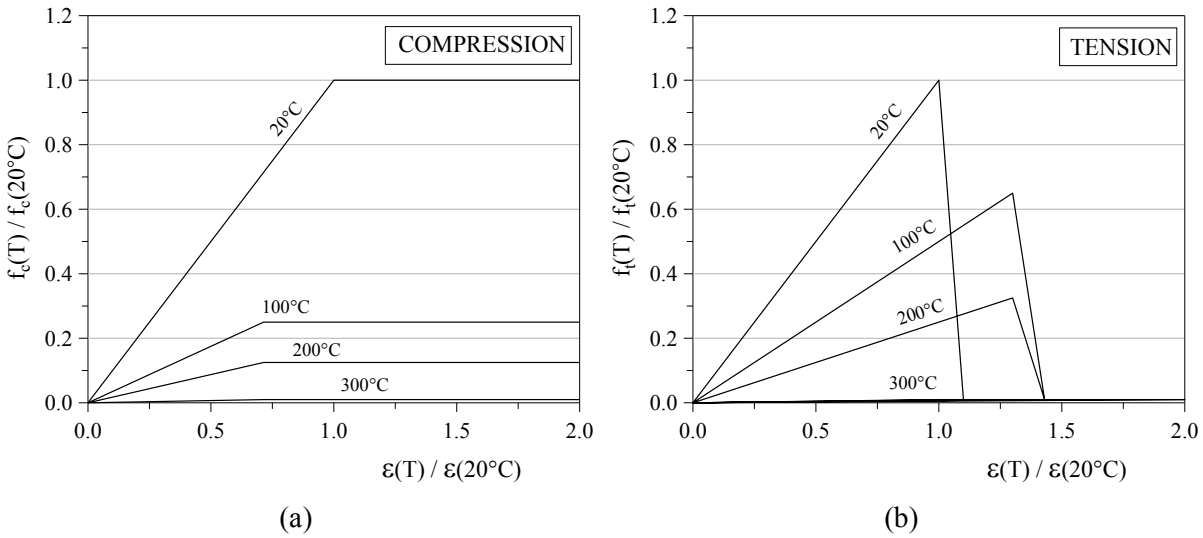

Fig. 3.12 - *Elasto-plastic (a) and elasto-brittle (b) strength-strain relationships at different temperatures for wood in compression and tension, respectively.*

Even though for the examined experimental tests only the behaviour in tension has to be defined, the CDP model was chosen as it can be used to simulate different tests such as beams and plates loaded out-of-plane, and columns and walls loaded in-a-plane. Elasto-plastic (Fig. 3.12a) and elasto-brittle (Fig. 3.12b) strength–strain relationships at different temperatures were defined for timber in compression and tension, respectively. The elasto–brittle relationship was introduced using two points defining the elastic limit at a specified temperature and the minimum value possible in Abaqus, which is $1/100^{th}$ of the strength value at ambient temperature (Fig. 3.12b). The temperature dependent reduction factors for strength and modulus of elasticity parallel to grain proposed by Eurocode 5 were then implemented.

Because the aim of this numerical investigation is the simulation of the experimental tests, the mean values of mechanical properties were adopted at ambient temperature. The mean strengths were calculated from the characteristic values (Table 3.1) using a 1.22 coefficient to account for the scatter of experimental data, which was supplied by the LVL producer [Nelson Pine Industries Ltd. 2008].

Timber is an orthotropic material, so its structural performance depends upon the load direction relative to the grain direction. Because of the axial load applied parallel to the grain, inducing only stress distributions parallel to the grain, an assumption of isotropic behaviour was made. The load was applied as a negative pressure on the end

surfaces of the specimens. Three load levels were used so as to simulate the experimental tests carried out.

The numerical model was first validated on the closed form solution at ambient temperature and then used in conjunction with the outcomes of the thermal analysis to simulate the performed fire tests.

The numerical elongation was obtained by applying a tensile force of 75 kN and assuming the material as linear-elastic. The numerical displacement was 0.334 mm but the model represents only half specimen, so the total elongation was 0.668 mm. Using the analytical formula, the elastic elongation was calculated as 0.667 mm, the same as the numerical prediction.

Property		Characteristic Value	Mean Value
Compression // to grain	$f_{c,0}$	45.0 MPa	54.9 MPa
Tension // to grain	$f_{t,0}$	30.0 MPa	36.6 MPa
Mean modulus of elasticity	E	-	10.7 GPa

Table 3.1 *- Characteristic and mean values of LVL properties.*

3.4. NUMERICAL RESULTS

3.4.1. *Evaluation of temperature and stress distributions using different meshes*

Graphic visualizations of temperature and stress distributions at different fire exposure times within the modelled cross-section obtained by using three different meshes are reported in Figures 3.13 and 3.14, respectively. In Figure 3.13 the residual cross-section can be estimated since the grey colour corresponds to charred wood. The charring temperature of 300°C is represented by the red line. The stresses (red contour in Fig. 3.14) are concentrated mainly in the part of cross-section where the temperature is still close to the ambient temperature (blue contour in Fig. 3.13).

Figure 3.15a compares the temperature distribution predicted by the thermal simulations using different meshes in the 3D numerical model. The curves obtained with meshes 'A' and 'B' are very close. The shape of the curve obtained with mesh 'C' is slightly dissimilar from the other temperature distributions especially at 10 mm from the surface exposed to fire. The dependency of thermal results upon the chosen mesh can be clearly recognized.

The stress distributions predicted by the combined thermo-mechanical simulations using different meshes and element types are compared in Figure 3.15b. The numerical element was loaded with 75 kN. Using linear elements, the curves obtained with mesh 'B' are very close to the results obtained with the denser mesh 'C' especially for increasing distance from the surface exposed to fire, while the curves obtained with the coarser mesh 'A' are slightly more distant. The stress differences between meshes 'B' and 'C' do not justify the significantly longer computational time required by the denser mesh. The time ratio between the coarser and finer meshes is 1 to 8 for a thermo-structural analysis. In terms of fire resistance, the increase obtained using mesh 'C' is about 14% compared with the prediction using mesh 'A', whereas the meshes 'B' and 'C' give the same failure time. When quadratic elements are used with mesh 'B', the results are not greatly different from the results obtained using linear elements with the same mesh. Mesh 'B' using linear elements was finally chosen as the best compromise between the computational time and the accuracy of results.

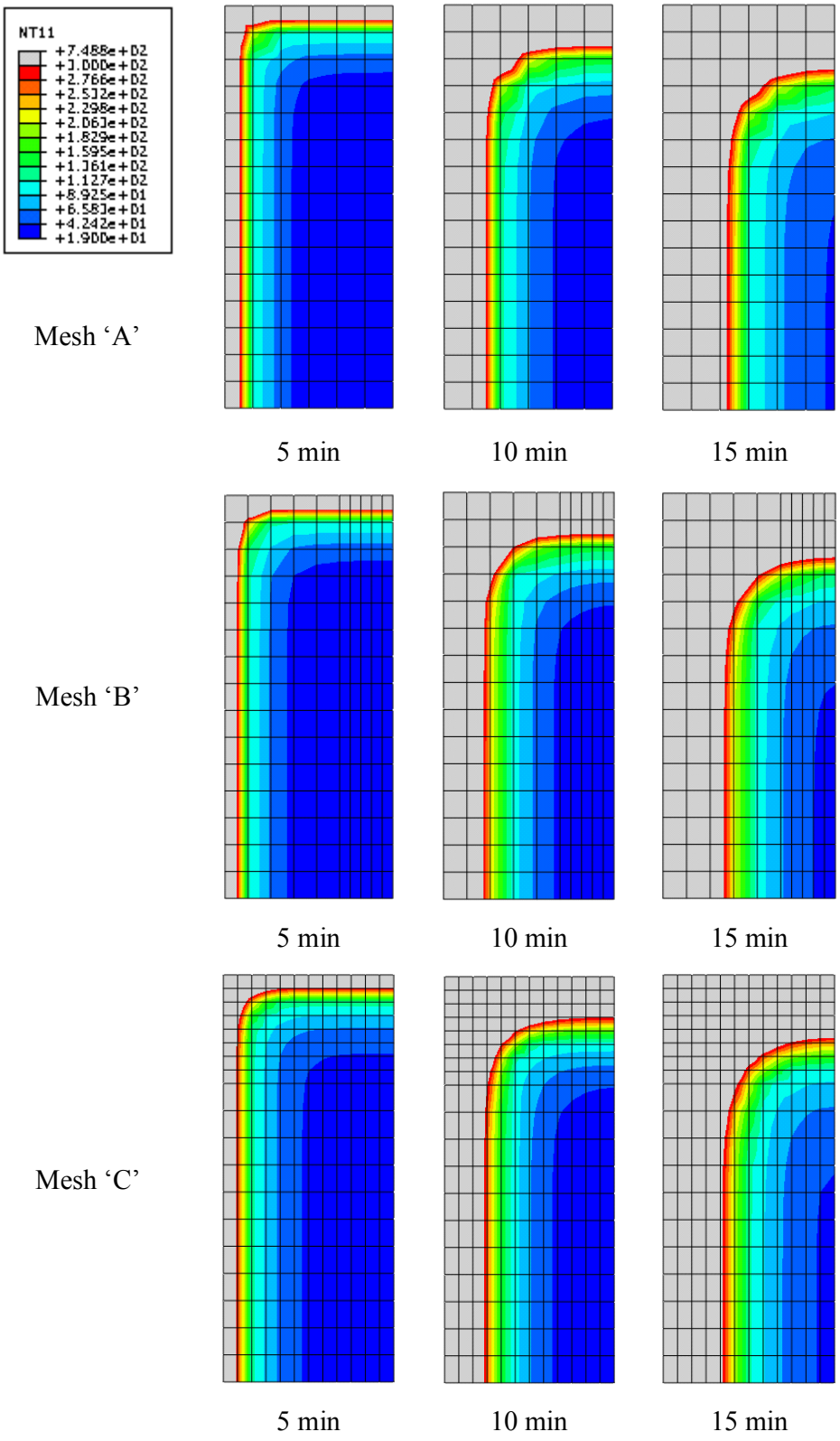

Fig. 3.13 - *Comparisons of temperature distributions within the modelled cross-section using three different meshes.*

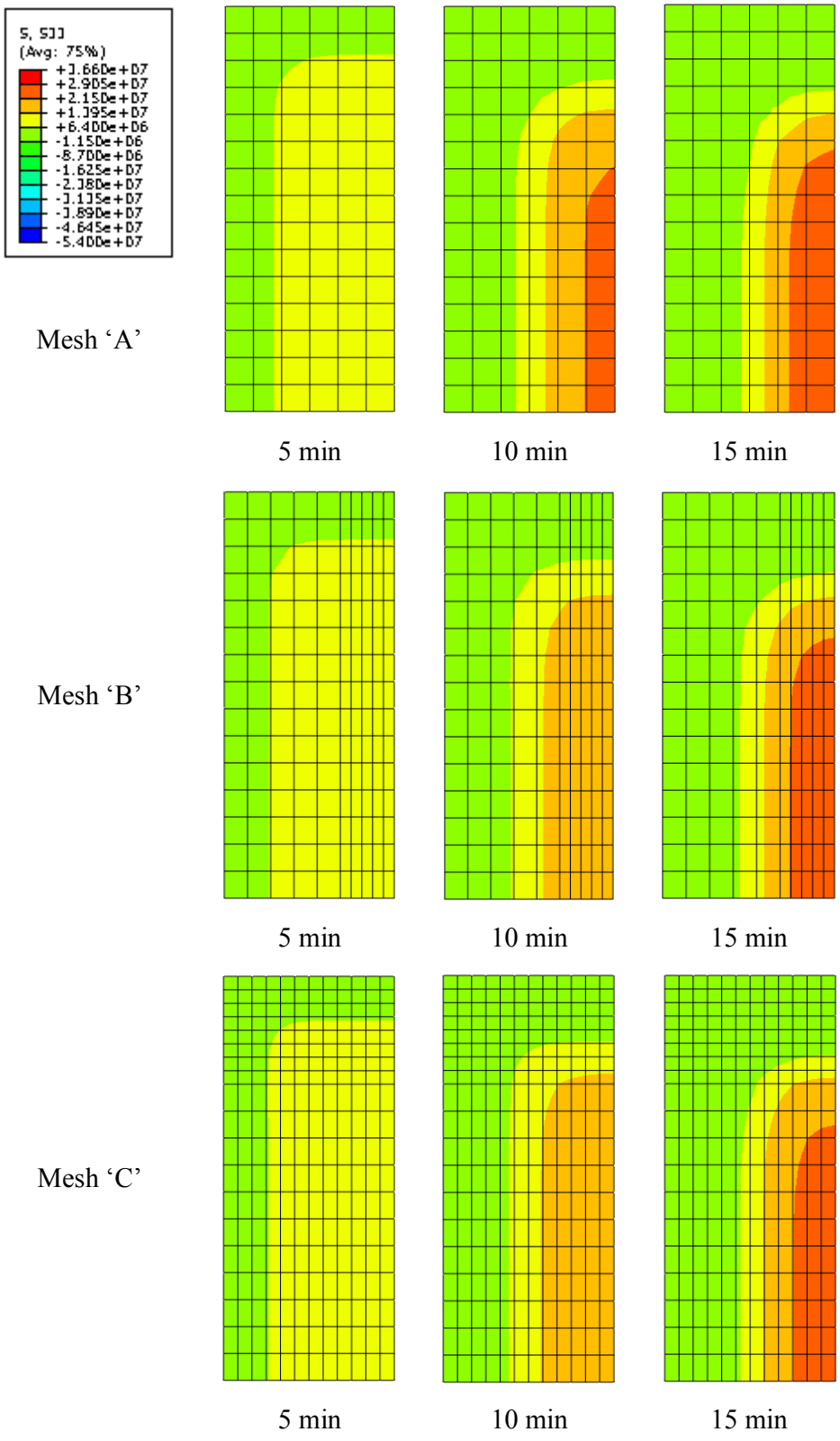

Fig. 3.14 - *Comparisons of stress distributions within the modelled cross-section using three different meshes.*

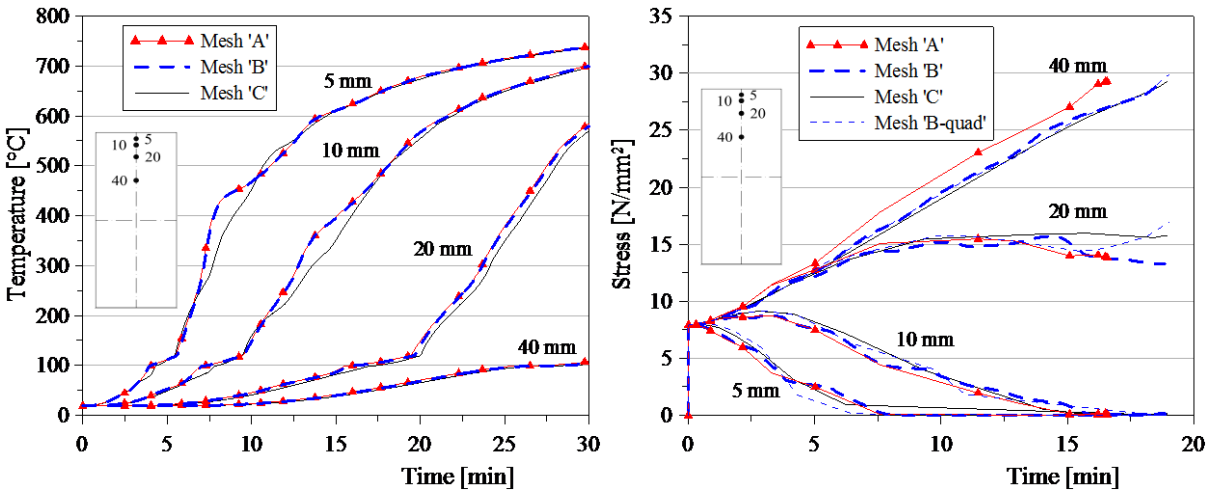

Fig. 3.15 - *(a) Temperature and (b) stress distributions in the cross-section at different depths using three different meshes.*

3.4.2. *Thermo-mechanical analyses*

Figure 3.16 shows the prediction of temperature distribution in the 3D numerical model after 30 min of fire exposure obtained by the thermal analysis.

Thermo-structural analyses allow the user to estimate the fire resistance of loaded elements and to predict the time to failure of the specimen when exposed to fire. Numerical analyses terminate when the solution appears to be diverging. If the convergence is not reached in some elements because the stress reaches the strength at that temperature, the last increment of the analysis can be assumed as the failure time of the numerical model. When the solution diverges, the numerical element is at its breaking point, as the stress approaches the ultimate tensile strength.

All numerical results presented in the following refer to the cross-section at mid-span of the tested specimens. In Figure 3.17a stress–temperature results of thermal–structural analysis with the applied load of 75 kN are plotted at different depths in the cross-section by assuming an elasto-brittle material (solid curves) and an elasto-plastic material in tension (dashed curves). The plastic material assumption is clearly a limit condition as it shows greater stress redistribution in the inner fibres, with a beginning of softening in the most inner ones. The piecewise linear curve is the wood strength variation as a function of temperature.

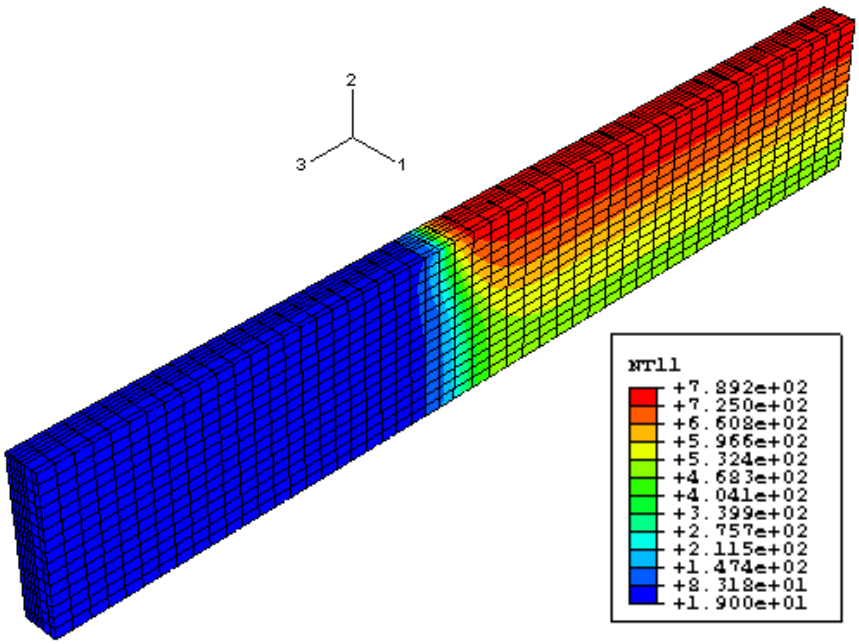

Fig. 3.16 - *Temperature distribution after 30 min of fire exposure.*

Linear elements were chosen in this model, so the stresses were computed at the integration point of each finite element, and the thermal state at these points was obtained through linear interpolation of the nodal temperatures assumed as an input for the mechanical analysis. The stress–temperature results (Fig. 3.17a), implementing different material behaviours in the model, show what happens when the numerical convergence is not reached. The solid curve at 31.5 mm represents the increasing stress in a node that did not converge at the end of the analysis.

In all the analyses carried out, convergence was not reached in elements that were mainly located in the middle of the cross-section. Elements far from the fire exposure have low temperature but are subjected to higher stresses because of stress redistribution in the section. Charred wood loses its mechanical capacity, so fibres more exposed to fire transfer their stress to inner fibres. This process continues until the residual cross-section of timber members is unable to support the increasing stress. Because of this, tensile stress increased in the inner and dropped in the outer fibres even if the applied load was constant throughout the fire exposure, as shown in Figure 3.17b, where thermal–structural results are plotted in terms of stress versus time of fire exposure for the 75-kN load level.

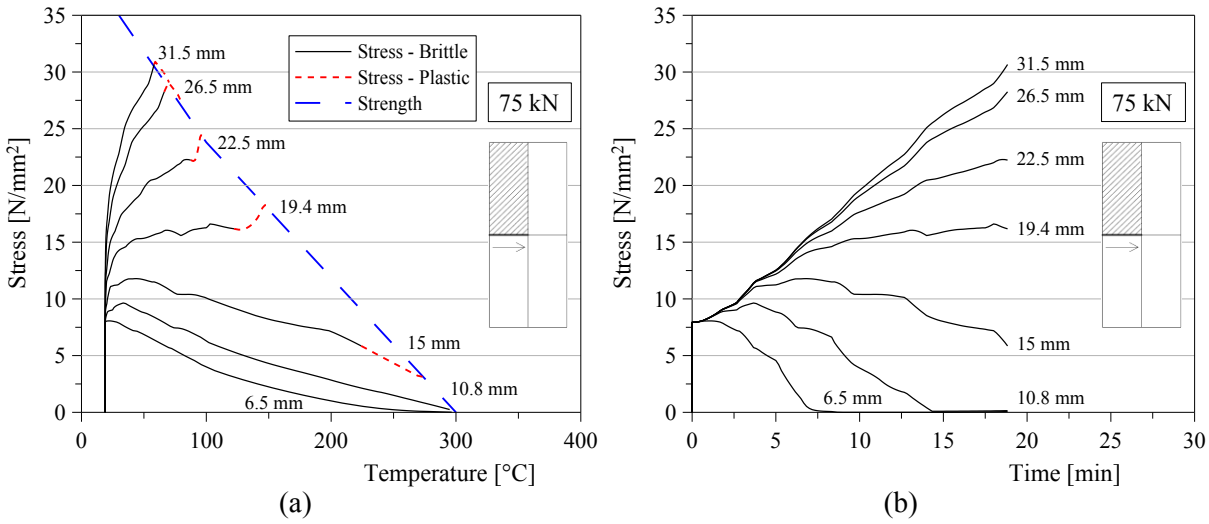

Fig. 3.17 - *(a) Stress and strength vs. temperature, and (b) stress vs. time at different distances from the exposed surface.*

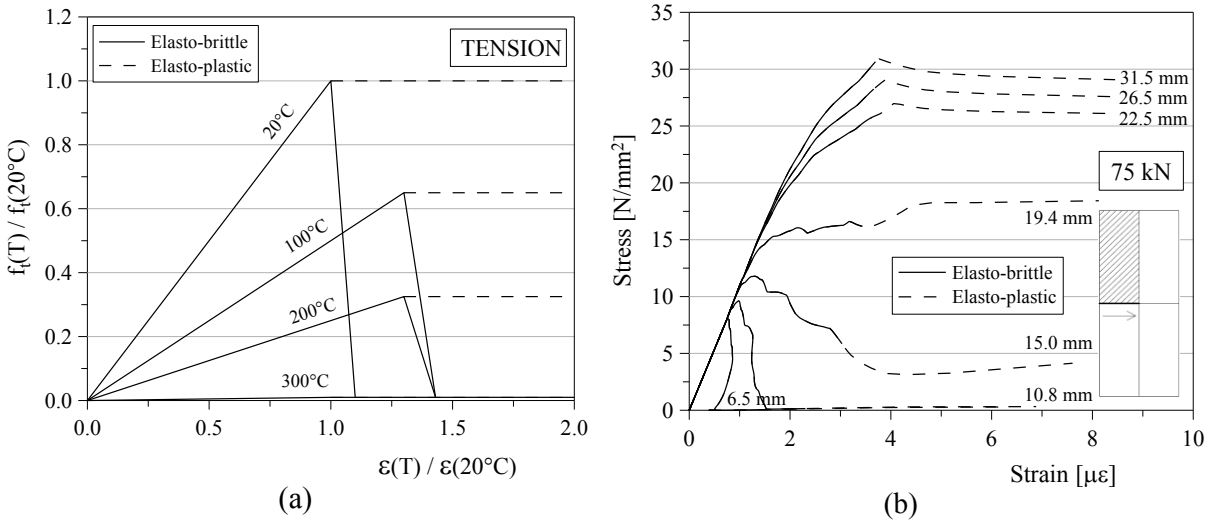

Fig. 3.18 - *Elasto-brittle and elasto-plastic strength-strain relationships at different temperatures (a) and stress-strain curves at different distances from surface (b) for timber in tension.*

Figure 3.18b compares stress–strain relationships by assuming an elasto-brittle (solid curves) and an elasto-plastic (dashed curves) behaviour in tension (Fig. 3.18a).

The temperature and stress distributions along the half-width of the specimen at the centroid of the cross-section are displayed for different fire exposure times in Figure 3.19. Five instants of time are considered, namely the time before the fire exposure, the failure time under a 75-kN load and three intermediate times (4.5, 9 and 13.5 min). Figure 3.19a allows the evaluation of the residual cross-section by referring to the rate of movement of the 300°C isotherm, assumed as the separation line between charred and

un-charred wood. A graphic visualization of the residual cross-section is possible using the numerical simulation. The charred material at different times is represented by grey colour in Figure 3.20a. Red colour corresponds to temperature of 300°C, whereas blue contour represents the temperature close to the ambient one. It can be noted that less than a quarter of the width had a temperature over 300°C at failure time of about 19 min. The residual portion appears to be heated, but it still has load-bearing capacity.

It was assumed that the 300°C isotherm determines the boundary between heated wood with residual strength and charred material without load-bearing capacity, as also shown by numerical results. The stress distribution in the wood cross-section depends upon the temperature variation because the applied load is constant during the fire test. At the beginning of the test, the stress is constant throughout the specimen and equal to the negative pressure applied at the end sections. As time goes by, the stress decreases in the fibres more exposed to the fire, and it is redistributed to the inner fibres, until the residual cross-section reaches its load-bearing capacity. This stress redistribution is evident in numerical results plotted at different times in Figure 3.19b. In the graphical visualization of stress distribution, the charred material with no load-bearing capacity is represented by grey colour (Fig. 3.20b), whereas the red contour corresponds to tension stresses in the residual cross-section. The highest stresses are concentrated in the middle of the section where temperature is still close to the ambient condition.

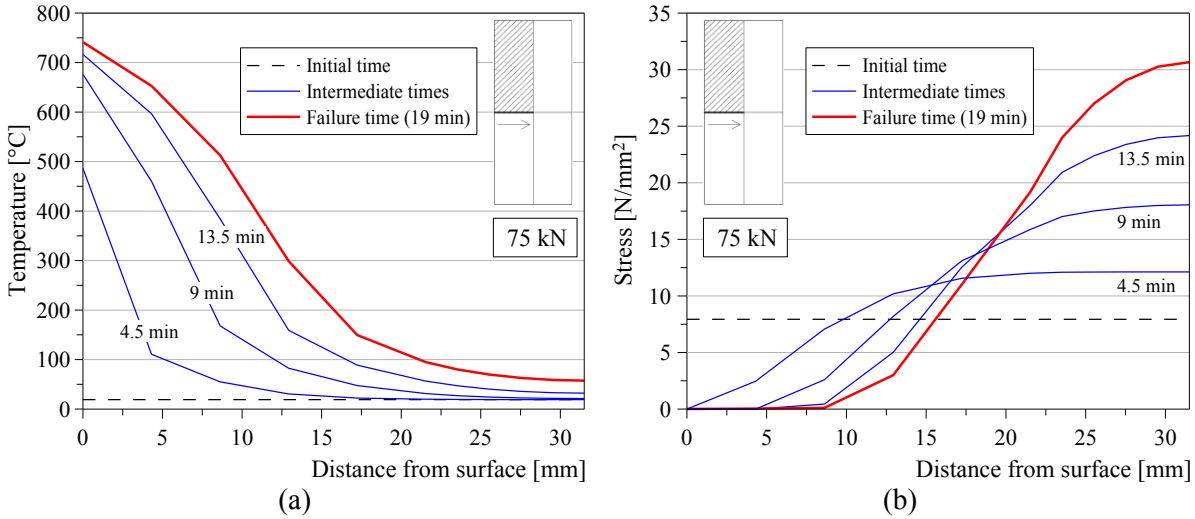

Fig. 3.19 - *(a) Temperature and (b) stress vs. distance from exposed surface at different fire exposure times along half-width of the specimen.*

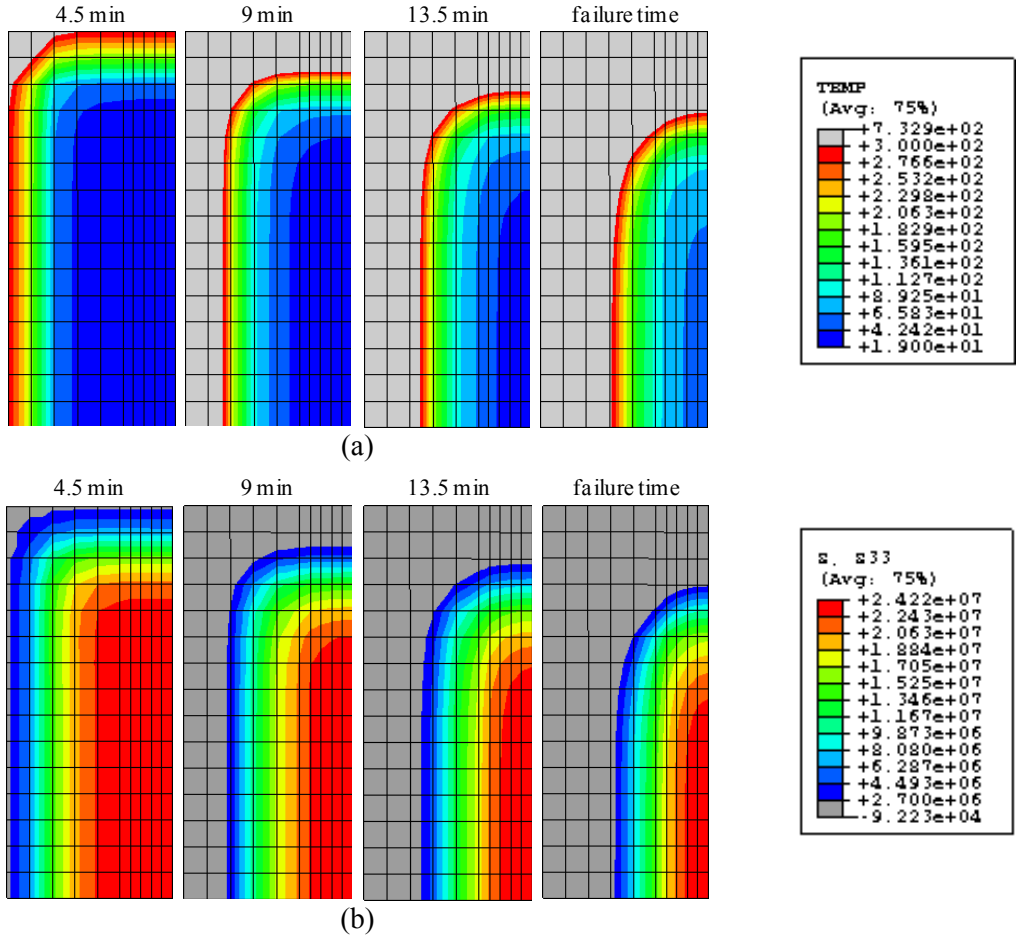

Fig. 3.20 - *Graphic visualization of residual cross-section (a) and stress distribution (b) at different fire exposure times.*

Figure 3.21 displays the thermal and mechanical states along the half-width (small dimension) of the specimen at the mid-depth of the cross-section. The stress distribution is evaluated at each time as an output of the numerical analysis. Such distribution of stresses can then be compared with the corresponding strength capacity that represents the available tensile strength at a specific thermal state. The temperature distribution at any instant is an output of the thermal analysis and can be used to calculate the related strength domain using the strength reduction factor with temperature proposed by Eurocode 5 [CEN 2004]. The results of the combined thermo-structural analysis at two times are reported, in particular after 9 min of fire exposure and after 19 min of fire exposure when numerical failure occurs. The failure time is the fire resistance of the residual structural element. Temperature and stresses are plotted versus the horizontal distance from surface directly exposed to fire at the level of the centroid of the cross-section. In Figure 3.21b, the 'stress' is the calculated stress in each element of the cross-

section (the demand), and the 'strength' is the estimated ultimate stress that would cause the failure of that element (the capacity). It can be seen that the stress and strength curves are very close at failure time, for all depths. This is due to the external fibres losing their strength and all stress redistributing to the inner fibres until ultimate strength was reached and failure occurred. At 9 min, the two curves are far apart because the applied tensile stress is markedly lower than the ultimate stress at all locations below the char layer. Furthermore, the temperature inside the element is still low (Fig. 3.21a), and less than one-third of the half section width has charred. Results presented until now were obtained defining the stress–strain relationship of wood as elasto-brittle (Fig. 3.12b).

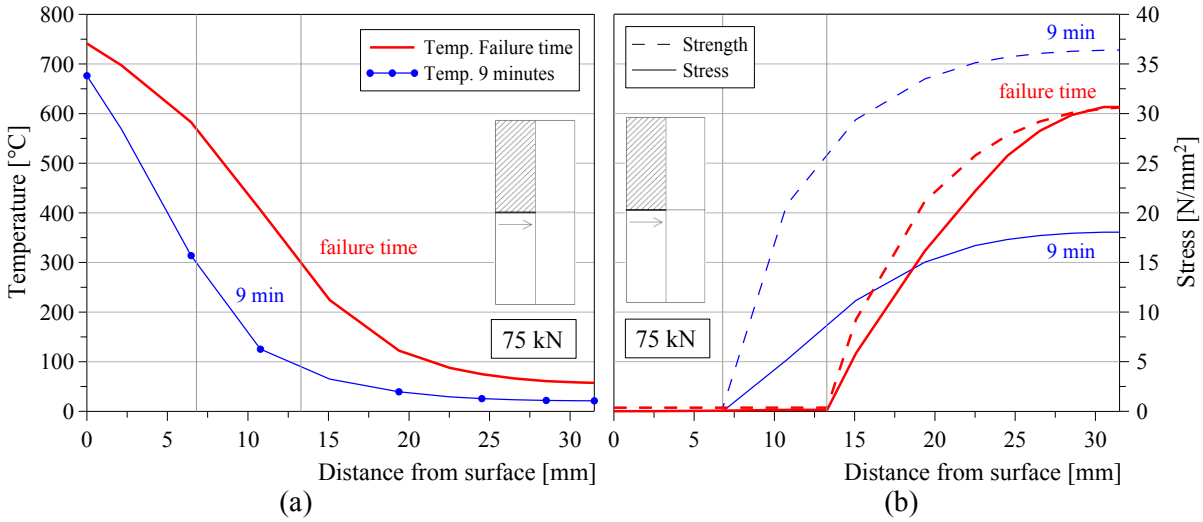

Fig. 3.21 - *Temperature, stress and strength distributions at different times for a 75-kN load.*

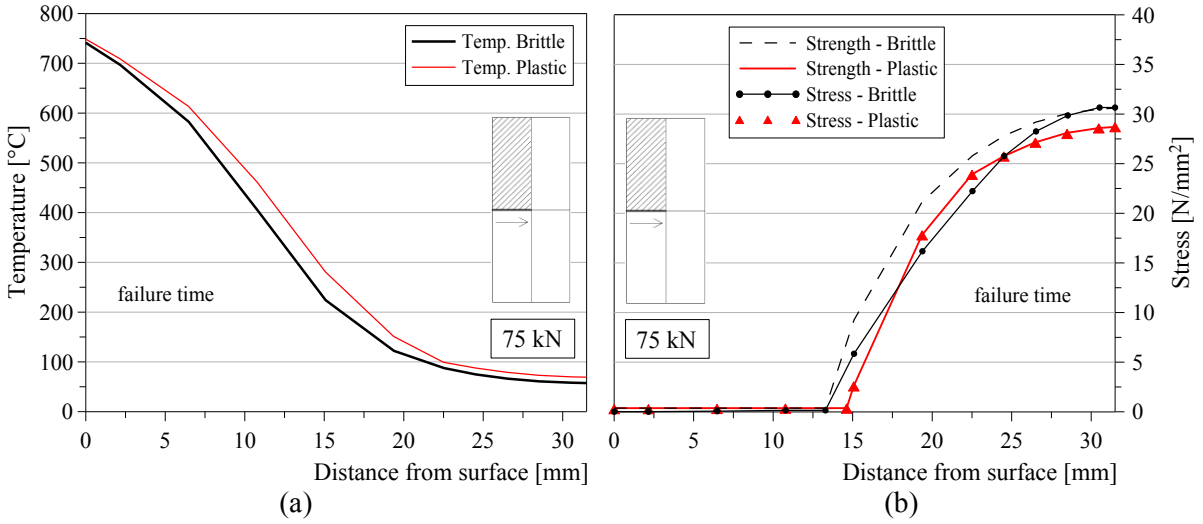

Fig. 3.22 - *Temperature, stress and strength distributions at failure time assuming elasto-plastic and elasto-brittle behaviour of wood for a 75-kN load.*

Figure 3.22 shows the corresponding curves as Figure 3.21 (but only for the failure time) if the thermo-mechanical analysis is carried out assuming wood as an elasto-plastic material in tension (Fig. 3.18a). The larger stress redistribution due to plasticity leads to a later failure. The temperature in the cross-section is higher in this case so the available strength (capacity) reduces. The stress and strength curves match extremely well along the entire depth of the cross-section.

Similar stress and strength distributions were also found for thermal and mechanical states along the half-depth (long dimension) of the specimen for the same tensile force. Figure 3.23 shows the thermal-structural results at failure time and after about 9 min of fire exposure along the vertical direction at the centroid level considering wood as an elasto-brittle material in tension.

In order to simulate the experimental tests, finite element analyses were carried out with the different tensile loads applied on timber specimens under fire conditions. Figures 3.24 and 3.25 display the thermal-mechanical states along half-width and half-depth of the specimens subjected to tension forces of 54 and 40 kN, respectively. These figures plot temperature, stress (demand) and strength (capacity) along the distance measured horizontally and vertically from the surface exposed to fire to the centroid of the cross-section. Results refer to failure time and to a second time equal to half failure time, about 28 and 14 minutes for the lesser of two loads (40 kN) and about 23 and 12 minutes for the other load (54 kN).

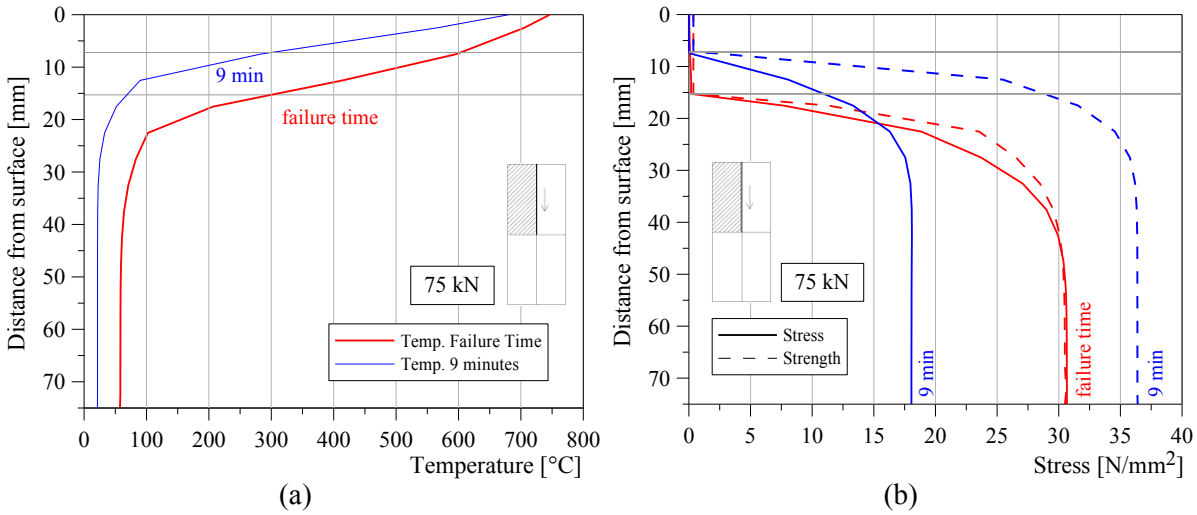

Fig. 3.23 - *Temperature, stress and strength distributions along half-depth of the specimen at the centroid level and at different times for a 75-kN load.*

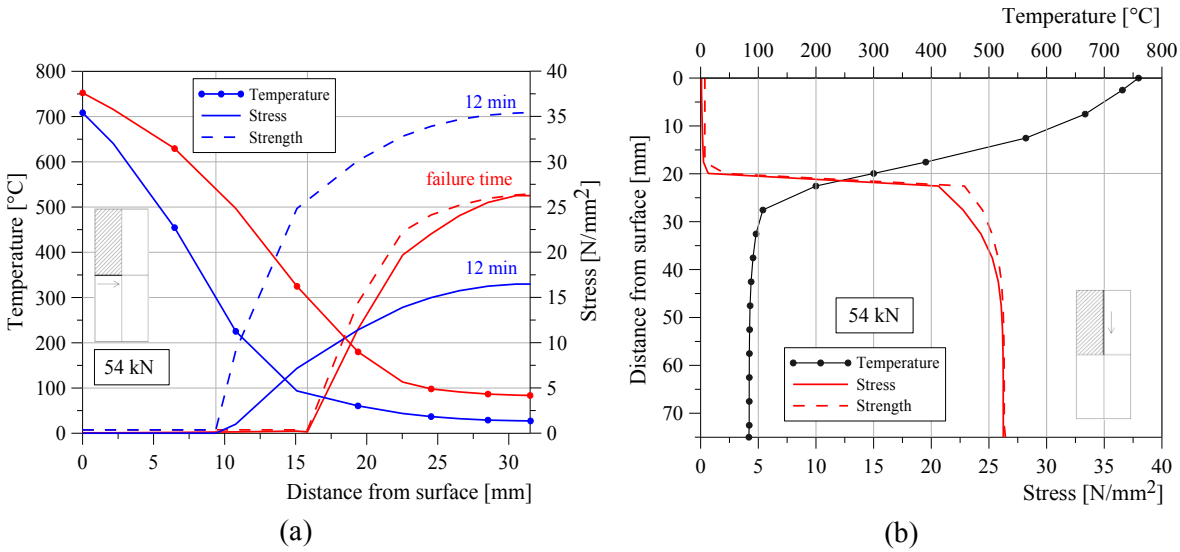

Fig. 3.24 - *Temperature, stress and strength distributions along half-width (a) and half-depth (b) of the specimen at the centroid level at different times for a 54-kN load.*

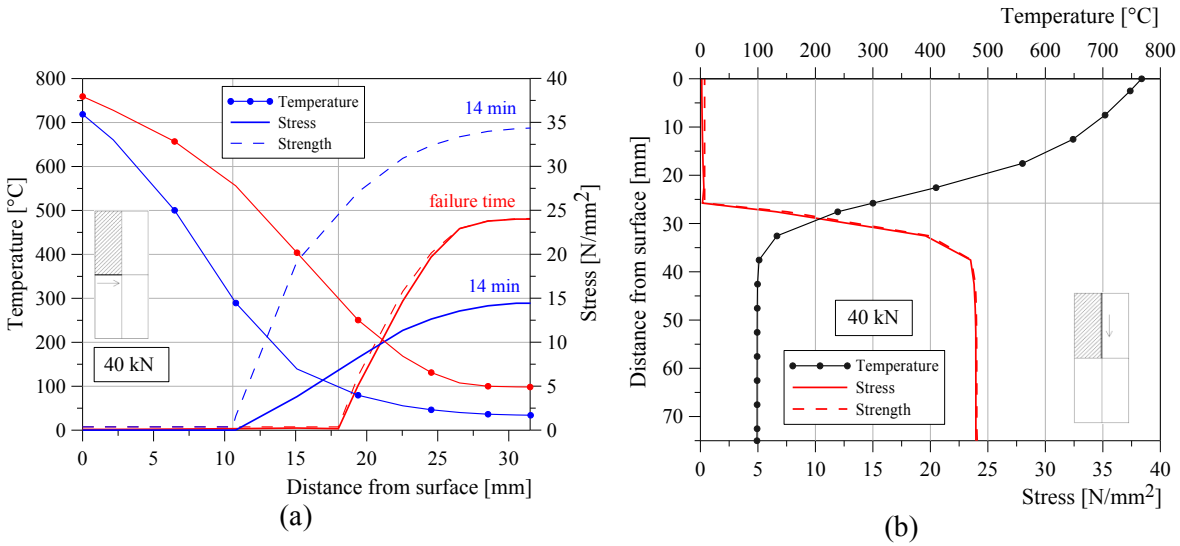

Fig. 3.25 - *Temperature, stress and strength distribution along half-width (a) and half-depth (b) of the specimen at the centroid level at different times for a 40-kN load.*

It is important to notice that the stress distribution under the load of 40 kN was very close to the strength domain (Fig. 3.25), as a proof of the larger stress redistribution achievable in the cooler cross-section, which can be justified based on the longer fire exposure and the lower tension load applied. Stress and strength curves with tensile force of 54 kN were intermediate between the other two load levels.

3.5. EXPERIMENTAL-NUMERICAL COMPARISONS

Experimental data were recorded in terms of temperature inside the custom-made furnace and within one specimen, elongation of the specimens, applied loads and failure times.

Figure 3.26a compares the temperatures recorded with thermocouples in one specimen and the numerical predictions using Abaqus code. Furthermore, the temperature distribution recorded in the cross-section is compared with the experimental data of fire tests previously performed in the same furnace on unloaded LVL specimens with the same mechanical properties and geometrical configurations (Chapter 2). The calculated temperature rose with a slight delay with respect to the experimental temperature, particularly in the inner fibres. This prediction of the temperature distribution is acceptable considering the high variability of wood material in general and, in particular, of fire test results.

The advancing of charring depth with time in the mid-point of each side of the LVL specimens was obtained from thermocouple data assuming the temperature of 300°C as the onset of charring. In Figure 3.26b, it is clear that the 300°C isotherm moves with different rates along the width and the depth of the cross-section. The charring rate along the depth (vertical direction of heat flux) is higher than along the width (horizontal direction of heat flux) of the cross-section as found also during other fire tests carried out on LVL members exposed to fire on three or four sides in furnaces of different sizes [Lane 2005; O'Neill et al. 2011]. Other experimental tests performed on solid and glued laminated timber members exposed to fire showed some qualitative differences in charring rate along the width and the depth of the cross-section [Frangi and Fontana 2003; Yang et al. 2009b]. The numerical trend of the charring depth is also reported in Figure 3.26b. The finite element simulation using Abaqus approximates the experimental curves quite well along both directions until the increase in charring rate becomes non-linear. The exponential rise of charring rate on the bottom of the cross-section is caused by the superimposition of heat fluxes coming from the bottom and the side of specimen when the residual width is small. At the beginning of the fire, the narrow side of the specimens are subjected to 1D charring, which changes to 2D charring after a while. Because of this, the charring depth on the narrow side of a rectangular cross-section

increases more than on the wide side [Frangi and Fontana 2003; Frangi and König 2011; SP Trätek 2010]. When the residual width of the cross-section is about one-third of the initial size (a charring depth of 20 mm), the average experimental charring rates on the bottom and the side of specimens are 0.83 and 0.69 mm/min, respectively. Only the charring rate on the side is comparable with the values specified by current codes [CEN 2004; SNZ 1993] because the code values are not intended for such small specimens.

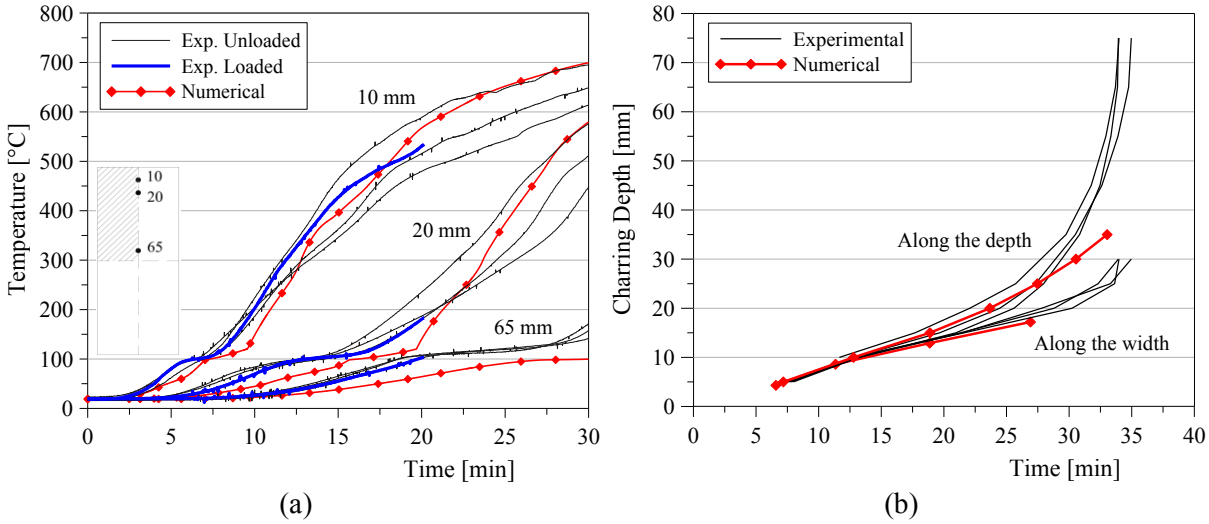

Fig. 3.26 - *Experimental-numerical comparison of (a) temperatures at different vertical depths and (b) charring depths along the width and the depth of the cross-section.*

Figure 3.27a compares experimental and numerical results in terms of specimen elongation under constant tension forces of 75 and 40 kN and in fire conditions. The numerical deformation increases slightly less than the elongation measured experimentally. The dashed curves were obtained assuming plastic behaviour for wood in tension. The difference between the recorded deformation and the numerical prediction could be justified by the delay of the temperature predictions using Abaqus and by the need to assume a modulus of elasticity different from zero (about 1/100th of the value at ambient temperature) at 300°C in the Abaqus model. Furthermore, the additional flexibility of the bolted connections with the steel plates was not modelled in Abaqus.

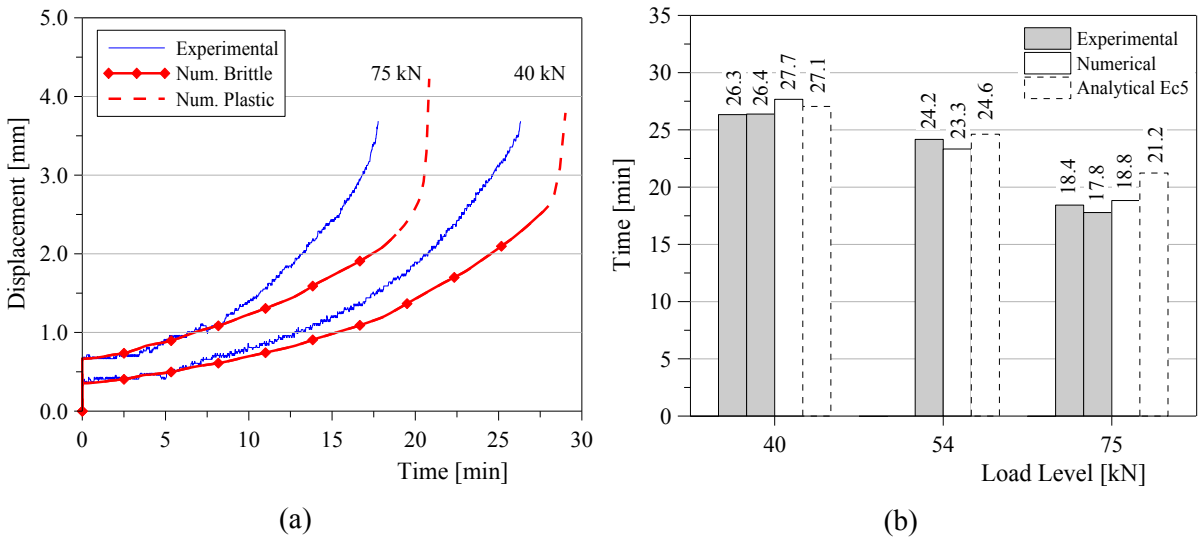

Fig. 3.27 - *Experimental-numerical comparison of (a) the elongation of specimens under two different tensile loads and (b) the fire resistance of specimens as failure time.*

The histogram in Figure 3.27b compares the numerically predicted assuming a brittle behaviour for wood in tension, analytically calculated using the 'reduced cross-section method' (RCSM) proposed by the Eurocode 5 [CEN 2004], and the experimentally measured fire resistance of LVL members loaded in tension. The fire resistance is clearly dependent upon the level of applied load. Some numerical analyses were performed also assuming an elasto-plastic behaviour for wood in tension, and the predicted fire resistance was greater than the prediction obtained using an elasto-brittle material. In particular, such resistance increase corresponded to 5%, 9% and 11% of the fire resistance obtained with an elasto-brittle model for members loaded with 40, 54 and 75 kN, respectively.

The difference between the numerical elasto-brittle prediction of fire resistance and the experimental values is less than 5% for all specimens except only one specimen loaded with 75 kN, which failed close to the connection with the steel plate, when the residual cross-section was still able to carry the load (5.6% difference). All the numerical elasto-plastic prediction results are non-conservative. The analytical method supplies a good prediction of failure time in comparison with experimental data, even if it overestimates the fire resistance for members loaded with 75 kN.

3.6. FIRE RESISTANCE PREDICTION

Figure 3.28a shows the numerical and experimental failure times of an LVL member exposed to fire on four sides and loaded with different tensile forces. The predicted fire resistance using Abaqus is plotted versus the ratio of the applied load. Further analyses were carried out with other seven load levels, in particular 20, 100, 150, 200, 250, 300 and 340 kN. These tensile forces range from 6% to 98% of the estimated ultimate mean strength at ambient temperature. For a member subjected to tensile load at ambient temperature, the mean tensile strength determined from the characteristic values (Table 3.1), supplied by the LVL producer [Nelson Pine Industries Ltd. 2008], led to a 346-kN failure load in ambient conditions. The predicted fire resistance of unloaded LVL members with cross-section of 63×150mm exposed to fire is about 39 min. At this time, all the cross-section has charred with temperatures over 300°C. The numerical curves were obtained using the 3D finite element model using both the approximation of temperatures recorded in the furnace during the fire tests and the ISO 834 fire curve [1999]. For members subjected to tension of over half of the ultimate strength at ambient conditions and exposed to the standard fire, the numerical failure of the members occurs slightly earlier than the failure times obtained using the furnace fire curve. The higher temperature reached in the first minutes of exposure to the standard fire curve justifies the anticipated failures.

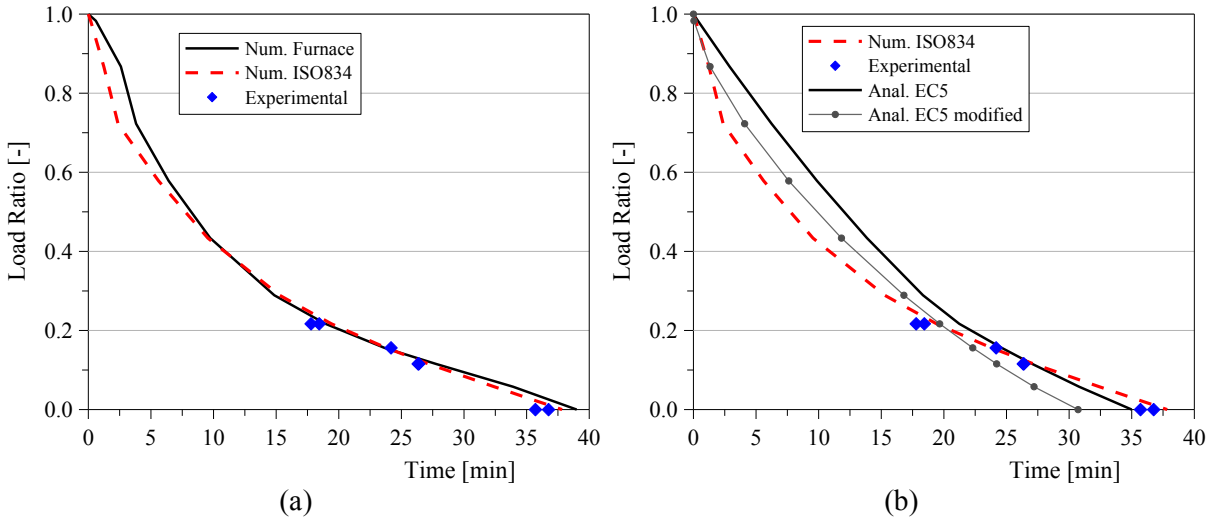

Fig. 3.28 - *Load ratio vs. failure time: (a) experimental-numerical and (b) analytical-numerical comparisons.*

In Figure 3.28b, the numerical curve obtained implementing the ISO fire curve in Abaqus is compared with load–time curves obtained as a result of analytical predictions of the fire resistance of small LVL members exposed to fire. The experimental failure times are also reported.

The analytical failure predictions were computed using the RCSM provided by Eurocode 5 [CEN 2004] to calculate the residual cross-section of timber elements under standard fire exposure and a variation of this method recommended by Cachim and Franssen [2010]. The Eurocode 5 assumes the same value of charring rate for all sides of a cross-section even if it would be more realistic to assume a greater charring rate on the narrow sides for very small cross-sections as shown by the experimental data. The fire resistance calculation does not take into account eventual superimpositions of heat fluxes from different directions [König 2005]. Furthermore, the Eurocode simplified approach does not consider what type of load is applied to the specimen; therefore, modified formulas for compression and tension were proposed to improve the estimation of the residual cross-section, increasing also the thickness of the so-called 'zero-strength' layer [Cachim and Franssen 2010; König 2005].

The analytical curves were derived assuming the notional charring rate of 0.7 mm/min suggested by Eurocode 5 for LVL even if the initial cross-section was smaller than a suggested minimum width that ensures validity of calculations [Frangi and Fontana 2003]. Very similar predictions were obtained by adopting the charring rates extrapolated from the experimental data and proposed by Frangi and König [2011]. The increased charring rate on the narrow side of the cross-section had a negligible influence on the fire resistance of members in tension, as found also for the bending moment resistance [Frangi and König 2011].

It can be observed that the analytical solution according to the Eurocode 5 method provides a good estimation of the numerically predicted fire resistance after 20 min of exposure. The analytical curve obtained using the modified formulas is conservative after this exposure time and non-conservative before; however, exposure times of less than 20 min and the corresponding levels of applied load are not realistic and relevant for structural design.

CONCLUSIONS

Chapter 2 presents and discusses the outcomes of the experimental tests conducted on small and medium size LVL cross-sections exposed to fire in a custom-made and a pilot furnace, respectively. The temperature distribution over the cross-sections was monitored using several thermocouples. A two-dimensional finite element conductive model implemented in Abaqus code is also presented. Different proposals for the thermo-physical parameters of wood were adopted in the modelling. Furthermore, a new proposal for the conductive model of LVL was made. This proposal assumes the same variations of density and specific heat as recommended in Eurocode 5, Part 1-2, but considers a variation of the thermal conductivity as suggested by other authors. The numerical model was used to simulate the heat transfer in timber cross-sections exposed to fire on one or more sides.

Chapter 3 presents and discusses the results of experimental tests conducted on small size LVL members subjected to a constant tension load during a two-dimensional fire exposure. Three different load levels were applied to the specimens. Temperature distribution within an instrumented cross-section and displacement were measured by thermocouples and potentiometer, respectively. A three-dimensional finite element model implemented in Abaqus code to simulate the fire tests is also presented. The thermal and mechanical states of the middle cross-section were evaluated at different times as results of combined thermal-structural analyses carried out with Abaqus. The 'concrete damaged plasticity' model readily available in Abaqus was used to describe the mechanical behaviour of wood. Elasto-brittle and elasto-plastic stress-strain relationships depending upon temperature were adopted to characterize the material in tension and compression, respectively. Further, wood was assumed as an elasto-plastic material both in tension and in compression. The stress distributions along the depth and the width of LVL elements were compared with the corresponding strengths at specific thermal states. The fire resistance of LVL members was predicted for different levels

of applied tensile load. The numerical predictions were compared with experimental data and analytical estimations based on the 'reduced cross-section method' (RCSM) proposed by Eurocode 5, Part 1-2.

The primary observations are reported herein after.

- The temperature distribution within small and medium size cross-sections was predicted respectively with acceptable approximation and with a delayed rise, particularly in the interior fibres.
- The new proposal for the thermal conductivity of wood led to better predictions for the medium size cross-sections and slightly worse, but still acceptable, predictions for the small cross-section, particularly for more distant fibres from fire exposure. It must be pointed out, however, that the small cross-section has less technical relevance than the other cross-sections as it is a narrow element with very low inherent fire resistance, probably needing additional passive protection if a given fire rating has to be achieved.
- Many variables characterize the heat conduction process within timber members exposed to fire and the related numerical modelling, therefore the small delay in the prediction of the thermal state within cross-sections can be considered as an overall acceptable approximation.
- The stress redistribution from the outer heated fibres to the inner cooler fibres took place depending upon the level of the applied load and on the time of exposure to fire.
- The stress redistribution in the residual cross-section subjected to lower applied loads appears to become similar to the stress redistribution obtained assuming an elasto-plastic rather than elasto-brittle behaviour of wood in tension, demonstrating a possible increase in wood plasticity under fire conditions.
- The numerical prediction of the specimen displacement was found to be underestimated with regard to the experimental values likely because of some simplifications in the numerical modelling such as assuming smeared cracking rather than fracture mechanics criteria in tension and neglecting bolted connections at specimen ends.

- The prediction of fire resistance was deemed to be acceptable, showing a difference of less than 5% with respect to the experimental results, especially considering the high variability of experimental data and the slightly delayed thermal simulation.
- The RCSM provided an acceptable solution of the fire resistance after 20 min of exposure, even if the initial cross-section was very narrow and quite atypical for structural applications.

PART II

FIRE BEHAVIOUR OF CROSS-LAMINATED TIMBER (XLAM) FLOOR PANELS

Abstract

The thermal and structural performance of cross-laminated timber (XLAM) floor panels exposed to fire was investigated experimentally and numerically. Large-scale fire tests of protected and unprotected XLAM panels were performed at Ivalsa Trees and Timber Institute (Italy). Finite element models were implemented in the software Abaqus to simulate the fire tests and to carry out parametric studies. Experimental and numerical results were compared with analytical predictions obtained using simplified design methods.

Chapter 4 reports a brief introduction on XLAM product. This recently developed wood-based material is now extensively used in Europe for domestic and public buildings since XLAM panels ensure the high structural, fire and insulation performances of massive timber elements.

Chapter 5 describes bending tests at ambient temperature and large-scale fire tests of XLAM floor panels. Three specimens exposed to standard fire curve were also loaded

out-of-plane with different levels of uniformly distributed load and in two cases collapse was reached. Other unloaded panels were protected using different cladding systems with the aim to investigate their thermal effects on XLAM cross-section. Experimental data obtained from the tests and discussed within the chapter includes Young's modulus and bending strength at ambient temperature, temperature distribution, charring depth, charring rate, residual cross-section, mid-span deflection, and failure time in fire conditions. Experimental fire resistances of protected and unprotected XLAM panels were compared with analytical predictions using simplified design methods such as the 'reduced cross-section method' proposed by Eurocode 5, Part 1-2 and a modified version recently developed for fire design of XLAM panels. The latter method was found to provide conservative estimations of the experimental failure times.

Chapter 6 presents a numerical modelling implemented in Abaqus finite element software for prediction of fire resistance of unprotected XLAM floors. A two-dimensional model for bending tests at ambient conditions was first implemented and then used to perform sequential thermal and structural analyses to simulate large-scale fire tests on unprotected XLAM panels loaded out-of-plane. The relationships proposed by the Eurocode 5, Part 1-2 for the dependency of thermal and mechanical properties of wood on temperature were employed. Numerical results in terms of temperature and stress distributions within a XLAM cross-section at different exposure times are presented and critically discussed. The stress redistribution within the cross-section due to the charring progress is clearly noticeable. The computed temperature distribution, charred depth, fire resistance and deflection were compared with the experimental measurements, showing an acceptable approximation. The numerical modelling was then used to carry out a parametric study aimed to derive the variation of the fire resistance upon the load level. The numerical results were also compared with the analytical predictions using the simplified method of the reduced cross-section recommended by the Eurocode 5, Part 1-2 for timber structures, and an improvement recently proposed for XLAM panels. Both methods provided an overall acceptable approximation, with the latter one always conservative.

Chapter 7 presents the finite element models implemented in Abaqus code to simulate fire tests of initially protected XLAM floor panels subjected to standard fire exposure. Thermal analyses were performed for predicting the temperature distribution within the XLAM cross-section protected with different cladding systems. The experimental-numerical comparisons in terms of temperature values highlight the importance of modelling the falling of the cladding when a certain temperature is reached. The fire resistance of panels protected with gypsum plasterboard and loaded out-of-plane was then predicted through sequential thermal and mechanical analyses. The relationships proposed by the Eurocode 5, Part 1-2 for the dependency of thermal and mechanical properties of wood on temperature were employed. Since the stiffness and strength degradation of wood with temperature is still subject of research, a parametric study with different variation laws was carried out. A limit case of timber with elasto-plastic behaviour in tension was also considered to demonstrate the capability of the numerical model to predict the formation of a plastic hinge also in fire conditions. The computed temperature and stress distributions within a protected XLAM cross-section at different exposure times are presented and critically discussed. The numerical predictions in terms of temperature distribution, fire resistance and deflection were compared with the experimental results, showing acceptable accuracy, particularly when the degradation laws of the Eurocode 5, Part 1-2 were adopted. The comparisons also show the need to model correctly the falling of the protective cladding for an accurate prediction of the thermal behaviour. The 'reduced cross-section method' and the adaptation for XLAM were used for analytical estimations to compare with numerical results.

CHAPTER 4.

CROSS-LAMINATED TIMBER (XLAM)

Cross-laminated timber (XLAM) is an innovative wood-based product developed in Europe in the mid of 1990s and now it is extensively used for single- and multi-storey buildings. XLAM is composed by several layers of solid timber boards stacked crosswise at a right angle and glued together (Fig. 4.1). Softwood such as spruce, pine and fir is currently used in XLAM production.

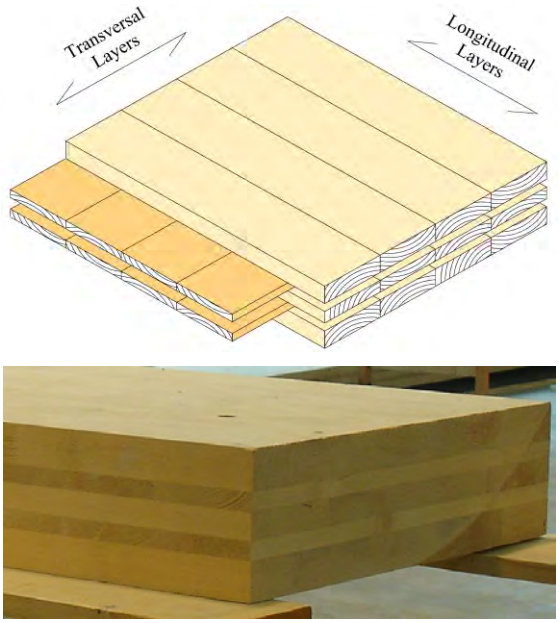

Fig. 4.1 *- Sketch and photo of a cross-laminated timber panel.*

Width and thickness of boards used to manufacture XLAM elements vary from 80 to 240 mm and from 10 to 45 mm, respectively. Board edges should be glued together to get better mechanical and building physical properties, but also for fire performance and aesthetical reasons (Fig. 4.2). Adhesives approved for load-carrying purposes are used to glue adjacent boards and layers, and to finger-joint the boards lengthwise. The glue application on the entire single layer area ensures a quasi-rigid connection between layers.

Fig. 4.2 *- XLAM cross-sections with glued board edges (left) and no glued board edges (right) [Promo_legno].*

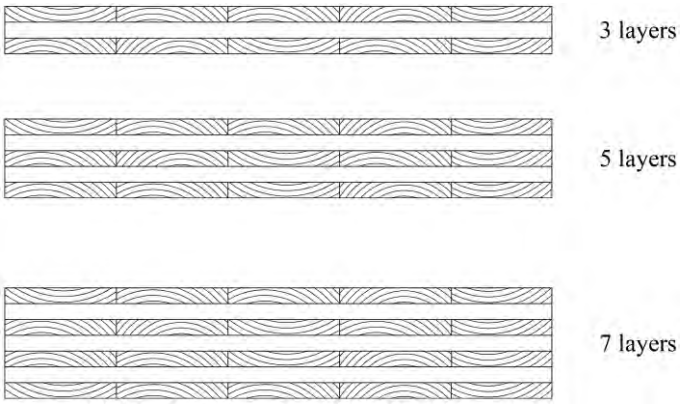

Fig. 4.3 *- XLAM cross-sections composed by 3, 5 and 7 layers.*

The number of layers in a XLAM cross-section varies from a minimum of three to seven or more (Fig. 4.3) and the total depth may range from 72 to 500 mm. Layers with the same or different thicknesses can be composed the XLAM panel section. Boards with different grading classes might be used for longitudinal (parallel) and transversal (perpendicular) layers to optimize mechanical and fire performances of XLAM product. Panel sizes vary by manufacturer anyway some restrictions depend upon the production process and the transport.

Currently, no European standards or codes are available for production of XLAM panels. Various XLAM products have a European Technical Approval (ETA) that allows manufacturers to place CE marking.

The general phases of a XLAM manufacturing process (Fig. 4.4) are herein listed:

- board selection and grading;
- board planning;
- finger-jointing of boards to produce a continuous lamination;

- assembly of finger-jointed boards to produce a bi-dimensional element corresponding to a single layer;
- glue application on layer surface;
- assembly of single layers;
- pressing using vacuum or hydraulic press;
- cutting of the product.

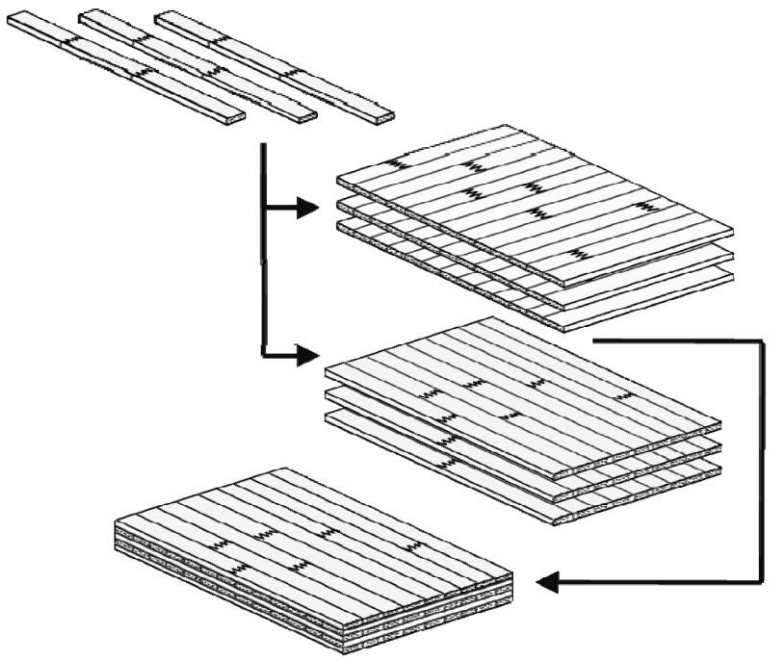

Fig. 4.4 *- Schematic view of XLAM manufacturing process [Promo_legno].*

The main advantages of XLAM panels are:

- dimensional stability;
- high in-plane and out-of-plane strength and stiffness properties;
- high shear strength against horizontal loads (seismic performance);
- good thermal insulation;
- good sound insulation;
- good fire resistance;
- high degree of prefabrication;
- easy assembling and short duration for erection;
- flexibility of utilisation.

The mechanical properties of XLAM panels are provided by each producer due to the different cross-section configurations. The structural performance of XLAM products depends upon the properties of the single layers and boards.

The external loads are carried by the longitudinal (parallel) layers, whereas the transversal (perpendicular) layers have very low strength and stiffness in the main panel direction since the stresses are perpendicular to the grains (Fig. 4.5). The so-called 'rolling-shear' (shear in the radial-tangential-plane) in the transversal layers leads to relatively low load-bearing capacities.

XLAM panel used as a floor and wall element has the outer layers parallel to the main floor direction and to the vertical loads, respectively (Fig. 4.6).

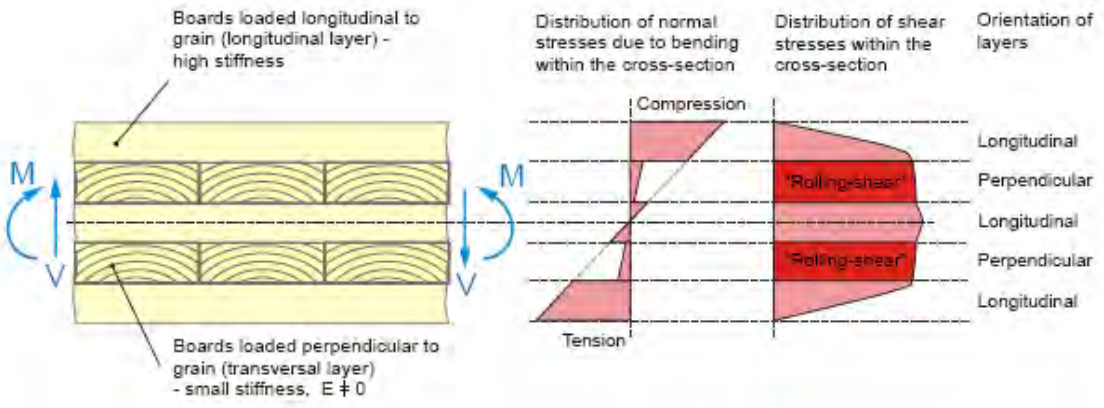

Fig. 4.5 - *Stress distributions along the depth of a XLAM panel subjected to a moment and a transversal force [Handbook 1 2008].*

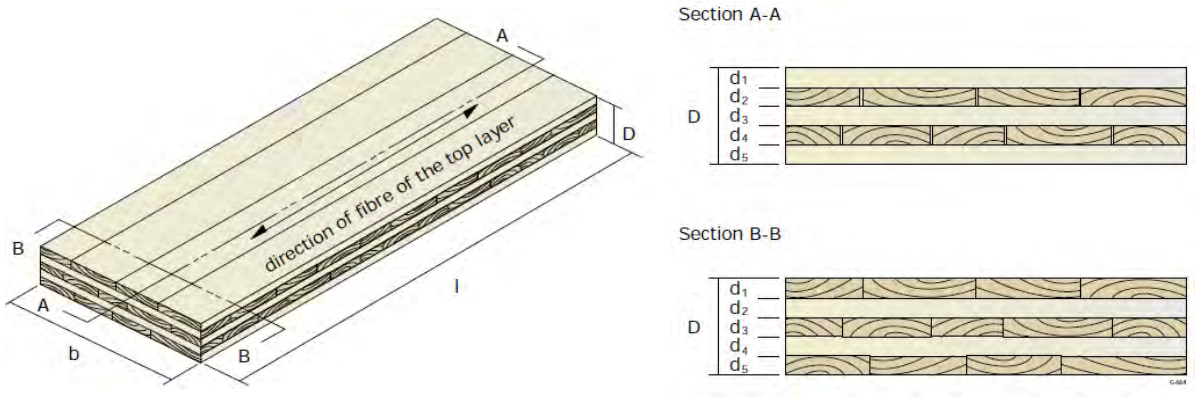

Fig. 4.6 - *Example of a XLAM floor panel [CLT Handbook 2011].*

The entire XLAM floors and walls are composed by several adjacent panels jointed together. Fast and simple on-site erection characterizes the construction system with XLAM panels. Different types of connections are used in this system, in particular between walls and foundations, and walls and floors (Fig. 4.7). Buildings made using XLAM elements are massive timber structures.

Fig. 4.7 - *Example of XLAM construction system.*

Fig. 4.8 - *On-site erection of a XLAM building [Stora Enso Timber].*

CHAPTER 5.

EXPERIMENTAL TESTS

5.1. INTRODUCTION

Timber construction systems are becoming more widespread all over the world for public and private buildings. Fire safety is an important design issue for timber structures since wood is a combustible material characterized by physical and chemical degradation with temperature. The use of massive timber elements, however, assures good structural performance in fire conditions due to the material insulating properties, which slow down the heat propagation within the cross-section and, therefore, the charring rate [Buchanan 2002]. Wood products have different fire behaviours, which depend upon the physical properties of the raw material, the manufacturing process, the adhesives used, the size of the cross-section, the structural utilization, etc. Cross-laminated timber (XLAM) is a wood product composed by cross layers of solid timber boards with the adjacent layers glued at a right angle (Fig. 5.1).

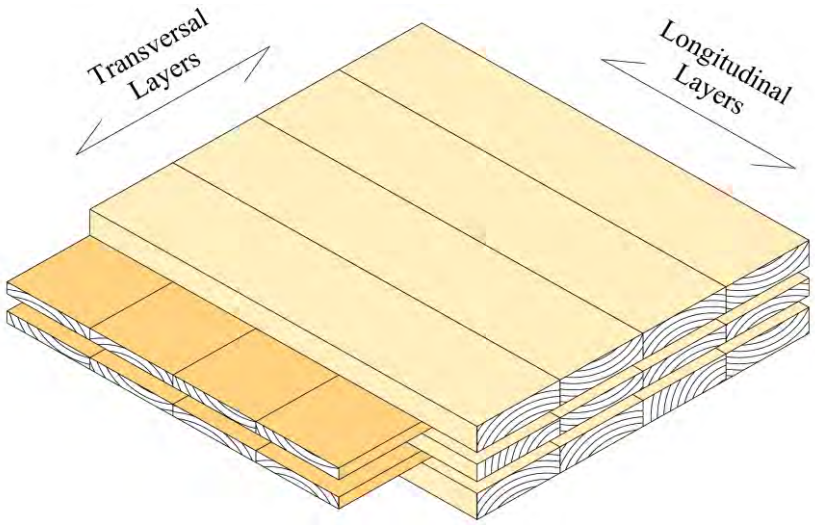

Fig. 5.1 - *Cross-laminated timber panel layout.*

Such product is now extensively used in Europe for single- and multi-storey buildings due to the improved in-plane stability, possibility to prefabricate entire walls and strips of floors, better acoustic and thermal properties, and rapidity of erection [BSPhandbuch 2010; Progetto Sofie 2007]. For these advantages and the possibility to obtain good seismic resistance, XLAM panels have recently been introduced also in North America [CLT Handbook 2011; Popovski and Karacabeyli 2011].

The fire resistance of XLAM panels depends upon several parameters including the number of layers and their thickness, the adhesives used during production, the use for floors or walls. At present, the European code for design of timber structures in fire conditions, the Eurocode 5, Part 1-2 [CEN 2004], does not provide specific information on XLAM panels. In recent years experimental studies have been carried out to investigate the fire performance of these panels manufactured by various producers with different characteristics. Small specimens were subjected to fire [Frangi et al. 2009a,b; Wilinder 2010], but also large- [Frangi et al. 2009b; Friquin 2010; Progetto Sofie 2007; Teibinger and Matzinger 2010] and full-scale fire tests [Frangi et al. 2008a] were performed. The aim of some tests was to investigate the thermal behaviour of unloaded protected or unprotected specimens; in other cases samples were loaded with different type and level of stresses to collect data also on their mechanical behaviour in fire conditions. Experimental data were used to evaluate the accuracy of analytical predictions obtained with simplified design methods. A recent proposal extends the 'residual cross-section method' for fire resistance provided by Eurocode 5 from sawn and glulam structures to XLAM panels taking into account their geometrical and structural characteristics [Schmid and König 2010; SP Trätek 2010].

This chapter presents and discusses the experimental results of bending tests at ambient conditions and large-scale fire tests on 5-layer XLAM floor panels carried out at Ivalsa Trees and Timber Institute in San Michele all'Adige, Italy. The XLAM panels were loaded with uniformly distributed load and subjected to one-dimensional fire exposure. Further data on fire behaviour of unloaded XLAM panels protected with different claddings or unprotected were also collected. The fire resistance was predicted using simplified design methods and then compared with experimental failure times.

5.2. BENDING TESTS AT AMBIENT CONDITIONS

5.2.1. Experimental setup

Four-point bending tests on cross-laminated timber (XLAM) panels were carried out in the Mechanical Testing Laboratory of Ivalsa Trees and Timber Institute (CNR-IVALSA), in San Michele all'Adige, Italy. The aim was to investigate the mechanical properties in terms of strength and stiffness at ambient temperature. The four-point bending tests were conducted on two series of 5-layer XLAM panels with different thickness and layer composition (Fig. 5.2). Length and width of all specimens were 5600 mm and 600 mm, respectively.

Eight 150 mm deep panels composed by bonded layers of 42, 19, 28, 19 and 42 mm (series 'S') were tested [Stora Enso Timber]. These XLAM panels were produced using boards of strength class C24 as in EN 338 [CEN 2009a], and formaldehyde-free adhesive, in particular polyurethane (PU) adhesive. The boards are jointed lengthwise by means of finger-joints. Other three tests on 95 mm deep panels composed by five bonded layers of 19 mm (series 'M') were executed [Martinsons]. Boards of strength class C24 were used to manufacture also this XLAM product, whilst the lamellas were glued with the melamine urea formaldehyde (MUF) resin.

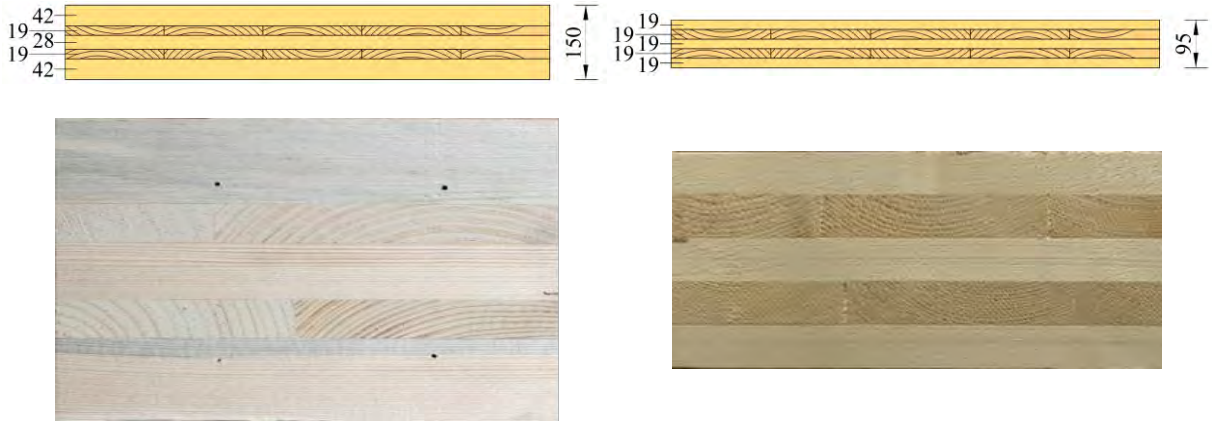

Series 'S' Series 'M'

Fig. 5.2 - *Cross-section of XLAM panels tested at ambient temperature.*

The simply-supported 5 m span XLAM specimens were loaded out-of-plane at the third points using two jacks distant 1700 mm from each other (Fig. 5.3). Five linear voltage displacement transducers (LVDTs) were positioned on each specimen to record deflections close to the supports, at 100 mm from the supports, and at mid-span (Fig. 5.4). The deflections other than at mid-span were found to be negligible as reported in the following paragraph.

Fig. 5.3 - *Photo of a specimen before the bending test at ambient condition (top) and setup of the test with dimensions in mm (bottom).*

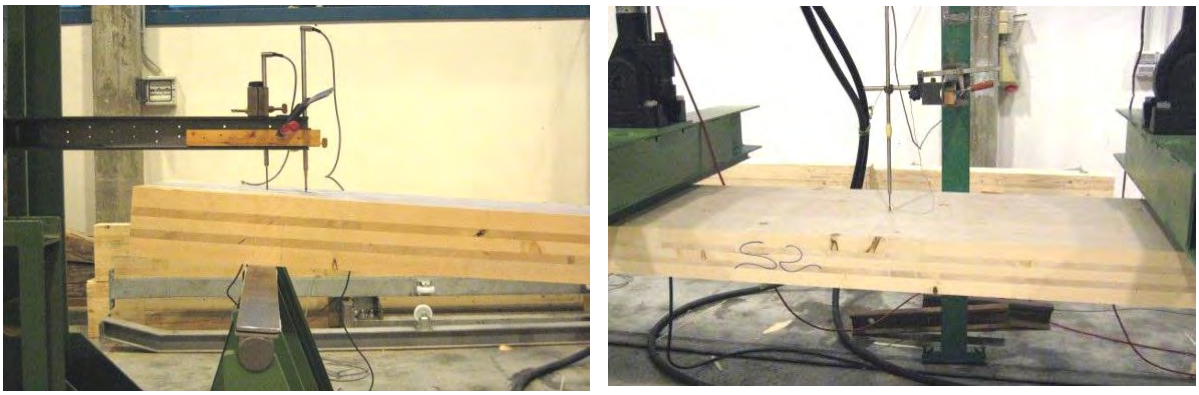

Fig. 5.4 - *Displacement transducers close to the support (left) and at specimen mid-span (right).*

5.2.2. Experimental results

Figure 5.5 plots experimental data in terms of total applied load versus mid-span deflection for specimens of series 'S' and 'M'. The linear trend of the curves clearly proves the elasto-brittle behaviour of panels. The total load was calculated as sum of the two jack loads. Figure 5.6 plots experimental data in terms of total applied load versus deflections recorded at 100 mm from supports for both specimen series. It can be noticed that these deformations are negligible compared to mid-span deflections.

Data collected for each jack show that specimens were not constantly subjected to symmetric vertical loads throughout the tests. Greater differences between applied loads can be noticed especially close to panel failure as plotted in Figure 5.7 for specimens of series 'S'.

The bending strength $f_{m,i}$ of every specimen i was calculated with the formula:

$$f_{m,i} = M_{u,i} / Z \qquad [5.1]$$

with:

$$M_{u,i} = P_{u,i} l / 6 \qquad [5.2]$$

$$Z = \frac{2}{\sum_{j=1,5} t_j} \left(\sum_{j=1,3} \frac{B t_{2j-1}^3}{12} + \sum_{j=1,3} B t_{2j-1} y_{2j-1}^2 \right) \qquad [5.3]$$

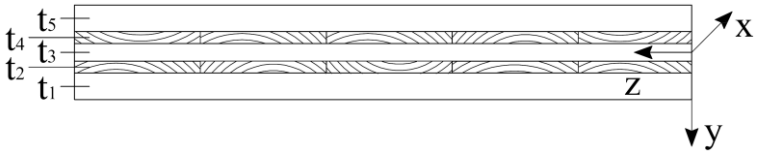

where $P_{u,i}$ and $M_{u,i}$ signify, respectively, the total load (sum of the two jack loads) and the bending moment at failure of specimen i, Z denotes the section modulus (Z = 2073 cm^3 and Z = 715 cm^3 for the tested panels of series 'S' and 'M', respectively), B is the panel width, t_j and y_j signify the depth and the centroid distance of the j_{th} layer from the centroid of the whole panel section, respectively. The section modulus Z was calculated considering only the layers in the main floor direction (layers parallel to face grain) and neglecting the mechanical contribution of transverse layers due to the significantly lower Young's modulus perpendicular to the grain. The global modulus of elasticity in bending $E_{m,g}$ was estimated according to EN 408 [CEN 2010].

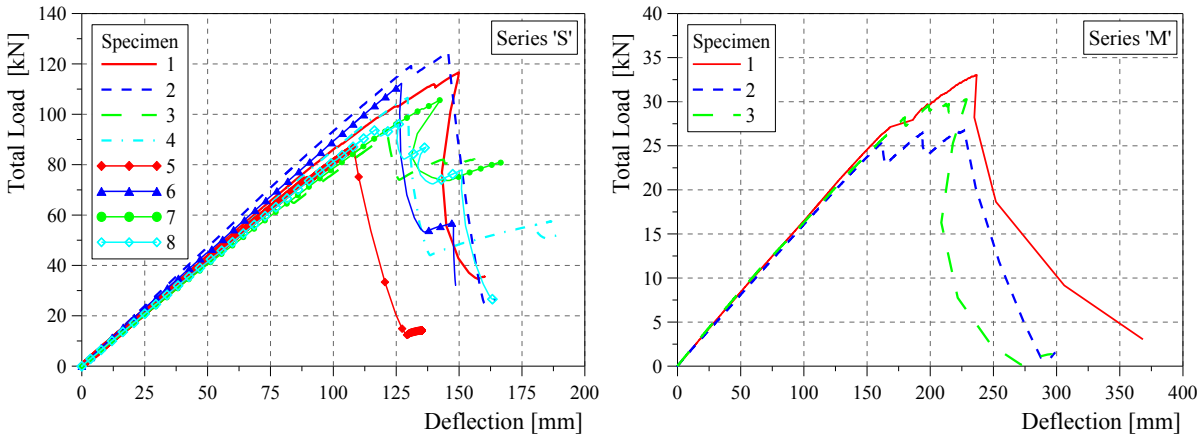

Fig. 5.5 - *Total load vs. mid-span deflection for bending tests at ambient condition.*

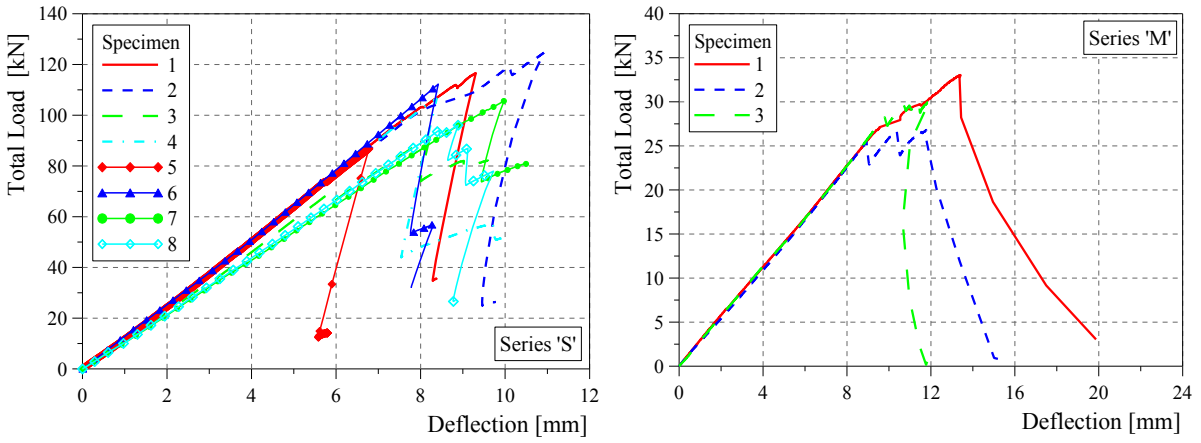

Fig. 5.6 - *Total load vs. deflection at 100 mm from supports for bending tests at ambient condition.*

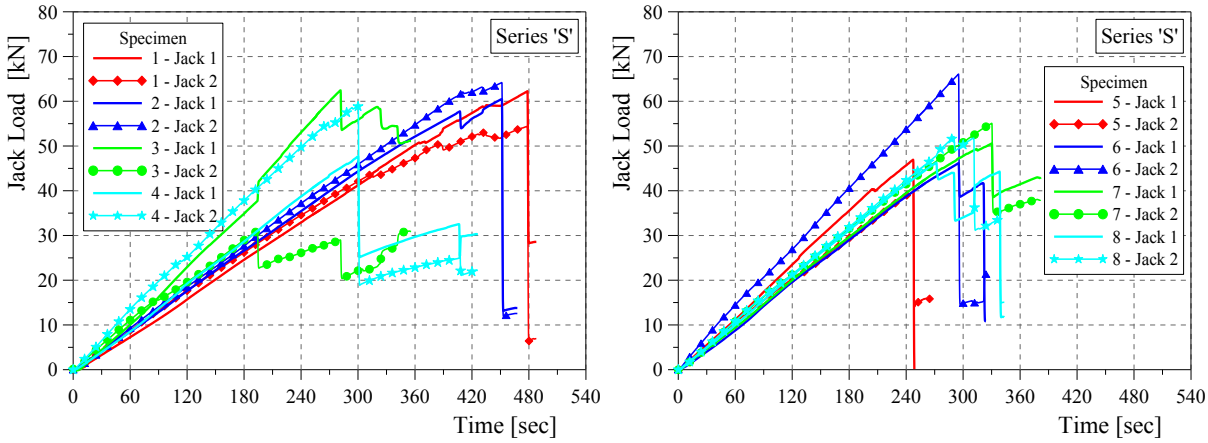

Fig. 5.7 - *Loads applied by each jack on specimens of series 'S' vs. time for bending tests at ambient condition.*

Tables 5.1 and 5.2 report the values of the total failure load $P_{u,i}$, bending strength $f_{m,i}$ and Young's modulus $E_{m,g,i}$ for both the specimen series along with the mean values and standard deviations.

Specimen No. [-]	P_u [kN]	$f_{m,i}$ [N/mm^2]	$E_{m,g,i}$ [N/mm^2]
1	116.62	46.41	12922
2	124.70	49.63	13746
3	91.44	36.39	12007
4	106.54	42.40	12657
5	86.60	34.54	12358
6	112.26	44.68	13039
7	105.66	42.05	11731
8	96.10	38.25	12055
mean value	105.02	41.79	12564
stand.deviat.	12.95	5.15	662

Table 5.1 - *Experimental results of bending tests on XLAM panels of series 'S' at ambient conditions.*

Specimen No. [-]	P_u [kN]	$f_{m,i}$ [N/mm^2]	$E_{m,g,i}$ [N/mm^2]
1	33.04	38.13	10745
2	26.80	30.93	10449
3	30.28	34.95	10468
mean value	30.04	34.67	10554
stand.deviat.	3.13	3.61	166

Table 5.2 - *Experimental results of bending tests on XLAM panels of series 'M' at ambient conditions.*

The same XLAM products were also tested at Jönköping University in Sweden [Wilinder 2010]. Fifteen and ten reduced specimens of 150 mm width and 2700 mm length were tested in bending at ambient temperature for series 'S' and 'M', respectively. A mean failure load about half the value obtained on large-scale panels of series 'S' tested at CNR-IVALSA was obtained. The estimated bending strength $f_{m,i}$ of 45.14 N/mm^2 was close to the value calculated for larger specimens. The mean failure load

obtained for specimens of series 'M' tested in Sweden was approximately 22% lower than the value found for panels tested at CNR-IVALSA, whereas the estimated bending strength was higher than the value calculated for larger specimens.

Figure 5.8 shows a XLAM specimen of series 'S' during the test at ambient conditions. The specimens failed in bending for fracture in tension of the bottom layer close to joints between boards or wood defects such as knots (Fig. 5.9).

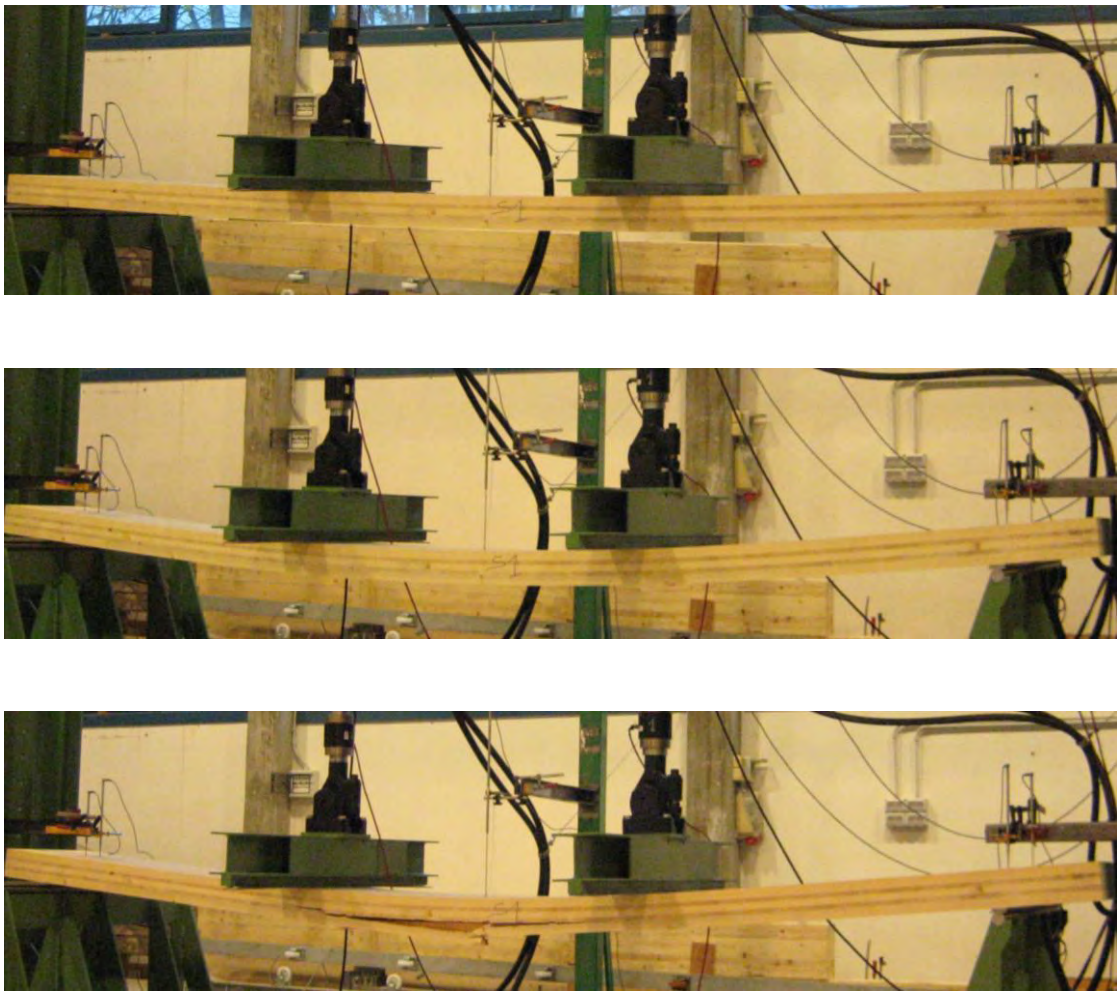

Fig. 5.8 - *A XLAM specimen during the bending test at ambient condition.*

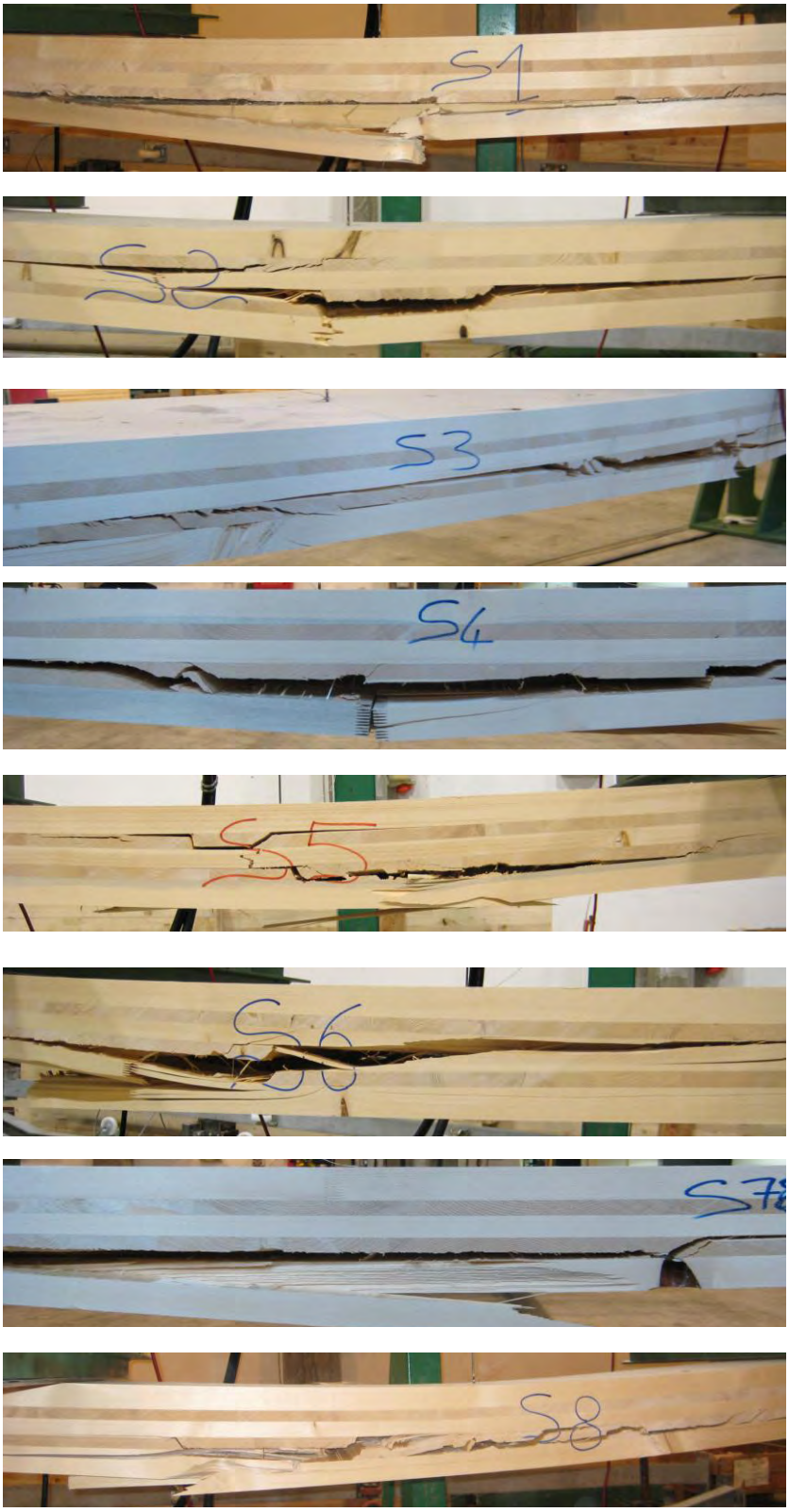

Fig. 5.9 - *Failure in bending of XLAM panels of series 'S' at ambient conditions.*

5.3. LARGE-SCALE FIRE TESTS

5.3.1. Experimental setup

Three large-scale fire tests were carried out on XLAM floor panels at the Fire Behaviour Laboratory of Ivalsa Trees and Timber Institute (CNR-IVALSA). The 5-layer panels of series 'S' had the same size of the specimens tested in bending at ambient condition (150×600×5600 mm). The measured density was approximately 449 kg/m^3.

The panels were placed above a horizontal furnace with 3.00×5.00 m opening (Fig. 5.10) and subjected to one-dimensional (1D) standard fire exposure [ISO 834-1 1999] on the bottom side. Temperature inside the furnace is controlled by eight thermocouples and two temperature regulators.

Fig. 5.10 - *Photos of the horizontal furnace at CNR-IVALSA.*

Lightweight precast concrete panels with REI 180 fire resistance were used to cover the remaining of furnace opening (2.40×5.00 m) during two tests (fire tests No. 1 and 2) (Fig. 5.11 and Fig. 5.12), whereas four unloaded XLAM panels with the same size as the loaded panels were used during the last test (fire test No. 3, specimens II to V) (Fig. 5.13 and Fig. 5.14). Two unloaded XLAM panels were protected using different methods as showed in Figure 5.15: (i) 15 mm thick gypsum fibreboard (GF) [Fermacell] complying with EN 15283-2 regulation [CEN 2009c] (specimen S3-IV) (Fig. 5.15a); and (ii) a cladding system made of 12.5 mm thick GF [Fermacell] placed at 40 mm distance from the bottom fibre of the XLAM panel, with the cavity completely filled with rock

wool (RW) insulation (specimen S3-III) (Fig. 5.15b). In the former cladding, the GF was fixed with staples (1.5×10×50 mm) directly to XLAM panels; whilst in the latter solution the GF was fixed with staples (1.5×10×40 mm) to ledges of 40×40 mm. The remaining two unloaded XLAM panels (specimens S3-II and S3-V) were left unprotected (Fig. 5.13).

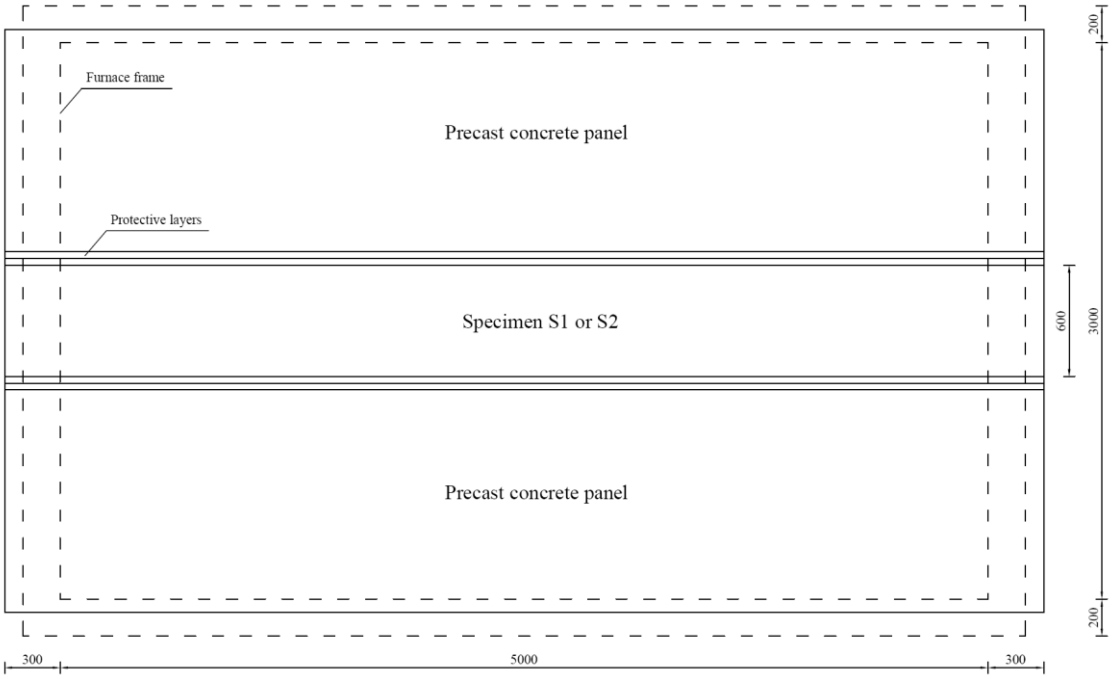

Fig. 5.11 - *Plane view of setup for large-scale fire tests No. 1 and 2 (dimensions in mm).*

Fig. 5.12 - *Setup of large-scale fire tests No. 1 and No. 2.*

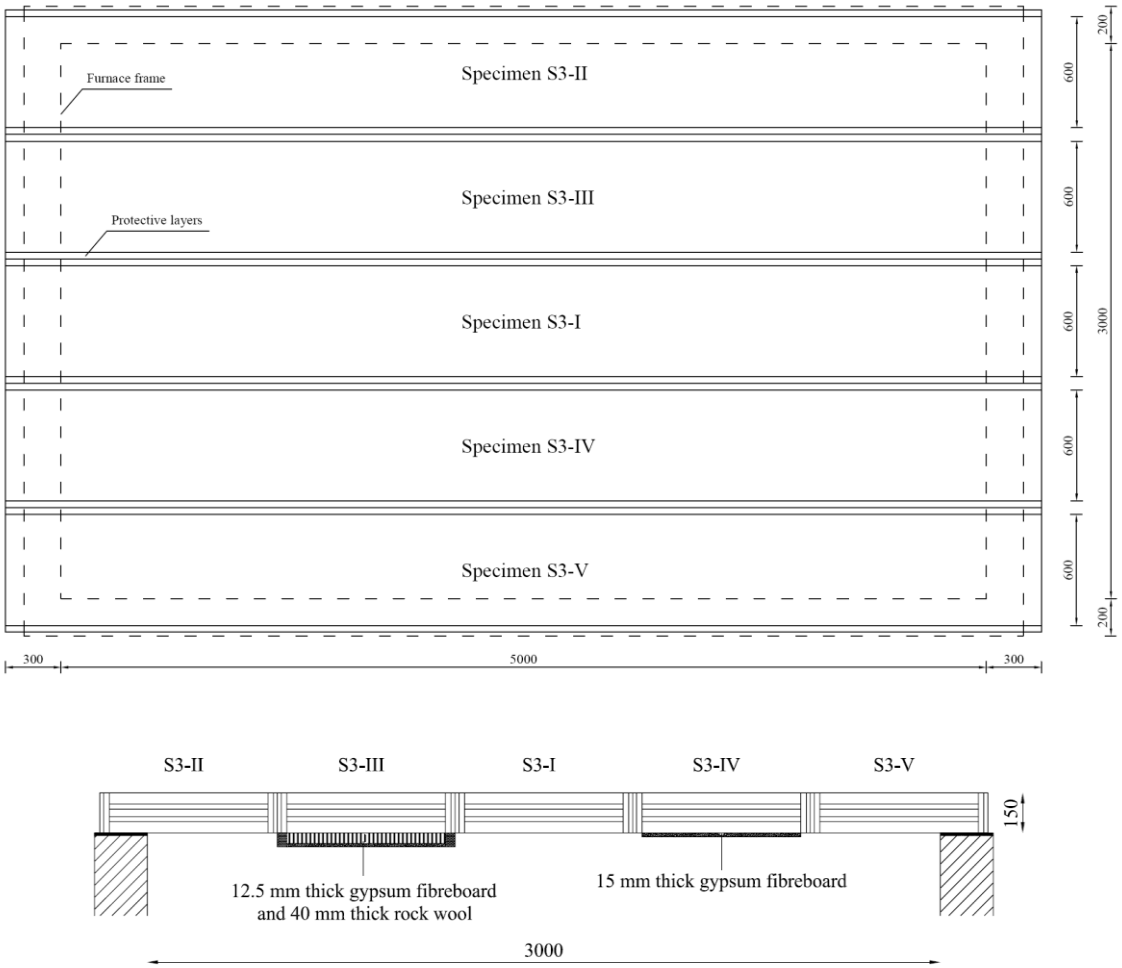

.13 - *Setup of large-scale fire test No. 3: plane view (top) and transversal cross-section (bottom) (dimensions in mm).*

Fig. 5.14 - *Setup of large-scale fire test No. 3.*

(a) (b)

Fig. 5.15 - *(a) Specimen S3-IV protected with gypsum fibreboard. (b) Specimen S3-III protected with gypsum fibreboard and rock wool.*

The edges of all XLAM specimens were protected with 21 mm thick wooden boards and 15 mm thick fire-rated (type F according to EN 520 [CEN 2009b]) gypsum plasterboard (GP) in order to ensure a 1D heat transfer in the tested panels (Fig. 5.16). This protection was made with short lengths of material so as not to provide any additional stiffness and resistance to the loaded panels. The GP was fixed to wooden boards with 3.5×30 mm screws (type Fe620005 [Rothoblaas]), whilst 3.5×40 mm screws (type HBS3540 [Rothoblaas]) fixed the wooden boards to XLAM specimens.

Fig. 5.16 - *Protection of specimen lateral edges with gypsum plasterboard and wood.*

Three XLAM panels were loaded out-of-plane with a uniformly distributed load of 5 or 10 kN/m^2 obtained using short lengths (about 800 mm) of steel rails (Fig. 5.17). The two load levels corresponding respectively to 11 and 21% of the ultimate mean strength at ambient condition were chosen as the latter one corresponds to the typical quasi-permanent load condition used in fire resistance design [CEN 2002a], and the former one is half that value.

Fig. 5.17 - *Photos of fire tests No. 1 (left) and No. 3 (right). The loaded specimens are in the centre of the furnace, and the unloaded precast concrete/XLAM panels are besides (left/right photo).*

The lower load level was applied to specimen S3-I, while the two other panels S1 and S2 were subjected to the higher load level. Specimen S2 was protected with one layer of 15 mm thick fire-rated (type F according to EN 520 [CEN 2009b]) GP [Knauf] in order to increase its fire resistance.

Loaded and unloaded XLAM panels were instrumented with thermocouples at different depths to record the temperature distribution within the cross-sections during the fire test (Fig. 5.18). Thermocouples type K (Chromel-Alumel) suitable for temperatures over 400°C were used according to EN 1363-1 [CEN 1999]. They were inserted in 5 mm drilled holes that were filled with gypsum fibre.

The temperatures in loaded panels S1 and S2 were recorded by nine thermocouples arranged in three parts of the specimen span in order to consider the possible non-homogeneous temperature distribution inside the furnace (Fig. 5.19). The three instrumented cross-sections were located at approximately 750 mm from furnace frame (thermocouples '1'), at mid-span (thermocouples '2') and close to third point (thermocouples '3'). Within each cross-section, three thermocouples T_a, T_b and T_c recorded the thermal gradient respectively at 21, 52 and 75 mm from the bottom surface, i.e. in the middle of the three lower layers of XLAM panel. The horizontal distance between each thermocouple was 250 mm. All thermocouples were inserted horizontally at 50 mm distance from the lateral edge of the specimens [CEN 1999]. Only the thermocouples T_b arranged in these specimens (S1 and S2) were introduced vertically.

Fig. 5.18 - *Details of thermocouples inserted in XLAM specimens.*

The temperature was recorded also on unexposed surface by three thermocouples (T_A, T_B and T_C) located approximately at fourth points and at half-breadth of specimen. Further three K-type thermocouples (T_i) were arranged in the GP-XLAM interface of specimen S2.

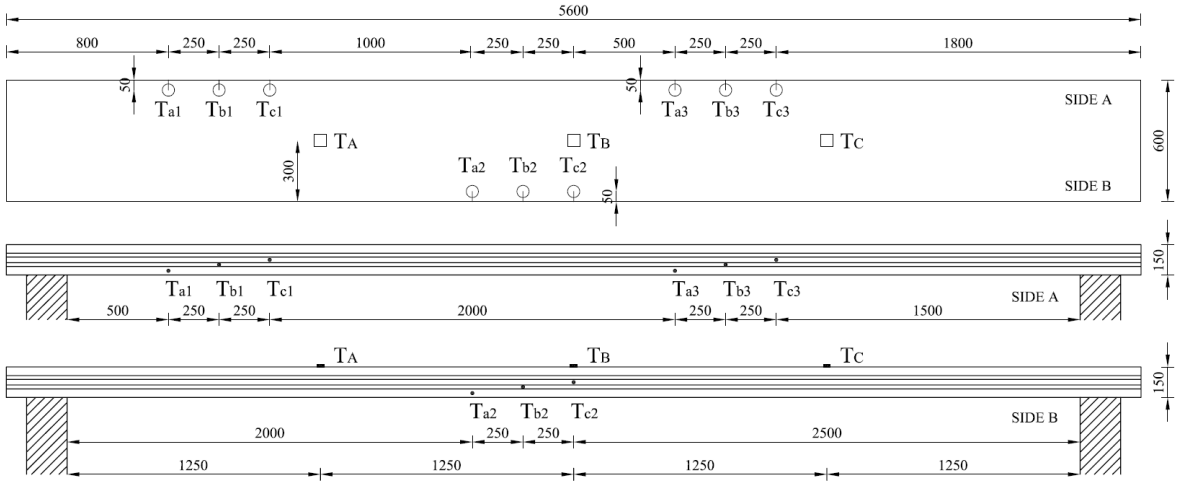

Fig. 5.19 - *Plane view of loaded specimens S1 and S2 (top) and longitudinal cross-sections (middle and bottom) of specimen S1 with thermocouple layout (dimensions in mm).*

The loaded and unprotected specimen S3-I was instrumented similarly to other loaded panels S1 and S2 (Fig. 5.20 and Fig. 5.21c). The temperatures were monitored in three cross-sections at different depths (21, 52 and 75 mm) from the exposed surface. Further three thermocouples (T_d) were inserted at 99 mm, i.e. in the middle of the fourth layer. Whereas no thermocouples were positioned on unexposed surface of specimens during the fire test No. 3.

The two unprotected and unloaded specimens S3-II and S3-V were instrumented with four thermocouples close to mid-span (T_{a2}, T_{b2}, T_{c2} and T_{d2}) at the same depths (21, 52, 75 and 99 mm) of loaded specimen S3-I (Fig. 5.20 and Fig. 5.21a,e).

Three thermocouples were placed in the protected and unloaded specimen S3-IV at 21, 52 and 75 mm from the bottom surface close to mid-span (T_{a2}, T_{b2} and T_{c2}), with two additional thermocouples placed at the GF-XLAM interface (T_i) (Fig. 5.20 and Fig. 5.21d). Lastly, the temperatures were monitored in specimen S3-III close to the mid-span at the depths of 52 and 75 mm (T_{b2} and T_{c2}), and at the GF-RW ($T_{i,1}$) and RW-XLAM ($T_{i,2}$) interfaces (Fig. 5.20 and Fig. 5.21b).

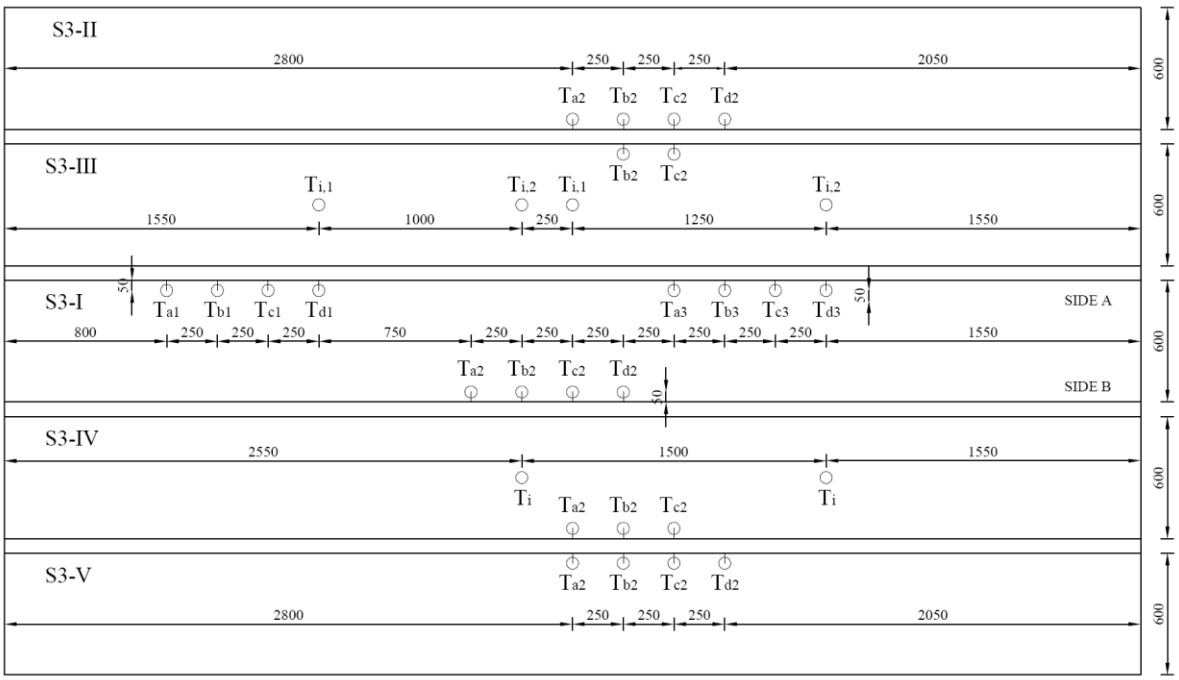

Fig. 5.20 - *Plane view of specimens during fire test No. 3 with thermocouple layout (dimensions in mm).*

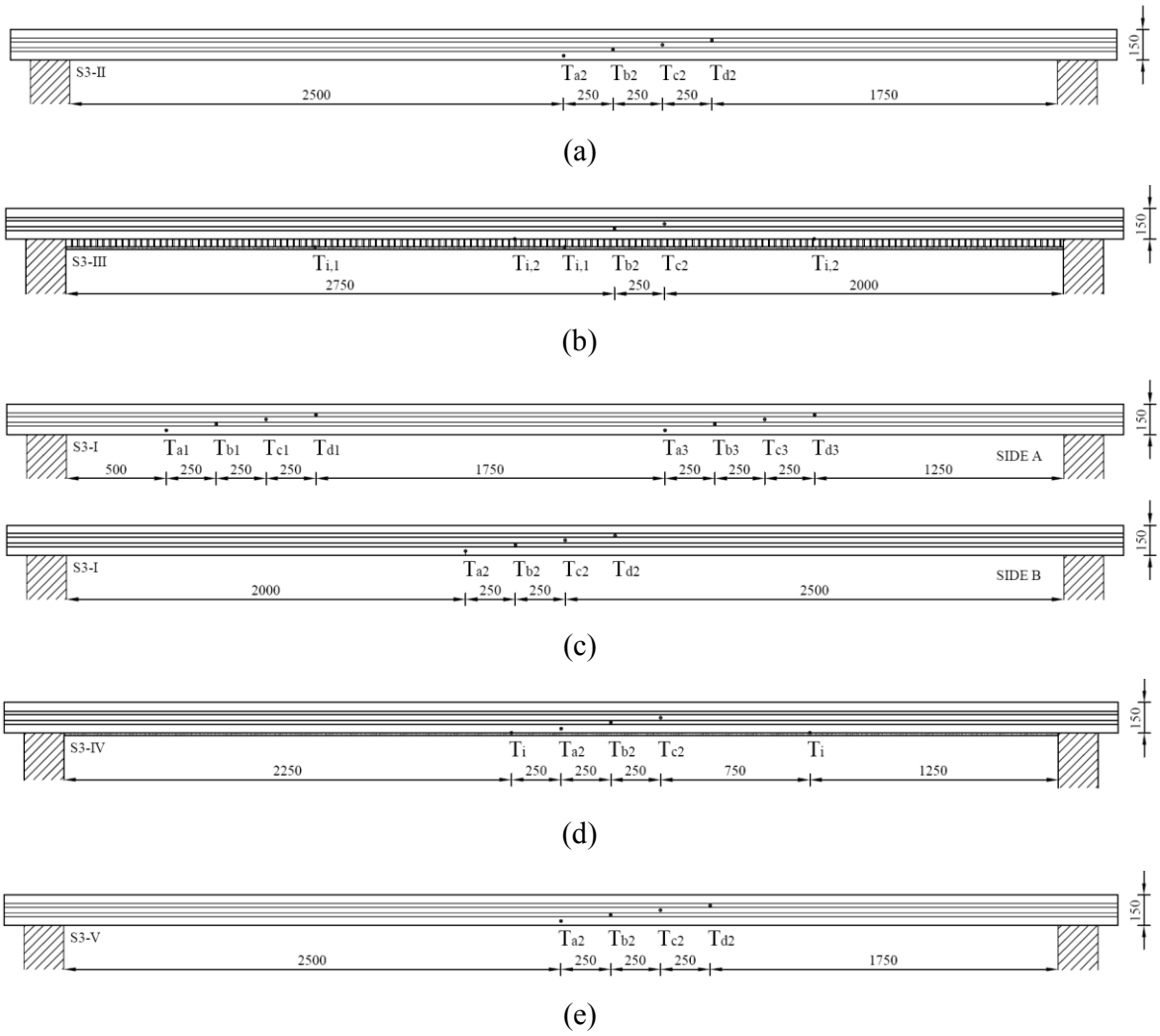

Fig. 5.21 - *Longitudinal cross-sections with thermocouple layout (dimensions in mm): (a) specimen S3-II; (b) specimen S3-III; (c) specimen S3-I; (d) specimen S3-IV; (e) specimen S3-V.*

The loaded specimens were laid on the furnace frame first, loaded on the unexposed surface next, and then subjected to the fire when the furnace was switched on (Fig. 5.22). The temperature in all thermocouples was monitored over time, and the mid-span deflection of the loaded panels was recorded using a LVDT.

Fig. 5.22 - *Some stages of large-scale fire tests.*

5.3.2. Experimental results

Fire resistance

Fire tests No. 1 and 2 were carried out until the collapse of the loaded panels (Fig. 5.23) that fell inside the furnace. Due to safety reasons, only some parts of the specimens could be removed, and therefore data on residual cross-sections are not available for these specimens (Fig. 5.24). The 99 min fire resistance found for specimen S1 is directly comparable with the failure time (100 min) obtained in Sweden on small-scale fire tests [Wilinder 2010]. The use of protective cladding made of 15 mm thick GP (type F) increased the fire resistance of specimen S2 to 110 min.

The third test was stopped before failure due to the high discharge of flames between specimens in order to avoid further equipment damage and to allow data collection of the residual cross-section (Table 5.3). The furnace was switched off and after about 16 min the imposed load was removed completely. Then the five specimens were removed one after another and extinguished with water (Fig. 5.25).

Table 5.3 summarizes the main results of the fire tests. Times of removal and extinguishing of panels were measured from the instant when the furnace was switched off.

Test No.	1	2	3	3	3	3	3
Specimen No.	S1	S2	S3-I	S3-II	S3-III	S3-IV	S3-V
Applied load [kN/m^2]	10	10	5	0	0	0	0
Protective cladding	no	yes	no	no	yes	yes	no
Ambient temperature [°C]	0	22	22	22	22	22	22
Test duration [min]	99	110	61	61	61	61	61
Failure	yes	yes	no	no	no	no	no
Removal time [min]	-	-	18.3	27.5	25.5	21.5	23.2
Extinguishing time [min]	-	-	19.4	28.3	26.2	22.3	24.2

Table 5.3 - *Summary of fire tests on XLAM panels.*

Fig. 5.23 - *Specimen S1 close to failure.*

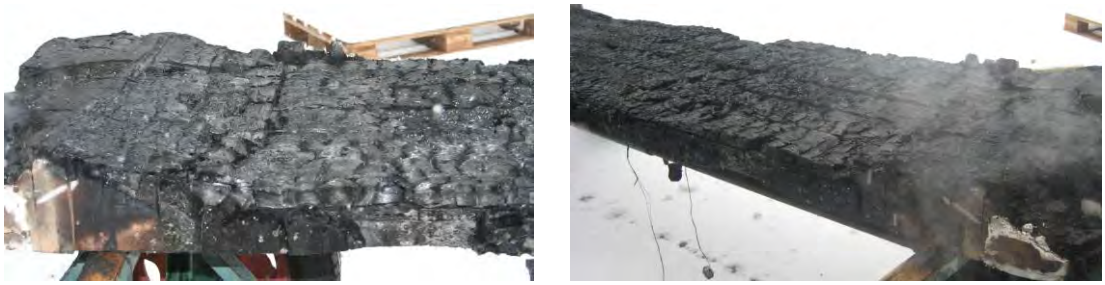

Fig. 5.24 - *Parts of specimen S1 after fire test.*

Fig. 5.25 - *Stages of fire test No. 3.*

Figure 5.26 displays the trend in time of the mid-span deflection of the panels uniformly loaded out-of-plane with 11 and 21% of the estimated failure load at ambient temperature. The significant reduction in deflection rate for the specimen subjected to the lower load level (specimen S3-I versus S1) can be clearly recognized. The effect of the protective cladding that caused a delay in the increase in deflection (specimen S2 versus S1) can also be noticed.

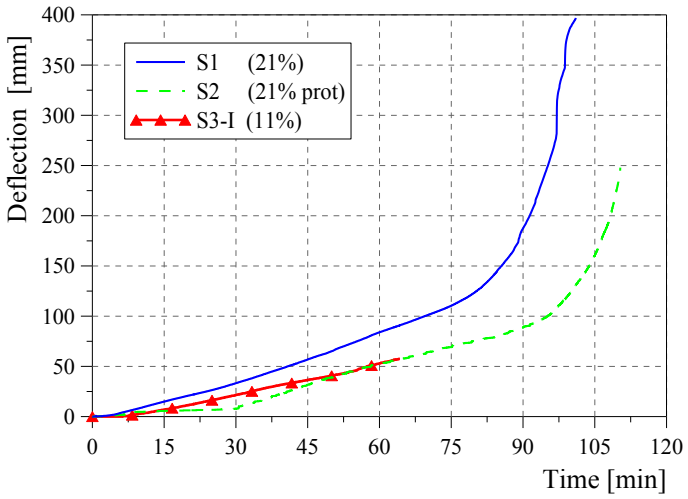

Fig. 5.26 - *Deflection of XLAM floor panels loaded out-of-plane and exposed to fire.*

Temperature distribution

Figure 5.27 shows the temperatures of loaded specimens S1 and S2 recorded by the thermocouples inserted at three different depths (21, 52 and 75 mm) and at GP-XLAM interface (T_d) of protected panel (S2). The experimental results of the thermocouples installed on the unexposed surfaces showed that the temperature remained constant throughout the tests and equal to the environmental value, demonstrating the excellent insulation properties of the panels.

Figure 5.28 plots the temperatures measured during the third test within unprotected specimens S3-I, S3-II and S3-V. The thermocouples located at 99 mm did not measure temperature variations respect to the ambient one. The thermocouple readings within timber cross-sections and at interfaces between timber and cladding of protected specimens S3-III and S3-IV are plotted in Figure 5.29. It can be noticed that the thermal state of timber cross-sections remained constant until 30 min and then it slightly changed but the temperature did not exceed 100°C throughout the test.

In all aforementioned figures, the experimental fire curves measured in the furnace during the tests are compared with the standard fire curve [ISO 834-1 1999]. The experimental curves ('Furnace') rose slower than the ISO curve until about 600°C. The 400°C temperature was reached about 2, 1.5 and 3 min later with respect to ISO curve during fire test No. 1, 2 and 3, respectively.

The temperatures at cladding-XLAM interfaces have a similar trend even if different insulating materials were used. The curves are characterized by a plateau around 100°C due to evaporation of water contained in gypsum, followed by a quick increase in temperature. A comparable thermal behaviour of GP and GF was observed also during fire tests performed at the Swiss Laboratories for Materials Testing and Research (EMPA) with the aim to investigate the fire behaviour of these protective claddings [Frangi et al. 2010b]. The rapid temperature increase behind claddings might indicate the falling of the protective layers that takes place when a temperature between 300°C and 600°C is attained. This temperature range is consistent with the suggested value of 400°C provided by a recent European guideline [SP Trätek 2010] for fire design of floor assemblies protected by type F GP or GF.

It can be noticed that the temperature at the GP-XLAM interface in specimen S2 rose slower than in specimens S3-III and S3-IV protected with GF (Fig. 5.30). The 300°C temperature was reached at the GP-XLAM interface about 40 min after the beginning of fire exposure, whereas the charring of panels protected with 15 mm thick GF and 12.5 mm thick GF plus 40 mm of RW started after approximately 32 and 27 min, respectively. This is in agreement with observations of Just et al. [2010] who found reduced failure times for wall cladding made of GF compared to type F GP.

Thermocouples between GF and RW ($T_{i,1}$ in Fig. 5.29a) in specimen S3-III recorded a temperature increment greater than at GF-XLAM interface (T_i in Fig. 5.29b) in panel S3-IV. This is mostly due to the different cladding thickness used in the two specimens. Furthermore, the temperature between RW and XLAM ($T_{i,2}$ in Fig. 5.29a) increased slowly until 100°C then it rose instantaneously to high values due to the GF failure and the consequent falling of RW that was not fixed to timber specimen. This is consistent with results of recent investigations on fire behaviour of GP and GF as protective claddings of timber structural elements, where the adverse contribution to the failure time of cladding of insulation in floor or wall cavities was highlighted with respect to assemblies with void cavities [Frangi at al. 2010b; Just et al. 2010].

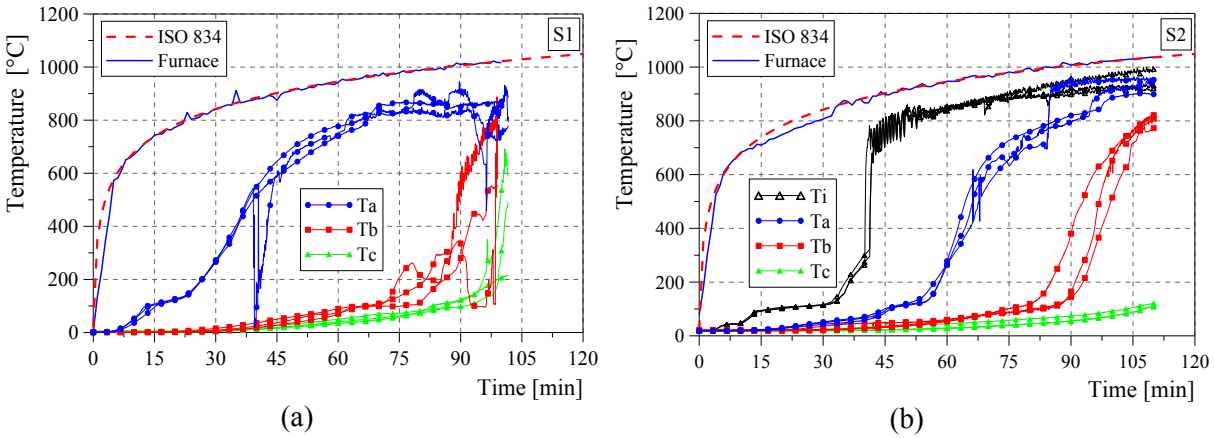

Fig. 5.27 - *Temperature distributions within unprotected and protected XLAM specimens S1 (a) and S2 (b) exposed to fire.*

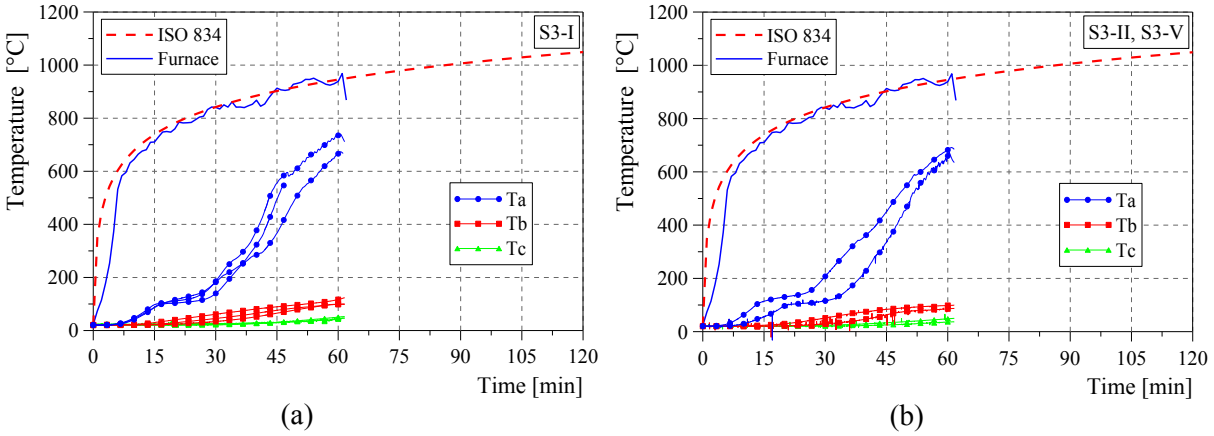

Fig. 5.28 - *Temperature distributions within unprotected XLAM specimens S3-I (a), and S3-II and S3-V (b) exposed to fire.*

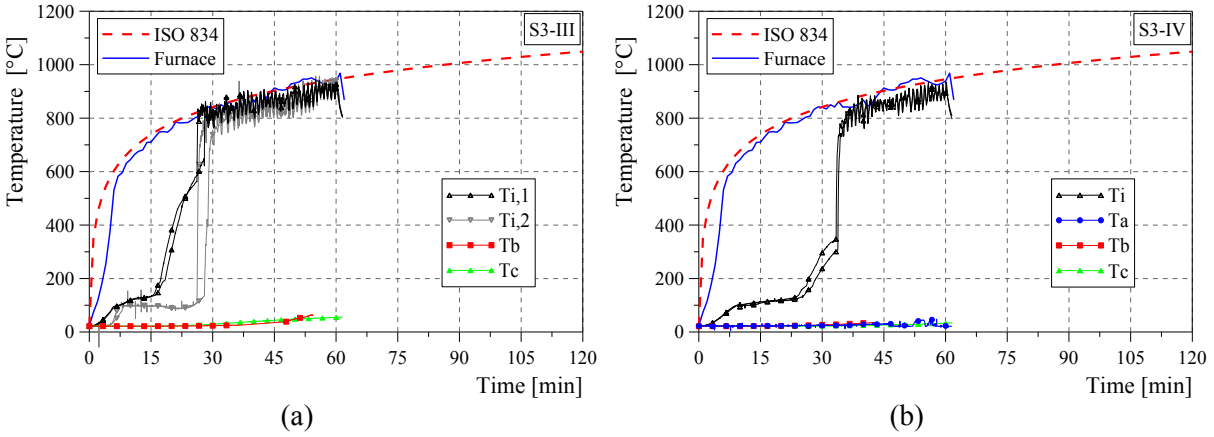

Fig. 5.29 - *Temperature distributions within protected XLAM specimens S3-III (a) and S3-IV (b) exposed to fire.*

The comparison between the temperatures recorded in protected and unprotected XLAM cross-sections (specimens S1 and S2) exposed to fire is presented in Figure 5.30b. The protective cladding leads to a delay in the beginning of wood charring as shown by thermocouples readings at 21 mm from the bottom surface of panel. This effect is reduced during the fire exposure due to the falling of the cladding. It was observed that the thermal states within specimens S1 and S2 were very similar after approximately 85 min of fire exposure.

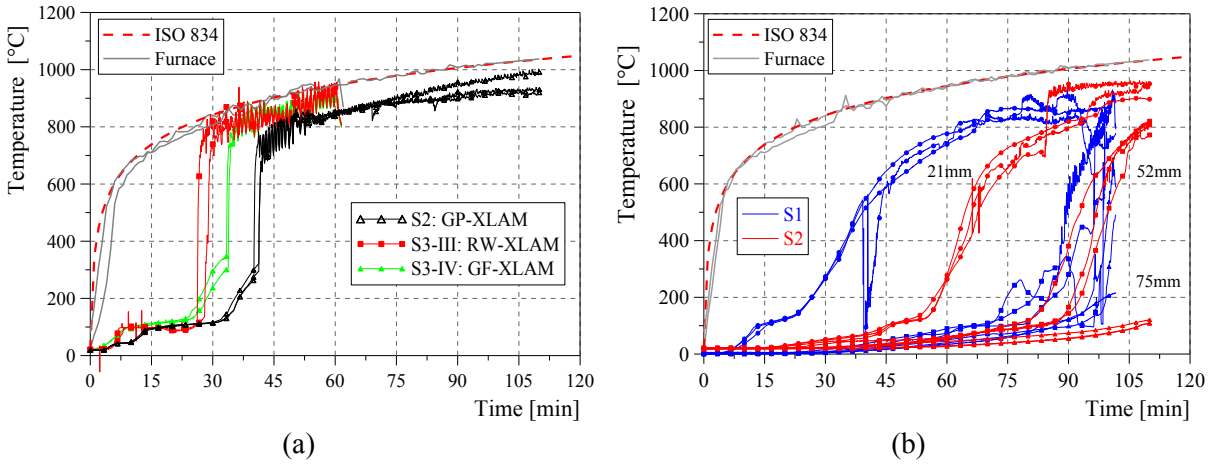

Fig. 5.30 - *Comparison of temperatures at cladding-XLAM interfaces (a) and within unprotected (S1) and protected (S2) XLAM panels (b).*

5.3.3. Charring rate

Evaluation via measurement of the residual cross-section

No data were collected on residual cross-sections of specimens S1 and S2 because they failed and fell inside the furnace.

At the end of fire test No. 3, all specimens were removed from furnace and extinguished with water to stop the charring. Then the charred material was removed from panels that were sawn in four parts. The residual cross-sections of specimens were measured in the transversal and longitudinal directions every 10 and 50 mm respectively (Fig.5.31). Figures 5.32, 5.33 and 5.34 show the specimens and their cross-sections after the fire exposure. Table 5.4 reports the measured residual sections of protected and unprotected specimens. The mean residual cross-section of the three unprotected panels was about 98 mm corresponding to 65.3% of the initial panel depth (150 mm). The difference in the two directions was less than 1.5 mm. The mean residual cross-section of the two protected panels was 107.5 mm corresponding to 71.6% of the initial panel depth (150 mm). The difference in the two directions was about 1.2 mm. The mean residual cross-sections of unprotected and protected specimens differ of approximately 6% because the protective layers delay the beginning of charring in timber elements. It can be noticed that the specimen protected only with GF (S3-IV) had a residual section of about 111 mm depth, slightly larger than that of the panel protected with GF and RW (S3-III).

Specimen No.	Protective cladding	Residual section			
		Longitudinal	Transversal	Mean value	
		[mm]	[mm]	[mm]	[-]
S3-I	no	95.88	97.49	96.68	64%
S3-II	no	97.67	98.88	98.28	66%
S3-III	yes	102.11	107.26	104.68	70%
S3-IV	yes	110.84	109.59	110.22	73%
S3-V	no	98.03	99.54	98.78	66%

Table 5.4 - *Measured residual cross-sections of unprotected and protected specimens exposed to fire during test No. 3.*

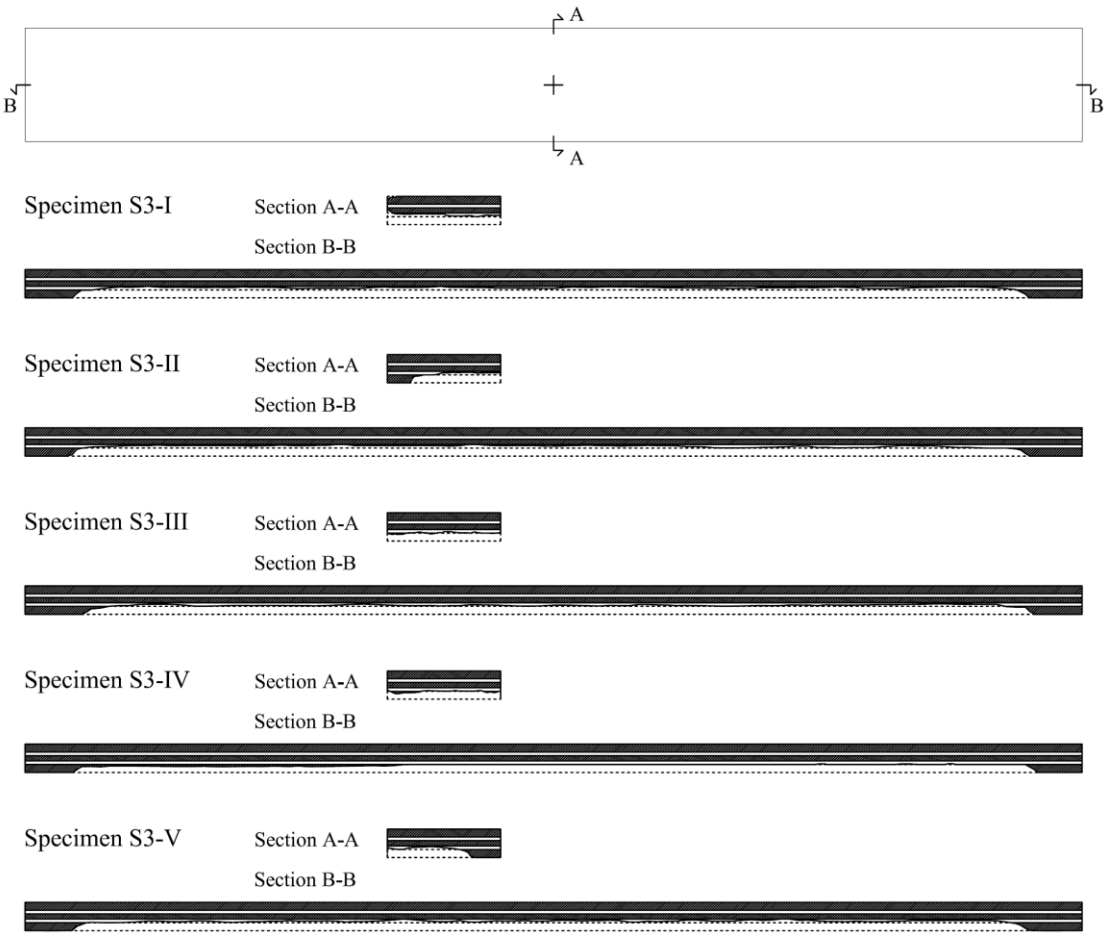

Fig. 5.31 - *Residual cross-sections of unprotected and protected specimens.*

Fig. 5.32 - *Unprotected specimen S3-I after fire exposure.*

Fig. 5.33 - *Unprotected specimens S3-II and S3-V after fire exposure.*

Fig. 5.34 - *Protected specimens S3-III and S3-IV after fire exposure.*

The charring rates β_0 reported in Table 5.5 were calculated considering the duration of fire test t_f and the time necessary to remove (t_r) and extinguish (t_e) the panels, namely:

$$\beta_0 = (d\text{-}d_r)/(t_f + t_r + t_e) \qquad [5.4]$$

where d and d_r signify the initial and mean residual depths of the panel, respectively.

Specimen No.	Time [min]	β_0 [mm/min]
S3-I	80.44	0.66
S3-II	89.26	0.58
S3-III	87.22	0.52
S3-IV	83.34	0.48
S3-V	85.18	0.60

Table 5.5 - *Charring rate evaluation via measurement of the residual cross-section for unprotected and protected specimens.*

The charring rate of the loaded specimen S3-I is similar to the value of 0.65 mm/min proposed by Eurocode 5, Part 1-2 [CEN 2004] for solid and glued laminated timber under 1D standard fire exposure. The low charring rates of specimens S3-II and S3-V can be justified considering that they were removed and extinguished as the last and third panel, respectively, and therefore they burned longer than the other specimen (S3-I) at a lower rate when the furnace was switched off. The presence of protective layers delays the beginning of charring specimens S3-III and S3-IV, thus leading to lower charring rates.

Evaluation via thermocouple readings

The charred depth (d - d_r) of all tested specimens can be obtained also indirectly from data recorded by thermocouples at different depths in the cross-section. The 300°C isotherm is assumed as the border between charred and heated wood as suggested by Eurocode 5, Part 1-2 [CEN 2004].

Table 5.6 reports the charring rate β_0 calculated as the displacement rate of the 300°C isotherm in the cross-sections of unprotected (S1) and protected with GP (S2) XLAM panels. The 300°C isotherm reached only one of the three thermocouples in specimen S1 at 75 mm depth from the exposed surface approximately one minute before the panel collapsed inside the furnace. The temperature increase at that depth and the consequent high charring rate might be caused by cracking of the specimen close to mid-

span, where the thermocouple (T_{c2} in Fig. 5.20 and Fig. 5.21c) was located, since the residual cross-section, estimated as 75 mm, was not able to bear the applied load. Moreover this was inserted at approximately 50 mm from the lateral side of the specimen where the protective layers made of wood and GP were fixed to ensure the 1D heat flux. In the last minutes of the fire test, however, some flames went into the gap between the specimen and the lateral cladding due to the high panel deformation, the cracking of the protective layers, the charring of the wood layer and possible pull out of screws. This event might have caused the increase in temperature measured by the thermocouple (Fig. 5.27a) because the residual cross-section of specimen S1 was subjected to a two-dimensional (2D) heat flux coming from the bottom and the side of the panel.

The cladding of specimen S2 delayed the charring at the depths of 21 and 52 mm of about 30 and 4 min, respectively, compared to the unprotected specimen S1. This comparison can be done since the fire curves during the tests were similar. The mean charring rate can be estimated as 1 mm/min assuming the start of charring at 40 min, when the temperature of 300°C was attained at the cladding-XLAM interface. The calculated value is high as the charring began at the time of the probable cladding failure, therefore the XLAM panel was directly exposed to a much higher furnace temperature than it would have been if it had been unprotected.

Specimen S1			Specimen S2		
Time [min]	$d - d_r$ [mm]	β_0 [mm/min]	Time [min]	$d - d_r$ [mm]	β_0 [mm/min]
0	0	0	40.1	0	0
31.4	21	0.67	61.0	21	1.00
88.2	52	0.58	92.4	52	0.99
97.8	75	0.77	-	75	-

Table 5.6 - *Charring rate evaluation via thermocouple readings for unprotected (left) and protected (right) specimens.*

The charring progress in unprotected specimens (S3-I, S3-II and S3-V) during test No. 3 was measured only by thermocouples at 21 mm distance from the bottom fibre of the panel due to the short fire exposure. For the same reason no thermocouples inserted

in protected panels (S3-III and S3-IV) collected data on charring. However the first layers of protected panels appeared to have charred when the residual cross-sections were measured at end of tests (Table 5.4 and Fig. 5.34). The thermocouples recorded the temperature until the end of test but the panel continued charring until their removal and extinguishing (Table 5.3). The 300°C isotherm reached the RW-XLAM interface in S3-III and the GF-XLAM interface in S3-IV after about 27 and 32 min of fire exposure, respectively. The corresponding charring rates calculated from the measured residual cross-sections (Table 5.4) considering the technical time to remove and extinguish the specimens, and assuming charring began when the 300°C isotherm reached the cladding-XLAM interface are 0.76 and 0.77 mm/min for specimen S3-III and S3-IV, respectively.

The average charring rates for unprotected panels S3-I, S3-II and S3-V calculated indirectly from thermocouple readings at 21 mm from the exposed surface are reported in Table 5.7. These charring rates are lower than the values obtained from the residual cross-section (Table 5.4).

Specimen No.	Time [min]	$d - d_r$ [mm]	β_0 [mm/min]
S3-I	39.17	21	0.54
S3-II	43.47	21	0.48
S3-V	35.43	21	0.59

Table 5.7 - *Charring rate evaluation via thermocouple readings for unprotected specimens during test No. 3.*

Discussion

Figure 5.35 plots the charred depths of unprotected panels obtained indirectly from thermocouple readings (solid symbols) and directly from residual cross-section measurements (empty symbols) versus time. The dashed curve represents the charred depth calculated assuming the constant 1D charring rate β_0 = 0.65 mm/min proposed by Eurocode 5, Part 1-2 [CEN 2004].

The charring rate values determined, directly and indirectly, from experimental data collected during the fire tests at CNR-IVALSA might have be influenced by several parameters, including: (i) the slower initial temperature rise in the furnace compared to a

standard fire exposure; (ii) the specimen position in the furnace frame; and (iii) the time required at end of the tests to extinguish the specimens in order to stop the charring.
Charring rates close to the Eurocode value were obtained in fire tests carried out by another author on reduced scale specimens made from the same XLAM product exposed to standard fire curve [Wilinder 2010].

Experimental research on XLAM panels exposed to fire pointed out that a considerable increase in charring rate occurred during the fire test due to the falling-off of charred layers and the consequent direct exposure to fire of un-charred wood [Frangi et al. 2009a,b]. This phenomenon was observed only for XLAM panels manufactured with five different PU adhesives, whereas the charred layers did not fall off in specimens produced using MUF adhesives. During the tests presented in this chapter, there was no possibility to take observations inside the furnace in order to identify the possible falling of charred layers. The collected experimental data did not evidence any quick temperature increases indicating the falling-off of charred layers even if a PU adhesive was used to manufacture the tested panels. It should be pointed out, however, that to draw final conclusions on this issue it would be necessary to repeat other tests with thermocouples located at the glued interface between laminations.

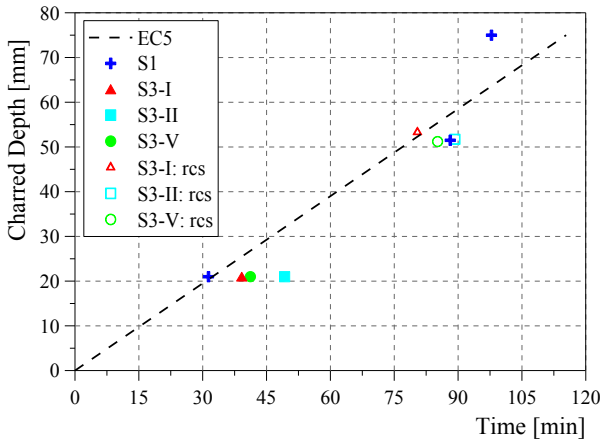

Fig. 5.35 - *Charred depth vs. time for unprotected specimens from thermocouple readings, from residual cross-section (rcs) measurements, and from Eurocode 5 (EC5).*

5.4. ANALYTICAL-EXPERIMENTAL COMPARISONS

The Eurocode 5, Part 1-2 [CEN 2004] provides two methods to evaluate the fire resistance of timber structural elements: (i) the 'reduced cross-section method' (RCSM); and (ii) the 'reduced properties method'. The former approach is the simplified method for fire design of XLAM floors since the latter method cannot be used for timber slabs [König 2005]. According to RCSM, an effective cross-section with unchanged mechanical properties is calculated by reducing the real residual cross-section to estimate the fire resistance of timber elements exposed to fire.

Recent experimental research has shown that the fire behaviour of XLAM panels depends upon the behaviour of the single layers, and two limit cases should be considered [Frangi et al. 2009a,b]: (i) the charred layer protects the inner layers and slows down the heat transmission in the panel; and (ii) the charred layer falls off and exposes the remaining inner layers directly to fire. In the first case, the XLAM panel can be considered as a thermally homogenous timber panel, whereas the second case can be compared with an initially protected timber structure where an increase in charring rate occurs when the cladding falls off. The falling-off of the charred timber layer mainly depends upon the type of adhesive, the number and thickness of layers. As mentioned previously, experimental data recorded in these tests does not provide evidence of the occurrence of this phenomenon, therefore only the first case was considered in these analytical predictions.

Although Eurocode 5 does not provide charring rates for XLAM panels, the value β_0 = 0.65 mm/min for solid and glued laminated timber exposed to 1D standard fire exposure [ISO 834-1 1999] was adopted to calculate the charring depth $d_{char,0}$:

$$d_{char,0} = \beta_0 t \qquad [5.5]$$

where t is the time of fire exposure in min.

Further, a 'zero-strength' layer of $k_0 d_0$ thickness characterized by neither strength nor stiffness has to be considered in addition to the charred depth $d_{char,0}$ in order to compute the effective cross-section d_{ef} according to RCSM (Fig. 5.36a):

$$d_{ef} = d_{char,0} + k_0 d_0 \qquad [5.6]$$

where d_0 and k_0 are a constant of 7 mm and a time-dependent coefficient, respectively.

Different laws for unprotected and protected timber elements are supplied by Eurocode 5 to determine the linear variation of k_0 with the fire exposure time (Fig. 5.37).
If the charring of initially protected timber elements starts before 20 min of fire exposure ($t_{ch} \leq 20$ min), the same k_0 variation adopted for unprotected has to be used (Fig. 5.37a).

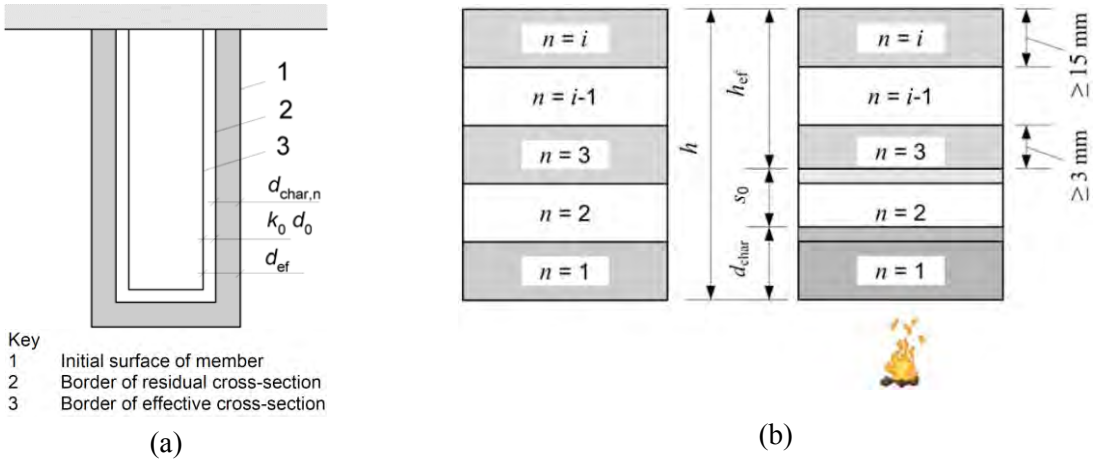

(a) (b)

Fig. 5.36 - *(a) 'Reduced cross-section method' [CEN 2004] and (b) the recent adaptation to XLAM panels [SP Trätek 2010].*

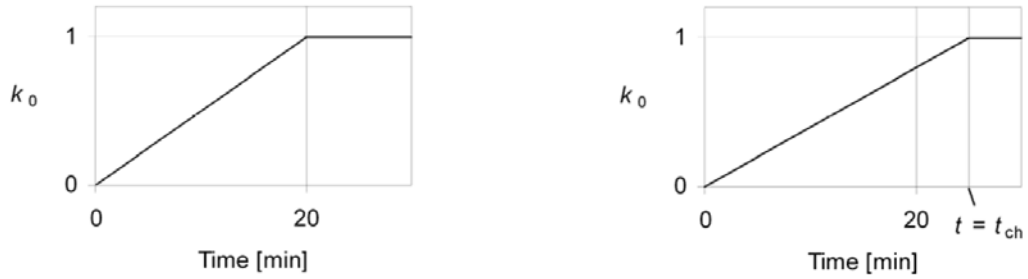

(a) (b)

Fig. 5.37 - *Variations of k_0 for unprotected elements and protected elements where $t_{ch} \leq 20$ min (a) and for protected elements where $t_{ch} > 20$ min [CEN 2004].*

The Eurocode 5 does not propose specific variations to consider different wood-based products such as XLAM rather than solid timber, different structural elements like floors or walls, and different stress distributions. Recent research has demonstrated that non-conservative predictions of XLAM resistance can be made by adopting a constant 'zero-strength' layer for any panel section and stress condition [Schmid and König 2010]. A new design method to evaluate this layer, the so-called 'compensating layer' s_0, for XLAM panels is suggested depending upon the number of layers, the thickness of

panel, the type of stress on the exposed side, the type of structure (wall or floor), and whether or not a protective cladding is used [Schmid and König 2010; SP Trätek 2010] (Fig. 5.36b). The fire resistance of XLAM panels is not linearly dependent upon the charred depth since their structural behaviour is affected by the layer direction and number of layers [Frangi et al. 2009a].

Table 5.8 reports the estimated failure times of unprotected and protected XLAM floor panels subjected to 1D fire exposure using the simplified Eurocode method (RCSM) and the newly developed adaptation to XLAM panels (RCSM for XLAM) [Schmid and König 2010, SP Trätek 2010]. In the latter method, the quantity s_0 was calculated with the formulas:

$$s_0 = \frac{h}{100} + 10 \qquad [5.7]$$

$$s_0 = \frac{h}{35} + 6 \qquad [5.8]$$

where h is the panel thickness in mm. These formulas can be used for unprotected (Eq. (5.7)) and protected (Eq. (5.8)) XLAM floor panels with five layers and the tension side exposed to fire to compute their effective cross-section d_{ef} according to Eq. (5.6). In this case the compensating layer' s_0 is adopted instead of the constant d_0.

XLAM panel	Unprotected		Protected	
Load level	11%	21%	11%	21%
RCSM	118 min	103 min	127 min	112 min
RCSM for XLAM	111 min	96 min	122 min	107 min
Experimental	-	99 min	-	110 min

Table 5.8 - *Analytical-experimental comparison of the fire resistance of unprotected and protected XLAM floor panels.*

The predictions of the fire resistance are made based on the uniformly distributed load levels used in fire tests and considering or not the presence of a protective cladding. The two inner layers in the direction perpendicular to face grain are conservatively neglected due to their lower stiffness. Furthermore, it is assumed that 3 mm is the minimum thickness of the charred layers [SP Trätek 2010], below which the strength and stiffness of the layers are neglected.

Two different situations have to be analyzed for initially protected elements according to Eurocode 5: wood charring (t_{ch}) starting when cladding failure occurs (t_f) (Fig. 5.38a) or before that time (Fig. 5.38b).

The first case ($t_{ch} = t_f$) was considered in the estimation of fire resistance for XLAM floors protected with a 15 mm layer of GP. The analysis of experimental data in terms of temperature within specimen S2 (Figure 5.27b) shows in fact that the charring temperature (300°C) and the hypothetical collapse temperature of floor cladding (400°C) were reached at the GP-timber interface approximately at the same time, namely 40 min from the onset of the fire test. In the analytical evaluations reported in Table 5.8 it is assumed that charring starts at 28 min as calculated using the conservative formula proposed by Eurocode 5:

$$t_{ch} = 2.8h_p - 14 \qquad [5.9]$$

where h_p is the thickness of the protective layer in mm. In the case under study, a 15 mm thick GP layer was used. The fire resistance increases of about 11% if the experimental time of 40 min is considered.

Analytical predictions were performed also with RCSM for XLAM adopting s_0 calculated with Eq. (5.8) for protected floors as recommended in recent guidelines for fire design [SP Trätek 2010].

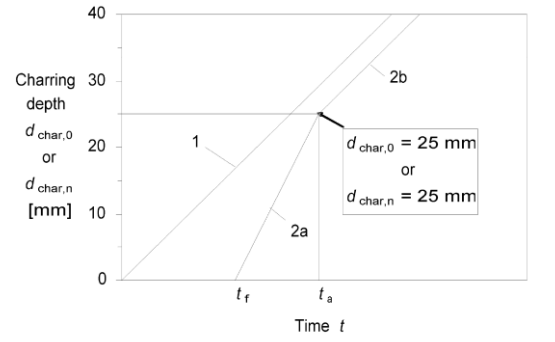

Key:
1 Relationship for members unprotected throughout the time of fire exposure for charring rate β_n (or β_0)
2 Relationship for initially protected members after failure of the fire protection
2a After the fire protection has fallen off, charring starts at increased rate
2b After char depth exceeds 25 mm charring rate reduces to the rate shown in table 3.1

(a)

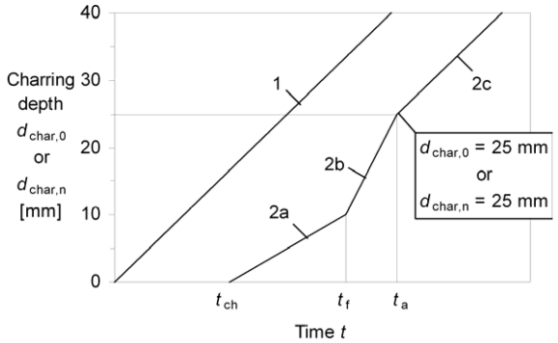

Key:
1 Relationship for members unprotected throughout the time of fire exposure for charring rate β_n (or β_0)
2 Relationship for initially protected members where charring starts before failure of protection:
2a Charring starts at t_{ch} at a reduced rate when protection is still in place
2b After protection has fallen off, charring starts at increased rate
2c After char depth exceeds 25 mm charring rate reduces to the rate shown in table 3.1

(b)

Fig. 5.38 - *Variation of charred depth vs. time when $t_{ch} = t_f$ (a) and $t_{ch} < t_f$ (b) for initially protected timber elements as suggested by Eurocode 5 [CEN 2004].*

The predictions of fire resistance for unprotected and protected elements using the RCSM are about 6.5% and 4.2% higher, respectively, than the values obtained with the recent extension of the RCSM to XLAM. The latter method also provides conservative predictions compared with the failure times of specimens during the experimental tests.

The fire resistance of the unprotected XLAM specimen S1 was calculated also assuming the charring rates β_0 evaluated indirectly from thermocouple readings (Table 5.6) to take the variation of heat flux from 1D to 2D into account. In particular, the charring rate values β_0 = 0.58 mm/min and β_0 = 2.4 mm/min were adopted before and after approximately 88 min of fire exposure, respectively. The charring rate in the last minutes of fire test was very high. The charred depth increased of 23 mm in less than 10 min, whereas the same depth would have charred after about 35 min assuming the constant Eurocode value β_0 = 0.65 mm/min. The failure times of XLAM panels loaded with 11% and 21% of the failure load at ambient temperature predicted using the experimental charring rate and the RCSM are 99 and 95 min, respectively. These estimations are conservative with respect to experimental results.

Figure 5.39 compares the experimental charred depths of unprotected (S1) and protected (S2) XLAM specimens obtained indirectly from thermocouple readings (Table 5.6) with the analytical predictions (dashed curves). The analytical curve for unprotected timber elements was determined assuming the constant charring rate β_0 = 0.65 mm/min proposed by Eurocode 5. Both the cases suggested by Eurocode 5 for initially protected timber member, namely start of wood charring at the cladding failure or before that time (Fig. 5.38), were considered. When the protective cladding falls off ($t_{ch} = t_f$), the charring starts at a double rate with respect to the value β_0 for initially unprotected elements since the timber element is directly exposed to high temperatures. The charring slows down when the charred depth exceeds 25 mm and the charring rate for initially unprotected elements β_0 = 0.65 mm/min can be assumed. If the charring begins before the cladding failure ($t_{ch} < t_f$), the initial charring rate is lower than the value for unprotected elements until the falling-off of protective layers occurs. The experimental results clearly show the delayed start of timber charring due to the presence of the cladding. It can be noticed that the experimental charring rate after the cladding failure is high throughout the fire test and it does not decrease when the charred depth is greater than 25 mm as assumed in the analytical predictions.

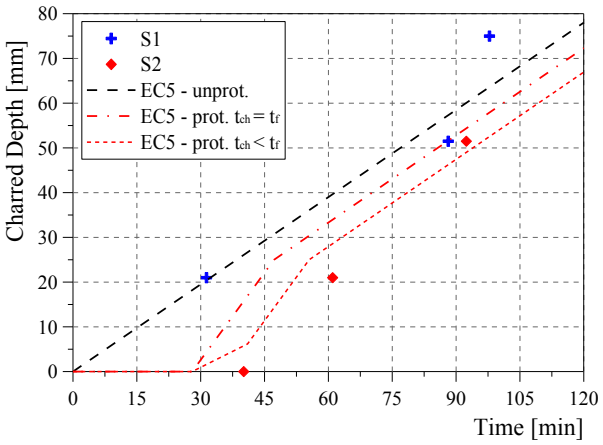

Fig. 5.39 - *Experimental and analytical charred depths vs. time for unprotected (S1) and protected (S2) XLAM specimens.*

Figure 5.40 plots the experimental deflection of loaded unprotected (S1 and S3-I) and protected (S2) specimens during the fire tests and the analytical estimations using RCSM and RCSM for XLAM. The deflection was calculated with the formula:

$$f = \frac{5}{384}\frac{ql^4}{EJ_{res}} \qquad [5.10]$$

where J_{res} is the second moment of area of the residual, resistant cross-section, q, l and E signify respectively the uniformly distributed applied load, the specimen span length and the Young's modulus.

The intermediate plateau of the analytical curves corresponds to the charring of the second (from the bottom surface), non load-bearing layer of the XLAM section.

The experimental curves measured during fire tests No. 1 and 3 are well approximated by the analytical estimations especially in the first 60 min of fire exposure (Fig. 5.40a). After that time, both analytical methods do not provide conservative predictions of deflection. Specimen S1 had a quick increment of displacement due to the 2D fire exposure that occurred before its failure. The deflection of protected specimen S2 is estimated with the same assumptions of t_{ch} e t_f adopted to calculate the fire resistance (Fig. 5.40b). The experimental curve is almost in the middle between the two analytical predictions, with the RCSM for XLAM method providing conservative estimations.

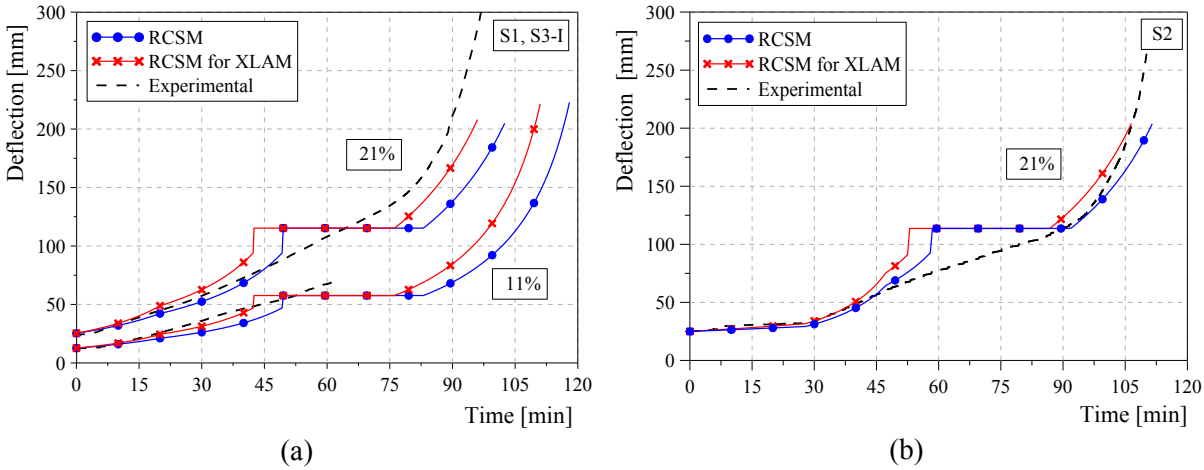

Fig. 5.40 - *Experimental-analytical comparisons of deflection of unprotected (a) and protected specimens (b) during the fire tests.*

CHAPTER 6.

NUMERICAL ANALYSES: UNPROTECTED PANELS

6.1. INTRODUCTION

The fire behaviour of structural timber elements is an important research topic in order to ensure the attainment of the required safety level in timber buildings. Several experimental investigations have been carried out on different wood products, such as laminated veneer lumber [e.g. Menis 2008; Tsai 2010], glued laminated timber [e.g. Yang et al. 2009a] and cross-laminated timber (XLAM) [e.g. Frangi at el. 2009a,b; Friquin 2010; Wilinder 2010]. Small- and large-scale tests were performed on loaded and unloaded specimens subjected to one- or two-dimensional heat fluxes in furnaces of different sizes.

The need for simple design methods has led to the development of analytical approaches [e.g. AWC 2003; CEN 2004; Frangi and Erchinger 2007] that need calibration on results of experimental tests which, however, are very expensive. It is therefore of interest to develop robust numerical models that can be used to extend the few experimental results available to different configurations (e.g. the specimen size) and/or load conditions. Some numerical models implemented in different software packages are already available in literature [e.g. Bobacz 2006; Franssen 2005; Mirianon et al. 2008; Takeda and Mehaffey 1998]. Thermal and mechanical simulations allow investigation of the effects caused by the fire exposure and the external loads on structural elements. The models, validated on experimental data, were used to investigate the behaviour of connections between timber members in fire conditions [e.g. Erchinger et al. 2010; Peng 2010; Racher et al. 2010], the influence of a particular adhesive on the fire resistance of wood elements [Klippel et al. 2011] and the performance of protected

elements [e.g. Bénichou et al. 2002; Frangi and Erchinger 2007; Lu et al. 2010; Teibinger and Matzinger 2010].

Current codes of practice such as Eurocode 5 Part 1-2 [CEN 2004] provide specific indications on advanced calculation methods, including thermal and mechanical properties of timber as a function of temperature. However, no specific information on XLAM is reported in this code. Some numerical simulations on XLAM panels were recently carried out to investigate their fire behaviour. Thermal and structural analyses were performed on protected and unprotected XLAM elements loaded in bending and subjected to one-dimensional fire exposure on tension or compression side [Schmid and König 2010]. Different depths, layer thicknesses and layer numbers of the XLAM cross-section were considered. Numerical predictions of fire resistance were compared with analytical estimations and experimental data. Comparisons of the numerical thermal behaviour of 3- and 5-layer XLAM and homogeneous timber panels exposed to standard fire [ISO 834-1 1999] on one side were also carried out [Frangi et al. 2009b; König and Schmid 2007]. Frangi et al. [2009b] assumed in their model of XLAM panel that the charred layers fell off due to the use of a polyurethane adhesive. This event caused the increase in charring rate due to the direct exposure of wood to fire in the absence of the protective char layer. The numerical results pointed out the influence of the number and thickness of layers on the fire behaviour of XLAM panels. The experimental charring depths measured after fire tests of small and large XLAM specimens were compared with the numerical predictions of residual cross-sections.

This chapter presents a numerical model implemented in the finite element code Abaqus. Thermal and mechanical analyses were carried out to simulate the bending tests at ambient temperature and the large-scale fire tests performed on unprotected XLAM floors and described in Chapter 5. The numerical results in terms of temperature, stress, deflection and fire resistance are discussed and compared with the experimental data and analytical predictions using simplified design methods.

6.2. MECHANICAL ANALYSIS AT AMBIENT CONDITIONS

A two-dimensional (2D) numerical model was implemented in the general purpose software package Abaqus [ABAQUS v.6.9]. The aim was to simulate the four-point bending tests at ambient temperature performed at Ivalsa Trees and Timber Institute (CNR-IVALSA) in San Michele all'Adige (Italy) on 5-layer XLAM floor panels of series 'S' (Chapter 5). The simply-supported specimens had a cross-section of 150×600 mm and a length of 5600 mm. The thicknesses of the five layers were 42, 19, 28, 19 and 42 mm.

Only half of the specimen longitudinal section was modelled in Abaqus due to material, restraint and load symmetry (Fig. 6.1). The out-of-plane concentrated load P_i was applied at the third point of the specimen and monotonically increased to failure, which is attained when the numerical convergence is no longer found. A simple support was defined on one end of the model, whilst on the other end, corresponding to the symmetry plane, a constraint that allows only the vertical displacement was imposed.

A mesh of 6240 linear quadrilateral elements type 'CPS4' of approximately 7×10 and 4.75×10 mm size for layers parallel and perpendicular to the main floor direction, respectively, was chosen (Fig. 6.2).

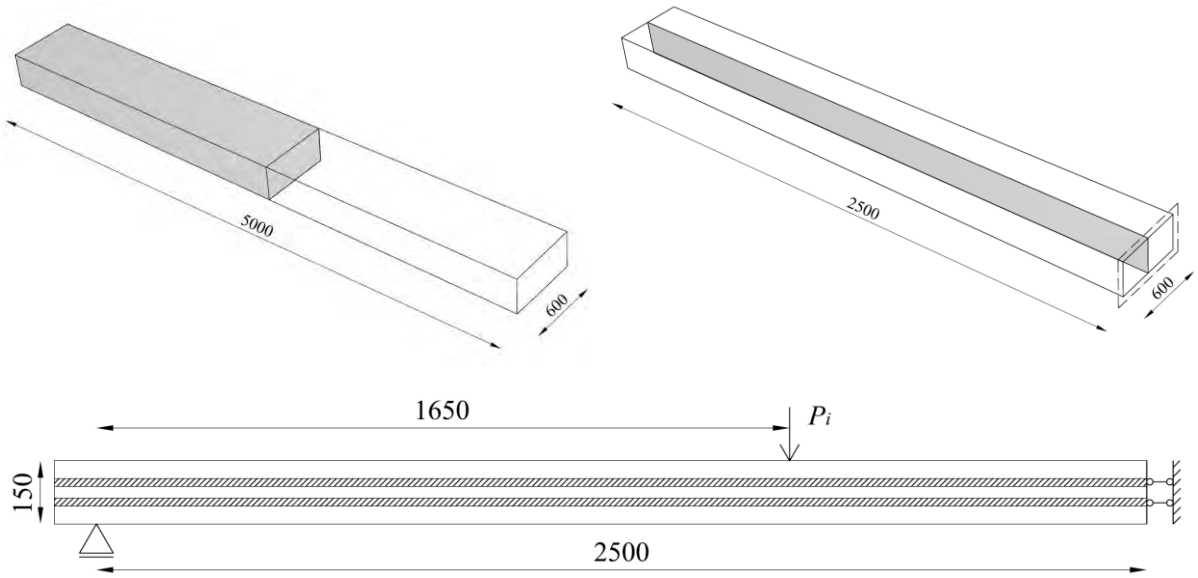

Fig. 6.1 *- Geometry of specimens and two-dimensional model implemented in Abaqus to simulate tests at ambient conditions (dimensions in mm).*

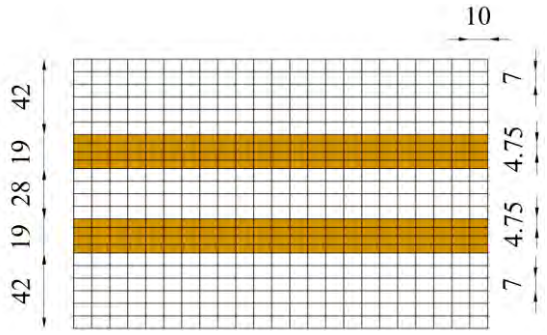

Fig. 6.2 *- Mesh adopted to model the longitudinal section of specimens tested at ambient conditions (dimensions in mm).*

The compound cross-section of XLAM panels was described in Abaqus by defining two different materials for layers parallel and perpendicular to the main floor direction. The materials were initially assumed as linear-elastic, and both hypotheses of orthotropic and isotropic behaviour were investigated. For orthotropic behaviour, the Young's moduli E, the shear moduli G and the Poisson's ratios υ in the longitudinal ('L'), radial ('R') and tangential ('T') directions suggested by Mirianon et al. [2008] were used (Table 6.1). For isotropic behaviour, a fictitious Young's modulus of 120 N/mm^2 was calculated for the layers perpendicular to the main floor direction based on a rolling shear modulus of 40 N/mm^2, whereas the actual Young's modulus parallel to the grain was used for the other layers. Poisson's ratios of 0.3 and 0.5 were adopted in the layers parallel and perpendicular to the main floor direction, respectively (Table 6.2).

Parallel and perpendicular layers	
E_L [N/mm^2]	12000
E_R [N/mm^2]	600
E_T [N/mm^2]	600
G_{LR} [N/mm^2]	700
G_{LT} [N/mm^2]	700
G_{RT} [N/mm^2]	40
υ_{RL} [-]	0.038
υ_{RT} [-]	0.558
υ_{TR} [-]	0.015

Table 6.1 *- Elastic constants for wood as an orthotropic material [Mirianon et al. 2008].*

Layers	Parallel	Perpendicular
E [N/mm^2]	12000	120
υ [-]	0.3	0.5

Table 6.2 - *Elastic constants for wood as an isotropic material.*

The stress distribution along the panel depth and the mid-span deflection obtained by assuming the materials as isotropic and orthotropic are plotted in Figure 6.3. Given the similarity of results, the isotropic behaviour was chosen as it allows the use of non-linear mechanical models such as the 'concrete damaged plasticity' (CDP) readily available in the Abaqus library, which would otherwise not be possible if an orthotropic material model was used.

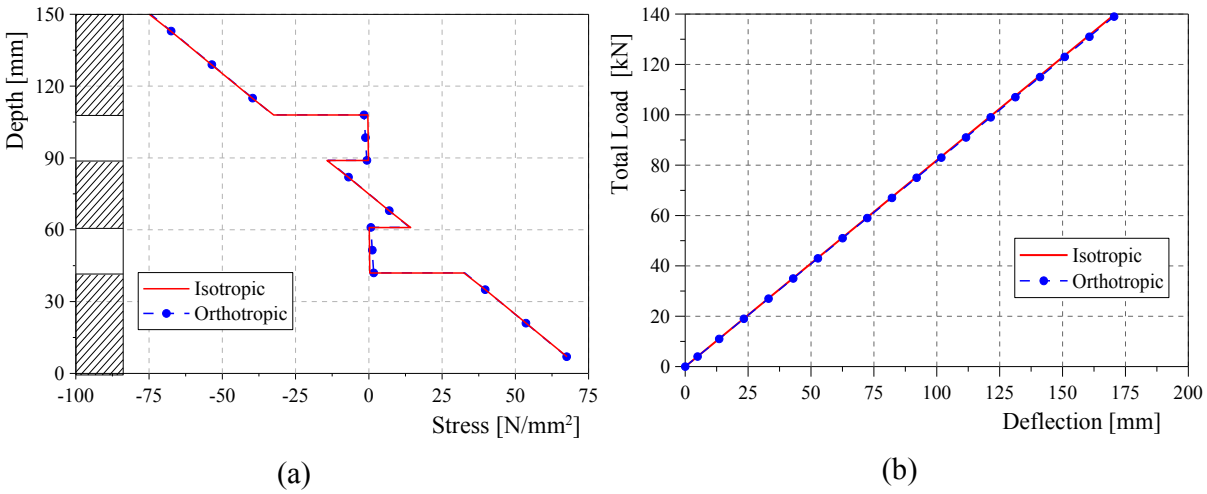

Fig. 6.3 - *Stress distribution along the mid-span panel depth (a) and load-deflection curve at mid-span (b) in the hypothesis of isotropy and orthotropy.*

The mechanical behaviour of the materials was then modelled more realistically by assuming an elasto-plastic and an elasto-brittle behaviour in compression and tension, respectively. Since a specific predefined material model of timber is not available in Abaqus, the CDP model was chosen, which can also be used for fire behaviour as it includes allowance for thermal degradation of mechanical properties. The CDP model allows the definition of different strength-strain relationships in compression and in tension, whereas only one Young's modulus can be adopted for both types of stresses.

Linear quadrilateral elements type 'CPS4' were used, with the mean values of mechanical properties parallel to grain obtained from bending (Chapter 5) and compression [Goina 2010] tests on XLAM specimens at ambient temperature. The Young's modulus E and the tensile and compression strengths (f_t and f_c) of the layers parallel to the main floor direction were assumed equal to 12564 N/mm^2, 41.79 N/mm^2 and 52.74 N/mm^2, respectively. The strength of the layers perpendicular to the main floor direction was determined as 1/10th of the value in the other direction. A fictitious Young's modulus of 120 N/mm^2 and the Poisson's ratios of 0.5 were adopted in the layers perpendicular to the main floor direction. The most important deformability component of the cross layers, in fact, is the shear component, and due to the anisotropy of timber only one property between the shear modulus and the Young's modulus can be correctly considered using an isotropic model.

Table 6.3 summarizes the values adopted for both parallel and perpendicular layers in the numerical modelling at ambient temperature.

Layers	Parallel	Perpendicular
E [N/mm^2]	12564	120
f_t [N/mm^2]	41.79	4.18
f_c [N/mm^2]	52.74	5.27
υ [-]	0.30	0.50

Table 6.3 - *Material properties adopted in the modelling.*

Figure 6.4 compares the experimental data and the numerical prediction of mid-span deflection versus the total applied load, demonstrating that the numerical model can provide an accurate prediction of the panel behaviour at ambient temperature. The finite element analysis assuming the material as isotropic with elasto-brittle and elasto-plastic behaviours in tension and compression, respectively, stopped when the load level of 105 kN was reached, which corresponds to the mean value of the experimental failure loads (Table 5.1). Furthermore, this numerical result is in close agreement with the numerical curve obtained by assuming a linear-elastic orthotropic material.

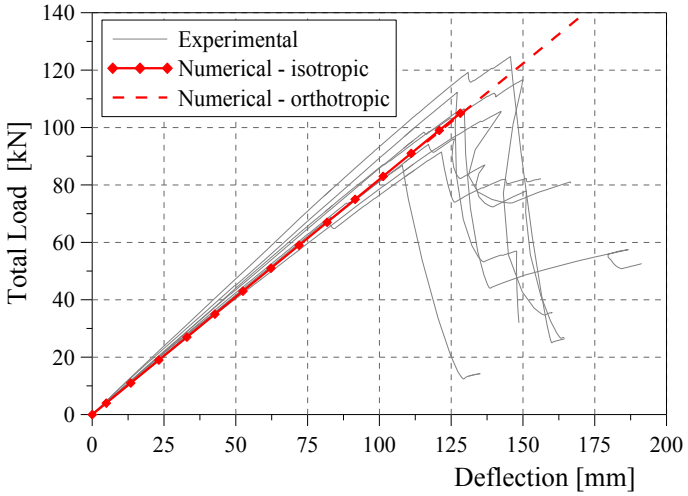

Fig. 6.4 - *Experimental-numerical comparison in terms of total load vs. mid-span deflection.*

6.3. THERMAL ANALYSIS IN FIRE CONDITIONS

6.3.1. *Model implementation*

Uncoupled heat transfer analyses were carried out in Abaqus [ABAQUS v.6.9] to describe the thermal state of unprotected 5-layer XLAM floor panels subjected to one-dimensional (1D) fire exposure during the fire tests performed at CNR-IVALSA (Chapter 5). Four XLAM specimens of series 'S' (S1, S3-I, S3-II and S3-V) were tested during tests No. 1 and 3 that had a duration of 99 and 61 min, respectively.

The 2D finite element model previously described for the mechanical analysis was used also for thermal investigations since the specimens tested at ambient temperature and in fire conditions had the same size (150×600×5600 mm) and restraint conditions (Fig. 6.5).

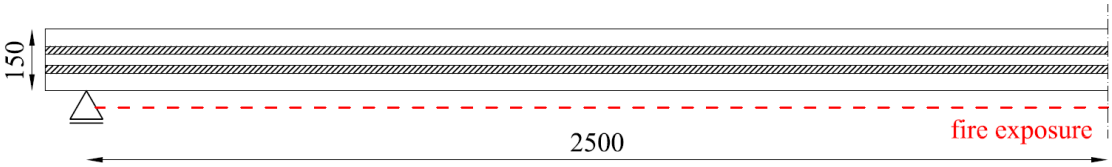

Fig. 6.5 *- Two-dimensional model implemented in Abaqus to simulate the fire exposure of unprotected XLAM panels (dimensions in mm).*

The fire exposure was modelled by using the temperature recorded in the furnace as an input and by imposing the thermal interactions with the surrounding environment as boundary conditions of radiation and convection on exposed and unexposed surfaces. The emissivity and the convection coefficient were assumed equal to 0.8 and 25 W/m^{2}K as suggested by Eurocode 5, Part 1-2 [CEN 2004] and Eurocode 1 [CEN 2002b], respectively. The ambient temperature measured at the beginning of the tests was adopted as initial thermal condition in the numerical model. In particular, temperature of 0°C and 22°C were assumed for specimens tested during fire tests No. 1 (specimen S1) and 3 (specimens S3-I, S3-II and S3-V), respectively.

The actual fire curves recorded during the tests were implemented in the thermal simulations because they rose slower than the standard fire curve ISO 834 [1999] in the

first minutes until about 600°C temperature as shown in Chapter 5. That is more evident in the last fire test (test No. 3) when the 400°C temperature was reached about 3 min later with respect to the standard fire curve.

The thermal properties of wood depend upon the temperature. Different proposals can be found in literature for effective thermo-physical properties [e.g. Bénichou et al. 2001; CEN 2004; Frangi 2001; Hopkin et al. 2011]. In this investigation, the relationships proposed by Eurocode 5 for conductivity, specific heat and density were implemented in Abaqus, assuming the experimentally measured 12% moisture content and 450 kg/m^3 density values at ambient temperature (Fig. 6.6).

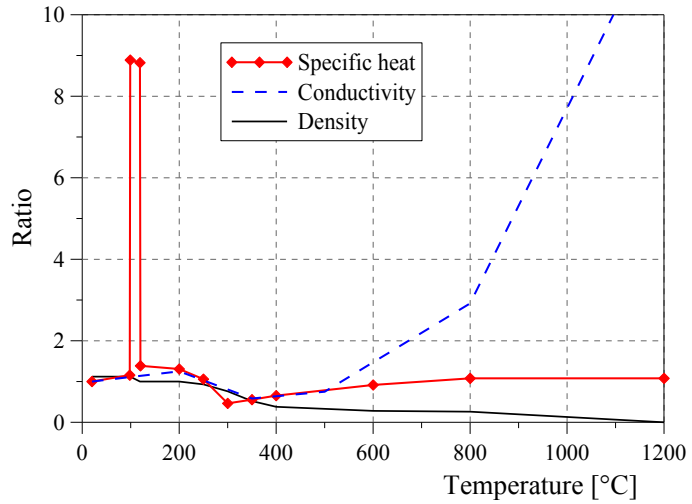

Fig. 6.6 *- Variations of wood thermo-physical properties with temperature according to Eurocode 5 [CEN 2004].*

Four-node linear heat transfer quadrilateral elements 'DC2D4', which are available in the Abaqus library, were used. Simulations using eight-node quadratic elements ('DC2D8') were also performed and results similar to those obtained with linear elements were observed.

The model was subdivided in 14790 elements of about 5 mm size (mesh 'B'), which is a good compromise between accuracy of solution and computational time. Some preliminary numerical analyses were performed using different meshes (Fig. 6.7) to investigate the dependency of the results upon the chosen mesh. Three meshes were tested, and the results were compared as discussed in the following paragraph.

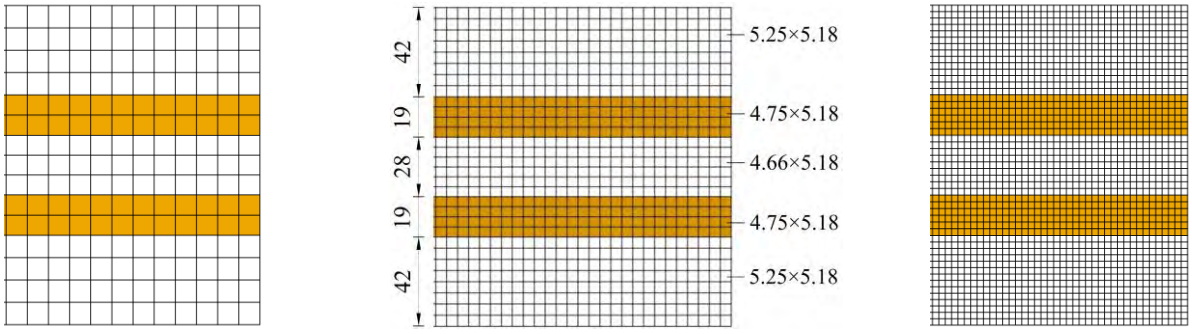

Fig. 6.7 - *Three different meshes adopted in the model of the longitudinal panel section (dimensions in mm).*

Meshes coarser (mesh 'A') and finer (mesh 'C') than the chosen one (mesh 'B') subdivide the entire longitudinal panel section in 3825 elements of about 10 mm size and in 41552 elements of about 3 mm size, respectively.

Similar 2D and three-dimensional (3D) thermal models were already implemented in Abaqus code and validated on experimental results obtained from small- and large-scale fire tests of specimens made of glued laminated timber and laminated veneer lumber subjected to 2D exposure on three or four sides (Chapter 3).

6.3.2. *Results*

The numerical results obtained by thermal analyses performed adopting different meshes show very similar temperature distributions at different depths from the exposed surface (Fig. 6.8a). The main difference was noticed with the coarser mesh (mesh 'A') that slightly anticipates the temperature increase. The chosen mesh with 5-mm length elements (mesh 'B') represents as good compromise between accuracy of solution and computational time.

Figure 6.8b compares the results obtained by implementing in the model with mesh 'B' the fire curves recorded during tests No. 1 and 3.

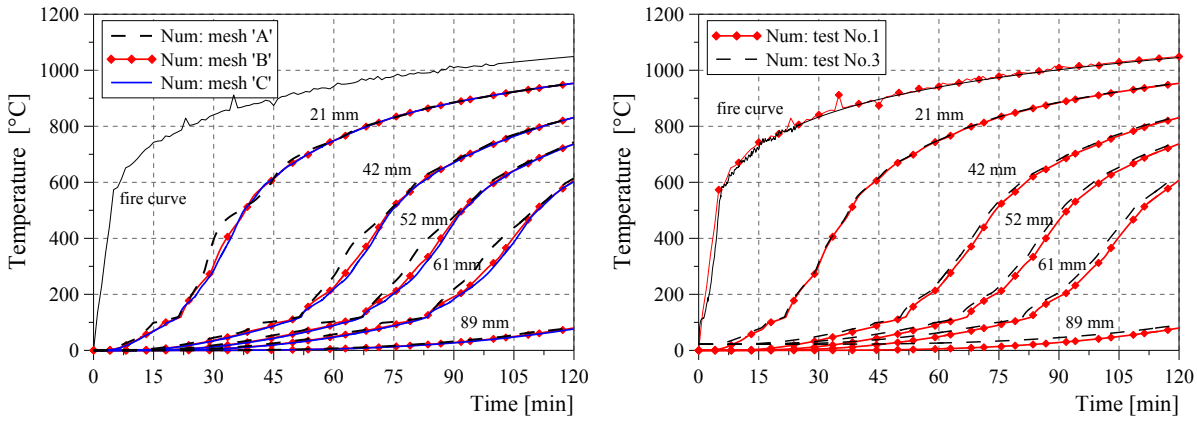

(a) (b)

***Fig. 6.8** - Temperature distributions within unprotected XLAM panels obtained by adopting three different meshes (a) and by implementing different fire curves (b).*

Figure 6.9a plots the comparisons between numerical and experimental temperatures within unprotected XLAM floor panels (specimens S1 and S3-I). The experimental data recorded by thermocouples at 21, 52 and 75 mm from the exposed surface are quite scattered. The numerical curves were obtained by implementing the fire conditions recorded during testing of specimen S1 (test No. 1). The thermal simulations are reasonably close to experimental data especially if their scatter is considered.

Figure 6.9b plots the charred depths versus the fire exposure time for specimen S1. The experimental values were obtained indirectly from data recorded by thermocouples in three cross-sections and at different depths from the exposed surface. The 300°C is

assumed as the border between charred and heated wood as suggested by Eurocode 5. Only one thermocouple at 75 mm from the exposed surface in the mid-span cross-section measured 300°C about one minute before the XLAM failure, which occurred after approximately 99 min of fire exposure.

The temperature increase observed in Figure 6.9a at 52 and 75 mm from the exposed surface in the last minutes of the fire test led to a higher charring rate, which is clearly visible in Figure 6.9b. This increase in charring rate at mid-span was due to the additional fire exposure from the lateral side of the specimen due to flames introduced between the XLAM panel and its lateral protective cladding because of the high panel deflection monitored towards the end of the test. This experimentally observed 2D heat flux, however, is unlikely to occur in real floor structures where each panel is connected to the adjacent ones.

The dashed curve in Figure 6.9b represents the charred depth based on the constant 1D charring rate β_0 = 0.65 mm/min proposed by Eurocode 5 for solid and glued laminated timber. The numerical prediction of charring (solid curve) shows a linear trend close to Eurocode curve. Neither the analytical approach nor the numerical model based on the 1D heat flux can predict the temperature increase recorded by the thermocouple located at 75 mm from the exposed surface.

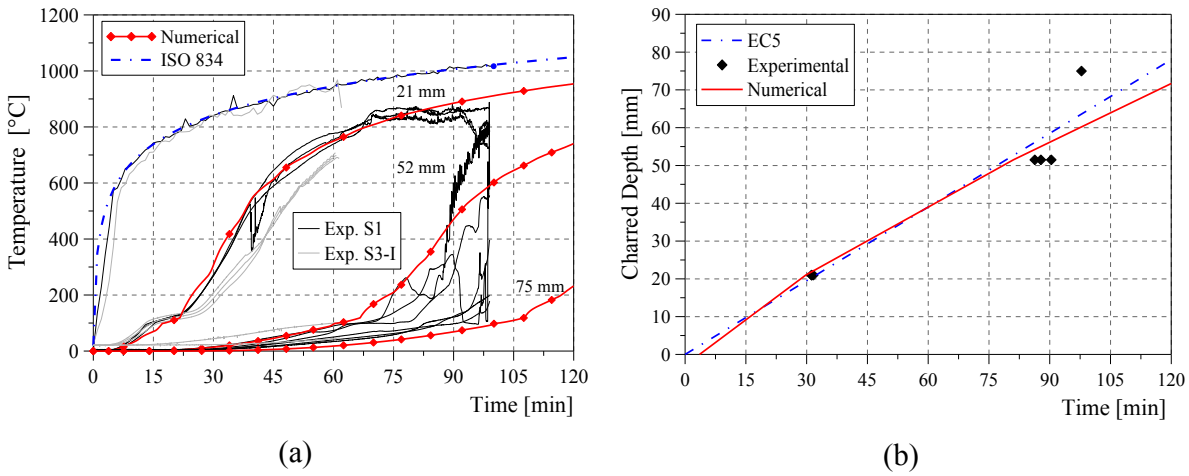

(a) (b)

Fig. 6.9 - *(a) Experimental and numerical temperature distributions within unprotected XLAM panels. (b) Charred depth vs. time from experimental data, numerical modelling and analytical predictions.*

6.3.3. *Discussion*

Since the 1D heat flux was unable to capture the increase in charring rate observed towards the end of the experiment, half of the transversal cross-section of the XLAM panel was modelled in Abaqus to implement the change of fire exposure from 1D to 2D. The model was subdivided in 1800 square elements (type 'DC2D4') of approximately 5 mm size (Fig. 6.10).

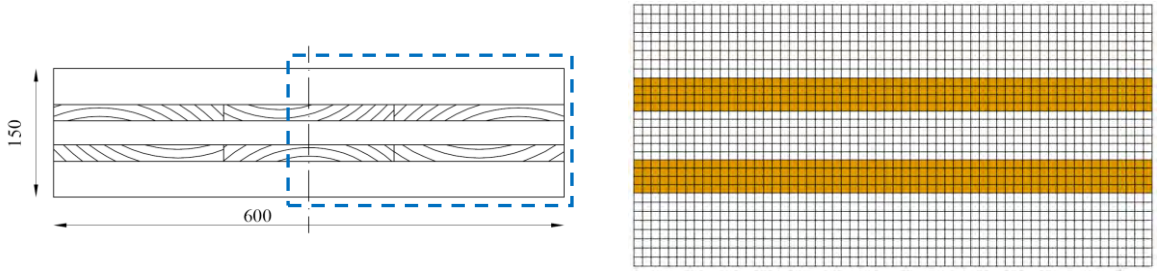

Fig. 6.10 - *Transversal cross-section of unprotected XLAM panels (left) and two-dimensional model implemented in Abaqus (right) (dimensions in mm).*

Two consecutive thermal analyses, on the cross-section exposed to fire conditions first on the bottom side (1D heat flux) and subsequently on both bottom side and lateral edge (2D heat flux), were carried out. The thermal interactions of radiation and convection were assumed on the exposed surfaces. Based on experimental observations, the 2D thermal analysis was started at 80 min from the beginning of the fire test, assuming as an input the temperature distribution at the end of the previous 1D thermal analysis. Graphic visualizations of temperature distributions within the modelled cross-section at different times are displayed in Figure 6.11. The charred material is represented by grey colour, whereas red colour corresponds to 300°C temperature. Figure 6.11a represents the thermal state after 80 min of 1D fire exposure from the bottom side of XLAM panel. It can be noticed that about half depth has still a temperature close to the ambient one (blue contour). The thermal state when the XLAM panel failure occurred (99 min) is showed in Figure 6.11b. At that time the cross-section was already subjected to a 2D heat flux started about 20 min before.

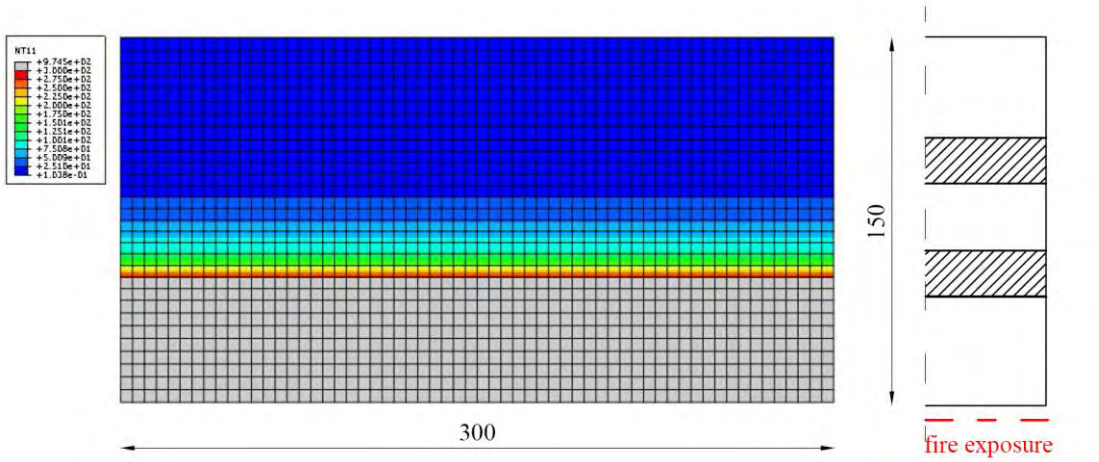

(a)

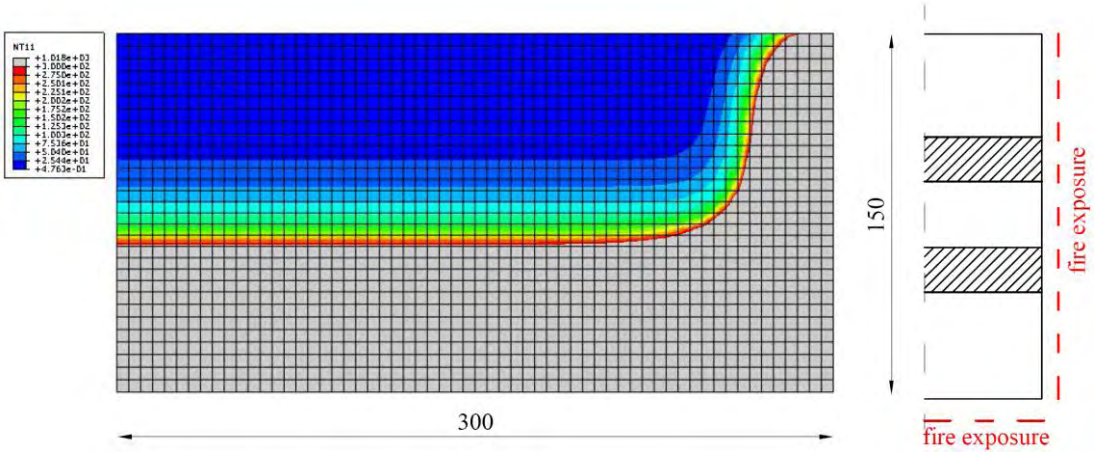

(b)

Fig. 6.11 - *Temperature distributions within the cross-section of unprotected XLAM panels after 80 and 99 min of fire exposure.*

The numerical variation of heat flux led to temperature increases close to the thermocouple records as displayed in Figure 6.12a by the dashed curves. Consequently, also the charring rate is higher, and the experimental charred depth after about 100 min of fire exposure obtained indirectly by thermocouple data is predicted with good accuracy (Fig. 6.12b).

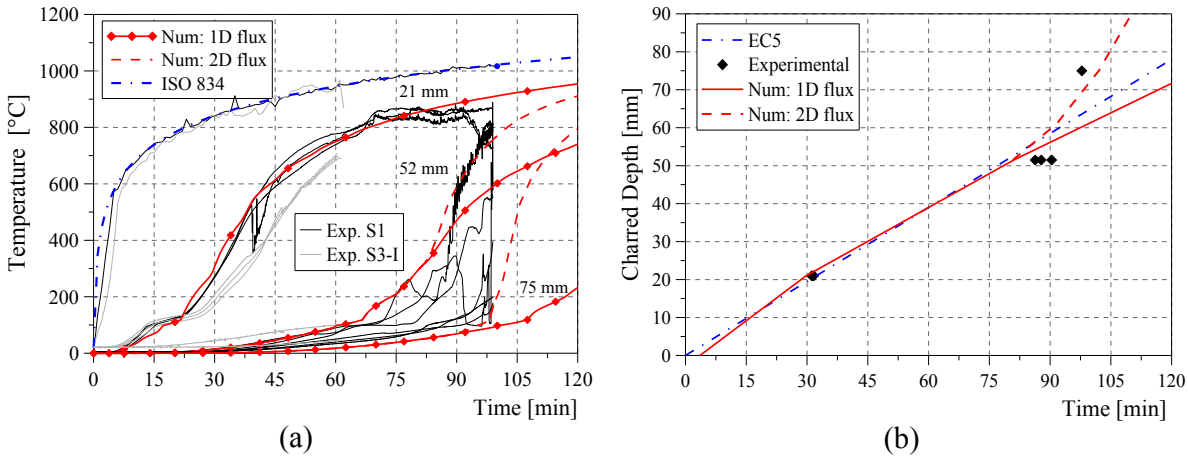

Fig. 6.12 - *Cross-section of unprotected XLAM panels subjected to different heat fluxes. (a) Experimental and numerical temperature distributions. (b) Charred depth vs. time from experimental data, numerical modelling and analytical prediction.*

Figure 6.13 compares the thermocouple readings with the temperature distribution obtained with the 1D heat model within the 150 mm deep panel at different fire exposure times. Five times are considered, namely the time before fire exposure, the experimental failure time corresponding to 99 min of fire exposure, and three intermediate times (30, 60 and 90 min). The dashed curves at 90 and 99 min plot the temperature obtained by using the numerical model of the cross-section subjected to 2D heat flux. Good correspondence between numerical and experimental values can be noticed throughout the test duration, particularly when the 2D heat flux is considered at the end of the experimental test.

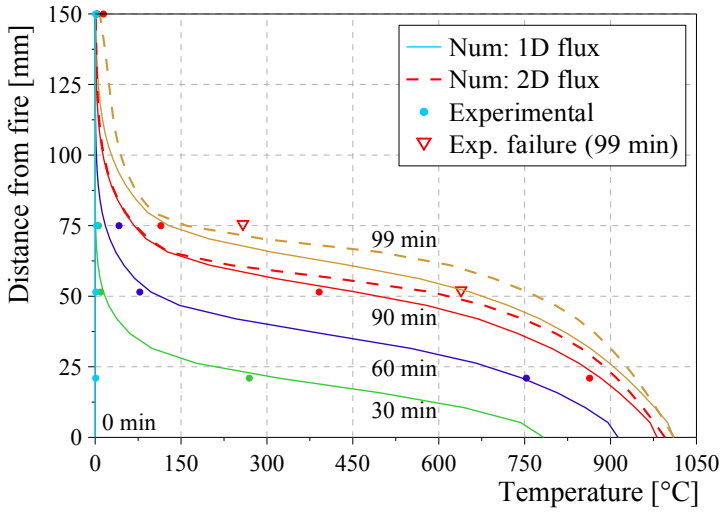

Fig. 6.13 - *Experimental and numerical temperature distributions along the panel depth at different exposure times.*

6.4. THERMO-MECHANICAL ANALYSIS IN FIRE CONDITIONS

6.4.1. *Model implementation*

Sequential coupled thermal-stress analyses were carried out in Abaqus [ABAQUS v.6.9] to predict the failure time of the unprotected 5-layer XLAM floor panels tested at CNR-IVALSA (Chapter 5). Two large-scale simply supported panels, specimens S1 and S3-I, were subjected to uniformly distributed load q_i of 5 or 10 kN/m^2, corresponding to 11% and 21% of their estimated mean failure load at ambient conditions, and then exposed to fire on the bottom side. The structural failure of specimen S1 occurred after about 99 min of fire exposure, whereas test No. 3 was stopped after 61 min before specimen collapse.

The same 2D finite element model previously described for the mechanical analysis at ambient temperature and the thermal analyses in fire conditions was used. Load, geometry and boundary conditions of the 2D model are displayed in Figure 6.14. The same restraint conditions used in the mechanical modelling at ambient temperature were adopted. The uniformly distributed load was defined as a uniform pressure on the unexposed surface of the numerical model.

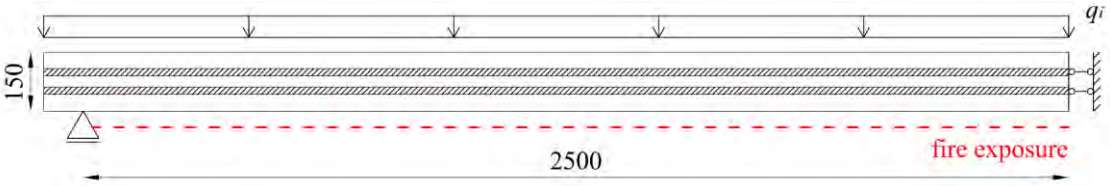

Fig. 6.14 - *Two-dimensional model implemented in Abaqus to simulate tests of unprotected XLAM panels in fire conditions (dimensions in mm).*

The thermal analysis describes the temperature distribution within the structural element in fire conditions. Its output is used as an input for the mechanical analysis. This procedure was chosen because mechanical stresses depend upon the thermal state in the cross-section, whereas the inverse relationship does not hold. The consecutive analyses must be performed using the same 2D model in terms of geometry and mesh (mesh 'B'

in Fig. 6.7) in order to assure perfect correspondence of node and element labels when the thermal state is converted to an input for the following mechanical simulation.

The elements of about 5 mm size used for the structural analyses are four-node quadrilateral, linear reduced-integration elements type 'CPS4R'. Some analyses were performed also using eight-node quadratic elements type 'CPS8R' but the larger computational burden was not justified by a significant improvement of results as shown in the following paragraph.

Like the thermal parameters, also the mechanical properties of wood depend upon the temperature and several proposals can be found in literature [e.g. Buchanan 2002; CEN 2004; Jong and Clancy 2004]. The strength and stiffness degradation with temperature suggested by the Eurocode 5, Part 1-2 [CEN 2004] for a standard fire exposure were assumed in this study (Fig. 6.15a). Strength reduction with temperature is greater in compression than in tension and this difference influences the fire performance of timber structural elements. The degradation of Young's modulus with temperature was defined in accordance with the Eurocode relationship for timber in tension since only one degradation law can be implemented in Abaqus, and experimental failures always occurred for fracture in tension of the lower layers.

Different stress-strain relationships in compression and tension, and their dependency upon temperature in accordance with Figure 6.15a, were implemented using the CDP model. Figure 6.16b plots the elasto-plastic and elasto-brittle stress-strain relationships for different temperature values in compression and tension, respectively, adopted for layers parallel and perpendicular to the main floor direction.

The same mean values of strength, Young's modulus and Poisson's ratio used to simulate bending tests at ambient temperature were assumed for the layers parallel and perpendicular to the main floor direction, as reported in Table 6.3. Moreover, the minimum value of tensile strength equal to 34.54 N/mm^2 obtained from tests on XLAM specimens at ambient temperature (Chapter 5) was adopted in a thermo-mechanical analysis. In this case the fire resistance of XLAM floor panels loaded with 21% of the estimated failure load at ambient temperature decreases of about 6% with respect to the numerical prediction using the mean value of tensile strength (41.79 N/mm^2).

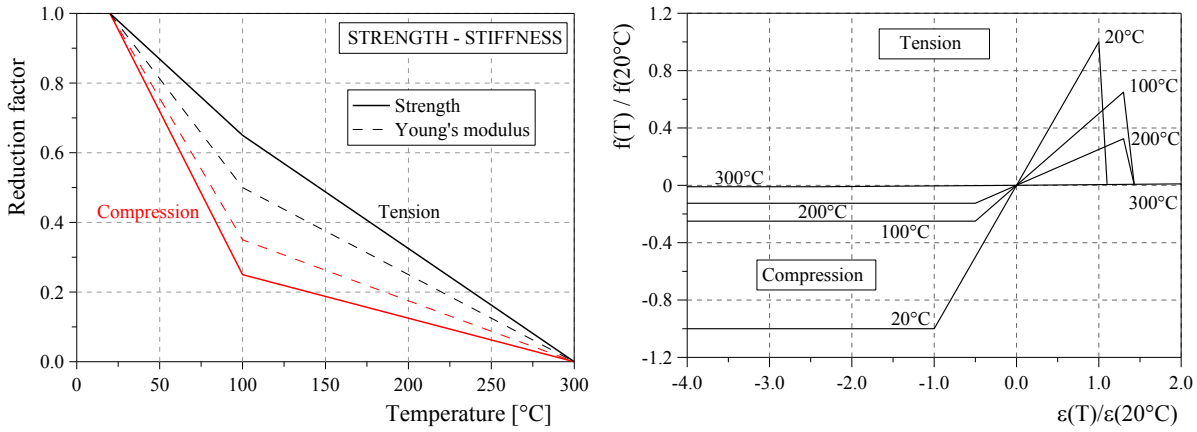

(a) (b)

Fig. 6.15 - *(a) Strength and Young's modulus reductions with temperature in compression and in tension as suggested by Eurocode 5 [CEN 2004]. (b) Strength-strain relationships in compression and tension at different temperatures for layers parallel and perpendicular to main floor direction.*

The failure of the panel can be assumed to occur at the time when the numerical model does not converge any more. At the same time, in some integration points the stress reaches the strength of the material at the corresponding thermal state. Therefore, the failure time to the last increment of the analysis provides the fire resistance of the structural element.

In the analyses of the experimental tests carried out at CNR-IVALSA, the convergence was not achieved in the elements located in the third layer of XLAM panel. This is the second resistant layer as the layers running perpendicular to the main floor direction do not carry significant amount of load due to their low Young's modulus parallel to the main floor direction.

6.4.2. *Results*

The numerical results here discussed refer to the cross-section at mid-span of a XLAM panel exposed to fire on bottom side and subjected to 21% of the estimated failure load at ambient temperature on the unexposed surface as during fire test No. 1 (Chapter 5).

Figures 6.16a and 6.16b compare the stress distributions along the XLAM panel depth obtained by adopting in the modelling three different meshes (Fig. 6.7), and by using both linear and quadratic elements, respectively. The stresses before the fire exposure, after 60 min of fire exposure and when the failure of the numerical model occurred are represented.

The fire resistance of XLAM floors adopting a coarser (mesh 'A') and a finer mesh (mesh 'C') differs respectively by about 5% and 1% from the prediction obtained using the chosen mesh (mesh 'B'). The main difference between numerical curves in Figure 6.16a is noticed with the coarser mesh (mesh 'A') that reaches stresses lower than the values attained using the other two denser meshes.

In Figure 6.16b the stresses before the fire exposure, after 60 min of fire exposure and at the numerical failure, namely 110 min from the beginning of fire, are represented for linear and quadratic elements used in the numerical model. The stress curves obtained by using both the element types slightly differ at failure time in the proximity of the interfaces between layers parallel and perpendicular to the main floor direction.

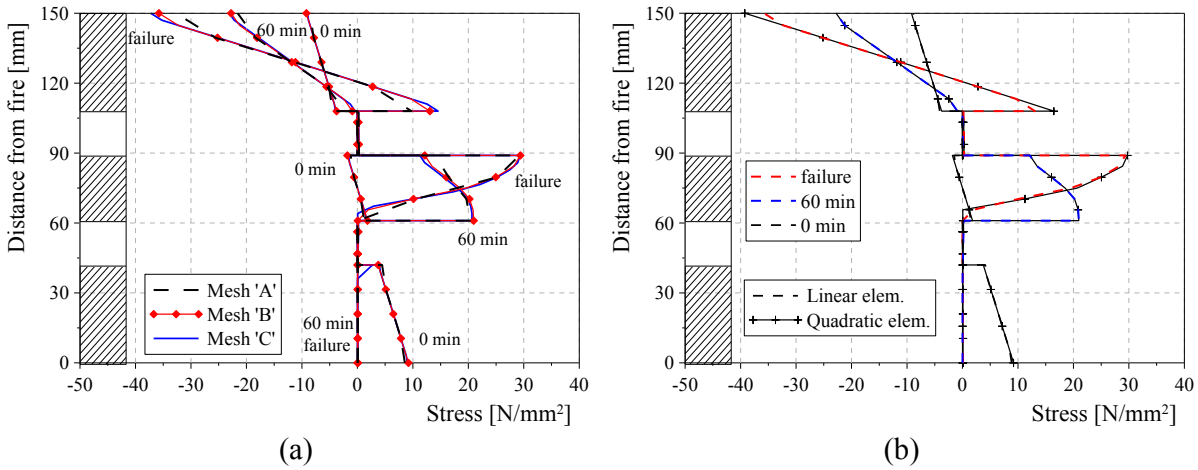

Fig. 6.16 - *Stress distributions along the XLAM panel depth at different exposure times obtained by using three different meshes (a), and linear and quadratic elements (b).*

Figure 6.17a plots the results of the thermo-mechanical analysis in terms of stress-temperature at different depths in the first, third and fifth layers from the surface exposed to fire of the XLAM section. The dashed curves represent the wood strength variation with temperature in compression and tension. The tensile stresses first increase due to the charring of the wood and reduction of the resisting section. Then the stresses drop to zero in the most exposed fibres (e.g. the fibre at 2.6 mm depth) when the charring temperature of 300°C, as proposed by Eurocode 5, is attained. More internal fibres (e.g. the fibres at 34.1 and 63.3 mm depth) show a more gradual stress reduction until the zero value is attained. As the distance from the exposed surface increases, the stress in the corresponding fibres does not reach the zero value as the failure occurs before the charring. The fibres more exposed to fire redistribute their stress in the upper fibres that have low temperature and maintain their mechanical capacity. Charred wood loses its strength and stiffness completely, while heated wood is subjected to high stresses due to the stress redistribution. This redistribution process continues until the residual cross-section is able to carry the increasing stresses even if the external applied load is constant throughout the fire exposure. It can be noticed in Figure 6.17a that some curves (i.e. 72.7 and 77.3 mm) stop very close to the maximum strength at that temperature since they represent the increasing stress in nodes where convergence is no longer found at the end of the analysis. Throughout the fire exposure, only the more distant layer from exposed surface (fifth layer) is always subjected to compressive stress (e.g. the fibre at 147.4 mm depth), while the other two resisting layers (first and third) are in tension.

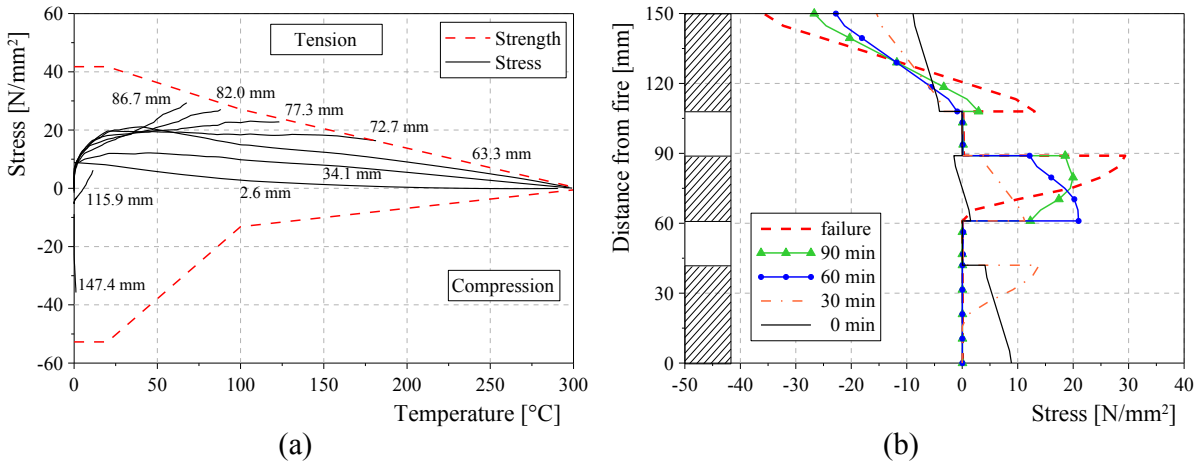

Fig. 6.17 - *(a) Stress and strength vs. temperature curves at different distance from exposed surface. (b) Stress distribution along the panel depth at different exposure times.*

The stress redistribution taking place in the 150 mm deep cross-section is described by the numerical results reported at different times in Figures 6.17b and 6.18. In particular, the stresses before the fire exposure, after 30, 60 and 90 min of fire exposure and when the numerical failure of the XLAM floor occurred (110 min) are represented. As previously discussed, the layers close to the fire exposure lose load-carrying capacity due to thermal heating and charring. For the equilibrium, this causes an increase in stresses in the more interior layers as the applied load is constant but the resisting section is reduced.

The green colour in the graphic visualization (Figure 6.18) represents the material with no load-bearing capacity, namely the charred wood and the layers perpendicular to the main floor direction. The red and blue contours correspond respectively to tension and compression stresses in the residual section.

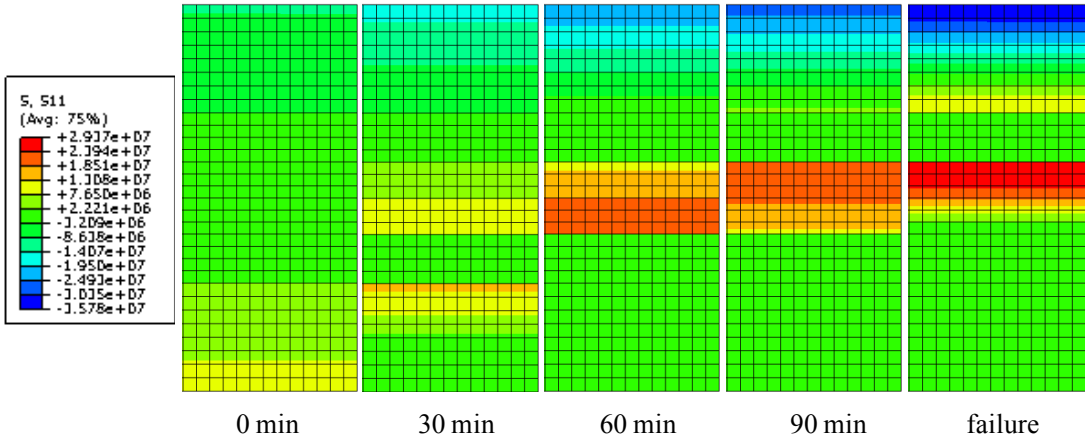

Fig. 6.18 - *Graphic visualization of stress distribution in the resisting section at different times from the onset of fire.*

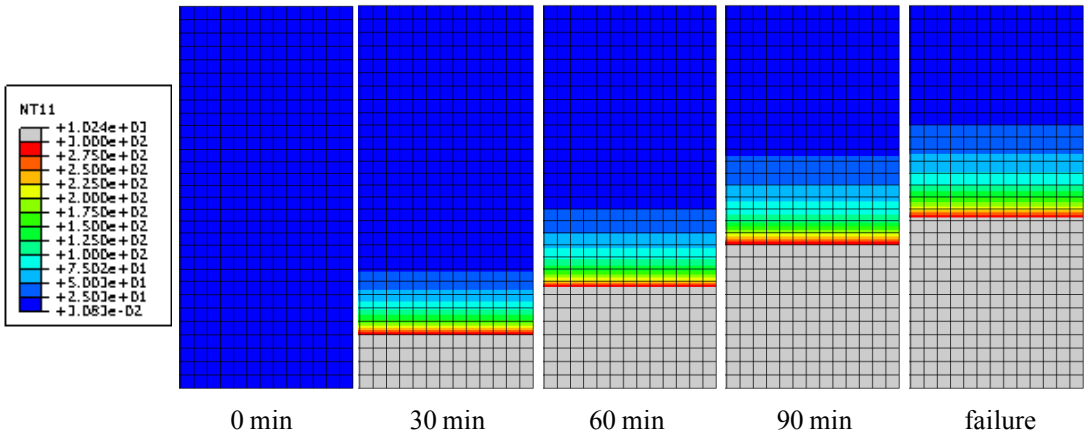

Fig. 6.19 - *Graphic visualization of residual section at different times from the onset of fire.*

The residual section can be determined by referring to the 300°C isotherm, considered as the separation between charred and un-charred wood. In Figure 6.19 the grey, red and blue colours represent the charred wood, the 300°C temperature and the ambient temperature, respectively. It can be noticed that approximately half of the panel depth has a temperature over 300°C at numerical failure time (110 min), whilst the more distant layer from fire exposure parallel to the main floor direction maintain almost unchanged its initial temperature throughout the test.

Figure 6.20 displays the numerical thermal and mechanical states along the panel depth at mid-span. The stress distribution is compared with the tension and compression strengths at the corresponding thermal state considering the reduction factors proposed by Eurocode 5. The thermal analysis supplies the temperature distribution used to determine the strength domain at any instant. In particular, Figure 6.20a represents the thermal and mechanical states after 110 min of fire exposure when the numerical failure of the panel loaded with 21% of the ultimate strength at ambient temperature occurs. It can be noted that the charring temperature (300°C) reaches the third layer from the bottom surface directly exposed to fire. The two lower layers are completely charred and therefore not stressed. The central layer is heated and the charring is ready to start. The stresses are redistributed in this layer and in the fifth one that is the most distant from fire. This layer maintains approximately the ambient temperature throughout the fire exposure therefore the tension and compression strength domains do not change along its depth. In the third layer the thermal state variation leads to a continuous change of strengths and stresses. The tensile stress distribution corresponds to the ultimate strength domain when numerical failure occurs, as can be clearly noted in Figure 6.20a. The failure time provides the fire resistance of a structural element, as the ultimate strength at a specific temperature is reached and the cross-section corresponds to the residual section.

In Figure 6.20a the stress distribution of the XLAM panel loaded with 11% of ultimate strength at ambient temperature is also represented at the same fire exposure time of 110 min so the temperature and strength curves do not change. The stress curve is far from the strength domain since the residual section of the XLAM panel is still able to support the applied load. The numerical failure occurs after about 128 min of fire exposure that is 18 min later than the floor subjected to a double load. At that time, half of the third layer is already charred and therefore the stresses are redistributed in the

residual heated part of this layer and in the fifth one where the temperature is still below 60°C (Fig. 6.20b). It can be noticed the considerable reduction of the compression strength domain with increasing temperature.

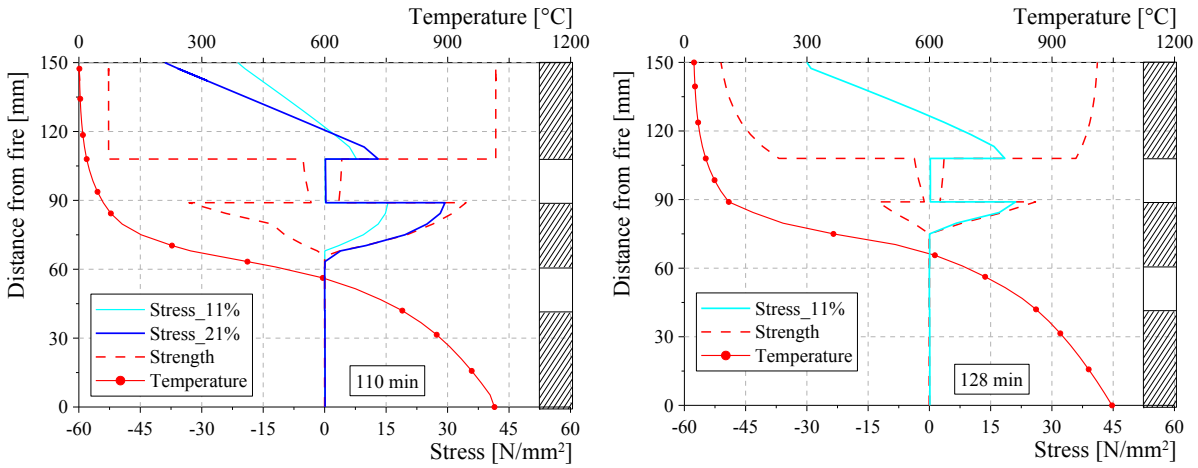

Fig. 6.20 - *Temperature, stress and strength distributions at failure time along the mid-span depth of XLAM floor panels loaded with 21% (a) and 11% (b) of the ultimate strength at ambient temperature.*

6.4.3. *Discussion*

The finite element model based on the 1D heat flux slightly overestimates the experimental fire resistance of the XLAM panel (specimen S1) loaded uniformly with 10 kN/m^2 (21% of failure load at ambient temperature). The difference between numerical and experimental failure time is about 10% (Table 6.4). This difference is due to the 2D fire exposure that occurred in the XLAM panel during the experimental tests because of the large mid-span deflection. This event led to a reduced residual cross-section and, consequently, to an anticipated failure.

Thermo-mechanical analyses considering the 2D heat flux were then performed using a 3D model implemented in Abaqus. Only a small block (50×150×300 mm) representing half cross-section of XLAM panel at mid-span was modelled due to computational burden (Fig. 6.21). The block was subjected to constant bending moment M = 9.38 kNm and 18.75 kNm corresponding to the value at mid-span due to the uniformly distributed load (5 or 10 kN/m^2) applied on the specimen during the

performed fire tests. A 50 mm thick steel plate was modelled to apply the bending moment through a couple of forces on the block. A 150×150×300 mm transition part was introduced between the plate and the block to ensure a uniform stress distribution within the examined block. For the same reason a part with the same size was modelled on the other end of block where the restraints were imposed. Both the transition parts were assumed to be made of XLAM with linear-elastic behaviour for both layers parallel and perpendicular to the main floor direction.

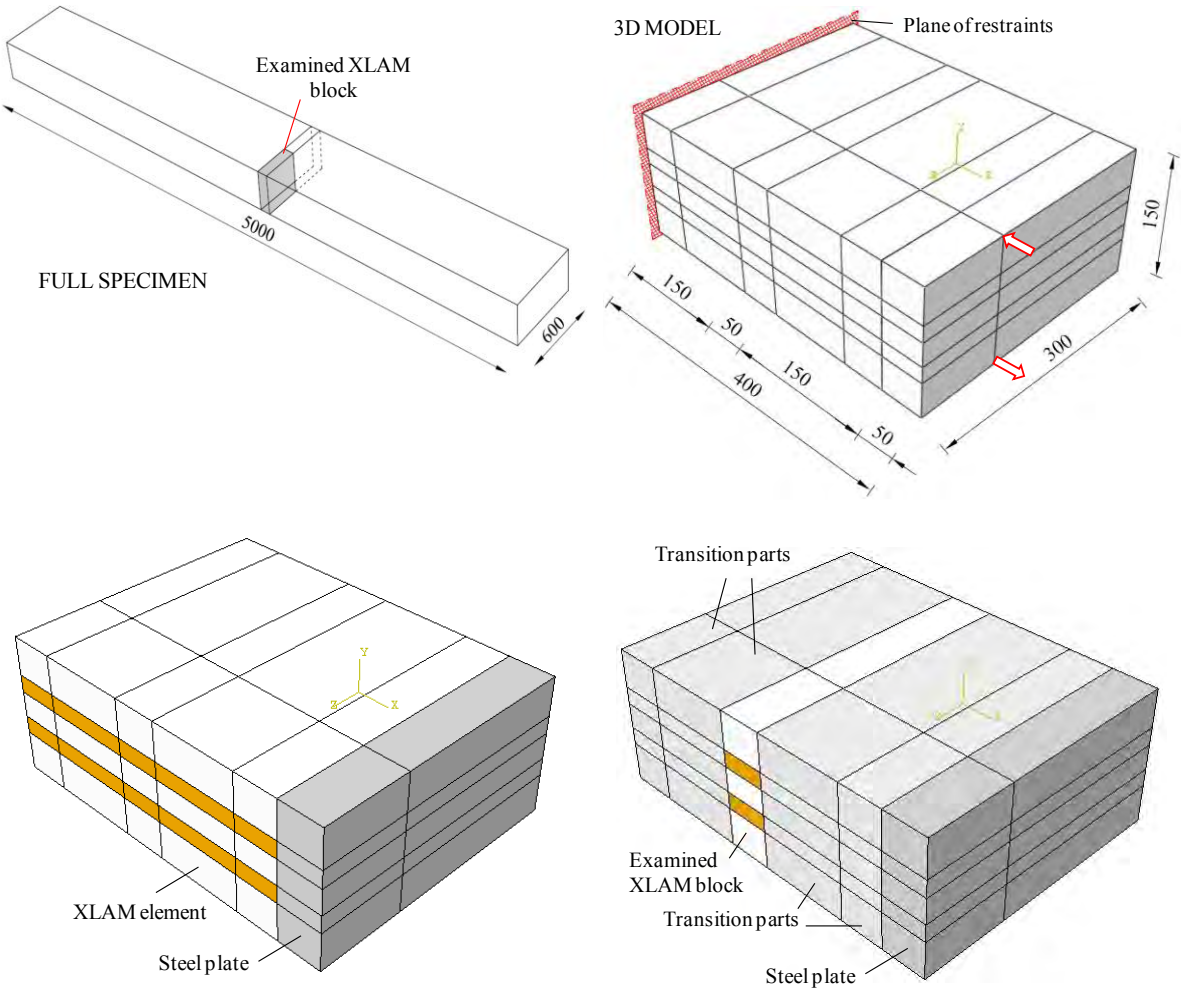

Fig. 6.21 - *Geometry of the three-dimensional model implemented in Abaqus for unprotected XLAM panels (dimensions in mm).*

Eight-node linear brick elements type ‘DC3D8’ and ‘C3D8R’ were used for the thermal and mechanical analyses, respectively. The cross-section of the 3D model is divided into 525 elements of different sizes. In particular, the mesh is denser in the part subjected to 2D heat flux coming from the bottom and lateral sides (Fig. 6.22).

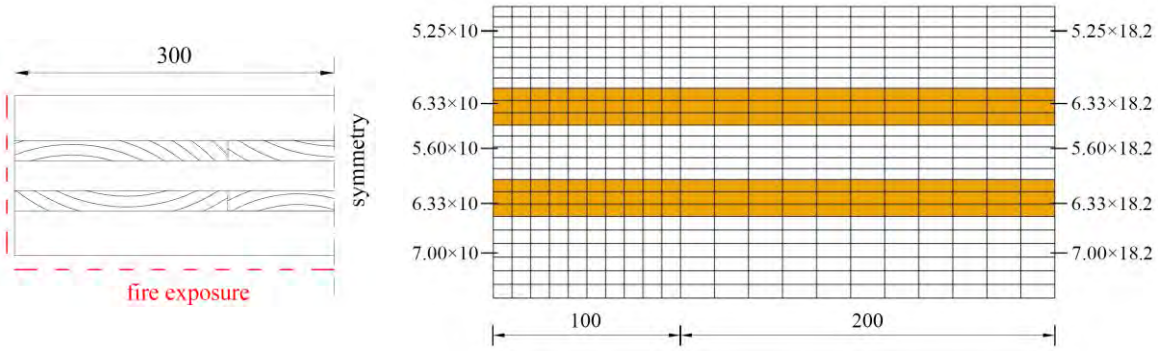

Fig. 6.22 - *Mesh adopted for unprotected cross-section of the three-dimensional model (dimensions in mm).*

Two consecutive thermal analyses were carried out to simulate the fire exposures on the bottom side (1D heat flux) and on both bottom side and lateral edge (2D heat flux), as described in a previous paragraph. The change of heat flux from 1D to 2D after about 80 min of fire exposure was imposed also on the transition parts.

Figure 6.23 displays the temperature distribution within the cross-section of the block at different times, namely after 101 and 121 min of fire exposure when the numerical failure of specimens loaded respectively with 21% and 11% of the failure load at ambient temperature occurred. The charred material is represented by the grey colour, whereas the red colour corresponds to 300°C. After 101 min from the beginning of fire exposure, the 300°C isotherm reached the third layer (second parallel layer).

Figure 6.24 displays the stress distribution within the cross-section of the block when the numerical failure of specimens loaded with 21% and 11% of the failure load at ambient temperature occurred. The green colour represents the material with no load-bearing capacity, namely the charred wood and the layers perpendicular to the main floor direction. The red and blue contours correspond respectively to tension and compression stress in the residual resistant layers, that is the third and fifth layers from the bottom.

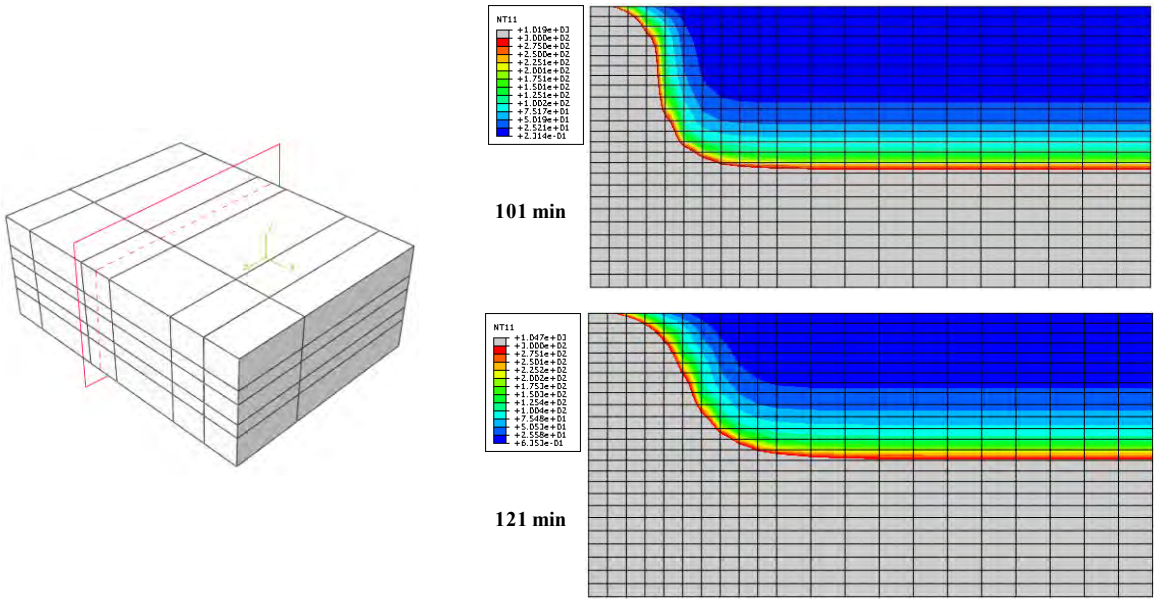

Fig. 6.23 - *Temperature distributions within the unprotected cross-section of the three-dimensional model at different times of fire exposure.*

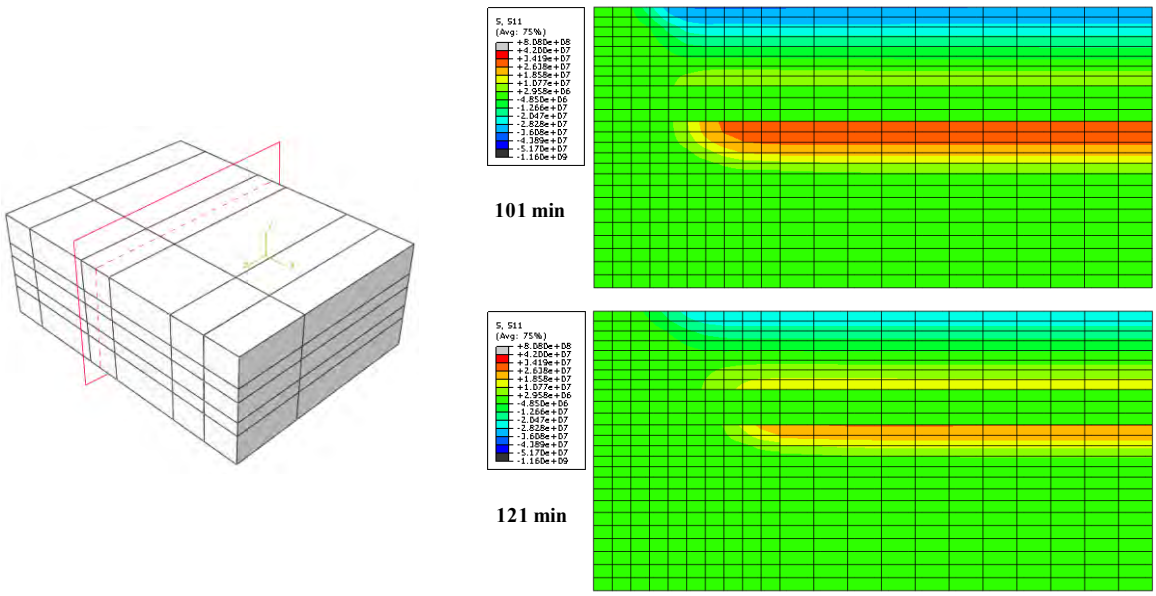

Fig. 6.24 - *Stress distributions within the unprotected cross-section of the three-dimensional model at different times of fire exposure.*

The numerical prediction using the 3D model led to results very close to the experimental value, as reported in Table 6.4.

Load level	11%	21%
Numerical (2D)	128 min	110 min
Numerical (3D)	121 min	101 min
Experimental	-	99 min

Table 6.4 - *Experimental-numerical comparison of the fire resistance of unprotected XLAM floor panels.*

Figure 6.25 plots the experimental and numerical deflections at mid-span of unprotected XLAM floor panels loaded with 11% and 21% of the failure load at ambient temperature and subjected to 1D fire exposure on the bottom surface. The numerical curve for the lower load level follows the experimental displacement until data are available. The deflection for the more loaded XLAM panel was measured until its failure occurred (99 min). In this case the numerical estimation of displacement is close to the experimental trend until the 80th min, when the specimen had a quick increment of deflection due to the 2D fire exposure that occurred on the specimen before the collapse in the furnace.

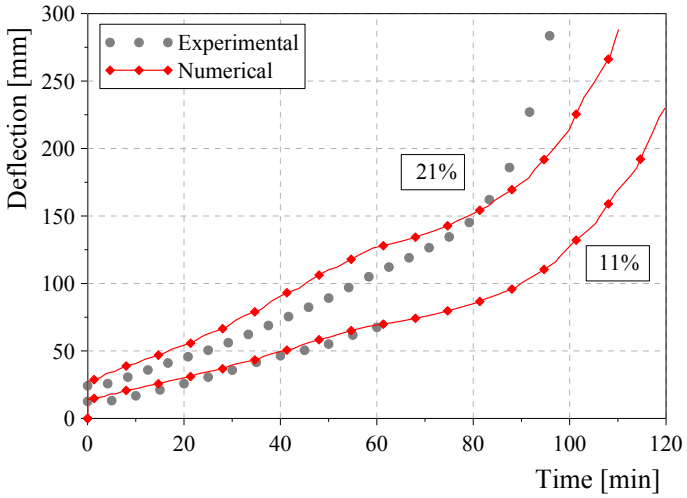

Fig. 6.25 - *Experimental and numerical deflections at mid-span of unprotected XLAM floor panels exposed to fire.*

6.5. PARAMETRIC STUDY

Once validated on the results of large-scale experimental fire tests, the numerical model was used to carry out a parametric study aimed to predict the fire resistance of XLAM floors. The same structural layout, depth and mechanical properties of the specimens tested at CNR-IVALSA were considered. In a real floor a 2D heat flux similar to that observed in the single panel experimental test is unlikely to occur as each panel is fastened to the adjacent ones. Therefore, a 2D numerical model of the floor displayed in Figure 6.14 and exposed to 1D fire exposure was used. Different out-of-plane load values ranging from about 5% to 87% of the estimated mean ultimate moment at ambient temperature were investigated.

The numerical results are plotted in Figure 6.26 as a ratio between applied load and mean collapse load at ambient temperature. The fire standard curve [ISO 834-1 1999] was used in all the analyses. The significant influence of the gravity load level on the fire resistance can be clearly recognized: the panel would classify as R120 for about 15% load level, R90 for about 31% load level, and R60 for about 34% load level.

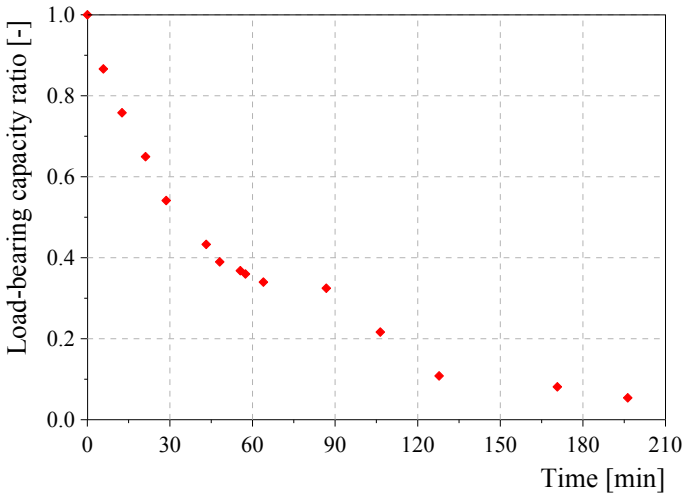

Fig. 6.26 - *Numerical predictions of fire resistance for XLAM floors exposed to fire and subjected to different load levels.*

6.6. ANALYTICAL-NUMERICAL COMPARISONS

The results of the parametric study can be used to check the approximation achievable using simple design methods, such as the 'reduced cross-section method' (RCSM) proposed by Eurocode 5, part 1-2 [CEN 2004]. This method, which was originally derived for structural elements made of sawn and glued laminated timber, has been recently extended to XLAM panels (RCSM for XLAM) [Schmid and König 2010; SP Trätek 2010].

The main difference between the two methods concerns the way the residual cross-section is calculated: in the former approach, a defined 'zero-strength' layer $k_0 d_0$ of 7 mm after 20 min of fire exposure is assumed, whereas in the latter approach the thickness of the so-called 'compensating layer' s_0 depends on the number of layers of the panel, the panel depth, the type of stresses on exposed side, the type of structural element (wall or floor), and the presence of protective cladding. The latter method was applied using the proposed formulas for unprotected 5-layer XLAM floor panels with the tension side exposed to fire [SP Trätek 2010]:

$$s_0 = 10 + \frac{h}{100} \qquad [6.1]$$

where h is the panel depth in mm.

Recent experimental research showed that the fire behaviour of XLAM panels depends upon the behaviour of the single layers, and two limit cases should be considered [Frangi et al. 2009a,b]: (i) the charred layer protects the inner layers and slows down the heat transmission in the panel; and (ii) the charred layer falls off and exposes the remaining inner layers directly to fire. As mentioned in Chapter 5, experimental data recorded during the performed tests does not provide evidence of the falling off of the charred timber layer, therefore only the first case was considered in the following analytical estimations.

The mean ultimate resistant moment M_{Ru} was determined with the formula:

$$M_{Ru} = \frac{(f_{m,mean} J_{res})}{(h_{res} - y)} \qquad [6.2]$$

where $f_{m,mean}$ is the mean value of the bending strength at ambient temperature obtained

experimentally, J_{res}, h_{res} and y signify respectively the second moment of area, the depth, and the centroid distance from the upper edge of the residual, resistant cross-section. All parameters, except the bending strength, vary with the fire exposure time since the panel cross-section is reduced by progressive charring.

The residual resisting cross-section was determined by neglecting the two layers perpendicular to the main floor direction and by assuming that the charred layers do not contribute to mechanical resistance of panel when their thickness is less than 3 mm [SP Trätek 2010]. The resistance of XLAM floors remains constant during the charring of layers perpendicular to the main floor direction as shown by the plateaus in Figure 6.27, where numerical and analytical predictions are compared.

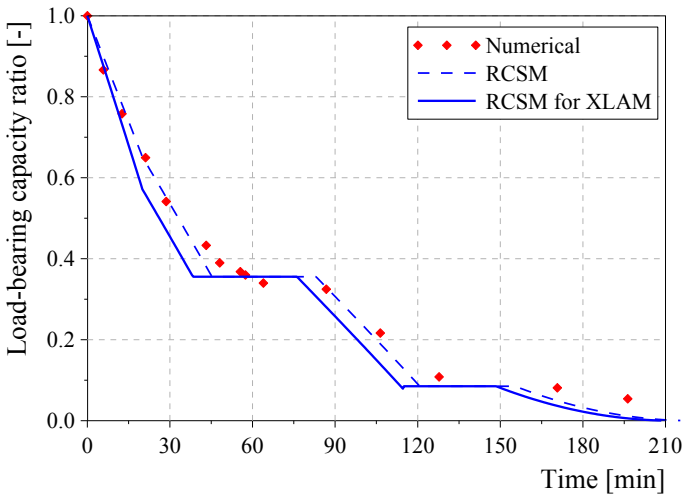

Fig. 6.27 - *Numerical and analytical predictions of fire resistance for unprotected XLAM floors exposed to fire.*

The predictions of fire resistance with the RCSM for XLAM are more conservative than the RCSM for load levels in the range 10% to 60% of failure load at ambient temperature. This method was calibrated to obtain the best results in the range 20% to 40% of bending resistance at ambient temperature [SP Trätek 2010]. The two analytical curves tend to coincide for high and low load levels. The fire resistance of XLAM floors loaded with 11 and 21% of ultimate load at ambient temperature, was estimated with a difference lower than 6.5% using the two simplified methods.

The numerical fire resistance is in good agreement with the analytical curve obtained with the RCSM for most of the load levels. The greater differences are noticed

close to the plateaus and for low stresses. The numerical failures of XLAM floors loaded as during the fire tests and subjected to ISO fire exposure [1999] occurred after about 128 and 108 min of fire exposure. These times differ approximately by 7.8% and 4.6% from the analytical estimations obtained using the RCSM (Table 6.5). However the RCSM for XLAM should not be used for fire exposure over 120 min [SP Trätek 2010].

Load level	11%	21%
Analytical - RCSM	118 min	103 min
Analytical - RCSM for XLAM	111 min	96 min
Numerical (2D)	128 min	108 min
Experimental	-	99 min

Table 6.5 - *Analytical, experimental and numerical comparison of the fire resistance of unprotected XLAM floor panels.*

Figure 6.28 compares experimental and numerical deflections also with the analytical values predicted using the RCSM and RCSM for XLAM. On the whole the RCSM for XLAM provides more conservative predictions. The numerical deflections show a trend similar to the analytical curves except for the plateau.

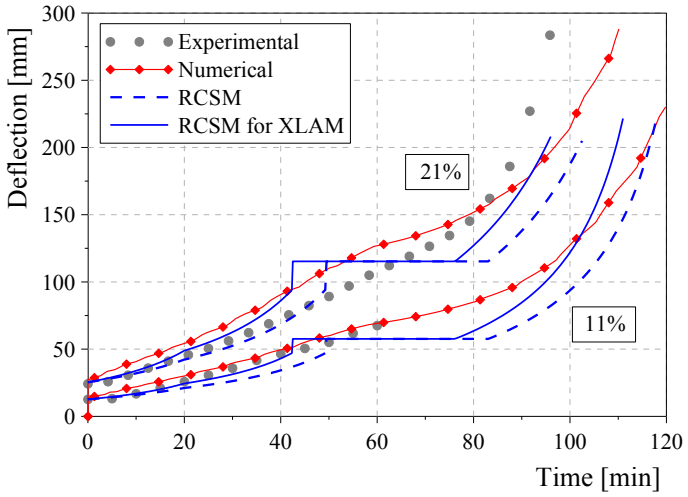

Fig. 6.28 - *Experimental, numerical and analytical deflections at mid-span of loaded unprotected XLAM floor panels exposed to fire.*

CHAPTER 7.

NUMERICAL ANALYSES: PROTECTED PANELS

7.1. INTRODUCTION

Some fire tests have been carried out on protected and unprotected cross-laminated timber (XLAM) panels [e.g. Frangi et al. 2009a,b; Friquin 2010; Schmid and König 2010; Teibinger and Matzinger 2010]. Experimental data were used to validate numerical models implemented in different software packages with the aim to analyse the thermal and structural performances of timber members exposed to fire. The numerical tools allow investigations of structural elements with different configurations (e.g. specimen sizes and protective materials) and/or load and exposure conditions without performing further expensive tests.

The fire behaviour of XLAM and homogenous timber panels with the same depths was investigated experimentally and numerically by Frangi et al. [2009b]. A numerical model was implemented in the finite element code Ansys and the falling of the charred layers in 3- and 5-layer XLAM panels was considered. The numerical results proved the influence of the number and thickness of layers on the fire behaviour of XLAM panels. Further, their charring rate was found to be strongly dependent upon the time when the charred layers fall off causing the direct exposure of the heated wood to high temperatures. Comparisons between the behaviour of XLAM and homogenous timber panels exposed to fire were performed also by König and Schmid [2007]. The temperature distribution within cross-sections with different depths and structural layout was described through thermal analyses carried out using both the software TempCalc [Fire Safety Design 1990] and Safir [Franssen 2005]. A computer program CSTFire, written as a Visual Basic macro embedded in Excel, was used for the sequential mechanical analyses. The numerical outcomes in terms of bending resistance and depth

of the 'zero-strength' layer were discussed and compared. The same computer programs were used in another numerical investigation focused on protected and unprotected XLAM elements [Schmid and König 2010]. The outcomes were compared with the analytical predictions obtained using the simplified 'reduced cross-section method' (RCSM) suggested by the Eurocode 5, Part 1-2 [CEN 2004] and a modified version for XLAM.

Several numerical investigations have been performed on timber frame assemblies exposed to fire using various software packages, such as Abaqus [e.g. Lu et al. 2010], Ansys [e.g. Frangi and Erchinger 2007; Tabaddor 2008; Winter and Meyn 2009] and Wall2D [e.g. Bénichou 2002; Takeda and Mehaffey 1998], in order to analyse also the influence of different cladding systems on fire performance of timber elements. The claddings lose their protective function after a specific fire exposure time, which is supplied by the producers or current codes of practice, such as Eurocode 5 [CEN 2004]. Data on failure time of protective layers made of different materials, such as gypsum plasterboard and gypsum fibreboard, were collected during experimental fire tests [e.g. Frangi et al. 2010b; Just et al. 2010; Just et al. 2011; Teibinger and Matzinger 2010]. This event influences the fire behaviour of initially protected timber members that are directly exposed to high temperatures. Therefore, the cladding fall should be modelled numerically to obtain realistic thermal simulations [e.g. Frangi and Erchinger 2007; Frangi et al. 2008b; König and Källsner 2006; Lu et al. 2010].

This chapter presents the finite element modelling implemented in Abaqus code to simulate the large-scale fire tests performed on XLAM floor panels initially protected with different cladding systems. The falling-off of protective layers was modelled since there was experimental evidence of the occurrence of this event. The numerical results in terms of temperature, stress, deflection and fire resistance are discussed and compared with data measured during the tests and analytical predictions using simplified design methods. Furthermore, the comparison between thermal and mechanical states within unprotected and protected XLAM panels is presented.

7.2. THERMAL ANALYSIS IN FIRE CONDITIONS

7.2.1. *Model implementation*

Uncoupled heat transfer analyses were performed to simulate the fire behaviour of the initially protected 5-layer XLAM floor panels tested at CNR-IVALSA (Chapter 5). Three protected XLAM specimens of series 'S' were exposed to one-dimensional (1D) fire on bottom side for about 110 and 61 min during tests No. 2 and 3, respectively. Different claddings were used to protect the 150 deep XLAM panels. A 15 mm layer of gypsum plasterboard type F (GP) and gypsum fibreboard (GF) was fixed directly to specimen S2 and S3-IV, respectively. A cladding made of 40 mm thick rock wool (RW) protected by 12.5 mm layer of GF was arranged to protect the third specimen (S3-III).

A two-dimensional (2D) numerical model was implemented in the general purpose finite element code Abaqus [ABAQUS v.6.9]. Only half of the longitudinal section of specimens (150×5600 mm) was modelled due to material, restraint and fire exposure symmetry (Figure 7.1).

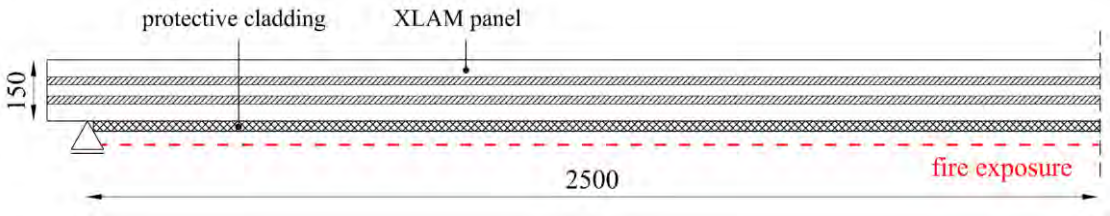

Fig. 7.1 - *Two-dimensional model implemented in Abaqus to simulate the fire exposure of protected XLAM panels (dimensions in mm).*

The model is composed by the XLAM longitudinal section jointed together with the cladding by means of a constraint. The compound cross-section of XLAM panels was described in Abaqus defining two isotropic materials with the same thermal properties for layers parallel and perpendicular to the main floor direction. Furthermore, a material for each protective layer made of GF, GP or RW was defined.

The fire exposure was described numerically by using the fire curve recorded during the tests No. 2 and 3 as an input and by imposing the thermal interactions of convection and radiation with the surrounding environment on exposed and unexposed

surfaces. The values proposed by Eurocode 1 [CEN 2002b] and Eurocode 5 [CEN 2004] for the convection coefficient and the emissivity were adopted, namely 25 W/m^{2}K and 0.8 respectively. The ambient temperature measured at the beginning of the tests was adopted as initial thermal condition in the numerical model. In particular, temperature of 0°C and 22°C were assumed for specimens tested during fire tests No. 2 (specimen S2) and 3 (specimens S3-III and S3-IV), respectively.

The thermal behaviour of the materials used, i.e. wood, GP, GF and RW, is strongly dependent upon the temperature. The thermo-physical properties that govern the heat transmission were defined as temperature-dependent in Abaqus. Different proposals can be found in literature for the variation of thermal conductivity, specific heat and density. In this investigation, the relationships suggested by Eurocode 5 [CEN 2004] and by a recent technical guideline [SP Trätek 2010] for wood and protective materials, respectively, were adopted (Fig. 7.2).

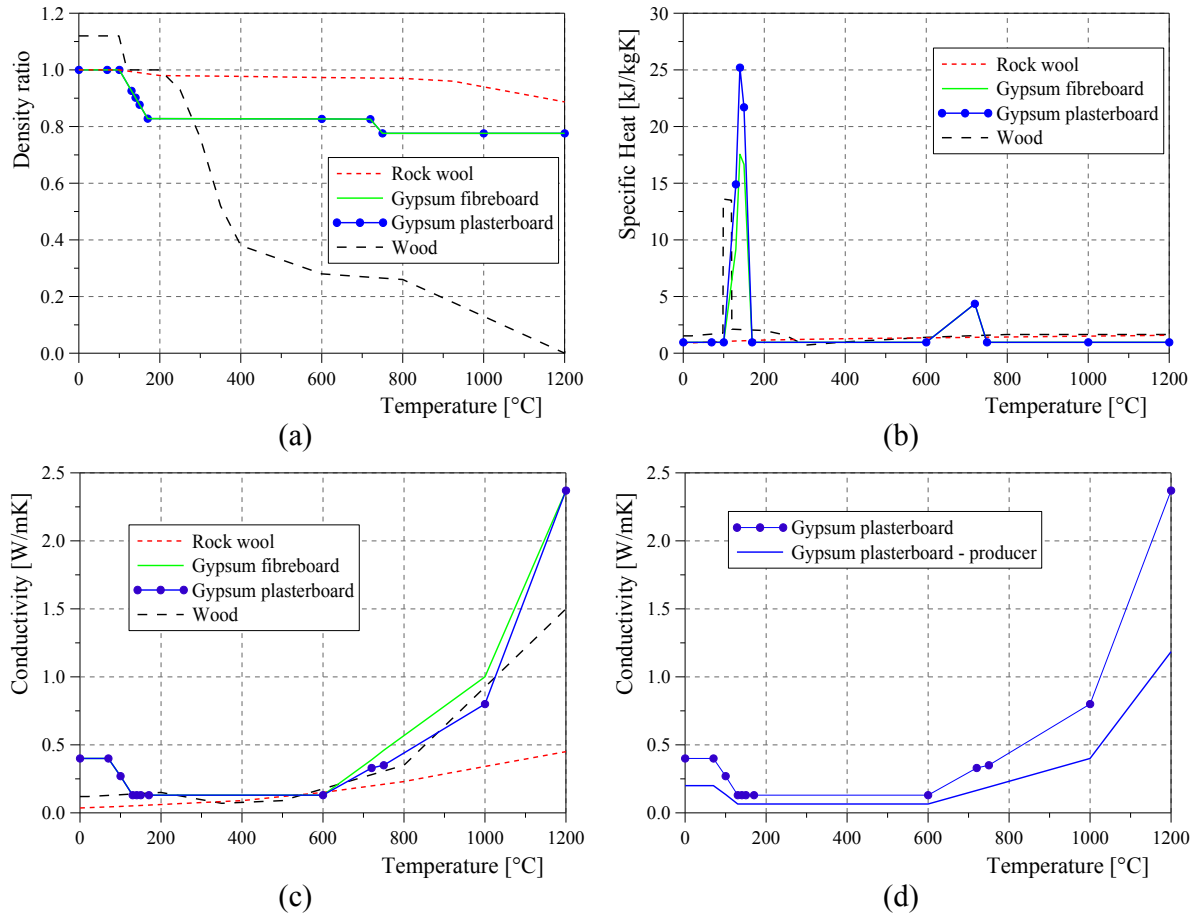

.2 - *Thermo-physical properties adopted to describe the behaviour of wood and fire-protective materials in fire conditions.*

Some thermal analyses were performed also assuming the thermal conductivity of GP at ambient temperature provided by the producer [Knauf]. In this case, the conductivity-temperature relationship was determined as a proportion of the curve proposed by the technical guideline [SP Trätek 2010] (Fig. 7.2d). The densities of about 800 and 1150 kg/m^3 at ambient temperature provided by the producers were adopted for GP [Knauf] and GF [Fermacell], respectively. The experimentally measured values at ambient temperature of moisture content and density of wood, 12% and 450 kg/m^3 respectively, were assumed in the analyses.

Observing the thermocouple records (Fig. 7.3), the falling of the protective layers was deduced since the temperature at the interfaces between the cladding and the XLAM specimen increased rapidly at a certain time. This event was simulated numerically through two sequential thermal analyses. The first analysis was carried out on the model that represents the XLAM floor panel and the cladding subjected to fire on the bottom side, whilst the second analysis considered only the unprotected panel directly exposed to high temperatures. The thermal state within the protected XLAM panel when the cladding falling occurred became an input for the following thermal analysis.

The time of the cladding fall was chosen in two different ways: (i) according to the technical guideline [SP Trätek 2010]; and (ii) based on the experimental data collected by thermocouples during the fire tests. In the former case, the value of 400°C is suggested as the critical temperature for floor claddings that lose their protective function.

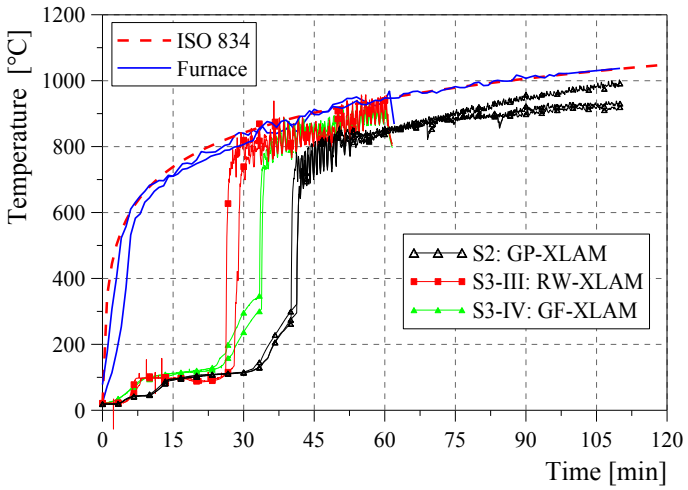

Fig. 7.3 - *Thermocouple records at interfaces between XLAM panels and protective layers.*

Specimen No.	S2	S3-III	S3-IV
Type of protective cladding	GP	GF+RW	GF
400°C at interface [min]	35.0	22.7	34.1
Experimental fall [min]	41.3	26.2	34.0

Table 7.1 - *Assumed times of falling of the protective layers.*

The times when the temperature of 400°C was numerically attained at the cladding-XLAM interfaces (criterion (i)) are listed in Table 7.1. The same table reports the times when the falling of the different claddings was assumed considering the sudden temperature increases recorded experimentally by the thermocouples (criterion (ii)).

Four-node heat transfer quadrilateral, linear elements 'DC2D4', which are available in Abaqus library, were used for the thermal analyses. Simulations using eight-node quadratic elements ('DC2D8') were also performed and results similar to those obtained with linear elements were observed.

The same mesh with elements of approximately 5 mm size chosen in the numerical model of unprotected XLAM panels (mesh 'B' in Fig. 6.7) were adopted since it resulted in a good compromise between the computational time required for the analyses and the accuracy of solution. A mesh with square elements of 5 mm size was used for the protective layers. The entire modelled longitudinal sections protected with a single layer of GP or GF and with a cladding system made of GF and RW were subdivided in 16770 and 20690 elements, respectively (Fig. 7.4).

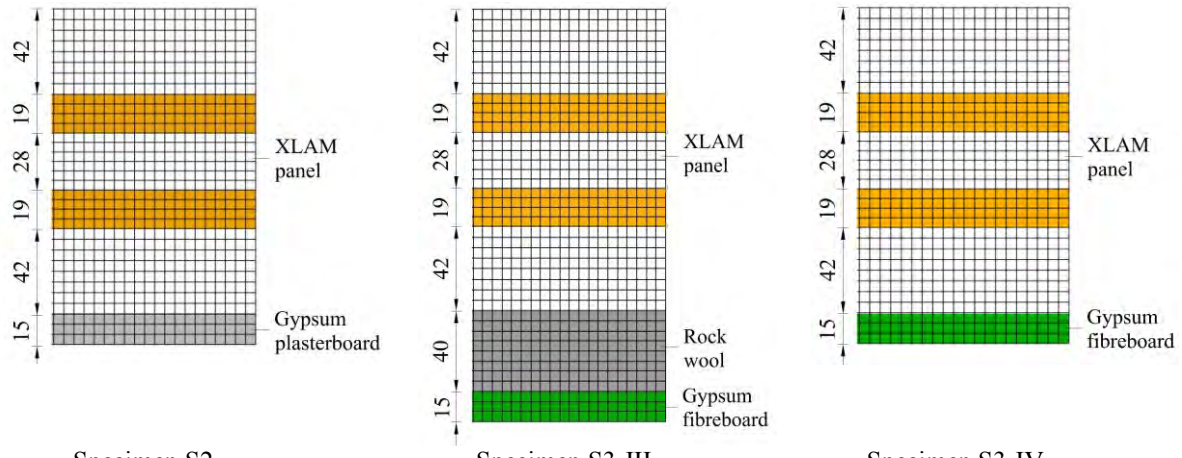

Specimen S2 Specimen S3-III Specimen S3-IV

Fig. 7.4 - *Mesh adopted to model protected XLAM panels in Abaqus (dimensions in mm).*

7.2.2. *Results*

The following figures compare the experimental data and the numerical results in terms of temperature within the floor panels subjected to 1D fire exposure. The thermal states at the interfaces between the XLAM panel and the cladding made of GP (specimen S2) and GF (specimen S3-IV) are plotted in Figures 7.5a and 7.5b, respectively. The numerical results clearly show that the experimental records can be modelled accurately only if the falling of the protective layers (dashed curves) is considered. Two different times of falling off were considered in the thermal analyses, as discussed previously. The simulations carried out considering the presence of the protection until the end of the fire exposure (solid curves) underestimate the temperature distribution. It can be noticed that the charring temperature of 300°C was reached at the cladding-XLAM interface when the protective layer made of GP or GF directly fixed to the XLAM panel fell off.

The GP falling corresponding to the sudden temperature increase recorded by the thermocouples occurred approximately after 41 min of fire exposure. The 300°C and the critical temperature of 400°C were numerically attained respectively 8 and 6 min before the experimental times (Fig. 7.5a).

The experimental falling of the GF was observed when the temperature at the interface was about 400°C according to the critical temperature proposed by the technical guideline [SP Trätek 2010] (Fig. 7.5b).

The temperature distribution in the cladding system made of GF and RW (specimen S3-III), in particular at the GF-RW and RW-XLAM interfaces, are displayed in Figures 7.6a and 7.6b, respectively. The experimental data points out the simultaneous falls of GF and RW approximately after 26 min from the beginning of the fire exposure. The thermal simulations assuming the criterion of the 400°C for the cladding fall are conservative with respect to the experimental records.

The numerical curves are close to experimental values recorded at interfaces of XLAM panels protected with GF and GF plus RW, whereas the temperature increase between GP and XLAM is anticipated by the numerical simulation.

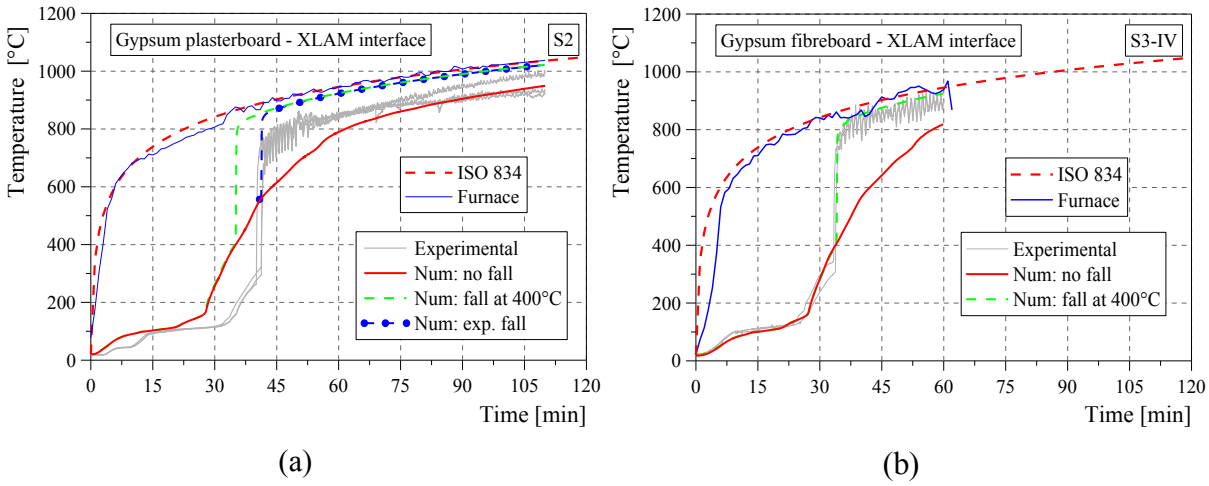

Fig. 7.5 - *Experimental and numerical temperatures at gypsum plasterboard-XLAM interface of specimen S2 (a) and gypsum fibreboard-XLAM interface of specimen S3-IV (b).*

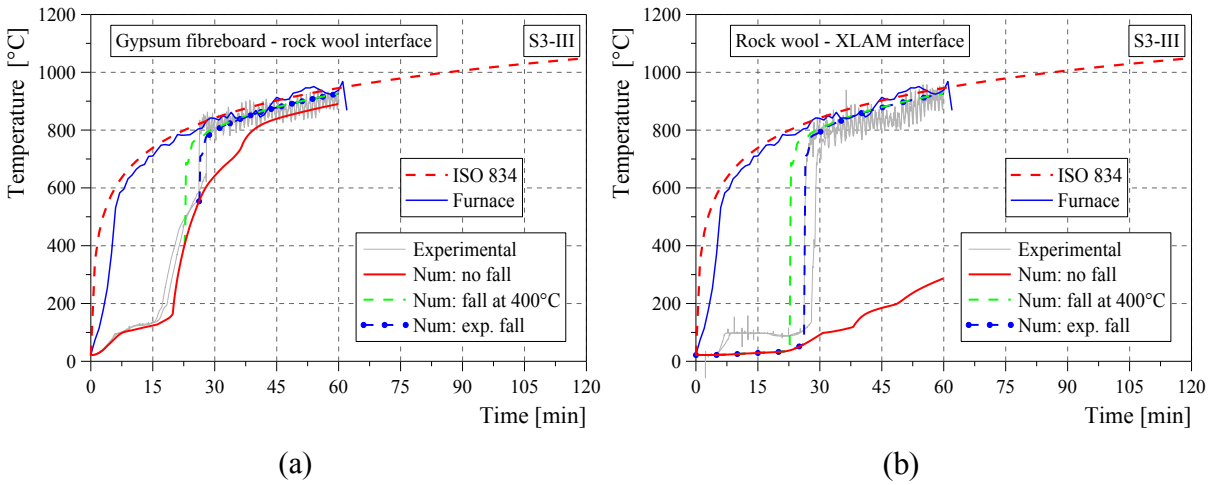

Fig. 7.6 - *Experimental and numerical temperatures at gypsum fibreboard-rock wool interface (a) and gypsum fibreboard-XLAM interface (b) of specimen S3-III.*

The temperature at 21 and 52 mm from the bottom surface of the XLAM floor panel initially protected with GP (specimen S2) are plotted in Figure 7.7. The numerical results clearly show that the temperature distribution within the XLAM section is underestimated if the fall of cladding is not considered in the model. A significant temperature increase was observed (Fig. 7.7) in the last minutes of the fire test (test No. 2) in the fibre at 52 mm from the bottom surface like during the fire test of unprotected XLAM panel (test No. 1). This increase is only partially simulated by the numerical model based on 1D heat flux.

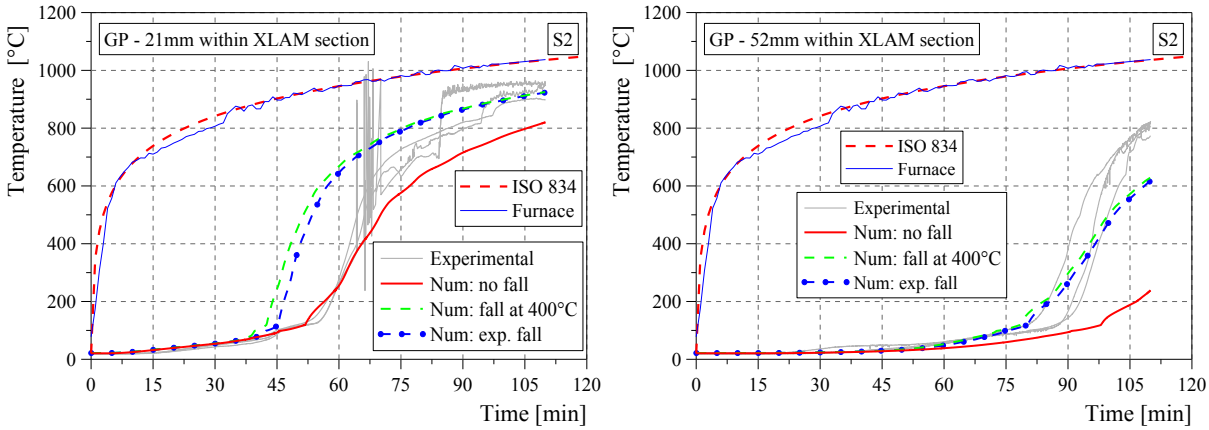

Fig. 7.7 - *Experimental and numerical temperatures within the XLAM panel protected with gypsum plasterboard (specimen S2) at 21 mm (a) and 52 mm (b).*

The thermal states at 52 mm within the XLAM sections protected with GF and RW (specimen S3-III), and GF (specimen S3-IV) are reported in Figures 7.8a and 7.8b, respectively. Fire test No. 3 had a short duration (about 61 min) therefore the thermocouples at 52 and 75 mm from the bottom surface did not measure significant temperature increases. The thermocouple inserted at 21 mm in the XLAM section of specimen S3-IV did not work during the test.

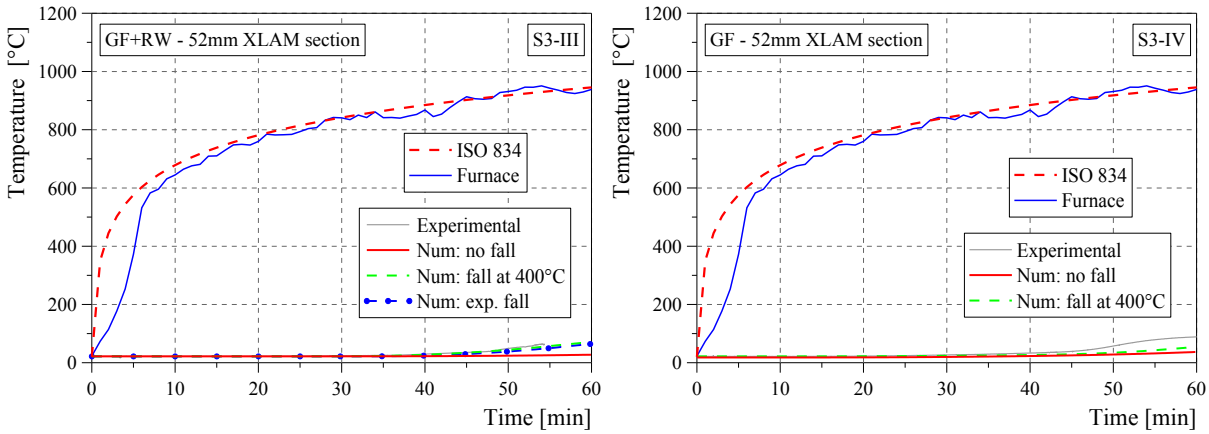

Fig. 7.8 - *Experimental and numerical temperatures at 52 mm within the XLAM panel protected with gypsum fibreboard and rock wool (a), and gypsum fibreboard (b).*

Figures 7.9, 7.10 and 7.11 display the temperature distribution along the depth of specimens protected with GP (specimen S2), GF and RW (specimen S3-III) and GF (specimen S3-IV), respectively. The grey colour represents material with a temperature greater than 300°C, which corresponds to red colour. Blue colour refers to ambient temperature. The thermal state is shown at five times, namely before the fire exposure, when the falling of the claddings was experimentally observed (Table 7.1) and after 30, 60 and 90 min from the beginning of the exposure. The cladding system of specimen S3-III is already fallen off after 30 min of exposure, whereas the other two specimens are still protected and the temperature at their cladding-XLAM interface is close to charring temperature (300°C). The thermal states within the XLAM panels differently protected are very similar after 60 and 90 min of fire exposure.

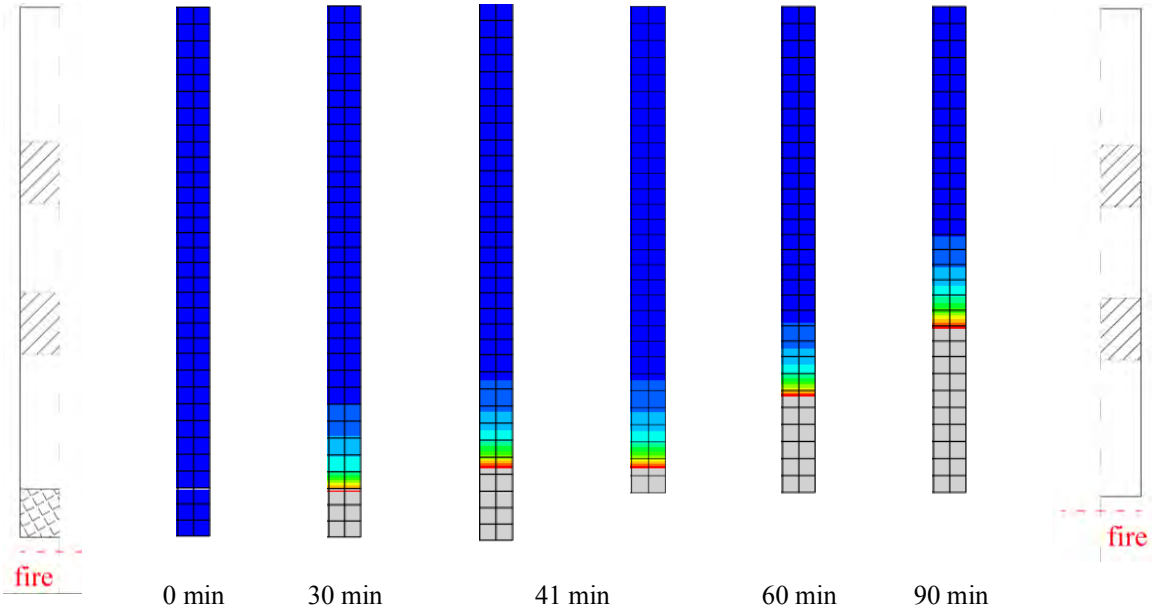

Fig. 7.9 - *Temperature distribution within XLAM panel protected with gypsum plasterboard (specimen S2) at different fire exposure times.*

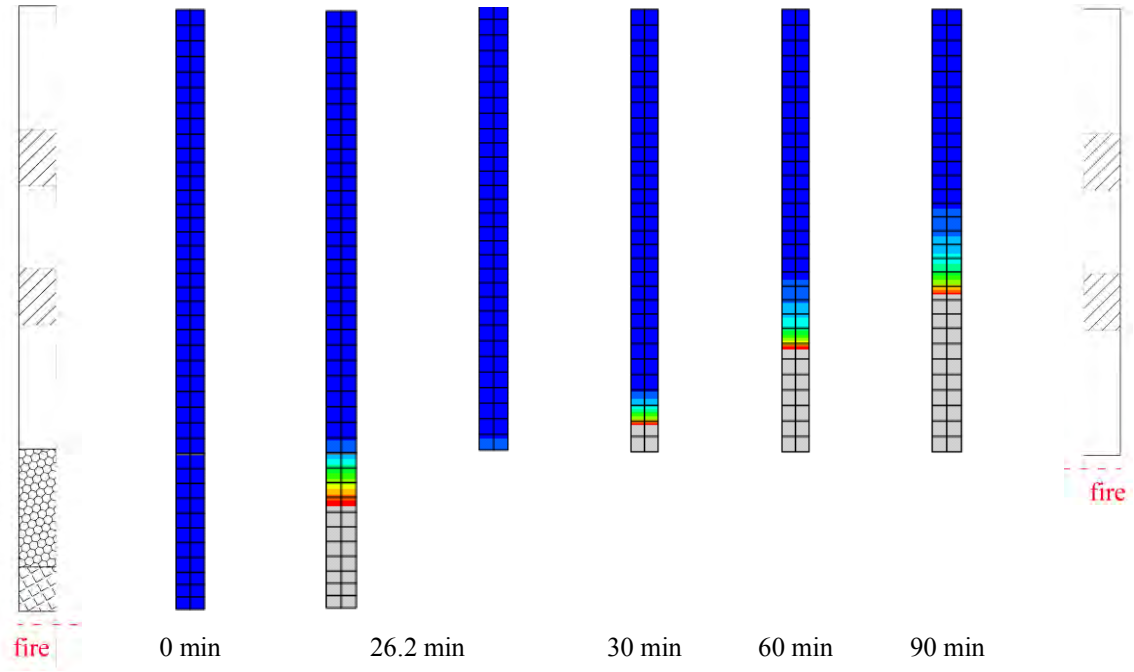

Fig. 7.10 - *Temperature distribution within XLAM panel protected with gypsum fibreboard and rock wool (specimen S3-III) at different fire exposure times.*

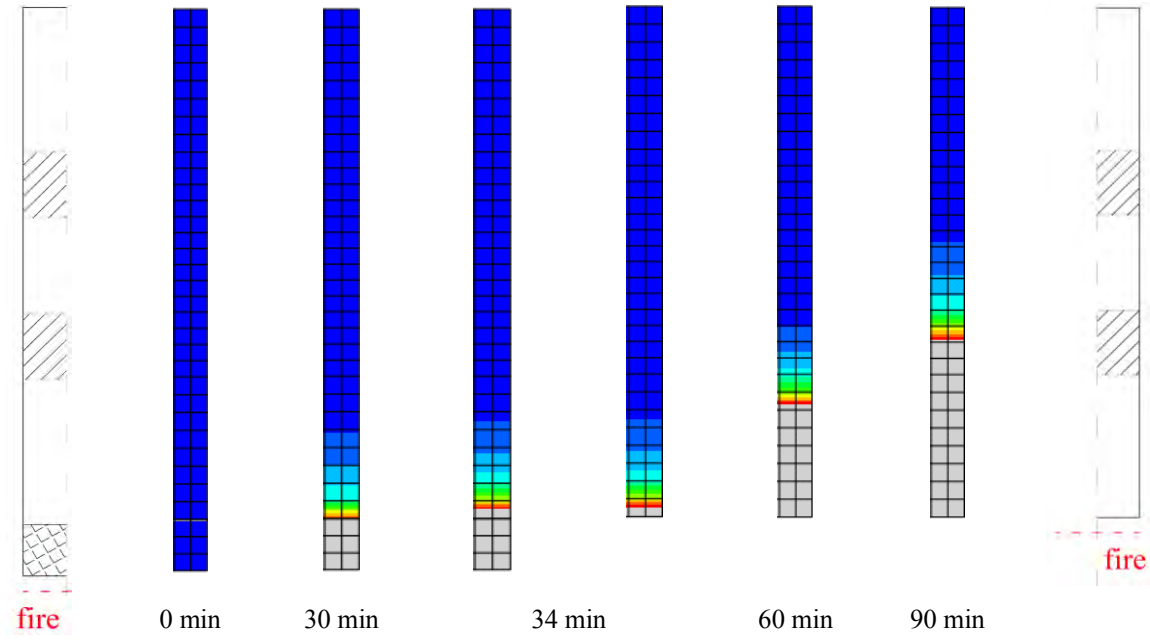

Fig. 7.11 - *Temperature distribution within XLAM panel protected with gypsum fibreboard (specimen S3-IV) at different fire exposure times.*

7.2.3. *Discussion*

Since the numerical prediction anticipated the temperature increase at GP-XLAM interface of specimen S2 (Fig. 7.5a), the value of thermal conductivity at ambient temperature provided by the GP producer [Knauf] and its variation with temperature (Fig. 7.2d) were adopted in the modelling. In this case, the analyses provided more accurate results than using the values suggested by the technical guideline [SP Trätek 2010]. The temperature distributions at GP-XLAM interface without falling of the protection were analysed defining the different conductivity-temperature relationships (Fig. 7.12a). The critical temperature of 400°C assuming the producer conductivity is numerically attained 5 min later the experimental time (41 min), whereas the beginning of the numerical charring coincides with the thermocouple records of 300°C.

Figures 7.12b and 7.13 plot the thermal states respectively at GP-XLAM interface and within the XLAM section obtained by modelling the cladding falling at two different times, as discussed previously (Table 7.1).

Figure 7.14a compares the thermocouple readings with the temperature distribution obtained numerically within the 150 mm deep cross-section at different fire exposure times. Seven times are considered, namely the time before fire exposure, the time of the cladding falling (41 min), the experimental and numerical failure times corresponding respectively to 110 and 120 min of fire exposure, and three intermediate times (30, 60 and 90 min).

Figure 7.14b plots the charred depth versus the fire exposure time of specimen S2. The experimental values were obtained indirectly from data recorded by thermocouples in three cross-sections and at different depths from bottom surface. The 300°C is assumed as the border between charred and heated wood as suggested by Eurocode 5 [CEN 2004]. The numerical results obtained by adopting different thermal conductivity-temperature relationships are also compared. It can be noticed that the experimental beginning of charring of XLAM cross-section is well simulated by the analysis performed using the conductivity value at ambient temperature provided by the producer.

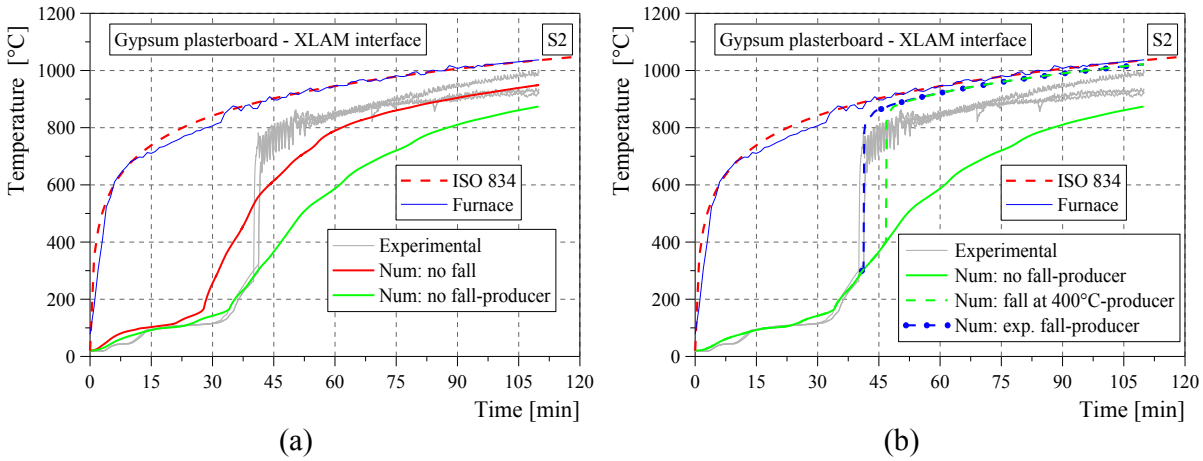

Fig. 7.12 - *Experimental temperatures at gypsum plasterboard-XLAM interface (specimen S2) compared with numerical results obtained by using different conductivity for gypsum plasterboard (a) and by modelling the cladding fall at different times (b).*

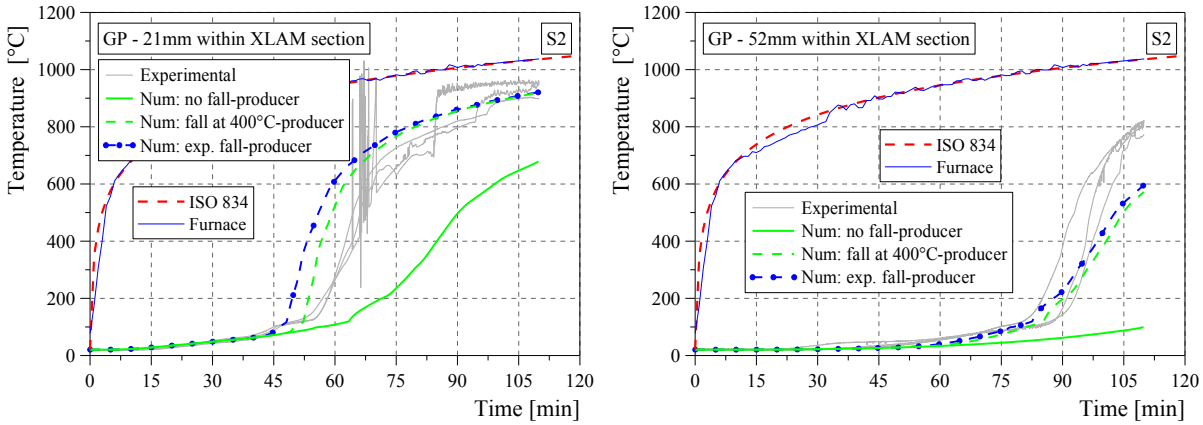

Fig. 7.13 - *Experimental and numerical temperatures within the XLAM panel initially protected with gypsum plasterboard (specimen S2).*

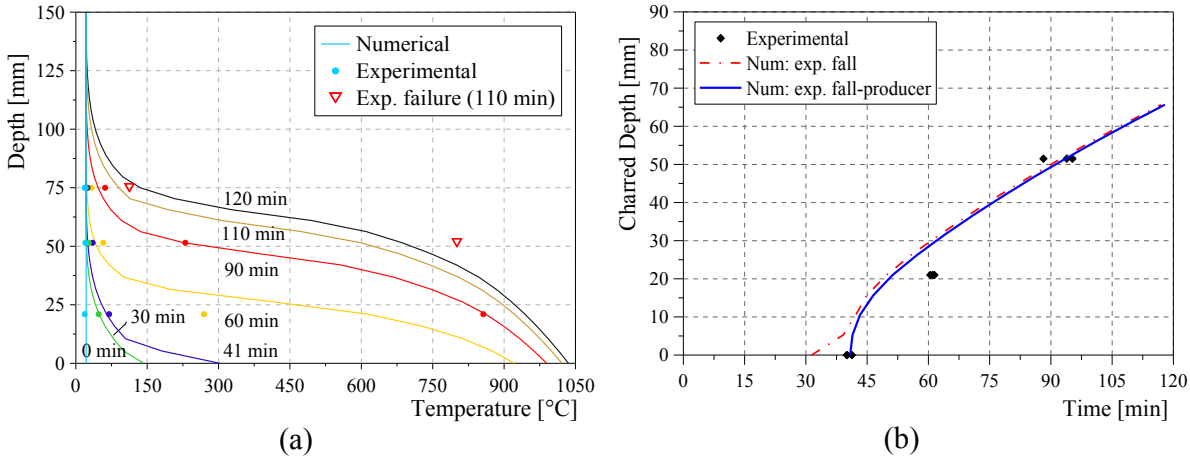

Fig. 7.14 - *(a) Experimental and numerical temperature along the panel depth at different exposure times. (b) Charred depth vs. time from experimental data and numerical modelling.*

The model is unable to capture the temperature increase observed towards the end of the test even if a different GP thermal conductivity was adopted. Therefore half of the transversal cross-section of specimen S2 was modelled in Abaqus to implement the change of fire exposure from 1D to 2D caused by the large deflection of the loaded panel specimen with respect to the adjacent unloaded panels. The model was subdivided in 1980 elements (type 'DC2D4') of approximately 5 mm size (Fig. 7.15).

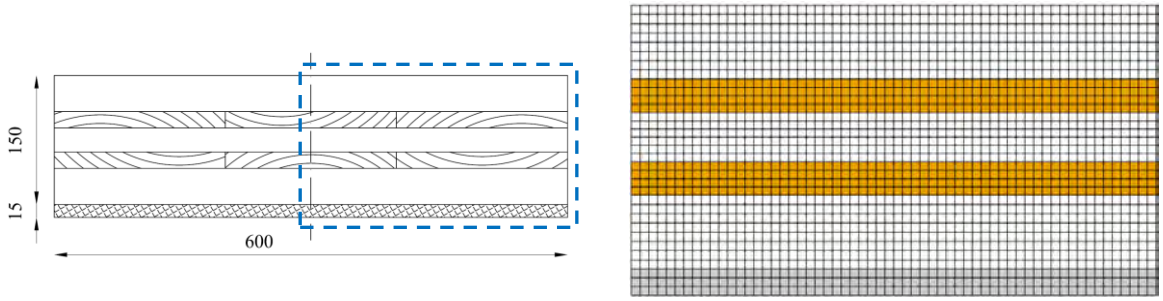

Fig. 7.15 - *Transversal cross-section of protected XLAM panels (left) and two-dimensional model of the cross-section implemented in Abaqus (right) (dimensions in mm).*

Three consecutive thermal analyses were carried out to simulate the 1D fire exposure on the bottom side of initially protected cross-section, and both the 1D and 2D heat fluxes on unprotected cross-section after the cladding fall. Based on experimental results, the 2D thermal analysis was started after 80 min of fire exposure. The temperature distribution at the end of each analysis became an input for the following thermal analysis.

Figure 7.16a plots the temperature at 52 mm obtained by modelling the falling of GP and the variation of heat flux from 1D to 2D in the transversal cross-section after about 41 and 80 min of fire exposure, respectively (dashed curve). It can be noticed that the temperature increase in the last minutes of fire test is in good agreement with the experimental values. This outcome explains the overestimation of the experimental fire resistance of the protected panel by the numerical model based on the 1D heat flux as discussed in the following paragraph. The variation of fire exposure led to an increase of charring rate (Fig. 7.16b) and consequently to a greater reduction of resisting cross-section.

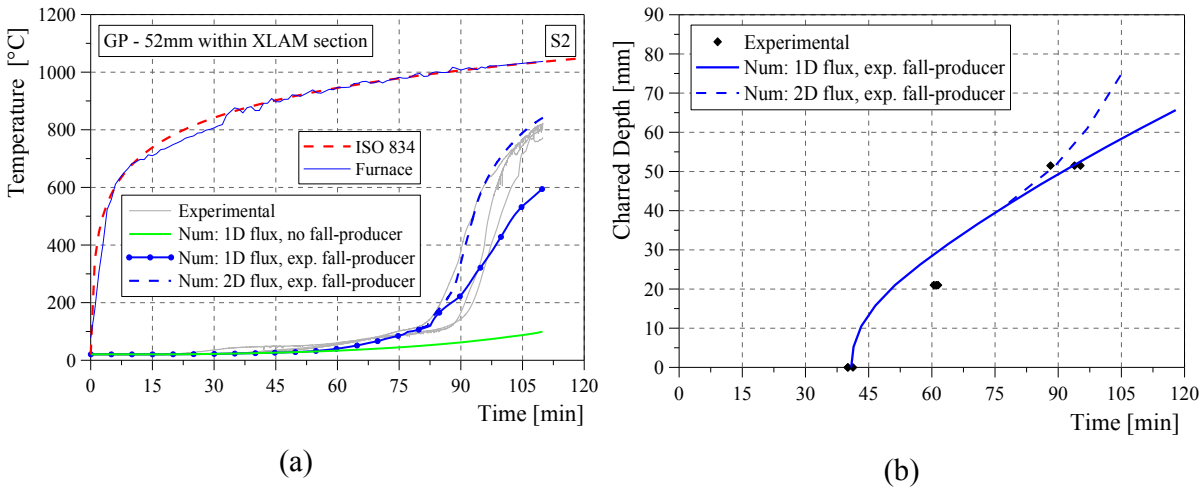

Fig. 7.16 - *Experimental data and numerical results in terms of temperature distribution within the initially protected XLAM panel (a) and charred depth (b) vs. fire exposure time.*

The graphic visualization of thermal states within cross-section when the GP cladding fell (41 min), the heat flux changed from 1D to 2D (80 min) and the numerical failure of XLAM panel occurred (120 min) are displayed in Figure 7.17. The charred material is represented by grey colour, whereas red and blue colours correspond to charring and ambient temperatures, respectively.

The charring of the XLAM panel starts after about 41 min of fire exposure when the 300°C isotherm attains the GP-XLAM interface and the protective cladding falls off (Fig. 7.17a). In Figure 7.17b the thermal state at 80 min is displayed. At that time, the heat flux changes from 1D to 2D. Only the lower layer (first layer from bottom) is completely charred, whereas about half cross-section has a temperature close to ambient temperature (blue colour). Half of the depth is charred at 120 min when the XLAM panel failure is imminent (Fig. 7.17c). At least 60 mm of panel width are already charred after about 40 min of 2D fire exposure (Fig. 7.17c).

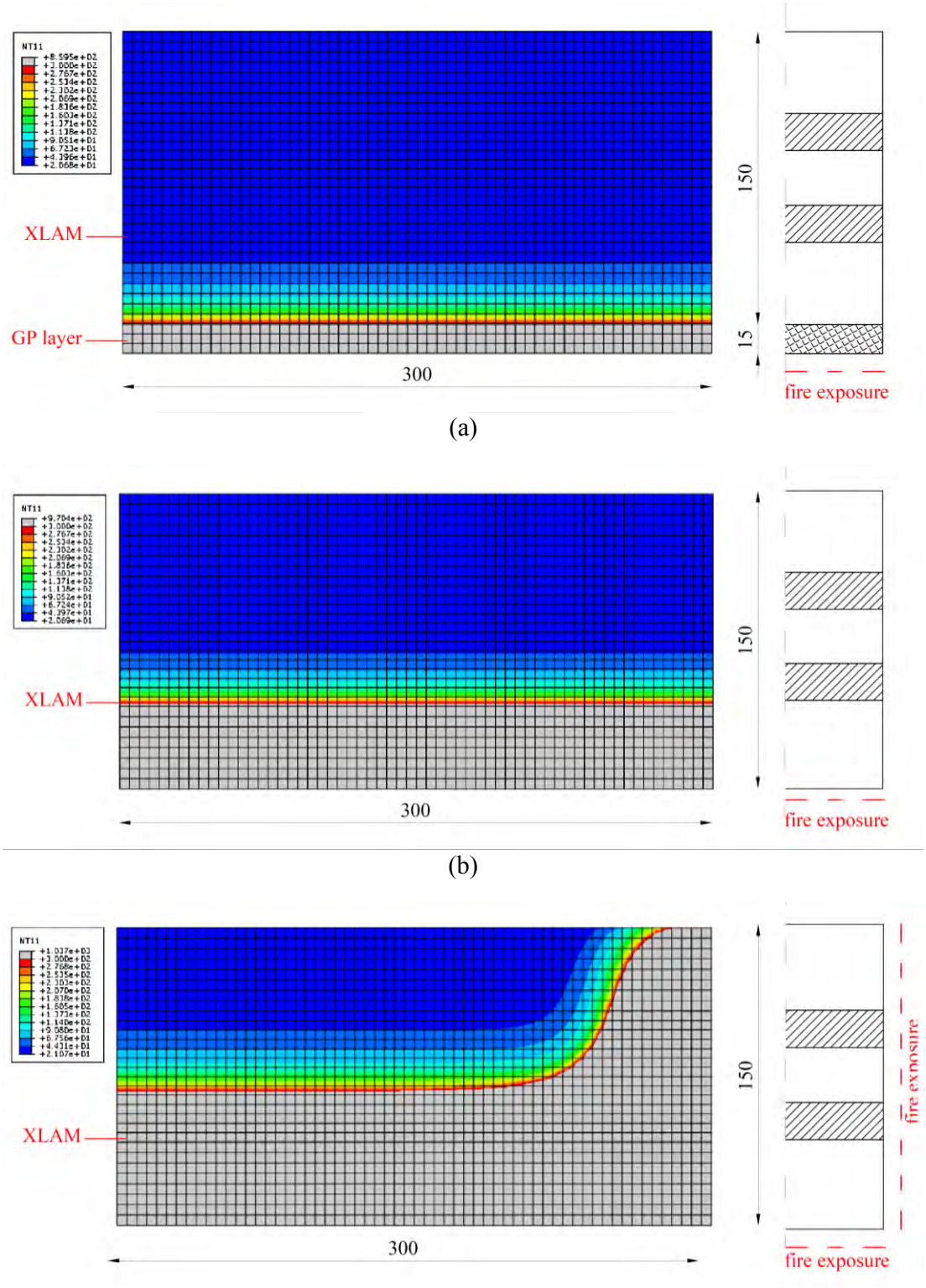

Fig. 7.17 - *Temperature distributions within cross-section of initially protected XLAM panels after (a) 41, (b) 80 and (c) 120 min of fire exposure.*

7.3. THERMO-MECHANICAL ANALYSIS IN FIRE CONDITIONS

7.3.1. *Model implementation*

Sequential coupled thermo-structural analyses were carried out in Abaqus [ABAQUS v.6.9] to simulate the experimental test carried out on a XLAM floor panel protected with F-type GP (specimen S2). The simply supported panel (150×600×5600 mm) was subjected to uniformly distributed load q_i of 10 kN/m^2 corresponding to 21% of the estimated mean load-carrying capacity at ambient temperature, and then exposed to 1D heat flux on the bottom side until the structural failure occurred after about 110 min (Chapter 5).

The same 2D finite element model described for the thermo-structural analyses of unprotected XLAM floor panels was used (Chapter 6). Unlike the thermal modelling of protected XLAM panel, the structural model represents only the XLAM part as the cladding contribution to the mechanical resistance of the floor assembly is negligible. Load, geometry and boundary conditions of the model are displayed in Figure 7.18. The uniformly distributed load applied during the fire was defined as a uniform pressure on the top surface of the panel. A simple support was defined on one end of the model, whilst on the other end, corresponding to the symmetry plane, a constraint that allows only the vertical displacement was imposed.

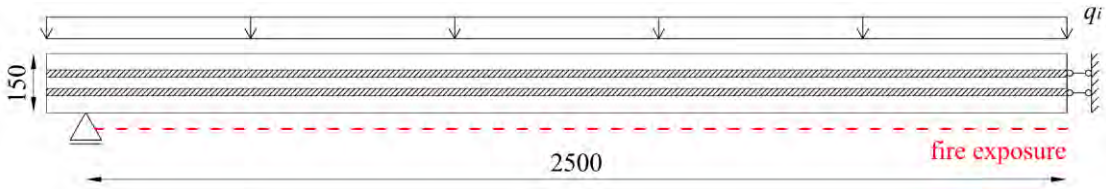

Fig. 7.18 - *Two-dimensional model implemented in Abaqus to simulate tests of initially protected XLAM panels in fire conditions (dimensions in mm).*

The thermal analysis simulates the exposure to high temperature, whilst the following mechanical analysis allows the evaluation of the fire resistance of loaded structural members. The temperature distributions within the member become an input for the mechanical model since the stresses induced by applied loads depend upon the thermal state in the section, whereas the inverse relationship does not hold. The correspondence of node labels must be ensured in order to implement the thermal states into the structural model, therefore a model with the same geometry and mesh (mesh 'B' in Fig. 6.7) must be utilized for both the consecutive thermal and mechanical analyses.

Four-node quadrilateral, linear elements with reduced integration (type 'CPS4R') were used for the structural analyses. The analyses of unprotected XLAM panels performed using quadratic elements with reduced integration ('CPS8R') did not provide a significant improvement of results in terms of fire resistance and stress distribution (Fig. 6.16b), therefore the linear elements were used. The model is subdivided in 14790 elements of approximately 5 mm size.

The mechanical properties of wood are dependent upon the temperature, like the thermal parameters. The temperature-dependent relationships suggested by the Eurocode 5, Part 1-2 [CEN 2004] for standard fire exposure were adopted (Fig. 7.19a).

The layers parallel and perpendicular to the main floor direction that compounded the XLAM cross-section were characterized in Abaqus by defining two isotropic materials with different mechanical behaviours. The mean values of strength and Young's modulus estimated from experimental data at ambient temperature were assumed for the layers parallel to the main floor direction (Table 7.2). The strength of the perpendicular layers were assumed as $1/10^{th}$ of the values in the main layers (Table 7.2), whereas a fictitious Young's modulus was calculated based on a shear modulus and a Poisson's ratio of 40 N/mm^2 and 0.5, respectively.

A plasticity model readily available in Abaqus for concrete, the 'concrete damaged plasticity' (CDP) model, was chosen to describe the mechanical behaviour, because there is not a specific predefined material model for wood. The different timber behaviour in compression and tension can be implemented in this plasticity model by taking also into account the influence of temperature on mechanical properties. Elasto-plastic and elasto-brittle strength-strain relationships were defined at different temperature for timber in compression and tension, respectively. Figure 7.19b plots the relationships defined for layers parallel and perpendicular to the main floor direction.

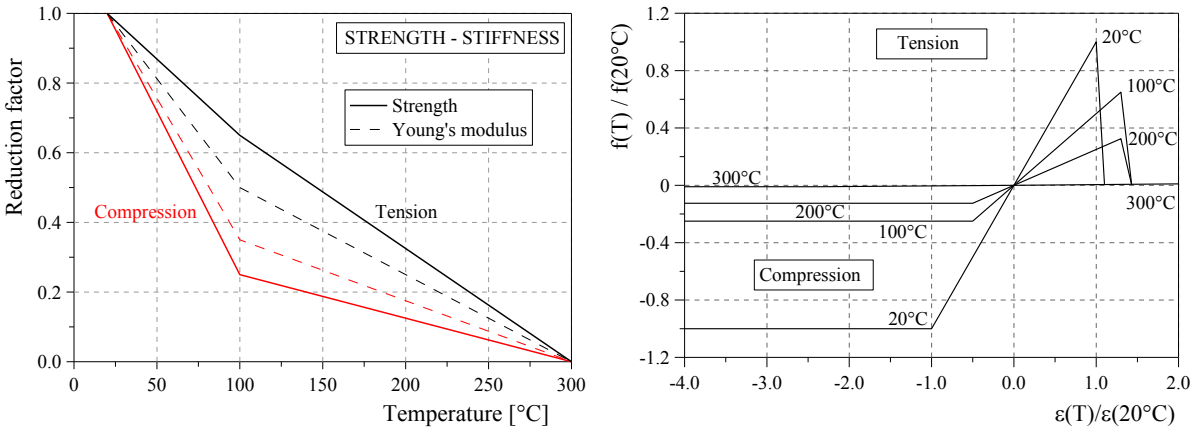

(a) (b)

Fig. 7.19 - *(a) Strength and Young's modulus reductions with temperature in compression and in tension as suggested by Eurocode 5 [CEN 2004]. (b) Strength-strain relationships in compression and tension at different temperatures for layers parallel and perpendicular to main floor direction.*

The CDP permits the definition of only one relationship for the variation of Young's modulus with temperature. The stiffness-temperature relationship suggested by the Eurocode 5 for timber in tension was implemented since the failure of structural elements in bending occurred mainly for fracture in tension of the lower layers.

The numerical failure of the XLAM floor panel was assumed to occur when the analysis terminates due to convergence problems. That happens when the strength at a determined thermal state is attained in some elements. Therefore, the failure time to the last increment of the analysis provides the fire resistance of the structural element.

In the analyses of the protected XLAM panel tested at CNR-IVALSA, the convergence was not achieved in the elements located in the third layer of the XLAM cross-section. This is the second resistant layer as the layers running perpendicular to the main floor direction do not carry significant amount of load due to their low Young's modulus parallel to the main floor direction.

Layers	Parallel	Perpendicular
Tension strength [N/mm^2]	41.79	4.18
Compression strength [N/mm^2]	52.74	5.27
Young's Modulus [N/mm^2]	12564	120

Table 7.2 - *Strength and stiffness values at ambient temperature*

7.3.2. *Results*

The numerical results presented here refer to the mid-span cross-section of a XLAM panel initially protected with F-type GP, loaded with 21% of the failure load at ambient temperature and subjected to 1D fire exposure.

The thermal state was obtained through a thermal analysis assuming the value of thermal conductivity at ambient temperature provided by the GP producer and modelling the falling of the cladding after about 41 min of fire exposure, as discussed previously.

The stress distributions within the XLAM cross-section at different times, namely the time before the fire exposure, the numerical failure time (120 min) and three intermediate times (30, 60 and 90 min) are plotted in Figure 7.20a.

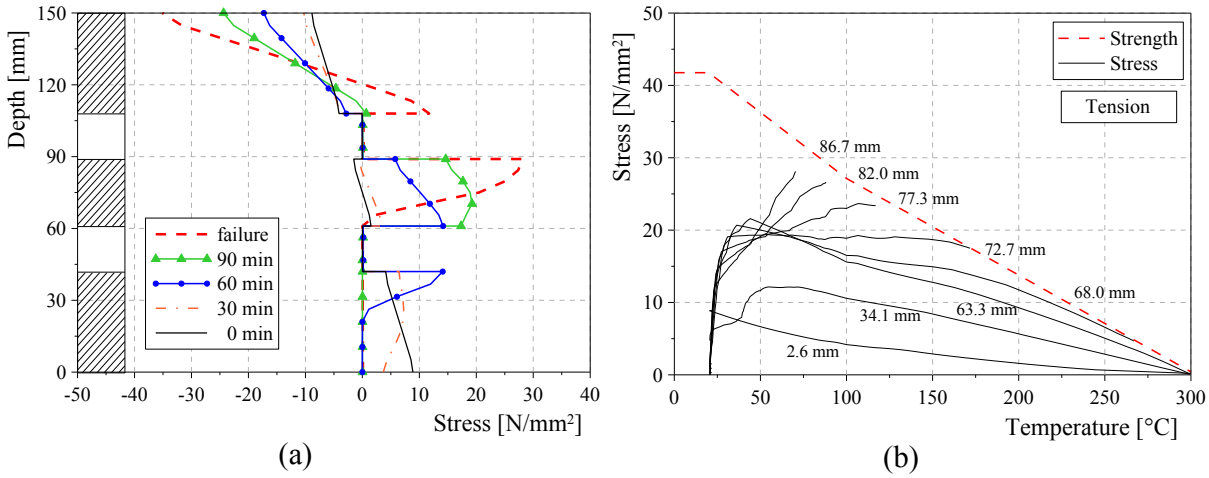

Fig. 7.20 - *(a) Stress distributions along the panel depth at different exposure times. (b) Stress and strength vs. temperature at different depths in the XLAM section.*

The stresses in the layers parallel to the main floor direction vary during the fire exposure because of the stress redistribution process that takes place in the timber cross-sections exposed to increasing temperatures. In the lower layer (first layer) the stresses are reduced immediately after the fire exposure and they are redistributed in the inner layers where the temperature is still low and the mechanical properties are almost unchanged. The stress drops to zero when the charring temperature, assumed equal to 300°C as suggested by Eurocode 5 [CEN 2004], is attained. At that temperature, charred wood loses its load-bearing capacity and the resisting cross-section decreases consequently until failure takes place. In the case under study, the failure occurs in the

third layer (second parallel layer) after approximately 120 min of fire exposure. At that time, the stress reaches the maximum tensile strength of timber at the corresponding thermal state. The residual cross-section at failure time includes two of the three layers parallel to the main floor direction (Fig. 7.21). However, one of these (the third layer) has a temperature ranging from 100°C to about 300°C so its load-bearing capacity is markedly reduced. The layer more distant from fire (the fifth layer) is the only one subjected to compressive stress, which is lower than the material strength also when failure occurs. In this layer the temperature remains constant at the ambient value throughout the fire exposure, therefore its mechanical capacity does not decrease.

Figure 7.20b shows the tensile stress redistribution in the XLAM layers parallel to the main floor direction. The variation of the tensile strength with temperature is represented by the dashed curve. In the fibres more exposed to fire, for example at 2.6 and 34.1 mm depth, the initial stress rises and then it drops due to the temperature increase. Conversely the inner fibres, for example at a depth of 72.7 mm, are subjected to an increasing stress until the maximum strength at that temperature is attained. The strength domain is not reached where the temperature is still low, i.e. at 82 mm.

Figures 7.21 and 7.22 display the temperature and stress distributions in the initially protected XLAM panel at different times, namely before the fire exposure, when the numerical failure occurred (120 min) and at three intermediate times (30, 60 and 90 min). In Figure 7.21 the grey, red and blue colours represent the charred wood, the 300°C temperature and the ambient temperature, respectively. It can be noticed that approximately half of the panel depth has a temperature over 300°C at numerical failure time (120 min), whilst the more distant layer (fifth layer) from bottom surface parallel to the main floor direction maintain almost unchanged its initial temperature throughout the test. In Figure 7.22 the green colour represents the material with no load-bearing capacity, namely the charred wood and the layers perpendicular to the main floor direction. The red and blue contours correspond respectively to tension and compression stresses in the residual resistant layers. The out-of-plane load applied on XLAM panel is the 21% of the estimated failure load, therefore the element is subjected to low stress before the fire exposure. Compressive and tensile stresses rise in the residual section with the increasing temperature until the maximum strengths (red and blue colours) at that specific thermal state are attained.

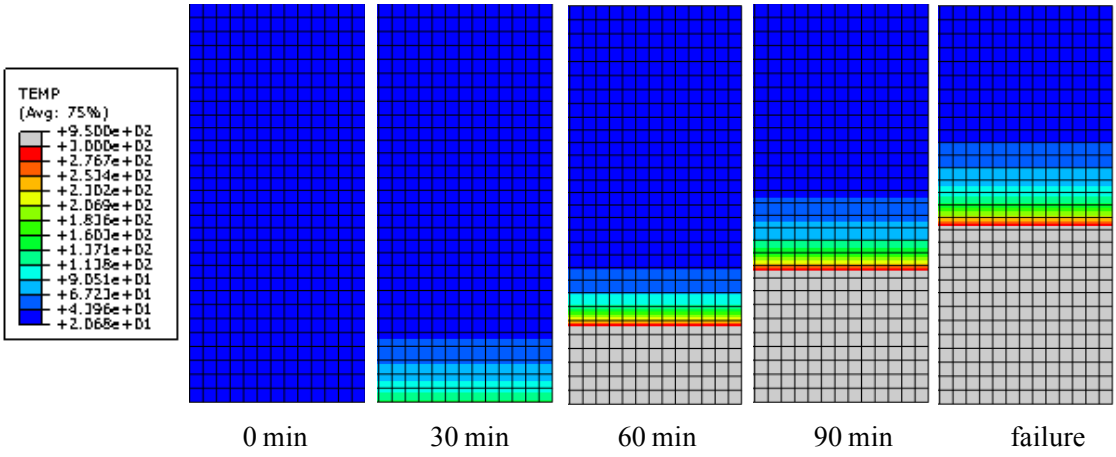

Fig. 7.21 - *Graphic visualization of residual XLAM section at different times from the onset of fire.*

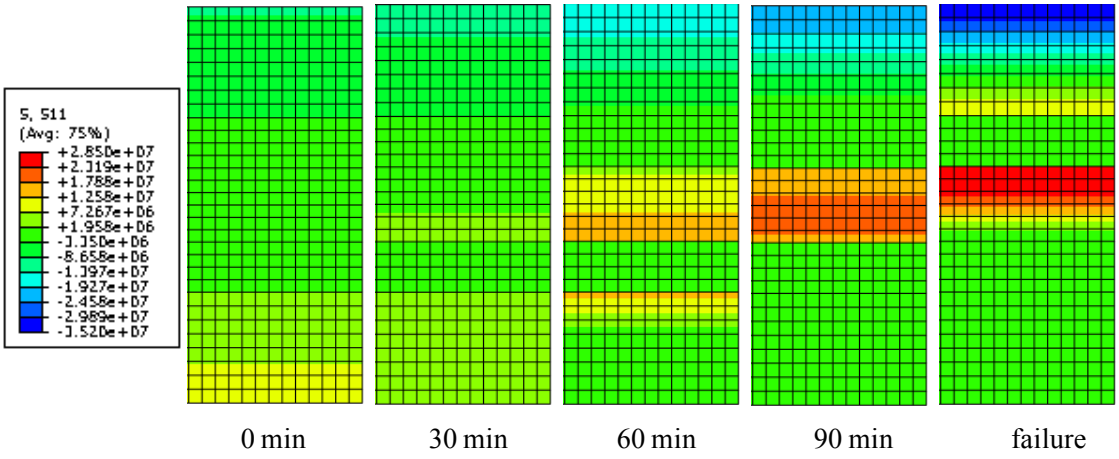

Fig. 7.22 - *Graphic visualization of stress distribution in the residual XLAM section at different times from the onset of the fire.*

Figure 7.23 compares stresses at different exposure times (30, 60 and 90 min) and depths in protected and unprotected XLAM sections. The stresses along the protected panel depth are lower than within unprotected panels at the same time (Fig. 7.23a). The GP cladding delays the heat transfer and the start of charring in the XLAM section, therefore the stress redistribution from hottest to cooler fibres is slowed down with respect to unprotected panels. Tensile stresses at different depths in protected and unprotected elements have similar trends with the increasing temperature (Fig. 7.23b). The plotted numerical results show the different temperature assumed in the models to describe the initial thermal state of specimens S2 and S3-IV according to experimental data.

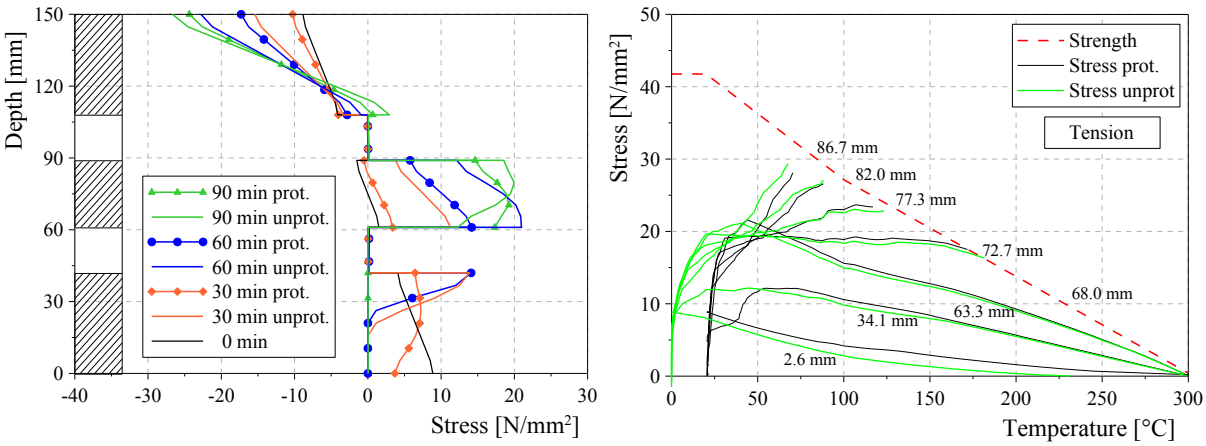

Fig. 7.23 - *(a) Stress distributions along the depth of protected and unprotected panels at different exposure times. (b) Stress and strength vs. temperature at different depths in the protected and unprotected XLAM sections.*

Figure 7.24a displays the numerical results of the thermo-mechanical analysis when the numerical failure occurred, that is approximately 120 min from the beginning of the fire exposure. At that time, only the two lower layers are completely charred and therefore not stressed. The charring has started also in the third layer that is mainly heated. The temperature distribution obtained by the thermal analysis was used to determine the strength domain along the panel depth according to the reduction laws proposed by the Eurocode 5 (Fig. 7.19a). The tension and compression stresses redistributed in the third and fifth layers are compared with the corresponding strength domains, which are almost constant along the fifth layer depth since the temperature does not change significantly. The tensile stress distribution in the third layer corresponds to the ultimate strength domain when numerical failure occurs (120 min).

The thermal and mechanical states within the XLAM section after 60 min of fire exposure are displayed in Figure 7.24b. At that time, the temperature in the section is still close to the ambient one, therefore the material strength is almost unchanged. The stress curve is far from the strength domain since the applied load is low (21%) with respect to the estimated ultimate strength.

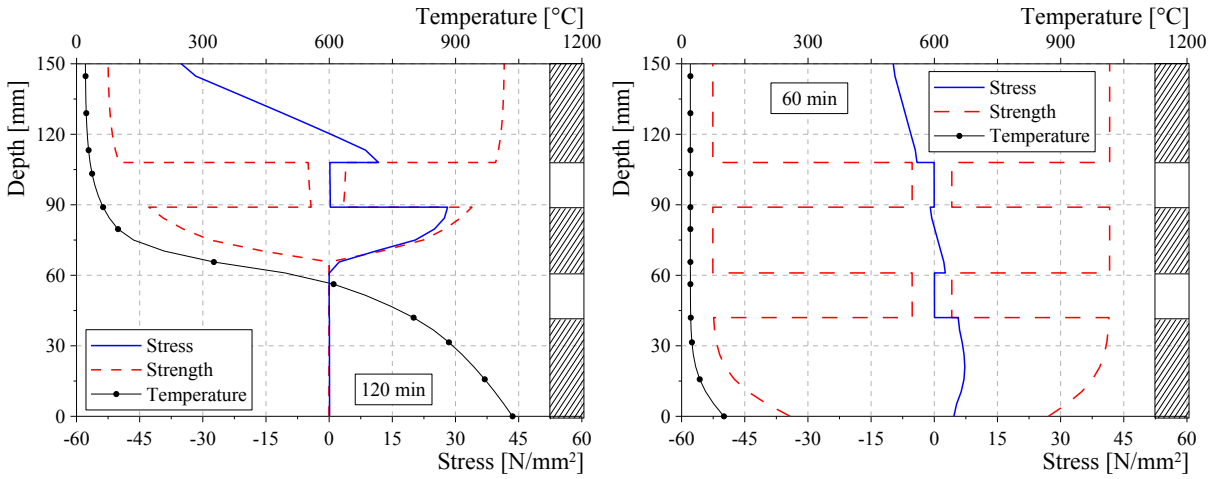

Fig. 7.24 - *Temperature, stress and strength distributions along the mid-span depth of the protected XLAM panel at failure time (a) and after 60 min of fire exposure (b).*

7.3.3. *Discussion*

The numerical modelling slightly overestimates (about 8%) the experimental fire resistance of the XLAM panel protected with GP and loaded uniformly with 10 kN/m^2 corresponding to 21% of the failure load at ambient temperature.

A similar difference was already found in the prediction of fire resistance of unprotected XLAM floor panels (Chapter 6). In that case, a change of heat flux from 1D to 2D due to flames introduced between the specimen and its lateral protection shortly before the failure was observed from experimental data due to the high deflection at mid-span. Therefore, a 3D model of a small block at mid-span of the XLAM panel loaded in bending was implemented in Abaqus to simulate the thermo-structural state at mid-span of an unprotected panel subjected to change of fire exposure from 1D to 2D after about 80 min. These numerical models provided a very accurate estimation of fire resistance and temperature distribution within the panel.

The variation of fire exposure from 1D to 2D led to an increase of charring rate, as observed also numerically (Fig. 7.16b), and consequently to a greater reduction of resistant cross-section causing the anticipate failure of the XLAM floor panel with respect to the 1D heat flux. Therefore, thermo-mechanical analyses considering the 2D

heat flux were performed using a 3D model of a small block at mid-span of the protected XLAM panel subjected to bending similar to the model already implemented in Abaqus for unprotected elements (Fig. 7.25). The 15 mm thick GP layer was introduced in the thermal model.

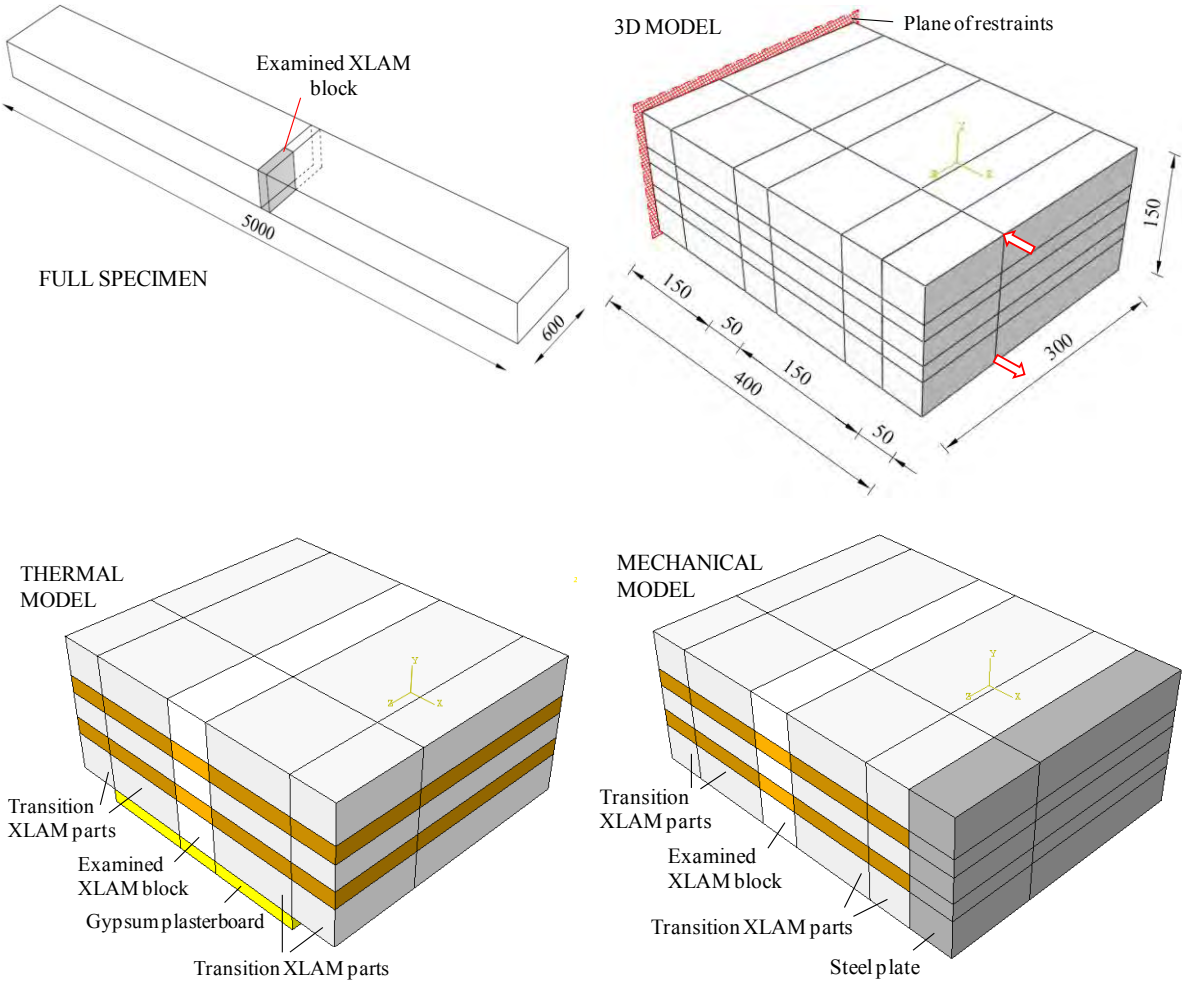

Fig. 7.25 - *Geometry of the three-dimensional models implemented in Abaqus for initially protected XLAM panels (dimensions in mm).*

Eight-node linear brick elements type 'DC3D8' and 'C3D8R' were used for the thermal and mechanical analyses, respectively. The transversal cross-section of the 3D model is divided into 567 elements of different sizes. In particular, the mesh is denser in the part subjected to 2D heat flux from the bottom and lateral sides (Fig. 7.26).

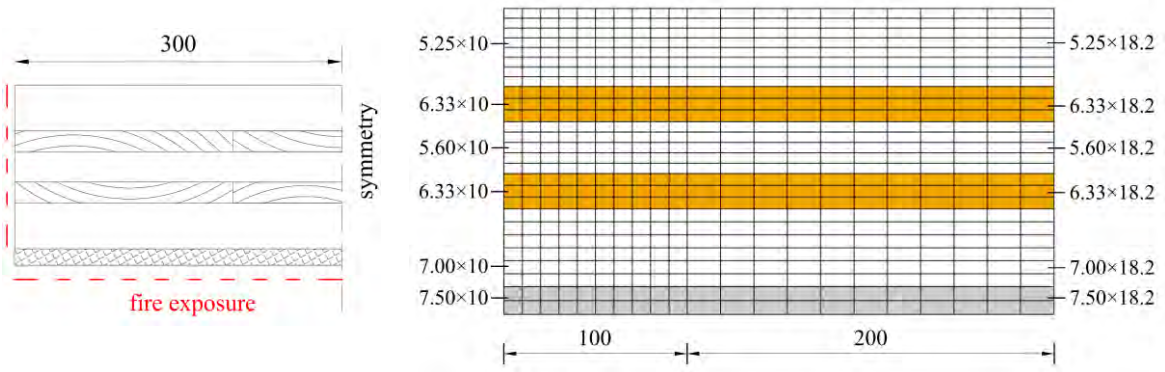

Fig. 7.26 - *Mesh adopted for protected cross-section of the three-dimensional model (dimensions in mm).*

The temperature distribution within the cross-section of the small numerical block was obtained through three consecutive thermal analyses by modelling the falling of GP and the variation of heat flux from 1D to 2D after about 41 and 80 min from the beginning of the fire exposure, respectively. Figure 7.27 displays the thermal state of the cross-section of the block at different times, namely close to the falling of GP (41 min), the change of heat flux (80 min) and the numerical failure of XLAM panel (109 min). The charred material is represented by the grey colour, whereas the red colour corresponds to 300°C temperature. Almost half of the XLAM cross-section depth has a temperature close to the ambient one (blue colour) after 80 min of 1D fire exposure from the bottom side. Conversely, only the two farther layers (fourth and fifth from bottom) have still a low temperature after 109 min, that is after about 29 min of exposure to 2D heat flux from bottom and lateral sides. Moreover, approximately 50 mm of the width are already charred due to the lateral heat flux.

The predicted fire resistance (109 min) is in good agreement with the experimental failure time (110 min), providing further confirmation of the model accuracy (Table 7.3).

Load level	21%
Numerical (2D)	120 min
Numerical (3D)	109 min
Experimental	110 min

Table 7.3 - *Experimental and numerical comparison of the fire resistance of protected XLAM floor panel.*

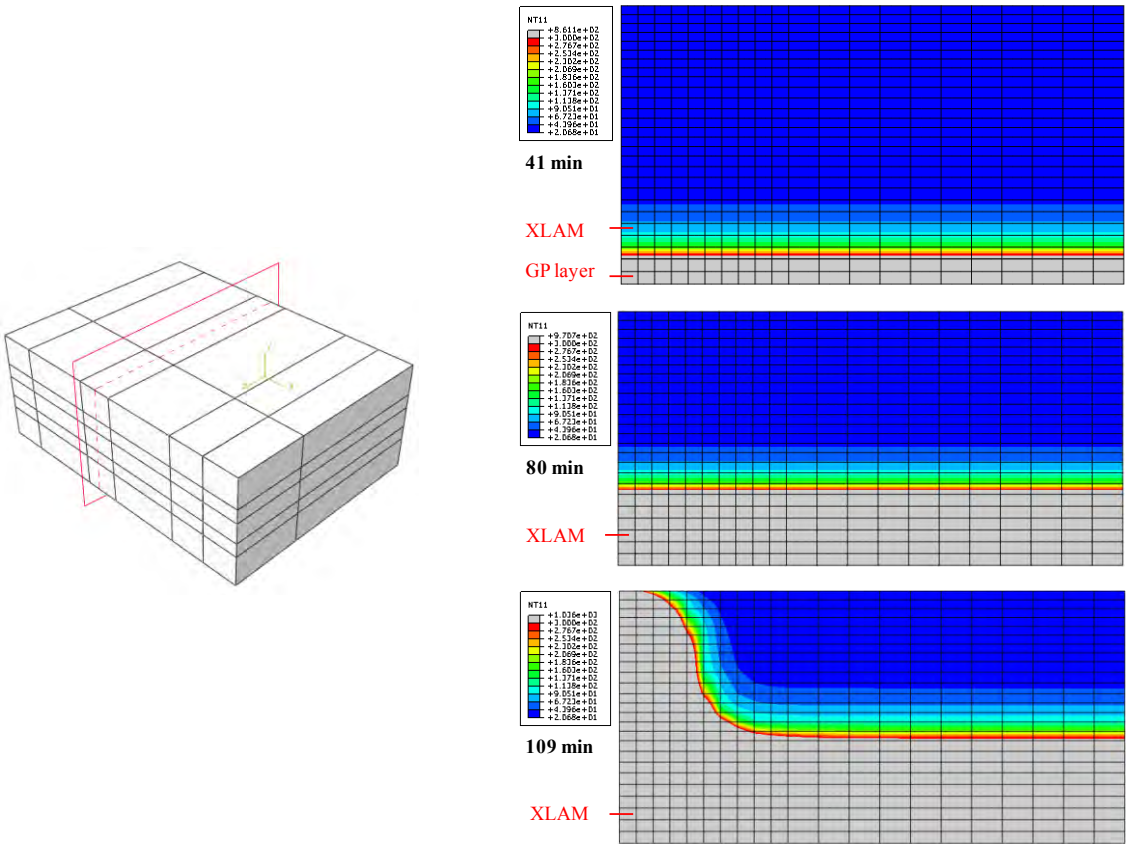

Fig. 7.27 - *Temperature distributions within the initially protected cross-section of the three-dimensional model at different times of fire exposure.*

The experimental and numerical mid-span deflections of protected XLAM panel are compared in Figure 7.28. The displacement was measured experimentally until the floor failure occurred (110 min). The numerical prediction of deflection is close to the experimental curve until the 60th min then the numerical simulation overestimates the displacement. After about 100 min of fire exposure the experimental and predicted deflections are again in close agreement before diverging near to the specimen failure when the experimental displacement increases rapidly.

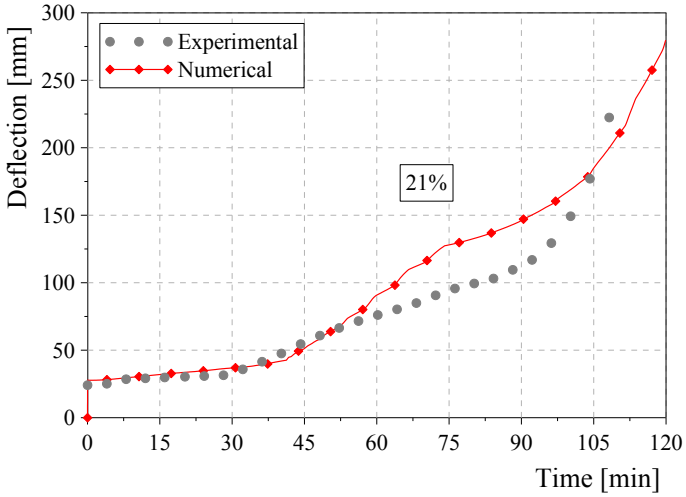

Fig. 7.28 - *Experimental and numerical deflections at mid-span of protected XLAM floor panel exposed to fire.*

7.4. PARAMETRIC STUDY

7.4.1. *Wood mechanical properties*

The dependence of the wood mechanical properties upon the temperature was implemented in the modelling by using the relationships proposed by the Eurocode 5, Part 1-2 [CEN 2004]. These general laws do not consider the possible dissimilar behaviour in fire conditions between solid wood and some wood-based products such as glued laminated timber and XLAM.

Since there is still some uncertainty within the scientific community on the type of degradation of mechanical properties with temperature to assume in the structural analysis, a parametric study was performed. The aim was to evaluate the influence of different strength and stiffness degradation laws with temperature on the fire resistance of initially protected XLAM floors loaded out-of-plane. The same structural layout, depth and applied load of the specimen S2 tested at CNR-IVALSA were considered. The numerical 2D model displayed in Figure 7.18 was used.

Thermo-mechanical analyses were carried out by changing either the strength-temperature relationship or the Young's modulus-temperature relationship (Fig. 7.29). Only in one analysis, modified degradations of both strength and stiffness were adopted simultaneously (Fig. 7.29b). In this analysis, the mechanical properties were maintained constant until the temperature of 290°C was attained and then they were dropped to zero at 300°C as proposed by the Eurocode 5. These variation laws were chosen to simulate the assumptions of the 'reduced cross-section method' (RCSM) provided by the Eurocode 5. The RCSM considers unchanged strength and stiffness for heated wood until 300°C temperature, where the charred material has no more load-bearing capacity. The initial (at ambient temperature) mechanical properties are adopted for a reduced residual cross-section, smaller than the effective one. This reduction in residual cross-section aims to provide conservative analytical predictions of fire resistance by neglecting the contribution of the heated wood, namely the part of the section close to the charred layer where the temperature varies from 300°C to almost ambient values.

Figure 7.29 plots the degradation relationships with temperature assumed in this parametric study for strength and Young's modulus in tension, and the laws proposed by

Eurocode 5. Almost all the adopted curves are bilinear with a knee at the temperature of 100°C like the Eurocode curves.

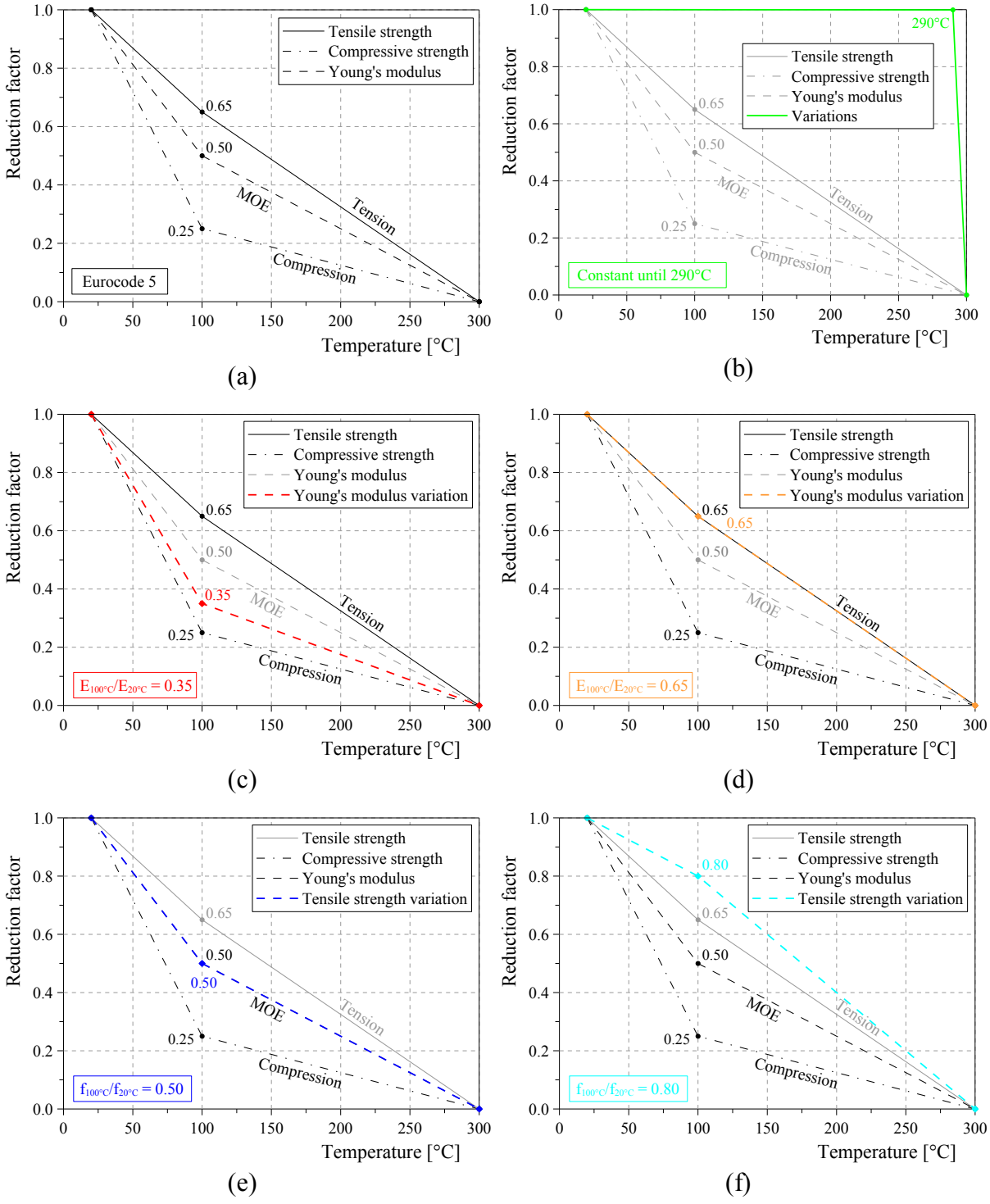

Fig. 7.29 - *Variations of Young's modulus (b,c,d) and tensile strength (b,e,f) with temperature adopted in the parametric study.*

The Eurocode variations of compressive and tensile strength were used when the modified Young's modulus degradations were considered. In particular, the reduction factor of Young's modulus at 100°C (0.50) was decreased to 0.35 and increased to 0.65 as plotted in Figures 7.29c and 7.29d, respectively. The adopted reduction of Young's modulus corresponds to the degradation law of the Young's modulus in compression suggested by the European design code. The tensile strength at 100°C (0.65) was decreased to 0.50 and increased to 0.80 as plotted in Figures 7.29e and 7.29f, respectively. In this case the Eurocode proposals for compression strength and tensile Young's modulus degradations were implemented.

The numerical failures with different assumptions for the mechanical property degradation still occurred in the third layer. The variations in Young's modulus degradation led to a fire resistance about 2% greater or lower than the prediction obtained using the Eurocode proposal for element loaded in tension. Differences of approximately 5% more and 7% less were found by increasing and reducing, respectively, the tension strength at 100°C. The fire resistance is overestimated of by 15% assuming the mechanical properties constant until the charring temperature. Table 7.4 summarizes the estimated fire resistance of initially protected XLAM panel loaded out-of-plane and exposed to 1D fire exposure.

Numerical results in terms of temperature, stress and strength distributions along the mid-span depth of a 5-layer XLAM floor panel are presented in Figure 7.30. The stresses within the section after 100 min of fire exposure obtained using different Young's modulus and tensile strength-temperature relationships are compared with the strength domain (dashed curve) at that specific thermal state.

Type of mechanical property degradation	Fire resistance	
Eurocode 5 properties	120.0	min
Tension strength: $f_{100°C}/f_{20°C} = 0.50$	111.5	min
Tension strength: $f_{100°C}/f_{20°C} = 0.80$	126.3	min
Young's modulus: $E_{100°C}/E_{20°C} = 0.35$	121.7	min
Young's modulus: $E_{100°C}/E_{20°C} = 0.65$	117.4	min
Properties constant until 290°C	138.6	min

Table 7.4 - *Fire resistance of initially protected XLAM panel estimated numerically adopting different mechanical properties-temperature relationships.*

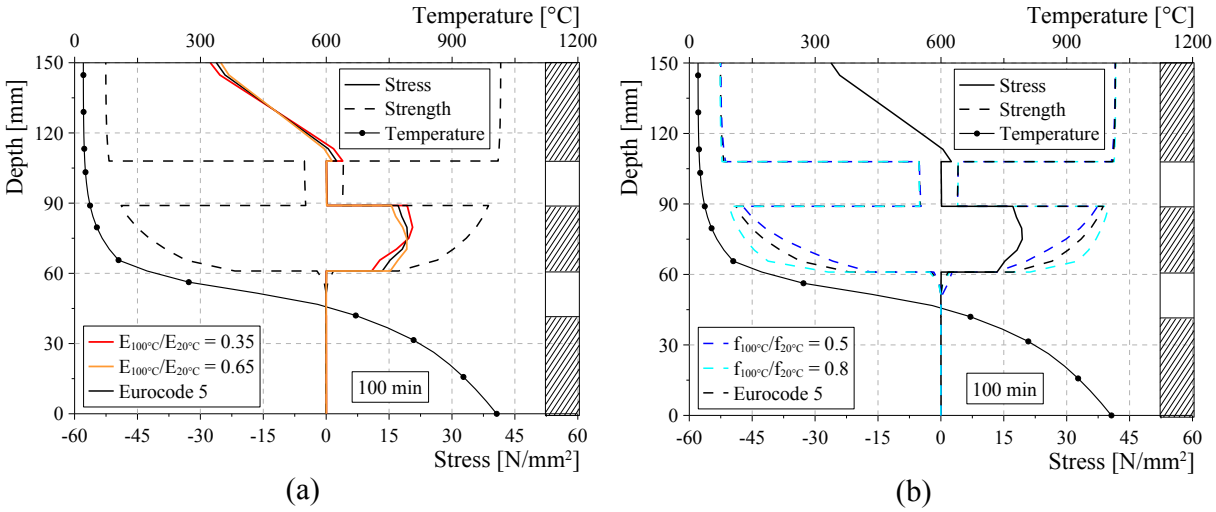

Fig. 7.30 - *Temperature, stress and strength distributions along the mid-span depth of initially protected XLAM panel after 100 min of fire exposure obtained assuming different degradations of Young's modulus (a) and tensile strength (b) with temperature.*

After 100 min from the onset of fire, the two lower layers are completely charred, whereas the third layer maintains part of its load-bearing capacity since the temperature ranges from 170°C to 36°C. The thermal state in the two layers more distant from fire is almost unchanged after 100 min of fire exposure. Differences between the stress distributions are noticeable only if the Young's modulus-temperature relationship is modified (Fig. 7.30a). Changes of tensile strength law lead to different strength domains, but they do not influence the mechanical state at this exposure time (Fig. 7.30b).

The thermo-structural states within the initially protected XLAM section at failure time obtained assuming different degradation laws of the mechanical properties with temperature are plotted in Figure 7.31. It can be noticed that the stress curves are close to the corresponding tensile strength domains in the third layer where the numerical failure occurred. Larger stress redistributions along the XLAM mid-span depth are obtained by increasing and reducing the degradations of Young's modulus (Fig. 7.31c) and tensile strength (Fig. 7.31f) with temperature, respectively.

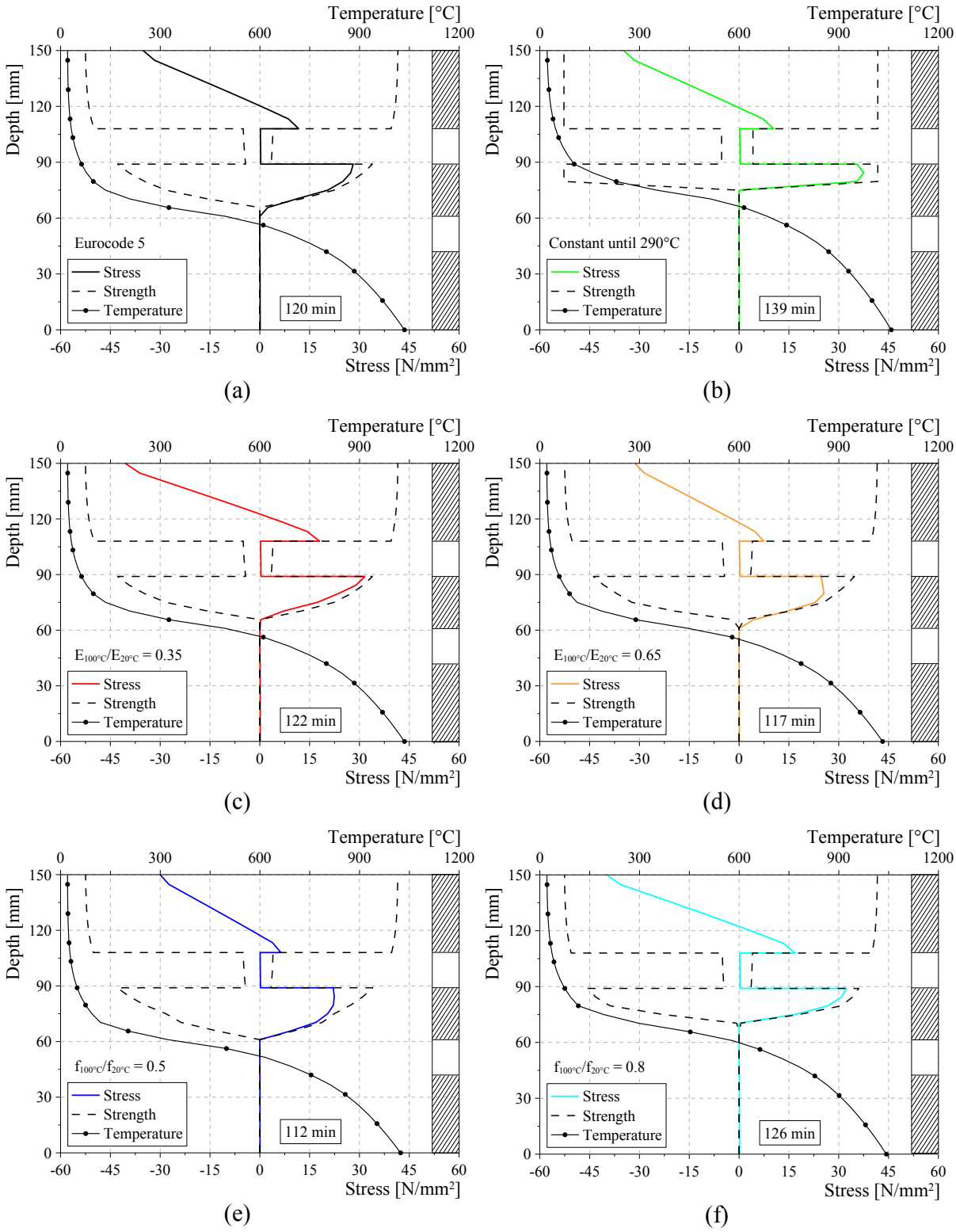

Fig. 7.31 - *Temperature, stress and strength distributions along the mid-span depth of initially protected XLAM panel at failure time obtained assuming different Young's modulus-temperature (a,b,c,d) and tension strength-temperature (a,b,e,f) relationships.*

Figure 7.32 plots the stress distribution during the fire test at 34 and 68 mm from the bottom surface obtained by assuming different mechanical properties-temperature relationships. Different variations of tensile strength with temperature provide stress curves with the same trend. The initial stress rises progressively and then drops to zero when the charring temperature (300°C) is attained (e.g. fibre at 34 mm depth). The stress is redistributed in the fibres more distant from fire (e.g. 68 mm depth) where the temperature is still low. Also in the inner fibres the stresses are gradually reduced to zero due to the increase in temperature. The stress distributions are compared with the corresponding strength domains determined according to the adopted property reduction laws. Stress and strength curves nearly coincide close to failure time.

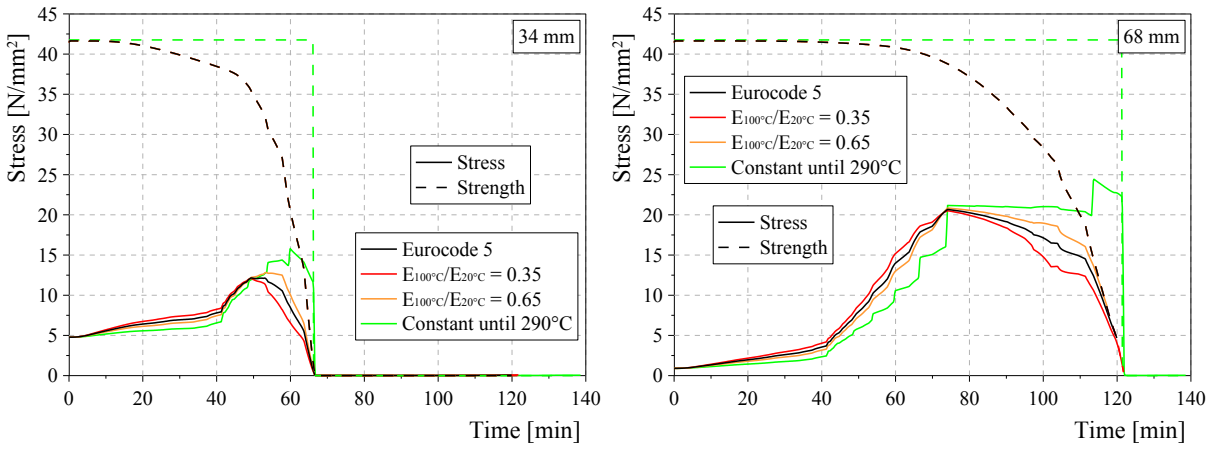

Fig. 7.32 - *Stress and strength vs. time at two different depths in the XLAM section obtained assuming different tension strength-temperature (a) and tensile Young's modulus-temperature (b) relationships.*

The estimated deflections at mid-span assuming the different degradation laws are compared in Figure 7.33. Different tensile strengths at 100°C provide curves with the same trend but different failure points. Conversely the variation in Young's modulus slightly affects the deflection, especially close to the failure.

A step curve is the result of the numerical simulation with constant properties that drop to zero at 300°C. This trend is caused by the charring of the mesh elements in the layers parallel to the main floor direction. The plateau after 70 min of fire exposure indicates the charring of the layer perpendicular to the main floor direction. The analytical deflection calculated with the RCSM (dashed curve) shows the same plateau but slightly anticipates the numerical curve. The simplified analytical method provides conservative results since the deflection is estimated considering a reduced resisting cross-section, whereas the actual residual section is considered in the numerical simulations.

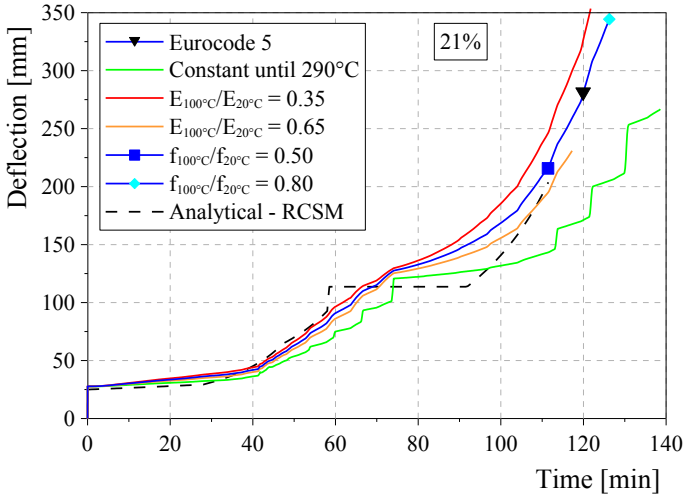

Fig. 7.33 - *Deflections at mid-span of initially protected XLAM floor panel obtained adopting different variations of mechanical properties with temperature.*

7.4.2. *Strength - strain relationships*

A thermo-structural analysis was performed also assuming elasto-plastic stress-strain relationships for wood both in tension and in compression. The thermo-mechanical state within the XLAM section at failure time obtained adopting this limit case is plotted in Figure 7.34b. In this case the numerical failure occurred after about 157 min of fire exposure due to the larger stress redistribution taking place in the section. At that time, the temperature in the panel is higher so the residual section and the strength domain reduce in comparison with the section and the domain at 120 min. Only the fourth and fifth layers are not charred and therefore all tension and compression stresses are carried by the last resisting layer parallel to the main floor direction (fifth layer) where the temperature is still low. The stress curve matches extremely well the corresponding strength domain along the un-charred floor depth and the failure occurs when a 'perfect' plastic hinge forms at mid-span. The formation of a perfect plastic hinge in this theoretical limit case provides a confirmation that the finite element model is correct.

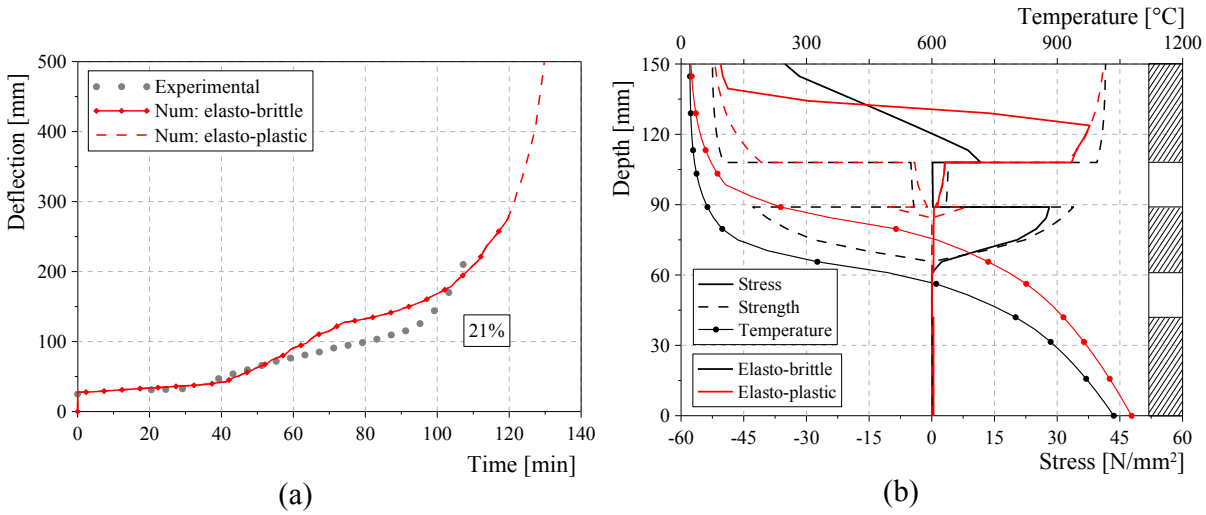

Fig. 7.34 - *Numerical results at mid-span of initially protected XLAM panel obtained assuming the material as elasto-brittle and elasto-plastic in tension: (a) deflections and (b) temperature, stress and strength distributions along the floor depth at failure time.*

7.5. ANALYTICAL-NUMERICAL COMPARISONS

The numerical results can be compared with analytical predictions using simplified design methods, such as the 'reduced cross-section method' (RCSM) proposed by Eurocode 5, Part 1-2 [CEN 2004]. This method, which was originally derived for structural elements made of sawn and glued laminated timber, has been recently extended to XLAM panels (RCSM for XLAM) [Schmid and König 2010; SP Trätek 2010]. The main difference between the two methods concerns the evaluation of the 'zero-strength' layer used to calculate the residual cross-section. A constant value of 7 mm after the start of charring (Fig. 5.37b) is adopted for this layer according to Eurocode 5. The RCSM for XLAM proposed some formulas to determine the thickness s_0 of the 'zero-strength' layer, referred to as 'compensating layer', considering the panel depth, the number of layers, the type of stress and structural element. The following formula is used for protected 5-layer XLAM floors exposed to fire on tension side:

$$s_0 = \frac{h}{35} + 6 \qquad [7.1]$$

where h is the panel depth in mm.

Two different situations have to be analyzed for initially protected elements according to Eurocode 5: wood charring (t_{ch}) starting when cladding failure occurs (t_f) (i) or before that time (ii). The first case ($t_{ch} = t_f$) was considered in the estimation of fire resistance for XLAM floors protected with a 15 mm thick layer of GP as proven by experimental data (Chapter 5). In the following analytical evaluations it is assumed that charring starts at 28 min as calculated using the conservative formula proposed by Eurocode 5 also for claddings consisting of one layer of F-type GP:

$$t_{ch} = 2.8 h_p - 14 \qquad [7.2]$$

where h_p is the thickness of the protective layer in mm.

The fire resistance and the deflection of initially protected 5-layer XLAM panels loaded with 21% of the estimated failure load at ambient temperature are predicted adopting the charring rate β_0 for solid and glued laminated timber (β_0 = 0.65 mm/min) proposed by Eurocode 5 and neglecting the two layers perpendicular to the main floor direction. Moreover, it is assumed that 3 mm is the minimum thickness of the charred

layers [SP Trätek 2010], below which the strength and stiffness of the layers are neglected. Table 7.5 reports the fire resistance of XLAM floor panels estimated analytically and numerically. The numerical failure occurred after about 120 min of fire exposure and this time differs approximately by 6.7% and 11% from the analytical estimations obtained using the RCSM and RCSM for XLAM, respectively.

Load level	21%
Analytical - RCSM	112 min
Analytical - RCSM for XLAM	107 min
Numerical (2D)	120 min
Experimental	110 min

Table 7.5 - *Analytical, experimental and numerical comparison of the fire resistance of protected XLAM floor panel.*

Figure 7.35a plots experimental, analytical and numerical charred depth versus fire exposure time. It can be noticed that the assumed time of start of charring (t_{ch}) is conservative with respect to experimental data. When the protective cladding falls off ($t_{ch} = t_f$), the charring starts at a double rate with respect to the value β_0 for initially unprotected elements provided by Eurocode 5 since the timber element is directly exposed to high temperatures (Fig. 5.38a). The charring slows down when the charred depth exceeds 25 mm and the charring rate for initially unprotected elements $\beta_0 = 0.65$ mm/min can be assumed. In Figure 7.35a it is also plotted the analytical curve obtained by assuming the start of charring before the falling of the protective layer ($t_{ch} < t_f$). In this case, the initial charring rate is lower than the value for initially unprotected elements. After the cladding failure observed experimentally at 41 min, the rate increases until the charred layer exceeds 25 mm and then it is reduced to $\beta_0 = 0.65$ mm/min.

Figure 7.35b compares experimental and numerical deflections also with the analytical values predicted using the RCSM and RCSM for XLAM. The experimental curves are well approximated by the analytical estimations as already discussed previously (Chapter 5). The plateau after approximately 50 min of fire exposure indicates the charring of the non load-bearing layer perpendicular to the main floor direction. On the whole the numerical deflection has a trend similar to analytical curves.

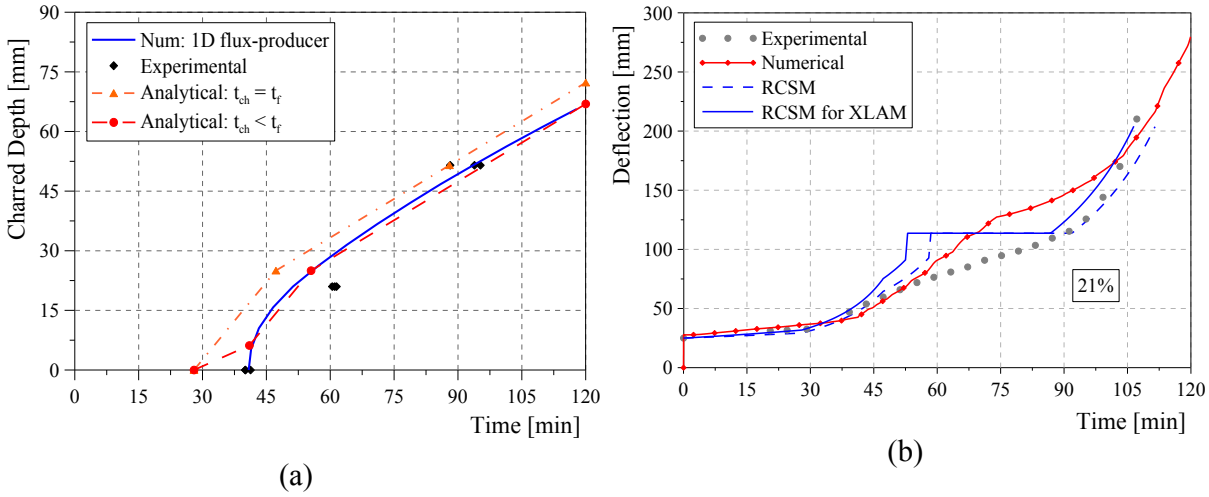

Fig. 7.35 - *(a) Charred depth vs. time from experimental data, numerical modelling and analytical predictions. (b) Experimental, numerical and analytical deflections at mid-span of loaded protected XLAM floor panel exposed to fire.*

CONCLUSIONS

Chapter 5 presents and discusses the results of experimental tests on 5-layer cross-laminated timber (XLAM) panels at ambient and fire conditions performed at Ivalsa Trees and Timber Institute (Italy). Two series of large-scale XLAM panels were tested in bending to collect data on mechanical properties. Protected and unprotected specimens with the same size were exposed to standard fire curve in a horizontal furnace to investigate their fire resistance. Three panels were loaded uniformly out-of-plane with two constant load levels and one of these was protected with a layer of gypsum plasterboard. The specimens subjected to the higher load level were tested to destruction. Additional four unloaded panels, two protected with gypsum fibreboard and two left unprotected, were exposed to standard fire curve. During all of the tests, temperatures were recorded by thermocouples inserted in the XLAM cross-section at different depths and locations. Other thermocouples were positioned at cladding-XLAM interfaces to collect additional information on the effect of thermal insulation on the temperature distribution and charring rates of the panel. The residual cross-sections were measured at the end of one test and the average charring rates were assessed and compared with values derived from thermocouple readings and with values proposed by Eurocode 5, Part 1-2 for solid and glued laminated timber. The experimental data of fire resistance and deflection were also compared with analytical predictions based on the 'reduced cross-section method' (RCSM) proposed by the Eurocode 5, Part 1-2 and a recently proposed extension of this method to XLAM (RCSM for XLAM).

The primary observations are reported herein after.

- Based on data readings from thermocouples, there was no evidence of falling off of charred layers during the fire tests. This is somewhat different from what observed in fire tests carried out by other authors on XLAM panels with the same type of glue. However, it should be pointed out that visual observation was not possible during the performed tests.
- The falling off of the cladding insulation layers was clearly noticed from the thermocouple readings as it corresponded to a significant increase in temperature at

the interfaces with the XLAM panels.

- The best fire performance was observed for cladding made of gypsum plasterboard, which delayed the start of charring in XLAM panels of about 10 and 40 min compared to panels protected with gypsum fibreboard and unprotected panels, respectively.
- A 15 mm thick layer of gypsum fibreboard slightly delayed the timber charring with respect to a cladding system made of a 12.5 mm layer of gypsum fibreboard with a 40 mm cavity filled of rock wool.
- The 150 mm thick unprotected XLAM panel loaded with 21% of the failure load at ambient temperature was found to possess a fire resistance of 99 min, which is more than adequate in a number of typical design situations.
- The fire resistance of the same floor panel can be improved of approximately 10% using a 15 mm thick layer of gypsum plasterboard (from 99 to 110 min).
- The charring rates determined directly from measurement of the residual cross-section and indirectly from thermocouple readings were comparable with the value suggested by Eurocode 5 even though the specimen position in the furnace and the technical time required to extinguish the panels at the end of test might have affected in some way their accuracy.
- The use of the RCSM allowed an easy yet slightly non-conservative design for fire resistance. However, the use of the RCSM for XLAM led to conservative predictions.
- The analytical evaluations of deflection for protected and unprotected XLAM panels using RCSM and RCSM for XLAM were in good agreement with experimental results.

Chapter 6 presents the models implemented in Abaqus finite element code to investigate the behaviour of unprotected XLAM panels loaded out-of-plane and exposed to standard fire on the bottom side. The layered nature of XLAM with very different properties in adjacent layers was numerically described by defining different isotropic materials for layers parallel and perpendicular to the main floor direction. The 'concrete damaged plasticity' model readily available in Abaqus was used to simulate the different wood behaviour in tension and compression. Elasto-brittle and elasto-plastic stress-strain relationships depending upon temperature were adopted to characterize the material in tension and compression, respectively. Strength and stiffness at ambient temperature

obtained from experimental tests were assumed. The numerical model was initially validated on experimental data collected during the bending tests of XLAM panels at ambient temperature. The same model was used to simulate the large-scale fire tests on 5-layer XLAM floors performed at Ivalsa Trees and Timber Institute. Sequential thermal and mechanical analyses were carried out to describe the temperature and stress distributions within the cross-section. The variation of thermal and mechanical properties with temperature proposed by the Eurocode 5, Part 1-2 was implemented. The temperature distributions obtained with the thermal analyses were adopted as an input for the structural model. The numerical predictions of fire resistance and deflection were compared with the experimental results presented in Chapter 5. A parametric study was carried out, where the load level applied on the XLAM panel was varied and the corresponding fire resistance was calculated and compared with the analytical estimations obtained using the RCSM and the new proposal for XLAM (RCSM for XLAM).

The primary observations are reported herein after.

- The thermal analyses provided an acceptable approximation of the temperature recorded by thermocouples within the cross-sections of unprotected XLAM floors, particularly when the actual two-dimensional heat flux observed during the experimental test was modelled.
- The results in terms of stress distributions at different depths clearly showed the increase and the following decrease of stresses with temperature in the fibres closer to the exposed surface until the 300°C temperature is reached, when the strength drops to zero.
- The stresses were redistributed in the cross-section from the more exposed fibres to the inner and cooler fibres until the residual cross-section was able to resist the applied load.
- At failure time, the stress reached the strength domain calculated as temperature function in different points of the cross-section. In the considered 5-layer XLAM panels, the failure occurred in the third layer from the exposed surface.
- On the whole the numerically predicted fire resistance was in good agreement with the experimental values, particularly when the actual two-dimensional heat flux observed during the experimental test was modelled, with a difference of about 2%.

- A clear dependence of the fire resistance on the load level was obtained.
- The analytical estimations based on the RCSM were in good agreement with the numerical predictions, whilst the RCSM for XLAM led to more conservative results. The greater differences were observed for the lower load levels.
- The numerical predictions of deflection followed the experimental trends and were fairly close to the estimated analytical curves.

Chapter 7 presents the finite element models implemented in Abaqus code with the aim to investigate the behaviour of initially protected XLAM floors exposed to fire on the bottom side. Numerical models similar to the modelling developed for unprotected XLAM panels were used. Thermal analyses were performed to describe the temperature distribution within XLAM panels protected by different cladding systems made of gypsum plasterboard or fibreboard. The obtained thermal states were compared with experimental data recorded by thermocouples during the fire tests on large-scale XLAM floor panels performed at Ivalsa Trees and Timber Institute (Italy). Subsequently, mechanical analyses were carried out to evaluate the fire resistance of a XLAM floor panel protected with gypsum plasterboard and loaded out-of-plane. The 'concrete damaged plasticity' model readily available in Abaqus was used to define the elasto-brittle and elasto-plastic stress-strain relationships depending upon temperature that characterize the wood behaviour in tension and compression, respectively. Strength and stiffness at ambient temperature obtained from experimental tests were assumed. The strength and stiffness degradation laws proposed by Eurocode 5, Part 1-2 were adopted initially. Then, a parametric study changing the degradation law of either the tension strength or the Young's modulus was performed to evaluate the influence on the fire resistance. In one case both properties were modified at the same time to reproduce the simplified assumption of unchanged material properties until the charring temperature (300°C), which is adopted by Eurocode 5, Part 1-2 in the RCSM for simplified fire design. A further mechanical analysis was performed by assuming wood as an elasto-plastic material in compression and tension. The numerical results were compared with experimental data and analytical predictions obtained using the RCSM and its extension for XLAM.

The primary observations are reported herein after.

- The comparison between numerical and experimental temperatures highlighted the need to model the falling off of the protective layers after a defined time of fire exposure in order to obtain a more realistic description of the thermal state.
- The temperature of 400°C at the cladding-XLAM interface suggested by recent technical guidelines for fire design was assumed as a criterion for the fall of protective layers. In the cases analysed, this criterion supplied slightly conservative and un-conservative results for gypsum fibreboard and plasterboard, respectively.
- A more accurate prediction of the thermal state within the cross-section of the XLAM panel protected with gypsum plasterboard was obtained by modelling the variation of heat flux from one-dimensional to two-dimensional shortly before specimen failure as experimentally observed.
- A significant stress redistribution within the cross-section from heated to cooler fibres was observed due to the reduction of timber mechanical properties with temperature.
- At failure time, the stress reached the strength domain calculated as temperature function in different points of the cross-section. In the considered 5-layer protected XLAM floors, the failure occurred in the third layer from the bottom surface.
- On the whole the numerically predicted fire resistance was in good agreement with the experimental value, particularly when a two-dimensional heat flux was modelled, with a difference of about 1%.
- The variations of the stiffness-temperature relationships affect the failure time, the stress distribution and the deflection of XLAM floor panels; conversely only the failure time changes if different tensile strength degradation laws are adopted.
- The limit case of elasto-plastic material in compression and tension clearly showed the larger stress redistribution in the cross-section at failure time when a 'perfect' plastic hinge formed in fire conditions, demonstrating that the model is robust and conceptually correct.
- The numerical estimation of deflection at mid-span was acceptable compared with the experimental one, especially considering the high variability that characterizes the wood material and the fire tests in general.
- The analytical and numerical predictions of deflections were in good agreement.

CONCLUSIONS AND RECOMMENDATIONS FOR FURTHER RESEARCH

The topic of this research is the performance of laminated veneer lumber (LVL) elements and cross-laminated timber (XLAM) floor panels in fire conditions. The investigation focused on some main research questions listed in the Introduction. The primary remarks of the entire research are herein reported for each research question.

- What is the actual resistance of large-scale timber structural elements exposed to fire on one or more sides and subjected to different types of load?

  Small- and large-scale tests were performed on LVL and XLAM specimens with different cross-sections. They were subjected to one- and two dimensional fire exposures in different furnaces. Some LVL and XLAM elements were loaded respectively in-plane and out-of-plane with different load levels. The high variability that characterizes the properties of timber and the fire tests influences also the experimental data. However, the experimental results highlight the good performance of timber elements in fire conditions, in particular of large LVL and XLAM specimens suitable for structural purposes. Unprotected LVL members with rectangular cross-section 63×150 mm exposed to standard fire on all sides and loaded in tension with 22% of the mean failure load at ambient conditions demonstrated a fire resistance of approximately 18 minutes. Unprotected XLAM panels with 150 mm depth exposed to standard fire on one side and loaded out-of-plane with 21% of the mean failure load at ambient conditions demonstrated a fire resistance of 99 minutes. Particularly the second value would be sufficient in a number of typical design situations, highlighting the inherent good structural performance of unprotected XLAM panels in fire conditions.

- What is the effect of protective cladding on the actual fire resistance of large-scale timber structural elements?

  Large-scale tests were performed on initially protected XLAM specimens subjected to one-dimensional fire exposure and protected with different types of cladding. The claddings made of a single layer of gypsum plasterboard or gypsum fibreboard fixed directly to the XLAM panel ensured at least 30 min of protection before losing their function. The XLAM floor panel protected with gypsum plasterboard was also loaded uniformly out-of-plane and its fire resistance was increased by about 10% with respect to an unprotected XLAM panel due to the delayed start of charring.

- Is it possible to model accurately the thermal state within protected and unprotected timber members, and the thermo-mechanical behaviour under load in fire conditions using general purpose software packages?

  Two- and three-dimensional finite element models were implemented in the general purpose software package Abaqus to simulate the fire exposure of the tested LVL and XLAM elements. The thermo-physical properties of wood depending upon the temperature as proposed by the European code for fire design of timber structures were adopted in the numerical modelling. Thermal analyses were carried out to investigate the thermal behaviour of protected and unprotected timber members exposed to fire on one or more sides. The temperature distribution within cross-sections of different sizes was described with acceptable accuracy compared to thermocouples records, especially considering the high variability of experimental data. Two- and three-dimensional models were implemented in Abaqus code to estimate the fire resistance of LVL and XLAM elements subjected to different levels of load in-plane and out-of-plane, respectively. A material model for non-linear behaviour readily available in Abaqus was used. Sequential thermo-mechanical analyses were executed to examine the structural performance of loaded timber members in fire conditions. Accurate predictions of the fire resistance were obtained with respect to experimental failure times. The differences are approximately 5% and 2% for small LVL elements and large XLAM floor panels, respectively.

  The proposed finite element model implemented in a general software package such as Abaqus can then be used effectively to predict the behaviour in fire conditions of timber members.

- What is the influence of the temperature-dependent properties of wood on the thermal and mechanical behaviour of timber members in fire conditions?

  The implemented finite element models were used to perform parametric studies aimed to investigate the influence of wood properties on fire behaviour. Thermal properties of wood proposed by different authors and variations of the mechanical property-temperature relationships suggested by the European code for fire design of timber structures were adopted in the modelling. The numerical outcomes highlight the considerable influence of adopted temperature-property laws on thermal and structural behaviour of timber exposed to fire. A 23% reduction of the tensile strength at 100°C was found to decrease the fire resistance of a XLAM panel by 7%. By comparison with the experimental results, it was concluded that the relationships provided by the Eurocode 5 provide accurate predictions.

- What is the accuracy of simplified design methods provided by current code of practice and new research proposals to estimate the fire resistance of timber elements under different load levels?

  The simplified 'reduced cross-section method' recommended by the European code for fire design of timber structures was used to estimate the fire resistance and the deflection of LVL and XLAM members. An extension of the afore-mentioned method to XLAM recently proposed in Sweden was also employed for analytical estimations. The analytical predictions are in good agreement with experimental results and numerical estimations. The new approach for XLAM was found to be always conservative, whilst the former one was found to be non-conservative for some load levels, even though the difference was always small.

Further experimental tests should be performed on elements made of LVL, XLAM or different wood-based materials in order to collect more data on their thermal and mechanical behaviour in fire conditions. For example, the dependency of the fire resistance of timber members on the load level should be further investigated by carrying out additional fire tests at different load levels. Also the effects of different protective claddings and their falling on the fire behaviour of initially protected timber elements should be subject of further experimental tests and numerical analyses. Other experimental research should be undertaken to clarify whether the falling of the XLAM charred layers does or does not occur, by carrying out further large-scale fire tests on unloaded panels instrumented with thermocouples at the interfaces of XLAM layers. The fire behaviour of XLAM panels loaded in-plane when used as walls should be explored with additional experimental testing.

Further experimental and numerical comparisons should be carried out to validate the thermal and mechanical modelling for different cross-sections and load levels. In order to improve the accuracy of the numerical simulations, further research should be performed on the dependency of thermal and mechanical properties of different wood-based products upon the temperature, which would enable further verification of the values and relationships proposed by the European code for fire design of timber elements. Additional research should address a number of important topics, including the numerical modelling of protected elements, the influence of the adopted strength and stiffness degradation laws with temperature on the fire resistance of timber members, and the numerical modelling of glued laminations when adhesives particularly sensitive to temperature are used. Last but not least, an important topic that should be investigated in future research is the fire resistance of connections between timber members. The Abaqus model should be extended to take into account the contact between timber and metal fasteners and plates, in terms of both heat conduction and structural resistance. After calibration on experimental results, the model should then be used to carry out parametric studies and then used to provide a data base of results used to check the accuracy of approximate design methods and to derive, if needed, better solutions.

REFERENCES

ABAQUS version 6.6. (2006). Hibbitt, D., Karlsson, B., Sorensen, P. Dassault Systèmes S.A.

ABAQUS version 6.9. (2009). Hibbitt, D., Karlsson, B., Sorensen, P. Dassault Systèmes S.A.

ANSYS® Academic Research, Help System, Coupled Field Analysis Guide, ANSYS, Inc.

AS/NZS 2005 (Australian/New Zealand Standard), AS/NZS 4357. *Structural laminated veneer lumber*.

American Wood Council (AWC) (2003). *Calculating the fire resistance of exposed wood members*. Technical Report 10, American Forest & Paper Association, Washington, USA.

Audebert M., Dhima D., Taazount M. and Bouchaïr A. (2011). *Numerical investigations on the thermo-mechanical behavior of steel-to-timber joints exposed to fire.* Engineering Structures; 33(12), 3257-3268.

Bénichou N., Sultan M.A., MacCallum C. and Hum J. (2001). *Thermal properties of wood, gypsum, and insulation at elevated temperatures.* Internal Report IR-710, Institute for Research in Construction - National Research Council of Canada, Ottawa, Canada.

Bénichou N., Kodur V.R. and Sultan M.A. (2002). *Experimental study and numerical modelling of the fire resistance of wood-stud wall assemblies.* Proceedings of the 4th Structural Specialty Conference of the Canadian Society for Civil Engineering, Montréal, Canada.

Bobacz D. (2006). *Behaviour of wood in case of fire. Proposal for a stochastic dimensioning of structural elements*. PhD Thesis, University of Natural Resources and Applied Life Sciences, Vienna, Austria.

BSPhandbuch - Holz-Massivebauweise in Brettsperrholz (2010). Institut für Holzbau und Holztechnologie, und holz.bau forschungs gmbh, Graz, Austria.

Buchanan A.H. (2002). *Structural Design for Fire Safety*. J. Wiley & Sons Ldt, Chichester, England.

Buchanan A.H. (2007). *Timber design guide*. New Zealand Timber Industry Federation Inc.

Cachim P.B. and Franssen J-M. (2009a). *Comparison between the charring rate model and the conductive model of Eurocode 5*. Fire and Materials; 33(3), 129-143.

Cachim P.B. and Franssen J-M. (2009b). *Numerical modelling of timber connections under fire loading using a component model.* Fire Safety Journal; 44(6), 840-853.

Cachim P.B. and Franssen J-M. (2010). *Assessment of Eurocode 5 charring rate calculation methods.* Fire Technology; 46(1), 169-181.

CEN 1999 (European Committee for Standardization), EN 1363-1. *Fire resistance tests - General requirements.* CEN, Brussels, Belgium.

CEN 2002a (European Committee for Standardization), EN 1990. *Eurocode 0 – Basis of structural design.* CEN, Brussels, Belgium.

CEN 2002b (European Committee for Standardization), EN 1991-1-2. *Eurocode 1 – Actions on structures – Part 1-2: General actions – Actions on structures exposed to fire.* CEN, Brussels, Belgium.

CEN 2004 (European Committee for Standardization), EN 1995-1-2. *Eurocode 5 - Design of timber structures. Part 1-2: General - Structural fire design.* CEN, Brussels, Belgium.

CEN 2004 (European Committee for Standardization), EN 14374. *Timber structures -*

Structural laminated veneer lumber - Requirements. CEN, Brussels, Belgium.

CEN 2009a (European Committee for Standardization), EN 338. *Structural timber – Strength classes.* CEN, Brussels, Belgium.

CEN 2009b (European Committee for Standardization), EN 520. *Gypsum plasterboards – Definitions, requirements and test methods.* CEN, Brussels, Belgium.

CEN 2009c (European Committee for Standardization), EN 15283-2. *Gypsum boards with fibrous reinforcement – Definitions, requirements and test methods. Part 2: Gypsum fibre boards*. CEN, Brussels, Belgium.

CEN 2010 (European Committee for Standardization), EN 408. *Timber structures – Structural timber and glued laminated timber – Determination of some physical and mechanical properties.* CEN, Brussels, Belgium.

CHH (Carter Holt Harvey) Woodproducts New Zealand: www.chhwoodproducts.co.nz.

CLT Handbook: cross-laminated timber (2011). Special Pubblication *SP-528E*, FPInnovations, edited by Gagnon S. and Pirvu C., Québec, Canada.

Erchinger C., Frangi A. and Mischler A. (2006). "*Thermal investigations on multiple shear steel-to-timber connections"*. Proceedings of the 9th World Conference on Timber Engineering, Portland, OR, USA.

Erchinger C., Frangi A. and Fontana M. (2010). *Fire design of steel-to-timber dowelled connections.* Engineering Structures, 32(2), 580-589.

Fermacell: www.fermacell.it

Fiori S. (2010). *Numerical-experimental analysis of cross-laminated timber floor panels exposed to fire.* Master Thesis, University of Trieste, Trieste, Italy (in Italian).

Fire Safety Design (1990). User's Manual for TCD 3.0 with TempCalc. Lund, Sweden.

Fragiacomo M., Menis A., Moss P.J., Buchanan A.H., and Clemente I. (2009). *Comparison between the conductive model of Eurocode 5 and the temperature*

distribution within a timber cross-section exposed to fire. Proceedings of the 42nd Meeting, CIB-W18, Duebendorf, Switzerland.

Fragiacomo M., Menis A., Moss P.J., Buchanan A.H. and Clemente I. (2010a) *Numerical and experimental evaluation of the temperature distribution within laminated veneer lumber (LVL) exposed to fire*. Journal of Structural Fire Engineering; 1(3):145-159.

Fragiacomo M., Menis A., Moss P.J., Clemente I. and Buchanan A.H. (2010b). *Numerical and experimental thermal-structural behaviour of laminated veneer lumber (LVL) exposed to fire*. Proceedings of the 11th World Conference on Timber Engineering, Riva del Garda, Italy.

Fragiacomo M., Menis A., Bochicchio G., Clemente I. and Ceccotti A. (2012a). *Fire resistance of cross-laminated timber floors. Part 1: Experimental study.* ASCE *Journal of Structural Engineering,* in review.

Fragiacomo M., Menis A., Moss P.J., Clemente I., Buchanan A.H. and De Nicolo B. (2012b). *Predicting the fire resistance of timber members loaded in tension.* Fire and Materials; in print.

Frangi A. (2001). *Brandverhalten von Holz-Beton-Verbunddecken.* PhD Thesis. Institute of Structural Engineering, ETH, Zurich, Switzerland (in German).

Frangi A. and Fontana M. (2003). *Charring rates and temperature profiles of wood sections*. Fire and Materials; 27(2), 91-102.

Frangi A., Fontana M. and Mischler A. (2004). *Shear behaviour of bond lines in glued laminated timber beams at high temperature.* Wood Science and Technology; 38(2), 119-126.

Frangi A. and Erchinger C. (2007). *Design of timber frame assemblies in fire*. Proceedings of the 40th Meeting, CIB-W18, Bled, Slovenia.

Frangi A., Bochicchio G., Ceccotti A. and Lauriola P. (2008a). *Natural full-scale fire test on a 3 storey XLam timber building.* Proceedings of the 10th World

Conference on Timber Engineering, Miyazak, Japan.

Frangi A., Erchinger C. and Fontana M. (2008b). C*harring model for timber frame floor assemblies with void cavities.* Fire Safety Journal; 43(8), 551-564.

Frangi A., Fontana M., Hugi E. and Jöbstl R. (2009a). *Experimental analysis of cross-laminated timber panels in fire.* Fire Safety Journal; 44(8), 1078-1087.

Frangi A., Fontana M., Knobloch M. and Bochicchio G. (2009b). *Fire behaviour of cross-laminated solid timber panels.* Fire Safety Science; 9, 1279-1290.

Frangi A., Fontana M., Hugi E. and Wiederkehr R. (2010a). *Fire safety of multi storey timber buildings.* Proceedings of the 11th World Conference on Timber Engineering, Riva del Garda, Italy.

Frangi A., Schleifer V., Fontana M. and Hugi, E. (2010b). *Experimental and numerical analysis of gypsum plasterboards in fire*. Fire Technology; 46(1), 149-167.

Frangi A. and König J. (2011). *Effect of increased charring on the narrow side of rectangular timber cross-sections exposed to fire on three or four sides*. Fire and Materials; 35(8), 593-605.

Franssen J-M. (2005). *SAFIR. A thermal/structural program modelling structures under fire*. Engineering Journal; AISC; 42(3), 143-158.

Friquin K.L. (2010). *Charring rates for cross-laminated timber panels exposed to standard and parametric fires*. Proceedings of the 12th World Conference on Timber Engineering, Riva del Garda, Italy.

Goina M. (2010). *Fire resistance of compressed wall made of cross-laminated timber panels.* Master Thesis, University of Trieste, Trieste, Italy (in Italian).

Handbook 1 – Timber Structures (2008). Educational Materials for Designing and Testing of Timber Structures – TEMTIS. Leonardo da Vinci Pilot Projects.

Hopkin D.J., El-Rimawi J., Silberschmidt V. and Lennon T. (2011). *An effective thermal property framework for softwood in parametric design fire: comparison of the*

Eurocode 5 parametric charring approach and advanced calculation models. Construction and Building Materials; 25(5):2584-2595.

ISO 834-1 (1999). *Fire-resistance tests. Elements of building construction. Part 1: General requirements*. International Organization for Standardization, Geneva, Switzerland.

Janssens M.L. (2004). *Modeling of the thermal degradation of structural wood members exposed to fire*. Fire and Materials; 28(2-4), 199-207.

Jones B.H. (2001). *Performance of gypsum plasterboard assemblies exposed to real building fires*. Fire Engineering Research Report 01/4. University of Canterbury, Christchurch, New Zealand.

Jong F. and Clancy P. (2004). *Compression properties of wood as functions of moisture, stress and temperature.* Fire and Materials; 28(2-4), 209-225.

Just A., Schmid J. and König J. (2010). *Gypsum plasterboards used as fire protection – Analysis of a database.* SP Report 2010:29, SP Technical Research Institute of Sweden, Stockholm, Sweden.

Just A., Schmid J. and König J. (2011). *Gypsum plasterboards and gypsum fibreboards – Protective times for safety design of timber structures. Proceedings of the 44th Meeting – CIB-W18, Alghero, Italy.*

Klippel M., Frangi A. and Fontana M. (2011). *Influence of the adhesive on the load-carrying capacity of glued laminated timber members in fire.* Proceedings of the 10th Symposium on Fire Safety Science, University of Maryland, Baltimore, USA.

Knauf: www.knauf.it

König J. and Walleij L. (1999). *One-dimensional charring of timber exposed to standard and parametric fires in initially unprotected and post-protected situations.* Report I-9908029. Swedish Institute for Wood Technology Research, Stockholm, Sweden.

König J. (2005). *Structural fire design according to Eurocode 5 – Design rules and their background*. Fire and Materials; 29(3):147-163.

König J. (2006). *Effective thermal actions and thermal properties of timber members in natural fires.* Fire and Materials; 30(1), 51-63.

König J. and Källsner B. (2006). *An easy-to-use model for the design of wooden I-joists in fire.* Proceedings of the 39th Meeting – CIB-W18, Florence, Italy.

König J. and Schmid J. (2007). *Bonded timber deck plates in fire.* Proceedings of the 40th Meeting – CIB-W18, Bled, Slovenia.

König J., Norén J. and Sterley M. (2008). *Effect of adhesives on finger joint performance in fire*. Proceedings of the 41st Meeting – CIB-W18, St. Andrews, New Brunswick, Canada.

Lane W.P. (2005). *Ignition, charring and structural performance of laminated veneer lumber.* Fire Engineering Research Report 05/3. University of Canterbury, Christchurch, New Zealand.

Laplanche K., Dhima D. and Racher P. (2004). *Predicting the behaviour of dowelled connections in fire: fire tests results and heat transfer modelling.* Proceedings of the 8th World Conference on Timber Engineering, Lahti, Finland.

Laplanche K., Dhima D. and Racher P. (2006). *Thermo-mechanical analysis of the timber connection under fire using 3D finite element model*. Proceedings of the 9th World Conference on Timber Engineering, Portland, OR, USA.

Lu L., Isgor O.B. and Hadjisophocleous G. (2010). *A computer model for light-frame wood floor assemblies under fire attack.* Proceedings of the 12th World Conference on Timber Engineering, Riva del Garda, Italy.

Mackerle J. (2005). *Finite element analyses in wood research: a bibliography*. Wood Science and Technology; 39(7), 579-600.

Martinsons: www.martinsons.se

Menis A. (2008). *Numerical and experimental investigations of LVL members exposed to fire.* Master Thesis. University of Trieste, Trieste, Italy (in Italian).

Mirianon F., Fortino S. and Toratti T. (2008). "*A method to model wood by using Abaqus finite element software. Part 1: Constitutive model and computational details.*" VTT Publications 687, VTT Technical Research Centre of Finland, Espoo, Finland.

Moss P.J., Buchanan A.H. and Fragiacomo M. (2009a). *Predicting the behaviour of timber connections subjected to fire.* Proceedings of the 20th Australasian Conference on the Mechanics of Structures and Materials. In: Futures in Mechanics of Structures and Materials, CRC Press; 857-863.

Moss P.J., Buchanan A.H., Fragiacomo M. and Austruy, C. (2009b). *Experimental testing and analytical prediction of the behaviour of timber bolted connections subjected to fire*. Fire Technology; Springer Science, doi: 10.1007/s10694-009-0096-6.

Moss P.J., Buchanan A.H., Fragiacomo M., Lau P.H. and Chuo T. (2009c). *Fire performance of bolted connections in laminated veneer lumber.* Fire and Materials; 33(5), 223-243.

Nelson Pine Industries Ltd. (2008). *Product Specification: LVL 02*. Nelson, New Zealand: www.nelsonpine.co.nz.

O'Neill J., Carradine D., Moss P.J., Fragiacomo M., Dhakal R. and Buchanan AH. (2011). *Design of timber-concrete composite floors for fire resistance*. Journal of Structural Fire Engineering; 2(3), 231-242.

Peng L. (2010). *Performance of heavy timber connections in fire*. PhD Thesis, Carleton University, Ottawa, Canada.

Peng L., Hadjisophocleous G., Mehaffey J. and Mohammad M.A. (2008). *Thermal investigation on heavy timber connections exposed to fire.* Canadian Society for Civil Engineering Annual Conference, Québec, Canada.

Popovski M. and Karacabeyli E. (2011). *Seismic performance of cross-laminated wood panels.* Proceedings of the 44th Meeting – CIB-W18, Alghero, Italy.

Promo_legno: www.promolegno.com

Progetto Sofie - Sistema costruttivo Fiemme (2007). Scientific Report, National Research Council of Italy – Trees and Timber Institute (Cnr-Ivalsa) and Provincia Autonoma di Trento, Italy.

Racher P., Laplanche K., Dhima D. and Bouchaïr, A. (2010). *Thermo-mechanical analysis of the fire performance of dowelled timber connection.* Engineering Structures; 32(4), 1148-1157.

Rigonat R. (2011). *Numerical-experimental analysis of the fire resistance of cross-laminated timber floors*. Master Thesis, University of Trieste, Trieste, Italy (in Italian).

Rogowski B.F.W. (1967). *Charring of timber in fire test. Symposium n°3: Fire and structural use of timber in buildings.* HMSO, London, England.

Rothoblaas: www.rothoblaas.com

Serrano E. (2004). *A numerical study of the shear-strength-predicting capabilities of test specimens for wood-adhesive bonds.* International Journal of Adhesion & Adhesives; 24(1), 23-35.

Shresta D., Cramer S. and White R. (1994). *Time-temperature profile across a lumber section exposed to pyrolytic temperatures.* Fire and Materials; 18(4), 211-220.

Schmid J. and König J. (2010). *Fire exposed cross-laminated timber – Modelling and tests.* Proceedings of the 43rd Meeting – CIB-W18, Nelson, New Zealand.

Schnabl S. and Turk G. (2006). *Coupled heat and moisture transfer in timber beams exposed to fire.* Proceedings of the 9th World Conference on Timber Engineering, Portland, USA.

Schnabl S., Planinc I. and Turk G. (2008). *Thermo-mechanical fire analysis of timber composite beams with interlayer slip.* Proceedings of the 10th World Conference on Timber Engineering, Miyazaki, Japan.

SNZ 1993 (Standards New Zealand), NZS 3603. *Code of practice for timber design*. Wellington, New Zealand.

SP Trätek (Technical Research Institute of Sweden) (2010). *Fire safety in timber buildings – Technical guideline for Europe.* SP Report 2010:19, SP Trätek, Stockholm, Sweden.

Steiger R. and Gülzow A. (2009). *Validity of bending tests on strip-shaped specimens to derive bending strength and stiffness properties of cross-laminated solid timber (CLT).* Proceedings of the 42nd Meeting – CIB-W18, Dübendorf, Switzerland.

Stora Enso Timber: www.clt.info

Tabaddor M. (2008). *Thermal and mechanical finite element modelling of wood-floor assemblies subjected to furnace exposure.* Research Report No. NC9140, Underwriters Laboratories Inc., USA.

Takeda H. and Mehaffey J.R. (1998). *WALL2D: a model for predicting heat transfer through wood-stud walls exposed to fire.* Fire and Materials; 22(4), 133-140.

Takeda H. (2003). *A model to predict fire resistance of non-load bearing wood-stud walls.* Fire and Materials; 27(1), 19-39.

Takeda H. (2010). *Effect of insulation on the fire resistance of wood-framed floor assembly.* Proceedings of the 11th World Conference on Timber Engineering, Riva del Garda, Italy.

Teibinger M. and Matzinger I. (2010). *Basis for evaluation of the fire resistance of timber constructions.* Final Report, Holzforschung Austria, Vienna, Austria.

Tsai W-H. (2010). *Charring rates for different cross sections of laminated veneer lumber (LVL)*. Master Thesis, University of Canterbury, Christchurch, New Zealand.

Wilinder P. (2010). *Fire resistance in cross-laminated timber.* Bachelor Thesis, Jönköping University, Jönköping, Sweden.

Winstone Wallboards Ltd. *GIB®Fire Rated Systems*. New Zealand: www.gib.co.nz.

Winter S. and Meyn, W. (2009). *Advanced calculation method for the fire resistance of timber framed walls.* Proceedings of the 42nd Meeting – CIB-W18, Dübendorf, Switzerland.

Xu B.H., Bouchaïr A., Taazount M., and Vega E.J. (2009a). *Numerical and experimental analyses of multiple-dowel steel-to-timber joints in tension perpendicular to grain.* Engineering Structures; 31(10), 2357-2367.

Xu B.H., Taazount M., Bouchaïr A. and Racher P. (2009b). *Numerical 3D finite element modelling and experimental tests for dowel-type timber joints.* Construction and Building Materials; 23(9), 3043-3052.

Yang T-H., Wang S-Y., Tsai M-J. and Lin C-Y. (2009a). *Temperature distribution within glued laminated timber during a standard fire exposure test.* Materials and Design; 30(3), 518-525.

Yang T-H., Wang S-Y., Tsai M-J. and Lin C-Y. (2009b). *The charring depth and charring rate of glued laminated timber after a standard fire exposure test.* Building and Environment; 44(2), 231–236.

ACKNOWLEDGEMENTS

This thesis would not be possible without the technical and financial support of the Department of Civil and Natural Resources Engineering of the University of Canterbury (Christchurch, New Zealand) and the Ivalsa Trees and Timber Institute (San Michele all'Adige, Italy) where the experimental tests were carried out.

Furthermore, several producers supplied the material utilized to fabricate the specimens. Fermacell S.r.l., Knauf Italia, Magnifica Comunità di Fiemme, Martinsons, Nelson Pine, Rothoblaas and Stora Enso are greatly appreciated for their useful collaboration.